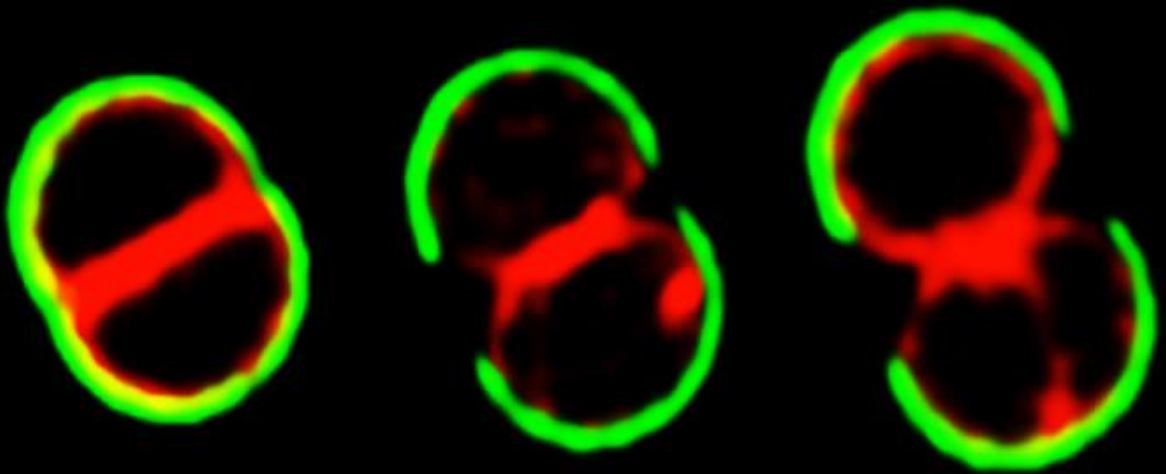


Mechanisms coordinating peptidoglycan  
synthesis with the cell cycle in  
*Staphylococcus aureus*

João Miguel Monteiro



Dissertation presented to obtain the Ph.D degree in Biology  
Instituto de Tecnologia Química e Biológica António Xavier | Universidade Nova de Lisboa

Oeiras,  
April, 2018



UNIVERSIDADE  
**NOVA**  
DE LISBOA







# Mechanisms coordinating peptidoglycan synthesis with the cell cycle in *Staphylococcus aureus*

João Miguel Monteiro

Dissertation presented to obtain the Ph.D degree in Biology

Instituto de Tecnologia Química e Biológica António Xavier | Universidade Nova de Lisboa

Oeiras, April, 2018





## Acknowledgments

I can say with certainty that my supervisor Dr. Mariana Pinho has been the most influential person in my scientific development. When I came into the lab I was brash and careless but you were always incredibly patient and believed in my abilities. Your guidance and knowledge have allowed me to achieve all the personal goals I set for my PhD. I could write a dissertation about how I think you are the best kind of P.I./leader/boss/supervisor, the kind that leads by example, that inspires others to fulfil their potential, but it's probably best that I focus on one particular moment. It was when we submitted our cell cycle paper, at 4 AM after a full day of revision. You told me to go ahead and press Enter, which I promptly did, and a pop-up window asked us if we were really sure and we just froze in place. I was exhausted, but the proudest I've ever been. Every time I write a text, prepare microscopy data or a graph I always think "Is this good enough for Mariana to see?" and most of the times it's not, so I do it over and then send it and you **still correct it**, and I am **extremely grateful** for that. Thank you Mariana.

I would like to acknowledge Dr. Sérgio Filipe, not only because of the great work collaborations over the years but also due to his insights into how to improve experiments and develop ideas. I have attended around 100 Lab Meetings during my stay at ITQB and I can say I've learned something completely new and interesting in



each and every one of them, thanks in no small part to Sérgio. Thank you for making Friday mornings a scientific joy.

I would like to thank Dr. Margarida Archer, member of my thesis committee, for helpful discussions on how to improve my work and presentation skills. I would also like to thank Prof. Adriano Henriques and Dr. Mónica Serrano for the engaging collaborations.

Thank you Prof. Hans-Georg Sahl for receiving me so well in Germany and for making sure that I was integrating with the group and the research. Your calm demeanour and vast knowledge of science really influenced my personal growth. Also, thank you for the canoe trip, it was awesome! I would also like to thank Prof. Gabriele Bierbaum for letting me work with her group, I had a fantastic stay there and wish there was more time to finish all the experiments we wanted to do. I'd also like to acknowledge Prof. Tanja Schneider and all the brilliant group members I worked with in Germany: Daniela, Marvin, Ina, Hannah, Anna and Patrick, you guys are too cool. A special thanks to my friends Anna Klöckner (did I spell that right?) and Mike Gajdiss for making my life in Bonn amazing.

I am truly a fortunate man for having the opportunity to work daily with talented, intelligent and dedicated people, whom I'd like to acknowledge. Nathalie (colleague) you are the ultimate evolution of the Post-doc, who knows where everything is, how to test every hypothesis, how to do every control that is needed, while teaching a bazillion students every week. There is a BN (before Nathalie) and an

AN (*anno* Nathalie) to describe the year you came to energize our lab. Pedrinho, you are probably the most unintentional funny person of all time and sometimes intentionally funny too. It's been great to work with you and watch you develop from a nervous kid to someone who can give a lecture about FACS. I'm proud of you and we'll always have Pisa. Also, have you made the sucrose? Thank you Raquel for always being inquisitive and ready to try new ideas and come up with models to show how things work, it's been inspiring. Bruno, the computer wizard, thanks for making my life easier using ones and zeroes and thanks for the great horror film recommendations. I would also like to thank former colleagues Pedro, Ana, Magda and James, miss you guys, and current members Helena and Trish. These were the people who first showed me how to perform experiments and to think critically and they have my eternal gratitude. I would also like to thank Ambre, Mário, Moritz, Andreia, Lúcia, Marta, Gonçalo, Rita, Joana, Denise and all former BCB and BCSP colleagues, with whom it's been a pleasure to work with. Special thanks to Teresa Baptista for making our lives in the lab much less stressful and therefore happier.

I would like to thank ITQB NOVA, which has been my home for the better part of the last decade. ITQB took me in fresh out of the University and has always provided everything I need for my scientific studies due to excellent work conditions. It's been an honour and a privilege to be part of this institute and while it is unlikely that I'll ever manage to give as much to ITQB as it has given

me, I've certainly tried (mostly by doing promotional videos). Of course none of this would be even possible without the financial support from Fundação para a Ciência e Tecnologia (FCT) and from the European Research Council (ERC), which I would also like to thank.

I'd also like to acknowledge the ITQB football crew, particularly Marcos, António, Carinhas, Bruno and Rui for contributing towards my weekly vent of accumulated frustration, which was fundamental during these years.

I would like to thank the friends who were closest to me during these years. Thank you Nathalie (partner) for making me happy every single day and for taking care of me, especially when I'm being difficult and obsessed with work. Thank you David, my n-duuude, can't even remember how my life was before you appeared in it, probably dull and not funny. Personal growth also meant coming to terms with the fact that you're better than me at every sport/activity that was ever invented, plus the ones which haven't been developed yet (VRball and Powerglove Tennis). I'll see you and Cátia in Kyoto for the best trip ever. Thank you Inês for being such a good friend and one of the few people who I know I can always count on. Thank you Matos the roommate for letting me stay at your home, where we could happily ignore each other most of the time with no hard feelings, and for being a true friend at every turn. Thank you Mónica for always listening and being supportive, even when

you're mad at me for not visiting. On the other hand I'm not the one who moved to the Swiss Alps. I would also like to thank my school buddies Rosa, André, Joaquim and Grifo, for all the great times during these years. Every time I need to explain my work to non-scientists it always goes through you guys first and you tell me I'm terrible every time. Perhaps one day I'll get this right.

I would like to say a final word for my family, particularly mom, dad and brother. Literally none of this would have been possible without you amazing people. At the end of the day, all that really matters is that you make the ones who you care about proud of you. I hope I've done that. Thank you for the genes and for the unconditional love and support.

**Table of Contents**

<b>Abbreviations and acronyms</b>	1
<b>Abstract</b>	5
<b>Resumo</b>	9
<b>Chapter I</b>	
<b>General Introduction</b>	13
Bacteria and us: an evolving relationship	15
The Bacterial Armour	27
The Division Machinery	41
Coordinating cell growth and peptidoglycan synthesis	52
References	59
<b>Chapter II</b>	
<b>Cell shape dynamics during the staphylococcal cell cycle</b>	77
Abstract	79
Introduction	80
Experimental Procedures	83
Results	103
<i>S. aureus</i> cells elongate during the cell cycle	99
The septum gives less than one hemisphere of each daughter cell	104
<i>S. aureus</i> grows by remodelling the entire cell surface	110
<i>S. aureus</i> enlarges via peptidoglycan synthesis and autolysis	112
Discussion	123
References	131

### Chapter III

<b>Recruitment of MurJ to the divisome directs peptidoglycan synthesis to the septum</b>	135
Abstract	137
Introduction	138
Experimental Procedures	141
Results	168
Localisation of peptidoglycan synthesis proteins during division	162
Order of arrival of peptidoglycan synthesis proteins to mid-cell	169
MurJ recruitment to the divisome triggers peptidoglycan incorporation at mid-cell	173
Discussion	185
References	188

### Chapter IV

<b>Building Bridges: the pentaglycine crosslinks in <i>S. aureus</i> peptidoglycan are required for cell integrity</b>	193
Abstract	195
Introduction	197
Experimental Procedures	202
Results and Discussion	219
The <i>femAB</i> operon is essential for the viability of <i>S. aureus</i>	213
Loss of FemAB activity leads to cellular lysis	216
Structure-based site directed mutagenesis of FemA	220
Concluding remarks	226
References	228

**Chapter V**

<b>Characterising the mode of action of novel small molecules effective against MRSA</b>	233
Abstract	236
Introduction	238
Experimental Procedures	241
Results	256
PC190723 prevents correct Z ring placement	249
DNAC-1 impairs cell wall synthesis in MRSA	253
DNAC-1 causes mislocalisation of PBP2/4 and FtsZ	256
DNAC-1 disrupts the bacterial membrane	259
Discussion	262
References	268

**Chapter VI**

<b>General Discussion and Conclusions</b>	273
New approaches to study an old foe	274
Dynamics of septum reshaping in <i>S. aureus</i>	278
One peptidoglycan synthesis machinery - two locations	280
Peptidoglycan crossbridges as targets for drug design	286
Mode of action of antibiotics and drug synergy	290
Final Remarks	296
References	298
<b><i>Curriculum Vitae</i></b>	303

## *Table of Contents*



## Abbreviations and acronyms

---

<i>AFM</i>	<i>Atomic Force Microscopy</i>
<i>Amp</i>	<i>Ampicillin</i>
<i>ANOVA</i>	<i>Analysis of Variance</i>
<i>bp</i>	<i>DNA base pairs</i>
<i>CA-MRSA</i>	<i>Community-associated MRSA</i>
<i>CCCP</i>	<i>Carbonyl cyanide m-chlorophenyl hydrazone</i>
<i>CET</i>	<i>Cryo-electron Tomography</i>
<i>CFP</i>	<i>Cyan Fluorescent Protein</i>
<i>CFU</i>	<i>Colony Forming Unit</i>
<i>Cm</i>	<i>Chloramphenicol</i>
<i>CRE</i>	<i>Carbapenem-resistant Enterobacteriaceae</i>
<i>CWSS</i>	<i>Cell Wall Stress Stimulon</i>
<i>dcw</i>	<i>Division and cell wall cluster</i>
<i>D-cyc</i>	<i>D-cycloserine</i>
<i>DIC</i>	<i>Differential Interference Contrast</i>
<i>DMPI</i>	<i>3-{1-[(2,3-Dimethylphenyl)methyl]piperidin-4-yl}-1-methyl-2-pyridin-4-yl-1H-indole</i>
<i>DMSO</i>	<i>Dimethyl Sulfoxide</i>
<i>ECDC</i>	<i>European Centre for Disease Control</i>
<i>EMCCD</i>	<i>Electron Multiplying Charge Coupled Device</i>
<i>Ery</i>	<i>Erythromycin</i>
<i>ESTK</i>	<i>Eukaryotic-like serine/threonine kinase</i>
<i>FDA</i>	<i>Food and Drug Administration</i>
<i>FDAA</i>	<i>Fluorescent D-amino acid</i>

---

## *Abbreviations and acronyms*

---

<i>FR</i>	<i>Fluorescence Ratio</i>
<i>GFP</i>	<i>Green Fluorescent Protein</i>
<i>GlcNAc</i>	<i>N-acetylglucosamine</i>
<i>HADA</i>	<i>Hydroxycoumarin-amino-D-alanine</i>
<i>HALA</i>	<i>Hydroxycoumarin-amino-L-alanine</i>
<i>HA-MRSA</i>	<i>Hospital-associated MRSA</i>
<i>HPLC</i>	<i>High-performance liquid chromatography</i>
<i>IPTG</i>	<i>Isopropyl <math>\beta</math>-D-1-thiogalactopyranoside</i>
<i>Kan</i>	<i>Kanamycin</i>
<i>LA</i>	<i>Luria-Bertani agar</i>
<i>LB</i>	<i>Luria-Bertani broth</i>
<i>LCA</i>	<i>Last Common Ancestor</i>
<i>mCh</i>	<i>mCherry fluorescent protein</i>
<i>MHC</i>	<i>Mueller-Hinton cation adjusted medium</i>
<i>MIC</i>	<i>Minimum Inhibitory Concentration</i>
<i>MOA</i>	<i>Mode of action (of an antibiotic)</i>
<i>MOP</i>	<i>Multidrug/oligosaccharidyl-lipid/polysaccharide protein</i>
<i>MRSA</i>	<i>Methicillin-resistant Staphylococcus aureus</i>
<i>MSSA</i>	<i>Methicillin-susceptible Staphylococcus aureus</i>
<i>MurNAc</i>	<i>N-acetylmuramic acid</i>
<i>NADA</i>	<i>Nitrobenzofurazan-amino-D-alanine</i>
<i>NMR</i>	<i>Nuclear Magnetic Resonance</i>
<i>NR</i>	<i>Nile Red</i>
<i>NRPS</i>	<i>Nonribosomal peptide synthetase</i>
<i>OD</i>	<i>Optical Density</i>
<i>Oxa</i>	<i>Oxacillin</i>
<i>P1</i>	<i>Phase 1 of the S. aureus cell cycle</i>

---

---

<i>P2</i>	<i>Phase 2 of the S. aureus cell cycle</i>
<i>P3</i>	<i>Phase 3 of the S. aureus cell cycle</i>
<i>PALM</i>	<i>Photo-activated Localisation Microscopy</i>
<i>PBP</i>	<i>Penicillin-binding Protein</i>
<i>PBS</i>	<i>Phosphate Buffer Saline</i>
<i>PCC</i>	<i>Pearson's Correlation Coefficient</i>
<i>PG</i>	<i>Peptidoglycan</i>
<i>PMF</i>	<i>Proton Motive Force</i>
<i>PMSF</i>	<i>Phenylmethylsulfonyl fluoride</i>
<i>PSSM</i>	<i>Position-specific Scoring Matrix</i>
<i>RBS</i>	<i>Ribosome Binding Site</i>
<i>SCCmec</i>	<i>Staphylococcal cassette chromosome mec</i>
<i>SDS-PAGE</i>	<i>Sodium dodecyl sulfate polyacrylamide gel electrophoresis</i>
<i>SEDS</i>	<i>Shape, elongation, division and sporulation protein</i>
<i>SEM</i>	<i>Scanning Electron Microscopy</i>
<i>sGFP</i>	<i>Superfast-folding GFP</i>
<i>SIM</i>	<i>Super-resolution Structured Illumination Microscopy</i>
<i>TEM</i>	<i>Transmission Electron Microscopy</i>
<i>TG</i>	<i>Transglycosylation</i>
<i>TGase</i>	<i>Transglycosylase</i>
<i>TIRF</i>	<i>Total Internal Reflection Fluorescence</i>
<i>TP</i>	<i>Transpeptidation</i>
<i>TPase</i>	<i>Transpeptidase</i>
<i>tRNA</i>	<i>Transfer RNA</i>
<i>TSA</i>	<i>Tryptic soy agar</i>
<i>TSB</i>	<i>Tryptic soy broth</i>
<i>Tun</i>	<i>Tunicamycin</i>

---

*Abbreviations and acronyms*

---

<i>UDP</i>	<i>Uridine Diphosphate</i>
<i>UV</i>	<i>Ultraviolet</i>
<i>Van</i>	<i>Vancomycin</i>
<i>VISA</i>	<i>Vancomycin-intermediate S. aureus</i>
<i>VRE</i>	<i>Vancomycin-resistant Enterococci</i>
<i>VRSA</i>	<i>Vancomycin-resistant S. aureus</i>
<i>WGA</i>	<i>Wheat Germ Agglutinin</i>
<i>WTA</i>	<i>Wall Teichoic Acid</i>
<i>X-Gal</i>	<i>5-bromo-4-chloro-3-indolyl-<math>\beta</math>-D-galactopyranoside</i>
<i>YFP</i>	<i>Yellow Fluorescent Protein</i>

---

## Abstract

The emergence and spread of antibiotic resistance in bacteria constitutes one of the major challenges to global public health and is predicted to further escalate during the 21<sup>st</sup> century. One of the most frequent multi-drug resistant pathogens is methicillin-resistant *Staphylococcus aureus* (MRSA), a gram-positive coccoid bacterium that causes difficult to treat infections with severe morbidity and mortality rates. Many of the commonly used antibiotics target steps in the biosynthesis of peptidoglycan (PG), a robust but flexible mesh-like macromolecule that withstands the intense internal turgor in the cell, among other functions. The integrity of the PG layer is of the utmost importance to bacteria, which must ensure that incorporation of new PG strands and remodelling of the existing ones is timely coordinated with the progression of the cell cycle. Despite its clinical relevance, many fundamental biological processes in *S. aureus* remain to be elucidated.

In this thesis we have used Super-Resolution Structured Illumination Microscopy (SIM) to show that *S. aureus* cells grow continuously during the entire cell cycle and undergo slight elongation. Cell growth is accompanied by PG synthesis, which occurs all around the periphery of the cells before the initiation of septum synthesis and strikingly shifts almost exclusively to mid-cell in preparation for division. Intrigued by the timely shift of peripheral

## *Abstract*

to septal PG incorporation, we decided to investigate the molecular mechanism mediating this transition. We studied the localisation of most proteins known to be involved in PG synthesis in *S. aureus* and determined that the putative PG precursor flippase MurJ localised to the septum in a manner dependent on the presence of divisome components DivIB, DivIC and FtsL, and that MurJ recruitment was required for septal PG incorporation. Inhibiting MurJ activity prevented PG incorporation both at the periphery and at mid-cell and affected the initiation of septum synthesis. Our data indicates that timely recruitment of MurJ to the divisome constitutes a novel mechanism which prokaryotes use to incorporate PG at two locations in the cell in the absence of an elongation machinery

We concluded our characterisation of the *S. aureus* cell cycle by investigating the dynamics of the process of reshaping the flat division septum into a curved surface (popping), following daughter cell splitting. We determined that this process occurs in less than 2 milliseconds and is dependent of both autolysin activity and internal turgor pressure. After splitting, the flat septum generated a curved surface which occupied approximately 40% of the cell surface and this proportion did not change with the progression of the cell cycle. This indicates that the new wall material coming from the septum of the mother cell is not selectively remodelled during the cell cycle.

In an effort to identify new targets which could be useful for pathogen specific drug design, we studied the Fem family of

transferases, which build the characteristic pentaglycine crossbridges present in the PG of *S. aureus*. Depletion of *femAB* expression in the background of community-associated MRSA (CA-MRSA) strain MW2 was lethal and caused cells to appear as pseudomulticellular forms that lysed due to extensive membrane damage, indicating that pentaglycine crossbridges are required to withstand internal turgor. Mutation of residues K180 and R181 of FemA, located in the  $\alpha 6$  helix, predicted to be involved in binding of tRNA, led to a severe decrease in FemA activity, indicating that the  $\alpha 6$  helix of FemA is important for protein activity and could be a good target for drug design.

A second approach to contribute to antibiotic development consisted on investigating the modes of action (MOA) of novel small molecules PC190732 and DNAC-1 using cell biology tools. We found that PC190732 caused delocalisation of *S. aureus* FtsZ away from the mid-cell, which in turn led to the concomitant delocalisation of PBP2, indicating that PC190732 caused cell death by interfering with divisome assembly and septal PG synthesis. In contrast, DNAC-1 led to rapid permeabilisation of the cell membrane, loss of membrane potential and consequent delocalisation of membrane-associated proteins FtsZ, PBP2 and PBP4.

This dissertation aimed to understand how PG synthesis is coordinated with the progression of the cell cycle in a clinically relevant pathogen, and to use this knowledge to contribute towards antibiotic research.

*Abstract*



## Resumo

A resistência a antibióticos em bactérias constitui um dos maiores desafios à saúde pública mundial na actualidade, e prevê-se que a situação vá piorar significativamente durante o Séc. XXI. Um dos grandes factores de risco são estirpes da bactéria Gram-positiva *Staphylococcus aureus* resistentes à meticilina (MRSA), que causam infecções hospitalares de difícil tratamento e com elevadas taxas de mortalidade. Muitos dos antibióticos de uso comum têm como alvo passos da síntese do peptidoglicano (PG), uma macromolécula robusta e flexível que suporta a elevada pressão interna na célula, entre outras funções. A integridade da camada de PG é de extrema importância para a bactéria, pelo que os processos de incorporação de novas cadeias de PG e de remodelação das cadeias existentes têm de ser coordenados de modo preciso com o ciclo celular. Apesar da relevância clínica de *S. aureus*, muitos dos processos biológicos fundamentais ainda não foram elucidados nesta bactéria.

Nesta dissertação utilizámos microscopia de superresolução (SIM) para mostrar que as células de *S. aureus* aumentam de volume durante todo o ciclo celular e alongam ligeiramente. Este crescimento celular é acompanhado de síntese de PG, que ocorre homogeneamente em toda a superfície da célula antes do início da síntese do septo, mas que surpreendentemente transita quase exclusivamente para o meio da célula, em preparação para a divisão

celular. Para investigar o mecanismo molecular subjacente a esta transição, estudámos a localização da maioria das proteínas envolvidas na síntese de PG em *S. aureus*. Verificámos que a localização no septo da proteína MurJ, a possível translocase dos precursores do PG, depende da presença dos componentes do divisoma DivIB, DivIC, FtsL, e que o seu recrutamento é necessário para a incorporação de PG no septo. Para confirmar esta hipótese usámos um inibidor de MurJ e verificámos que a incorporação de PG tanto na periferia da célula como no centro foi drasticamente reduzida, e que tal preveniu o início da síntese do septo. Os nossos estudos indicam que o recrutamento da MurJ para o divisoma constitui um novo mecanismo pelo qual procariotas inserem novo PG em duas localizações distintas da célula, quando não possuem uma maquinaria de alongação.

Concluimos a nossa caracterização do ciclo celular de *S. aureus* ao investigar a dinâmica do processo de remodelação do septo plano para uma superfície curva, que ocorre imediatamente após a separação das células-filhas. Este é um processo extremamente rápido, que ocorre em menos de 2 milisegundos, e que depende tanto de actividade enzimática de hidrólases do PG como de pressão osmótica interna na célula. Após a separação das células-filhas, a remodelação do septo gera uma superfície curva que ocupa aproximadamente 40% da superfície total da célula. Surpreendentemente, esta proporção não sofre alterações durante o ciclo celular, indicando que, ao contrário do que se pensava até à data, o

septo da célula-mãe não é selectivamente remodelado durante o ciclo celular.

De modo a identificar novos alvos moleculares que possam ser explorados no desenvolvimento de antibióticos específicos contra *S. aureus*, decidimos estudar as proteínas Fem, transferases que sintetizam as pontes de pentaglicinas características do PG de *S. aureus*. A redução da expressão de *femAB* na estirpe MW2, uma estirpe MRSA isolada na comunidade (CA-MRSA), resultou em células pseudo-multicelulares e na conseqüente lise celular devido a ruptura da membrana, o que indica que as pontes de pentaglicinas são necessárias para o PG suportar a pressão osmótica interna da célula. A mutação dos aminoácidos K180 e R181, contidos na hélice  $\alpha 6$  da FemA, levaram a uma diminuição acentuada da actividade da proteína, o que sugere que esta região é importante para actividade e que pode constituir um bom alvo para o desenvolvimento de antibióticos contra *S. aureus*.

De modo a contribuir para o desenvolvimento de antibióticos, investigámos o mecanismo de acção (MOA) em *S. aureus* de duas novas moléculas – o PC190732 e o DNAC-1 – através de técnicas de biologia celular. Observámos que o PC190732 causou a deslocalização de FtsZ para fora do septo, com concomitante deslocalização de PBP2, o que indica que o PC190732 leva à morte celular por interferir com a síntese de PG no septo. Em contraste, o DNAC-1 levou à rápida permeabilização da membrana celular, dissipação do potencial

## *Resumo*

de membrana e consequente deslocalização da FtsZ, PBP2 e PBP4, proteínas associadas à membrana.

Esta dissertação teve como objectivo determinar como é que a síntese de PG é coordenada com o ciclo celular de uma bactéria de importância clínica e usar esse conhecimento para contribuir para a investigação de antibióticos.

# Chapter I

---

## General Introduction



## **Bacteria and us: an evolving relationship**

To study bacteria is to study Life itself. It is the journey of how life appeared in our planet and how it thrives under the most extreme of circumstances. It is to realize that Nature will always find a way to improvise, to adapt and to overcome any challenge. It is to witness the constant struggle of organisms, competing and cooperating with each other, screaming for their right to exist.

Modern bacteria descend directly from unicellular microorganisms that were the first lifeforms to appear on Earth and were the dominant species for about 3 billion years thereafter<sup>1,2</sup>. Bacteria have spent this time evolving diverse metabolic pathways that allow the use of a wide range of energy sources. Hence bacteria can survive in virtually every ecological niche, from the deepest ocean bed<sup>3</sup> to the highest mountain peaks<sup>4</sup>, from ice-cold marine environments<sup>5</sup> to volcanic springs and hydrothermal vents<sup>6</sup>. Some bacteria produce spores that are resistant to cosmic rays and UV radiation<sup>7</sup>, leading scientists to speculate that spores could withstand interstellar travel and, in turn, that life on Earth has been seeded by meteorites carrying microorganisms (Panspermia). Others form vast photosynthetic blankets over the oceans and have single-handedly caused the oxygenation of the Earth's atmosphere and the consequential mass extinction of most anaerobic species at the time. Some bacteria live inside other bacteria, which themselves colonise an animal host, the three organisms thriving in a symbiotic circle<sup>8</sup>.

The Microbiome

All higher order multicellular organisms studied to date, from plants to animals including humans are complex ecological environments inhabited by thousands of prokaryotic species, along with other microorganisms, the so called microbiome<sup>9</sup>. Microorganisms that establish commensal or mutualistic relationships with the host are collectively described as microflora and often constitute an important part of the host's metabolism. The gut flora in particular is known to provide protection against pathogenic species<sup>10</sup>, to indirectly stimulate the development of the immune system<sup>11</sup> and to break down complex metabolites using enzymes the host lacks<sup>12</sup>. Accordingly, sudden changes in microbiota composition have been implicated with numerous health afflictions, from cardiovascular disease<sup>13</sup> to type 2 diabetes<sup>14</sup>. Exciting new avenues of microbial research have been exploring the notion that the composition of intestinal microbiota might influence cerebral development and social behaviour<sup>15,16</sup>. Although the long-standing myth that there are ten times more microbial cells than human cells in our bodies has been recently debunked, current estimates still predict that microbes outnumber our own cells<sup>17</sup>. This has prompted many scholars and lay media outlets to enthusiastically propose that we are more bacterial than human, or that bacteria are in control of our brains, a hyperbolic argument that undermines the complexities of interspecies relationships. Instead, perhaps the definition of what is self and what is foreign needs to be revised, taking into consideration



that in reality the human body functions as an association of eukaryotic and prokaryotic cells.

### The Eternal War

The concept of “good bacteria”, the usage of bacterial supplements for direct consumption (probiotics), or medical therapies based on using bacteria are ideas that only started to gain significant traction in public knowledge towards the tail end of the 20<sup>th</sup> century. Bacterial infections are traditionally regarded as some of the worst public health challenges Mankind has faced. Some infectious diseases such as the plague, caused by *Yersinia pestis*, have historically appeared in waves of epidemics, with the 14<sup>th</sup> century wave (Black Plague) claiming two thirds of the European population at the time. Other infectious diseases such as tuberculosis or cholera, caused by *Mycobacterium* spp. and *Vibrio cholera*, respectively, have constantly existed since antiquity<sup>18</sup> and are far from being eradicated from the modern world.

Serious bacterial infections were typically a death sentence until Alexander Fleming’s discovery of penicillin in a mouldy Petri dish in 1928<sup>19</sup>. Penicillin was one of the first discovered antibiotics and considered a miracle drug at the time, effective against a wide range of bacterial infections and easily tolerated by patients. Penicillin is part of a family of molecules called  $\beta$ -lactams, which target the aptly named penicillin-binding proteins (PBPs), enzymes involved in bacterial wall synthesis. Following a large push to

overcome the limitations associated with mass producing the drug, it was readily deployed to the Allied frontlines during World War II to treat infections in wounded soldiers<sup>20</sup>. Penicillin usage became widespread in clinical practices and soon thereafter, bacterial strains resistant to penicillin started to appear. What follows can be described as an arms race between humans and bacteria: new drugs have sequentially been developed to deal with resistant strains and as soon as they are introduced, bacteria develop resistance against them, prompting the need for new drugs. This cycle propagated throughout the 20<sup>th</sup> century and the situation has escalated to a point in which the so called “superbugs”, bacteria resistant to several classes of antibiotics, have emerged<sup>21-24</sup>. Superbugs are poised to become the most serious public health challenge that Humanity will face in the 21<sup>st</sup> century, threatening to take us back to a pre-penicillin dark age of medicine<sup>25</sup>.

### *Staphylococcus aureus* in the Age of Antibiotic Resistance

One of the higher risk superbugs is the Gram-positive human pathogen *Staphylococcus aureus*, which is the focus of this dissertation. *S. aureus* are small (~1 µm) non-motile coccoid Firmicutes which form golden (Latin *aureus*) colonies when cultivated in blood plates and appear as grape-like clusters when observed under the microscope. These bacteria are usually part of the human microbiota, colonising the skin and the nasopharynx asymptotically in about as much as a third of the human population<sup>26,27</sup>. When the skin or mucosal

protective layers are breached, *S. aureus* is capable of causing a wide range of infections, from skin and soft tissue infections to pneumonia, septicaemia, infective endocarditis and osteomyelitis<sup>28</sup>. Transmission is usually through skin-to-skin contact between carriers or through contact with contaminated objects or surfaces<sup>29-32</sup>. *S. aureus* is primarily a threat in healthcare settings, where it affects immunocompromised individuals or debilitated patients recovering from surgery<sup>32</sup>.

Antibiotic resistance in *S. aureus* has been eloquently described as a process that occurs in waves<sup>21</sup>. The first wave of resistant strains in the 1940s expressed a plasmid-encoded  $\beta$ -lactamase, capable of degrading the  $\beta$ -lactam penicillin, thus rendering it inactive<sup>33,34</sup>. To counter this, methicillin, a semisynthetic derivative of penicillin that binds PBPs but is insensitive to  $\beta$ -lactamase, was developed in 1959<sup>35</sup>. The emergence of methicillin resistant *S. aureus* strains (MRSA) marked the second wave of resistance<sup>21</sup>. MRSA strains acquired the resistance determinant *mecA*, contained in an exogenous DNA mobile element designated SCC*mec* (staphylococcal cassette chromosome *mec*), which was inserted in the genome<sup>36-39</sup>. *mecA* is proposed to have originated from *Staphylococcus sciuri* through horizontal gene transfer, due to the presence of a *mecA* evolutionary ancestor in all isolates of this species<sup>40</sup>. It encodes for PBP2A, an enzyme that has low affinity for  $\beta$ -lactams and thus is still active in the presence of these antibiotics<sup>41,42</sup>. This mechanism of resistance then confers high level resistance to all classes of  $\beta$ -lactams

(penicillins, cephalosporins, carbapenems). Adjacent to *mecA* in the SCC<sub>*mec*</sub> are *mecR1*, encoding a membrane signal transduction protein and *mecI*, a transcriptional regulator. These genetic elements ensure that *mecA* expression is usually repressed<sup>43</sup>. However, heavy methicillin (mis)usage in the 1970s has created selective pressure that resulted in isolates that have mutations in the *mecA* or *mecI* promoter regions, which loosened the control over *mecA* expression<sup>44</sup>. These strains with permissive PBP2A expression thus constitute the ongoing third wave of MRSA<sup>21</sup>.

In spite of the development of several generations of new antibiotics, infections by MRSA have reached global epidemic proportions. MRSA now represents >60% of nosocomial isolates of *S. aureus* in a variety of countries<sup>45</sup> and carriage of hospital-acquired MRSA (HA-MRSA) is endemic among hospitalized patients<sup>22,46</sup>. The 2016 surveillance atlas from the European Centre for Disease Control (ECDC) reports that the proportion of isolates resistant to methicillin in staphylococcal infections sits above 20% in 10 out of 30 European countries analysed. MRSA prevalence is particularly high in Southern and Eastern European countries, for example in Portugal approximately 44% of isolates are MRSA strains (Fig. 1).

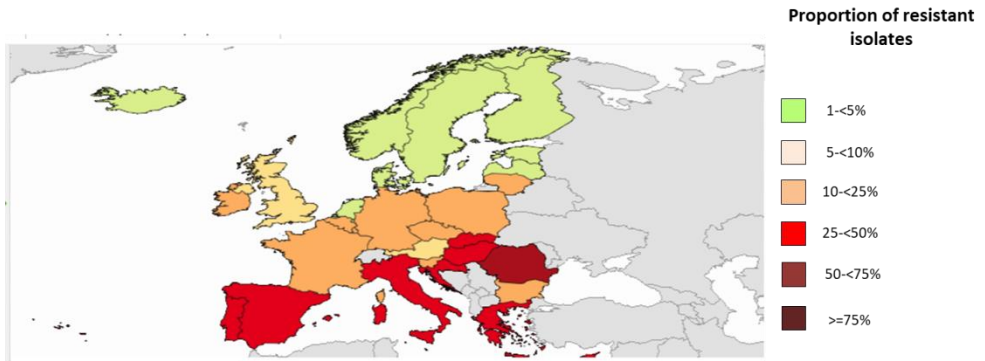


**Figure 1. MRSA prevalence in Europe in 2016.** Surveillance Atlas for infectious diseases of the European Centre for Disease Control, showing the proportion of methicillin resistant *S. aureus* (MRSA) isolates found in bloodstream infections reported in Europe in 2016. The prevalence of MRSA is particularly high in Southern and Eastern Europe. Adapted from <http://atlas.ecdc.europa.eu>.

Usually confined to healthcare settings, MRSA infections have started to emerge in communities during the late 90s. These community-acquired MRSA strains (CA-MRSA) constitute the 4<sup>th</sup> wave of *S. aureus* resistance and have been reported in the US, Canada, Asia, South America and Europe<sup>47-50</sup>. Contrasting with HA-MRSA, CA-MRSA strains can infect otherwise healthy individuals without predisposing risk factors. CA-MRSA strains constitute a major public health concern in the US in particular, where the vast majority of infections are caused by a clone known as pulse-field type USA300<sup>51</sup>. USA300 is an extremely virulent strain, infamous for causing life-threatening infections that progress unusually rapidly

and spread from host-to-host with ease, even when compared to other MRSA strains<sup>49,52,53</sup>.

Traditionally, MRSA strains are reliably susceptible to the glycopeptide vancomycin<sup>54</sup>. Vancomycin is an inhibitor of cell wall synthesis which is extracted from soil prokaryote *Amycolaptosis orientalis* and that started being commercialized *ca.* 1954<sup>55</sup>. Vancomycin therapy was typically a last resort measure against difficult to treat MRSA infections, mainly because vancomycin is significantly nephrotoxic, but also due to increased awareness of how bacteria acquire resistance<sup>54</sup>. Nevertheless, the increasing spread of MRSA demanded an over-reliance on vancomycin use and unsurprisingly, the turn of the century witnessed the emergence of vancomycin intermediate (VISA) and vancomycin resistant (VRSA) *S. aureus* strains<sup>56,57</sup>. As of today, *S. aureus* has managed to evolve resistance to virtually every sophisticated antibiotic that has been developed against it, including protein synthesis inhibitors such as minocycline<sup>58</sup> and linezolid<sup>59</sup> or the potent membrane depolarization effect of daptomycin<sup>60</sup>. Resistance mechanisms are often quite inventive too, for example in order to avoid exposure to daptomycin, resistant *S. aureus* strains have evolved to release phospholipids that sequester this antibiotic, preventing it from reaching the bacterial membrane, where it is active<sup>61</sup>. The extraordinary ability of this species to overcome every challenge it has been presented with is truly a testament to Nature's adaptability.

An exciting recent report by Ling and colleagues<sup>62</sup> describes a new natural antibiotic, teixobactin, an inhibitor of cell wall synthesis with exceptional activity against several Gram-positive pathogens. Importantly, serial passages of both *S. aureus* and *M. tuberculosis* strains in the presence of low dosage teixobactin, a method commonly used to simulate acquisition of resistance through selective pressure, failed to produce resistant mutants<sup>62</sup>. It is possible that teixobactin is part of a family of undiscovered natural products which have evolved to minimize resistance development by target microorganisms and their introduction into the clinic could be an important, even definitive, step in the struggle against superbugs. Yet the lessons learned from the 20<sup>th</sup> century antibiotic development/resistance acquisition cycles mandate a cautious optimism, as bacteria have proven time and time again that they will have a say.

### The State of Antibiotic Development

Most antibiotics in current clinical use were discovered in the 50s, known as the Golden Age of antibiotic discovery, and have since lost patent protection which equates to now being sold as low-cost generics. Thus, large pharmaceutical companies now channel their resources towards the development of cancer and chronic disease therapies, which provide tremendous financial returns<sup>63,64</sup>. Development of new drugs used to treat infections is mostly handled by start-up small biotechnology companies nowadays and following

the drug development cycle and introduction to the market, sales of new molecules often severely underperform<sup>64</sup>. Examples of recent drugs in the market are fidaxomicin, a highly potent antibiotic specific for the treatment of *Clostridium difficile* infections<sup>65</sup>, or glycopeptides oritavancin/telavancin, which were specifically developed to treat serious MRSA infections<sup>66</sup>. Yet despite the advantages in patient treatment provided by these new drugs, the reality is that in the market they compete directly with generic vancomycin and daptomycin, which are much more affordable, and so remain the preferential treatment<sup>64</sup>. Moreover, new drugs have to be used only as a last resort, in order to ensure that they will still be efficient when the common therapies fail, as was the case when vancomycin was introduced. These restrictions, while logical and necessary, severely harm sales of new antibiotics which in turn decrease the push to invest in new solutions.

An avenue of drug development that is considerably more marketable is towards synergistic therapy, where a new molecule is commercialized as an adjuvant in combination with an existing antibiotic. A prime example of those is the  $\beta$ -lactam/ $\beta$ -lactamase inhibitor combination therapies, of which the amoxicillin/clavulanic acid combination (Clavamox, Augmentin) remains the golden standard. The recent emergence of *Klebsiella pneumoniae* strains resistant to these treatments (carbapenem-resistant Enterobacteriaceae or CRE) has spurred on efforts to find new treatment combinations. A promising solution for the coming CRE



scourge is a combination of new  $\beta$ -lactam, relebactam, with the old imipenem plus  $\beta$ -lactamase inhibitor cilastatin, which is being developed by Merck, Inc. and is currently in Phase 3 clinical trials<sup>67</sup>. Other antibiotic classes which have been used for many decades but have seen a significant push in development recently are **i)** macrolides, protein synthesis inhibitors, most which are derivatives of “old” drug erythromycin that achieve high tissue penetration and thus are effective at treating intracellular infections<sup>68</sup>; **ii)** fluoroquinolones, that inhibit DNA gyrase and topoisomerase IV, of which Zabofoxacin (Dong Wha Pharmaceutical Co. Lda.) is currently in Phase 3 and showing high activity against upper respiratory tract infections (*S. aureus*, *Streptococcus pneumoniae*, *Moraxella catarrhalis*)<sup>69</sup>; **iii)** oxazolidinones, protein synthesis inhibitors, such as MRX-1 (MicuRx Pharmaceuticals, Phase 2) which is being developed primarily as a response to the emergence of vancomycin-resistant enterococci (VRE) but also works well against MRSA<sup>70</sup>. Another class of antibiotics that has only recently started being considered for therapy are the defensin mimetics. Defensins are small antibacterial peptides that form part of the innate immunity in animals and plants. Because defensins are small molecules, synthesizing them *in vitro* is a fairly simple process; unfortunately the first attempts to produce defensin mimetics led to molecules with low potency and stability<sup>64</sup>. The hopes for defensins as viable treatment options now rest with brilacidin (Polymedix), a defensin-mimetic designed to mimic the amphiphilic properties of antimicrobial peptides<sup>71</sup>. Brilacidin is

currently in Phase 2 trials and showing high activity against MRSA, while analogs with enhanced specificity towards Gram-negative superbugs are in concurrent development<sup>71</sup>.

Besides the aforementioned teixobactin breakthrough, no other new classes of antibiotics have been discovered in the past 50 years, and antibiotic resistance is evolving faster than the arrival of new drugs into clinical practice<sup>62</sup>. There is a clear urgent need for continued antibiotic development and the more solutions, the better.

## The Bacterial Armour

Survival of most bacteria depends on their ability to build a robust cell wall that can interface with the external *milieu*. Therefore it comes as no surprise that the vast majority of natural or synthesized antibiotic classes target the bacterial wall. The cell wall composes the thick outermost layer of the cell in Gram-positive bacteria (excluding encapsulated species) or sits underneath the outer membrane in Gram-negatives<sup>72,73</sup>. In both types of prokaryotes, the scaffold of the cell wall is the cross-linked polymer peptidoglycan (PG), also known as murein. PG is a mesh-like structure that can be up to 20-40 nm in thickness in Gram-positives<sup>74</sup>. The cell is under constant osmotic stress due to high internal pressure, which is sustained by the long glycan strands of peptidoglycan, crosslinked to each other through flexible peptide bridges. This generates a robust but elastic structure that prevents the protoplast from lysing<sup>75</sup>. In most Gram-positive bacteria, the cell wall envelope is also composed of polysaccharides, teichoic acids and proteins that are covalently linked or immobilized to PG<sup>76</sup>.

### Peptidoglycan Structure

The basic architecture of PG is remarkably well conserved in Eubacteria. Glycan strands are composed of alternating 1,4-linked N-acetylglucosamine (GlcNAc) and N-acetylmuramic acid (MurNAc) disaccharides. Glycan length can range from 6 disaccharide units in *S. aureus*<sup>77</sup> to 20-50 units in *Escherichia coli* or *Bacillus subtilis*<sup>75,78</sup>. Attached

to the carboxyl group of the MurNAc residue is a chain of amino acids commonly known as stem peptide, whose length and composition varies considerably between bacterial species<sup>79</sup>. Stem peptides are typically composed of L- and D- amino acids and one dibasic amino acid in the third position of the chain. This amino acid is either L-lysine, which is found in most Gram-positive species including *S. aureus* (Fig. 2A); or *meso*-diaminopimelic acid, found in most Gram-negative bacteria and some Gram-positives, such as *B. subtilis*<sup>79,80</sup>. One disaccharide unit containing a stem peptide is commonly known as a muropeptide (Fig. 2A).

Another structural feature of PG is the presence of crosslinks, which are peptidic connections between glycan strands. Crosslinks can be done directly from the D-alanine moiety in the fourth position of the stem peptide to the *meso*-diaminopimelic acid of another muropeptide, as is observed in *E.coli* and *B.subtilis* PG<sup>72,79</sup>. Alternatively muropeptides can be cross-linked via peptide bridges (crossbridges) that show significant interspecies variation. For instance, Gram-positive bacteria *Weissella viridescens* and *Enterococcus faecalis* build crossbridges composed of D-alanine<sup>81</sup> or D-alanine-D-alanine<sup>82</sup>, respectively, while *S. pneumoniae* can alternate between L-alanine-L-alanine and L-alanine-L-serine crossbridges or do direct crosslinking of glycans<sup>83</sup>. In contrast, *S. aureus* crosslinks its PG using pentaglycine bridges between the D-alanine in the fourth position of a muropeptide and the L-lysine in the third position of another (Fig. 2B). This unique feature likely confers high structural flexibility to the

whole PG macromolecule, which possibly allows for the high degree of crosslinking (up to 90%) that has been observed in *S. aureus* strains<sup>84,85</sup>.

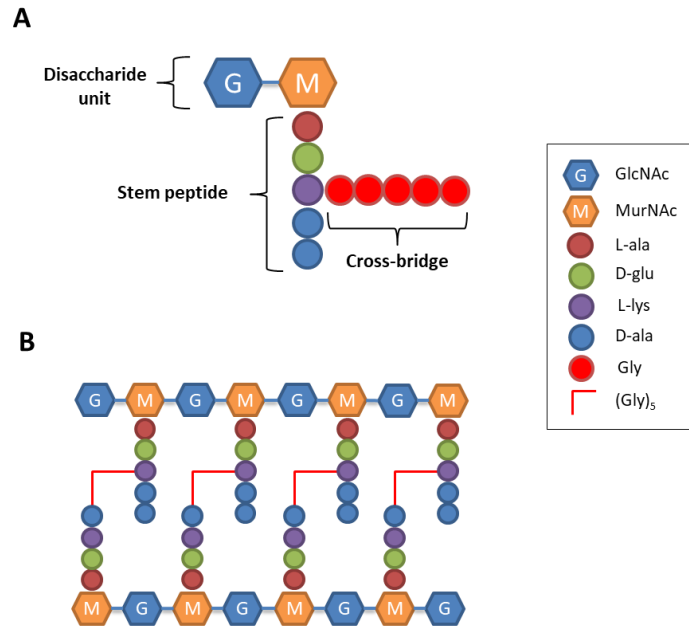


**Figure 2. Structure of *Staphylococcus aureus* peptidoglycan.** (A), A muropeptide of *S. aureus* PG consists of a GlcNAc-MurNac disaccharide with a five amino acid stem peptide linked to MurNac and a pentaglycine crossbridge connected to L-lysine. (B), Crosslinking of glycan strands in PG, using pentaglycine bridges, is done between the D-ala in the fourth position of the stem peptide of the first muropeptide and the L-lysine in the second muropeptide.

One of the most complex unsolved challenges in biochemistry pertains to the spatial structure of peptidoglycan, which likely varies from bacteria to bacteria, even among ones that possess identical PG chemical compositions<sup>86</sup>. The two main models proposed for the organization of PG are the layered<sup>87,88</sup> and the scaffold<sup>89,90</sup> (hedgehog)

models, which differ on the orientation of PG growth in respect to the membrane. The former depicts layers of PG growing parallel to the membrane, while the latter states that glycan strands grow outward from the membrane and orthogonal to it. In Gram-negative species the scaffold model does not seem compatible with the architecture of PG, because vertical alignment of the long glycan chains (average 30 disaccharide units) would far exceed the maximum sacculus thickness measured to date (7 nm)<sup>89,91</sup>. Accordingly, cryo-electron tomography (CET) observations in *Caulobacter crescentus* revealed loosely packed and disordered PG sheets running in parallel to the bacterial membrane, favouring the layered model<sup>92</sup>. More recently, Turner and colleagues<sup>93</sup> used atomic force microscopy (AFM) to probe a variety of Gram-negative species and found large pore structures distributed randomly in the sacculus, also consistent with a loose configuration. As mentioned above, glycan chain length is quite small in *S. aureus* (average 6 disaccharide units). Therefore it has been suggested that the vertical alignment of highly crosslinked PG would be more resistant to mechanical stress than short layers aligned along the membrane, favouring the scaffold model<sup>89</sup>. However, a recent approach to this problem by Kim *et al.*<sup>94</sup>, using solid-state NMR, revealed a surprisingly ordered and densely packed structure with parallel orientation to the membrane, as predicted in the layered model. Interestingly, the authors also characterized PG from *E. faecalis*, which has a (L-Ala)<sub>3</sub> crossbridge structure, as well as *S. aureus*

mutants with shortened crossbridges and could conclude that bridge length is likely a key determinant in the spatial organization of PG<sup>94,95</sup>.

### Building the Wall - Overview

Peptidoglycan biosynthesis is a multi-enzymatic pathway that spans three compartments of the bacterial cell: the cytoplasm, the inner and the outer leaflets of the bacterial membrane, as depicted in Fig. 3. A detailed description of this pathway will be given in the following sections. As mentioned above, most of the known antibiotics target specific steps in this pathway; brief descriptions of their molecular targets will be given, when applicable.

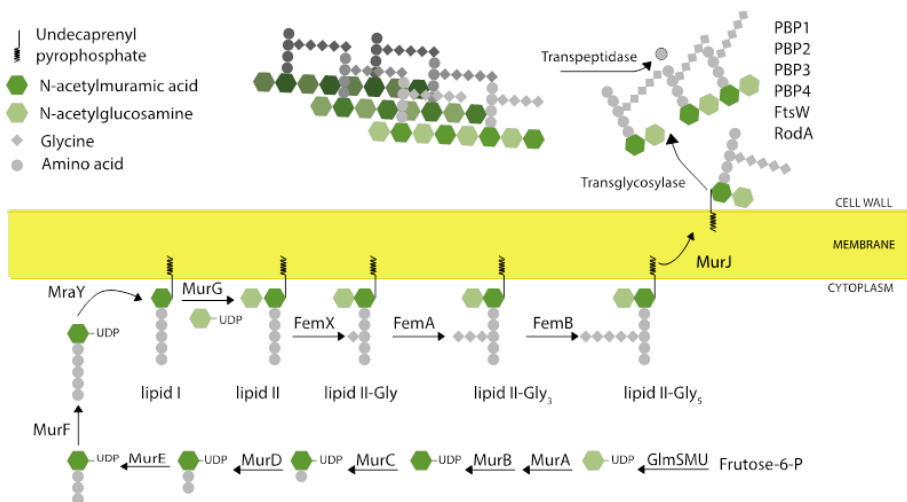


**Figure 3. PG biosynthesis in *Staphylococcus aureus*.** Synthesis of PG can be divided in three stages, each taking place in a different bacterial compartment. (1) the first stage takes place in the cytoplasm, with the synthesis of the soluble precursor UDP-MurNac-pentapeptide, which is then transferred to lipid carrier undecaprenyl-pyrophosphate, giving Lipid I (2) During the second stage, at the inner side of the membrane, a GlcNAc moiety is transferred to lipid I, giving lipid II, which is further modified by

the addition of a pentaglycine bridge, before being flipped across the membrane. (3) In the last stage, at the outer leaflet of the membrane, lipid II is incorporated into the growing PG network by transglycosylation and transpeptidation reactions. Adapted from <sup>96</sup>.

### Building the Wall – The cytoplasmic steps

PG synthesis in *S. aureus* starts with the reversible conversion of Fructose-6-P to the nucleotide sugar-linked precursor uridine diphosphate-GlcNAc (UDP-GlcNAc) by GlmSMU proteins<sup>97</sup>. The first committed step in PG synthesis is the conversion of UDP-GlcNAc and phosphoenolpyruvate into uridine diphosphate-MurNAc (UDP-MurNAc) and inorganic phosphate. This reaction is catalysed by MurA and MurB enzymes<sup>98-100</sup>. This is followed by synthesis of the stem peptide, beginning at the carboxyl group of UDP-MurNAc, with amino acids L-ala, D-glu, L-lys being sequentially added by the MurC, MurD and MurE enzymes, using adenosine triphosphate (ATP) as a source of energy <sup>101-104</sup>. In the last cytosolic steps, alanine racemase (Alr) converts L-alanine to D-alanine and D-alanine:D-alanine ligase (Ddl)<sup>105</sup> forms a dipeptide bond between two D-ala moieties, which are subsequently ligated to the stem peptide through MurF activity<sup>106</sup>. This originates the basic cytoplasmic PG precursor UDP-MurNAc-pentapeptide. Fosfomycin and D-cycloserine are two naturally occurring antibiotics produced by species of *Streptomyces* which shut down PG synthesis at the cytoplasmic stage. The former inactivates MurA by alkylating an active site cysteine residue<sup>107</sup>, while the latter



is a cyclic analogue of D-alanine that can compete for the active site of both Alr and Ddl, thus inhibiting the activities of these enzymes<sup>108,109</sup>.

### Building the Wall - The inner membrane steps

During the second stage of PG biosynthesis, the UDP-MurNAc-pentapeptide is transferred to the membrane acceptor undecaprenyl pyrophosphate, also known as bactoprenol, through the activity of the MraY translocase, giving the PG intermediate lipid I<sup>110</sup>. Bactoprenol is a lipophilic molecule which allows the transport of hydrophilic molecules across the cell's hydrophobic membrane. Lipid I is then converted into Lipid II by the activity of MurG, an enzyme that adds an UDP-GlcNAc moiety to lipid I via  $\beta$ -1,4-linkage<sup>111</sup>. At this point, the FemXAB family of transferases add directly and sequentially five glycines to the L-lys residue of the stem peptide in lipid II<sup>112</sup>. This pentaglycine bridge, which is a unique feature of *S. aureus* among prokaryotes, is used at a later stage to crosslink several layers of PG. First identified as factors required for the full expression of methicillin resistance, termed *fem* or *aux* factors<sup>113,114</sup>, each Fem protein uses glycyl-charged tRNA molecules as substrate<sup>112</sup>. Furthermore, each Fem protein has strict substrate specificity, with FemX being responsible for adding the first glycine, FemA the second and the third, and FemB the fourth and fifth glycines, and no Fem protein can substitute for another<sup>115-117</sup>.

Following the synthesis of the pentaglycine bridge, lipid II is further modified by amidation at the D-Glu residue of the stem

peptide by the glutamine amidotransferase GatD and the MurT ligase, possibly working in a bi-enzyme complex<sup>118,119</sup>. The amidated Lipid II-pentaglycine precursor is then finally translocated (flipped) across the membrane. The identity of the lipid II flippase has been a subject of heated debate. Two possible candidates based on experimental evidence are MurJ, a member of the MOP (multidrug/oligosaccharidyl-lipid/polysaccharide) exporter superfamily<sup>120-122</sup>, or FtsW, a member of the SEDS (sporulation, elongation, division and synthesis) protein family<sup>123,124</sup>. Although *in vitro* flippase activity has been demonstrated for *E. coli* FtsW<sup>123</sup>, recent work by Meeske and colleagues<sup>125</sup> proposed that SEDS proteins are peptidoglycan transglycosylases that likely function together with a cognate PBP during PG polymerization. Moreover, flipping of lipid II in *B. subtilis* was shown to require MurJ ortholog YtgP (also a MOP) or in its absence, backup flippase Amj which shows homology to MurJ<sup>121</sup>. This makes MurJ the most likely flippase, at least in Gram-positives.

Several antibiotics are known to inhibit steps of the inner membrane stage of PG biosynthesis. For example, transfer of the soluble UDP-MurNAc-pentapeptide to bactoprenol can be blocked either directly, using tunicamycin, a nucleoside which binds to MraY<sup>126,127</sup>, or indirectly using bacitracin, a molecule that prevents the turnover of bactoprenol<sup>128</sup>. Others include murgocil<sup>129</sup> or cyslabdan<sup>130</sup> which target MurG or FemA, respectively. Recently developed molecules 3-{1-[(2,3-Dimethylphenyl)methyl]piperidin-4-yl}-1-methyl-2-pyridin-4-yl-1H-indole (DMPI) and 2-(2-Chlorophenyl)-3-

[1-(2,3-dimethylbenzyl)piperidin-4-yl]-5-fluoro-1H-indole (CDFI), both from Merck, are likely MurJ inhibitors<sup>131</sup>. While the antibiotics mentioned above directly inhibit enzymes, the so called nonribosomal peptide synthetase (NRPS)-derived natural products such as ramoplanin and the more recently described teixobactin and lysobactin<sup>132</sup>, recognize the reducing end of lipid-linked cell wall precursors, namely lipid I and lipid II, and bind to it, halting PG synthesis at that point<sup>132</sup>.

### Building the Wall - The outer membrane steps

At the third and final stage of PG biosynthesis, lipid II is released from bactoprenol (which is recycled) and is incorporated into the growing PG network via transglycosylation (TG) and transpeptidation (TP) reactions<sup>82</sup>. The new subunit of PG is attached to the growing glycan chain through transglycosylation between the reducing end of the MurNAc in the nascent glycan chain and the C-4 carbon of the glucosamine residue in the lipid-linked precursor, using the phosphodiester-muramic acid bond as a source of energy<sup>133</sup>. This reaction can be catalysed by the transglycosylase (TGase) domain of bifunctional PBP2<sup>134</sup> or monofunctional TGases MGT and SgtA<sup>135</sup> in *S. aureus*. The moenomycin family of phosphoglycolipid antibiotics reversibly bind the TGase domain of these proteins. SEDS protein RodA has also been shown to have TGase activity<sup>125</sup>.

TP and crosslinking, in turn, are done by first cleaving the D-alanine-D-alanine bond at the terminus of the stem peptide in one glycan

subunit. This breakage then drives energetically the reaction between the resulting peptidyl end (D-ala) and an acceptor group present in another glycan. In *S. aureus* the acceptor group is the last glycine of the synthesised pentaglycine crossbridge, whereas in bacteria with direct crosslinking the acceptor is the dibasic amino acid in the stem peptide<sup>97</sup>. The TP reaction is done by the transpeptidase (TPase) domain of the PBPs. Molecules containing  $\beta$ -lactam rings, such as penicillin, methicillin, cephalosporins and carbapenems are collectively known as  $\beta$ -lactam antibiotics.  $\beta$ -lactam rings bind and irreversibly acylate the catalytic serine in the PBPs TPase active site, acting as suicide substrate homologues<sup>136,137</sup>. This causes the enzyme to lose activity which in turn prevents the transpeptidation of PG strands. The inhibition of TP can also be achieved with glycopeptide vancomycin, although the mechanism is quite different. Vancomycin is a very large hydrophilic molecule that can form hydrogen bonds with the D-ala-D-ala termini of the PG stem peptides, and thus, through steric hindrance, prevents access of the PBPs to their crosslinking substrates<sup>138</sup>.

### Building the Wall – The PBPs

In contrast to bacteria such as *E.coli* and *B.subtilis*, which contain genomic sequences encoding for 12 and 16 PBPs, respectively, in methicillin-susceptible *S. aureus* (MSSA) strains there are only four PBPs – three high-molecular weight PBPs 1-3 and one low molecular weight PBP4<sup>139,140</sup>. PBP1 is essential for cell viability<sup>141</sup>. Inactivation of

the TPase domain of PBP1 was shown to cause a decreased degree of PG crosslinking but not loss of viability, suggesting that this protein fulfils a second, unknown essential function to the cell<sup>142</sup>. PBP2 is a Class A PBP that is the only bifunctional PBP in the cell, possessing both N-terminal TGase and C-terminal TPase domains, which are highly conserved. The TPase domain of PBP2 is essential in MSSA strains and it seems to be sufficient to ensure cell survival in the absence of other PBPs<sup>143</sup>. It has been postulated that the main function of the TPase domain of PBP2 is the very initial crosslinking of mucopeptides up to pentameric molecules, gradually losing affinity to the substrate as its degree of polymerization increases<sup>144-146</sup>. This protein localizes at mid-cell and this localisation was shown to be dependent on interactions with its transpeptidation substrates, as treatment with cell wall targeting antibiotics affects its localisation pattern<sup>147</sup>. The function of PBP3 remains elusive, as this protein was shown to be non-essential for viability and its deletion did not lead to any observable phenotypes<sup>148</sup>. PBP4 is also dispensable for cell viability, however it has been shown to be important during PG polymerization<sup>146,149</sup>. Deletion of PBP4 causes a severe decrease in higher-order crosslinking during PG synthesis, which in turn results in decreased stiffness of the whole cell envelope, as measured by atomic force microscopy (AFM)<sup>150</sup>. Also interestingly, PBP4 activity has been linked to methicillin resistance in CA-MRSA strains, but not in HA-MRSA strains<sup>151</sup>. PBP4 is recruited to mid-cell through interactions with wall teichoic acids (WTA), components of the cell

wall envelope important for cell morphogenesis and virulence. It has been postulated that this mode of regulation constitutes a temporal cue that ensures that extensive cross-linking of PG layers is stalled until the remaining components of the envelope are assembled<sup>152</sup>. MRSA strains contain an additional PBP – PBP2A, acquired from another species. Unlike PBP2, PBP2A lacks a TGase domain but its TP domain is virtually insensitive to  $\beta$ -lactam acylation. When MRSA strains are challenged with  $\beta$ -lactam treatment, PBP2's TGase domain and PBP2A's TPase domain cooperate in the assembly of PG, possibly in a protein complex<sup>153,154</sup>. As PBP2 localisation requires substrate recognition, PBP2A could recognize its substrate and recruit acylated PBP2 to the mid-cell, where both proteins ensure PG incorporation.

### Peptidoglycan Remodelling

Growth and division of the bacterial cell requires not only synthesis of new PG but also its breakage, remodelling and recycling. This is done by enzymes collectively known as PG hydrolases or autolysins. There is seemingly a specific PG hydrolase for every glycosidic and amide bond present in peptidoglycan, although not all bacterial species possess the full set of hydrolases<sup>155</sup>. Hydrolases can be generally classified as muramidases, glucosaminidases, amidases, endopeptidases and carboxypeptidases. These enzymes fulfil numerous functions in the cell, from regulating cell growth to lysing the mother cell during sporulation or generating holes in the cell wall for the deposition of structures such as flagella. Peptidoglycan can be

regarded as a large mesh sustaining the cell, defining its shape<sup>74</sup>. In order for the cell to grow, new material must be inserted in the PG network, causing the mesh to expand. This expansion must require the rupture of covalent PG bonds by hydrolases<sup>156,157</sup>. Evidence for this theory comes from observations that both Gram-positive<sup>158</sup> and Gram-negative<sup>159</sup> bacteria shed peptidoglycan fragments during growth, a process termed peptidoglycan turnover. These fragments can constitute up to 40% of the existing PG in one generation, as seen during *E.coli* growth<sup>159</sup>. Because PG hydrolytic activity needs to be regulated, it has been proposed by Höltje that PG synthases and hydrolases form multi-enzymatic complexes that are coordinated in space and time during the bacterial cell cycle<sup>160</sup>. This would ensure that hydrolases are only active in sites of new synthesis. For Gram-positive bacteria, that have multiple layers of PG, an inside-to-outside growth model has been proposed<sup>161,162</sup>. This model supports the notion that new material is inserted underneath the existing layers, cleaved by autolysins in order to stretch and bear the mechanical stress. Gradually, the outermost layers are degraded and released as turnover material to the surrounding medium.

Hydrolytic activity is also required for daughter cell separation. At the end of the bacterial life cycle, the division septum must be cleaved, allowing the mother cell to split into two equal daughter cells. In *S. aureus*, this process seems dependent on the major hydrolase Atl, a bifunctional enzyme with both amidase and endo- $\beta$ -N-acetylglucosaminidase domains<sup>163,164</sup>. Null mutants of *atl*

show a variety of phenotypic alterations, including a disordered division pattern, formation of large cell clusters due to defective cell separation and impairment of biofilm formation<sup>163,165</sup>. In accordance to its role in daughter cell separation, Atl products bind to precise locations of the equatorial rings of the staphylococcal cell, both at the septum but also at the next division plane<sup>166,167</sup>. Interestingly this mechanism of localisation seems to be dependent on an exclusion strategy mediated by wall teichoic acids, as reported by Schlag and colleagues<sup>168</sup>. Evidence for hydrolase activity being involved in cell separation also comes from an *S. pneumoniae* mutant lacking glucosaminidase LytB<sup>169</sup>, and *E. coli*<sup>170</sup> and *Neisseria gonorrhoeae*<sup>171</sup> mutants lacking amidases AmiA-C. In each case, cell populations were composed of long chains of unseparated cells, indicating that following septation, the daughter cells failed to split properly. A recent report by Klöckner et. al.<sup>172</sup> showed that *Chlamydia pneumoniae*, an intracellular pathogen that lacks a typical peptidoglycan layer, expresses an essential hydrolase AmiA that surprisingly contains a penicillin-binding domain. Chlamydial AmiA was effective at separating daughter cells in an *E.coli* amidase mutant, suggesting functional conservation of this enzyme<sup>172</sup>. Because chlamydiae lack true PG, it is likely that AmiA fulfils a second essential role not related to hydrolytic activity, which highlights the fact that many functions of autolysins remain to be understood.



## The Division Machinery

The cell cycle of prokaryotes is in essence a straightforward and regular process. Most bacterial cells double their internal content, replicate their genetic material, synthesise a septum at mid-cell and divide into two identical daughter cells by binary fission. At the core of the cell cycle is a macromolecular protein machinery responsible for cell division called the divisome, which is coordinated by the conserved tubulin homologue FtsZ<sup>173</sup>. Many genes involved in the divisome, including *ftsZ*, are contained in the universal division and cell wall (dcw) cluster, which is conserved in many bacterial species<sup>174</sup>. FtsZ undergoes GTP-dependent polymerization into filaments, with a repeating arrangement of subunits, which form a ring around the longitudinal midpoint (the septum) of the cell. This structure is commonly referred to as the Z-ring<sup>175</sup>. Up until the turn of the millennium, it was believed that all bacteria and archaea used an universal cytokinetic machinery based on the Z-ring<sup>176</sup>. This turned out not to be true, as whole genome sequencing revealed that species of *Chlamydia*<sup>177</sup> and the *Planctomycetes*<sup>178</sup> phylum, along with the entire archaeal kingdom of *Crenarchaea*<sup>179</sup> manage as well without FtsZ. Nevertheless, these are exceptions to the rule: the Z-ring instructs and directs division in prokaryotes.

The assembly of the divisome follows a sequential order of events that have been extensively studied in model organisms *B. subtilis* and *E.coli*<sup>180</sup>. This process can be generally divided into two

stages, which will be described in depth in the following sections. During the first stage the division site is selected and FtsZ assembles into a ring which is tethered to the membrane, resulting in a structure called the proto-ring. In the second stage the proto-ring recruits additional proteins including cell wall synthases, forming the mature divisome, which then constricts the membrane leading to cytokinesis and cell separation.

### Division Site Selection

Correct positioning of the Z-ring at the future site of cell division (mid-cell) is dependent on protein systems acting as space regulators. These systems can be either negative, in the sense that they inhibit FtsZ polymerization at inappropriate sites or positive, by localizing at mid-cell and promoting Z-ring assembly there. Two well studied examples of negative space regulation are the Min system and nucleoid occlusion<sup>181,182</sup>, depicted in Fig. 4A. In the Min system, a MinCD protein complex that inhibits FtsZ polymerization either oscillates from one end of the cell to the other, creating a gradient where the concentration is highest at the cell pole (as seen in *E.coli* and *Neisseria sp.*), or is directly recruited to the cell poles by DivIVA, which has affinity for negative membrane curvature (in *B.subtilis*). In both cases, the middle of the cell becomes the preferential zone for the Z-ring to form<sup>183</sup> (Fig. 4A). The nucleoid occlusion system, in turn, prevents premature septation until replication of the chromosome is complete<sup>184</sup>. Nucleoid occlusion effectors Noc in *S. aureus*<sup>185</sup> and *B.*

*subtilis*<sup>186</sup> or *E.coli* homologue SlmA<sup>187</sup> bind specific DNA sequences that are heterogeneously distributed inside the cell, being more abundant near the origin of replication, which is positioned at mid-cell during initial stages of the cell cycle. As DNA replication progresses, the origin of replication and the nucleoid effectors are gradually moved towards the cell poles, which allows for polymerization of FtsZ at the middle<sup>188,189</sup> (Fig. 4A). Examples of positive space regulators that promote Z ring assembly include *S. pneumoniae* mid-cell anchored protein MapZ<sup>190</sup> or the SsgAB<sup>191</sup> protein complex in actinomycetes, which directly recruit FtsZ to mid-cell.

Division site selection in *S. aureus* is a more complex affair. Cells divide sequentially in three specific orthogonal planes, a trait that is rather uncommon in prokaryotes<sup>192</sup>. This results in cell clusters that resemble a bunch of grapes, giving the genus its namesake (from greek *staphylē*). Remarkably, in order to divide precisely in the correct plane, each generation of cells must 'remember' the previous two planes used by their immediate ancestor, indicating a mechanism of molecular memory.

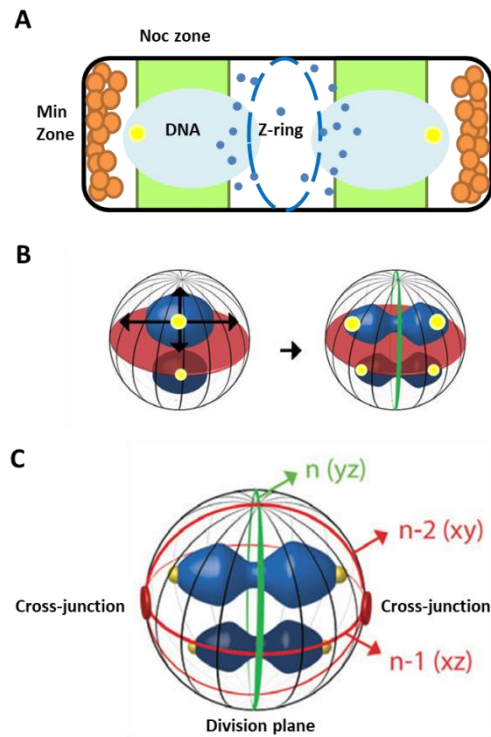


**Figure 4. Division site selection in bacteria.** (A), Bacterial division begins with polymerization of FtsZ as a ring structure at mid-cell (Z-ring), which in *B. subtilis* is spatially regulated by the Min and nucleoid occlusion systems. The MinCD system, which inhibits FtsZ polymerization, is recruited to the negatively curved cell poles, creating a Min zone that prevents Z-ring assembly. Nucleoid occlusion effector Noc binds specific DNA sequences that are more abundant near the origin of replication (yellow circles) and prevents FtsZ polymerization through steric hindrance (Noc zone), avoiding the bisection of the nucleoid. (B), Schematic of an *S. aureus* cell that has formed an equatorial division septum (in red). Prior to the next cell division, each daughter cell will replicate and segregate the DNA along its long axis, positioning the origin of replication (yellow spheres) at the edge of the nucleoid. The next plane of division can be any of the infinite number of planes (meridians) shown, however only one (in green) will not bisect the nucleoid. (C), Schematic of a cell showing the current division plane (in green,  $n$ ), the previous division plane ( $n-1$ , in red) and the division plane from two generations prior ( $n-2$ , in red). Each division plane is placed

orthogonally to the previous generation plane. In each cycle, the origins of replication (yellow spheres) segregate towards the cross-junctions (red discs) of the two previous planes used, by an unknown mechanism. This epigenetic information automatically defines the next division plane (in green). Panels (B) and (C) were adapted from <sup>185</sup>.

While *S. aureus* seems to lack any apparent Min system or homologues<sup>193</sup>, it does use nucleoid occlusion to avoid guillotining of the DNA by the divisome. As reported by Veiga et. al.<sup>185</sup>, mutants lacking Noc were shown to form multiple Z-rings that were no longer placed in perpendicular planes to each other. Furthermore, inhibiting DNA replication or promoting condensation with chloramphenicol, in the presence of Noc, led to abnormal non-orthogonal FtsZ structures. These data suggested that division site selection in *S. aureus* is determined by the axis of chromosome segregation<sup>185</sup>. DNA segregation in bacteria invariably occurs along the longer axis of the cell, presumably due to conformational entropy of the replicating nucleoid in a confined space<sup>194</sup>. However, spherical cells possess an infinite number of cell axes with the same length which are theoretically valid for chromosome segregation, resulting in an infinite number of possible division planes (Fig. 4B). Yet *S. aureus* always chooses the one division plane that is precisely orthogonal to both planes from the two previous generations. The authors proposed a model where the chromosome origins of replication would always segregate towards the intersection points of the last two planes of division (cross-junctions). In this scenario there is only

one plane that does not bisect the nucleoid. That plane is perpendicular to the previous plane and will automatically become the next division plane (Fig. 4B and C)<sup>185</sup>. This model is consistent with previous observations by Electron Microscopy (EM), showing that the surface of *S. aureus* contains “scars” from the two previous division cycles<sup>195</sup> and by AFM analysis on purified cell wall preparations, which revealed a large belt of PG in the division plane with a ‘piecrust’ structure, which remains after division as an orthogonal rib<sup>196</sup>. These cross-junctions, scars or orthogonal ribs may then constitute epigenetic information that specifies the division planes in cocci. Nevertheless, this model presumes the existence of a yet unknown factor that pulls the origins of DNA replication towards the cross-junctions.

### Assembly of the Proto-ring

Once the division site is selected, FtsZ polymers have to be tethered to the cytoplasmic membrane, as FtsZ lacks membrane interacting domains. This is achieved through interactions with FtsA and either SepF (in Gram-positives) or ZipA (in  $\gamma$ -proteobacteria)<sup>175</sup> (Fig. 5). FtsA is an ATP-binding actin homologue that associates with the membrane through its C-terminal amphipathic helix and constitutes the second most conserved protein in bacteria, after FtsZ<sup>197</sup>. Purified FtsA was shown to assemble into actin-like protofilaments in artificial lipid monolayers and mutations that disrupt these filaments were found to lead to defects in cell

division<sup>198,199</sup>. Moreover, FtsA was shown to be required for FtsZ treadmilling<sup>200</sup>. Treadmilling is the molecular mechanism wherein subunits are added to one end of a polymer while other subunits are removed from the opposing end. Importantly, the rate that subunits are added to one end is higher than the rate of subunit removal in the other end, which generates apparent movement of the whole filament. Using high resolution total internal reflection fluorescence (TIRF) to image FtsZ in an artificial membrane bilayer, Loose and colleagues<sup>200</sup> found that ATP-bound oligomers of FtsA promote the treadmilling of FtsZ filaments. Interestingly, *ftsA* mutants of *B. subtilis* can still divide, albeit slowly, and this deficiency can be compensated by overexpression of the other membrane tether, SepF, suggesting that these two proteins perform similar functions in this organism<sup>201</sup>. FtsZ polymerization must not only be tightly regulated in space and time but also in extent. Inactivation of EzrA, an inhibitor of FtsZ polymerization that is conserved in the Firmicutes phylum, leads to the presence of extra Z rings away from mid-cell in *B. subtilis*, which results in asymmetric division<sup>202</sup>. EzrA was also shown to be involved in cell size homeostasis in *S. aureus*, with *ezrA* mutants showing abnormally large phenotypes and misplacement of the Z ring<sup>203,204</sup>. Its counterpart, ZapA, is a Z-ring associated protein which seems to promote FtsZ polymerization, as it was shown to stimulate the formation of higher order FtsZ assemblies *in vitro* and to be essential in cells producing lower amounts of FtsZ<sup>205</sup>. Together these proteins constitute the proto-ring (Fig. 5).

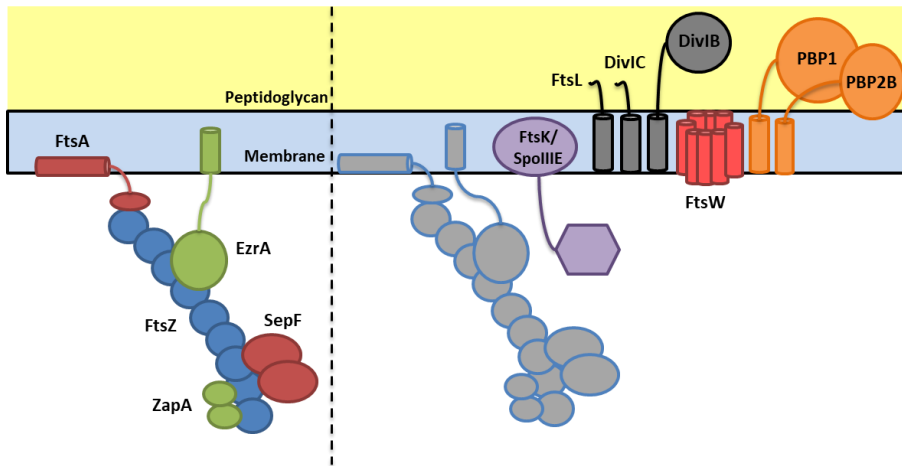


**Figure 5 – Divisome assembly in *B. subtilis*.** The assembly of the divisome begins with polymerization of FtsZ, the extent of which is controlled by ZapA and EzrA, which act as positive and negative regulators, respectively. The Z-ring is tethered to the membrane through protein interactions with FtsA and SepF. Together these proteins constitute the proto-ring. During the second stage of divisome assembly, the proto-ring recruits a large group of proteins to mid-cell, including FtsW, enzymes involved in PG synthesis (PBP1, PBP2B), PG hydrolases, DNA translocases (FtsK/SpoIIIE family) and the FtsL/DivIB/DivIC trimeric protein complex, of unknown function. The resulting megacomplex constitutes the mature divisome. The dashed line represents the time delay between the two stages of divisome assembly.

### Divisome Maturation

Following the assembly of the proto-ring, this structure recruits a second group of divisome proteins including FtsW, PG synthases, PG hydrolases, DNA-binding proteins (FtsK/SpoIIIE), and proteins that presumably promote interactions between the Z ring and the PG synthesis machinery<sup>180,206</sup>. The time delay between the two stages of divisome assembly has been reported to be at least 20% of



the cell cycle in *B. subtilis*<sup>207</sup>. Despite decades of research into the divisome, the biochemical functions of many of the second stage proteins remains unknown. A group of membrane spanning proteins DivIB, DivIC and FtsL in Gram-positives and their orthologues FtsQ, FtsB and FtsL in Gram-negatives are conserved in all species for which divisome assembly has been investigated<sup>208,209</sup>. DivIC and FtsL are unstable proteins by themselves, but when together with DivIB can form a strong heterocomplex that is recruited to the divisome and that is required for mid-cell localisation of PBP2B in *B. subtilis*<sup>208,210</sup>. DivIB, DivIC and FtsL appear to be structural proteins due to lack of enzymatic domains and are fairly similar in structure, each possessing a short N-terminal cytoplasmic domain, a single transmembrane domain and a larger periplasmic domain. Studies using conditional mutants have shown that the expression of DivIB is essential for *S. aureus* growth and that depletion of *divIB* causes a blockage in the completion, but not the initiation of septum formation<sup>211</sup>.

Another group of proteins that are recruited during the second stage of divisome assembly are the members of the conserved FtsK/SpoIIIE family of DNA translocases<sup>212,213</sup>. All members possess a C-terminal ATPase domain which forms homo-hexameric DNA motors responsible for the translocation of DNA away from the division site, avoiding bisection of the nucleoid by the septum<sup>213,214</sup>. These proteins bridge two essential steps of the bacterial life cycle: septum synthesis and DNA replication and segregation, and the

timing of their recruitment likely constitutes a major molecular checkpoint for cell cycle progression. Also of particular note is FtsN, a PG-binding protein found in *E.coli* with homologues in *Caulobacter crescentus* but otherwise poorly conserved in bacteria<sup>215</sup>. The exact function of FtsN is still unknown, however it is the last essential division protein to arrive at mid-cell and it was shown to be required for the recruitment of the *E.coli* Tol-Pal complex<sup>216</sup>, which mediates outer membrane invagination, the PG hydrolase AmiC<sup>217</sup> and to stimulate the activity of PG synthase PBP1b *in vitro*<sup>218</sup>. In light of these data, it has been proposed that the arrival of FtsN functions as a signal indicating that divisome assembly is complete, triggering septation in *E.coli*<sup>219</sup>. No homologues of FtsN have been found in Gram-positive bacteria, suggesting a different mechanism to initiate PG synthesis at mid-cell exists in these organisms.

Following divisome maturation and septal peptidoglycan synthesis and remodelling, the division macromolecular machinery constricts along the axis of the cell, causing cytokinesis to complete and the mother cell divides. The origin of the force that leads to cell envelope constriction has gathered substantial interest during these past years. The “iterative pinching model”, proposed by Li and colleagues<sup>220</sup> states that bending of the FtsZ polymers could generate the force necessary to constrict the membrane. A cycle of GTP-dependent FtsZ polymerization, membrane attachment and depolymerisation would lead to constriction, a mechanism functionally similar to the eukaryotic cell actomyosin ring, wherein

myosin motors pull actin bundles together, generating a contractile force<sup>221</sup>. However, this model has been challenged recently by observations that permanent cell wall deforming requires several minutes of applied bending force<sup>222</sup>. The fast dynamics of FtsZ subunit turnover<sup>223</sup> and treadmilling<sup>224,225</sup>, which occur on the seconds-scale, make it unlikely that the Z-ring exerts a direct sustained mechanical force on the membrane<sup>226</sup>. Additionally, computational models predict that the Z-ring can generate pulling forces of up to 100 pN<sup>227</sup>, a value which sits well below the opposing force exerted by the cell's internal turgor, which in *B. subtilis* is estimated to be close to  $10^6$  pN/nm<sup>228</sup>. Alternatively, PG synthesis and turnover at the septum could provide the required force for cytokinesis, and the function of FtsZ treadmilling would be to dynamically organize the synthesis machinery<sup>226</sup>. In support of this notion, the speed of PBP3 movement in *E.coli* was shown to be linearly correlated with the speed of FtsZ treadmilling<sup>225</sup> and the ~100 seconds time-scale dynamics of FtsZ clusters also matched well with the ~40 seconds incorporation time for newly synthesised PG strands in growing cells<sup>229</sup>.

## Coordinating cell growth and peptidoglycan synthesis

The morphological diversity that exists in bacteria is truly staggering. Traditionally, bacteriology research has focused mostly on pathogenic species, which tend to maintain a cylindrical or spherical regular shape but others are bent, flat sided, triangular, helical and even square-shaped, among a myriad of other possibilities. There are bacteria that create bulbous extensions of their cells, bacteria that live in colonies where each individual cell is partially differentiated, behaving as a primitive multicellular organism; bacteria that grow as branched filaments, not unlike a tree, and bacteria that shapeshift during their cell cycle<sup>230,231</sup>. In truth every prokaryote adopts the shape that allows it to better thrive in the particular ecological niche that it inhabits, with that particular shape gradually perfected through evolution. Cell morphology influences most of everything in the bacterial lifestyle from nutrient accessibility, to colonization of surfaces, to motility and survival against other species<sup>230</sup>. The morphology of most bacteria is dictated by their cell wall, functioning as an exoskeleton. This became apparent in the late 50s when isolated cell wall sacculi were shown to retain the particular shape of the original cell<sup>232</sup>. Moreover, mutations that affected cell shape were almost always mapped to genes involved in cell wall synthesis<sup>233-235</sup>. Interestingly, it seems that there is a trend that correlates increased complexity of PG synthesis to deviations from the basic shape, the sphere<sup>236</sup> (summarized in Fig. 6).

Truly spherical cocci, such as *Staphylococcus* and *Neisseria*, synthesise peptidoglycan mainly at the division septum<sup>237,238</sup>, a process that is coordinated by FtsZ and the divisome, as described above. Adapting a more complex shape than the sphere requires an additional level of spatio-temporal regulation of PG synthesis, which can translate to having independent macromolecular protein machineries acting on different locations of the cell. Elongated ellipsoids (also called ovococci) such as streptococci, lactococci and enterococci possess specific PBPs solely dedicated to peripheral growth, acting independently from the PBPs associated to the divisome<sup>236</sup>. In *S. pneumoniae* peripheral PG synthesis, catalysed by dedicated PBP2b, is localised in equatorial rings close to mid-cell, which mark sites of the previous division<sup>239,240</sup> (see Fig. 6). This PG insertion occurs in tandem and in close proximity to septal synthesis, which is done by PBP1a and PBP2x<sup>240,241</sup>, and leads to the slight elongation observed in these bacteria. The mechanism that coordinates this extraseptal PG synthesis is unknown, although it has been postulated that FtsZ could control both modes of synthesis<sup>242</sup>.

Elongation in rod-shaped bacteria is mechanically more complex<sup>243</sup>. Rods such as *B.subtilis* possess a machinery dedicated to elongation, the so called elongasome, that is coordinated by the cytoskeletal actin homologue MreB<sup>244</sup>. MreB assembles in short patches that move circumferentially along the cell and presumably direct the enzymes required for lateral PG synthesis, including the SEDS transglycosylase RodA, the transpeptidase PBP2 and the

putative signalling protein RodZ<sup>244,245</sup>. Similarly to the mechanisms proposed for divisome constriction, it has been suggested that peripheral PG synthesis provides the force that drives processive movement of the MreB patches along the cell<sup>244,246</sup>. Interestingly, MreB-dependent elongation is not ubiquitous in rods. Rods that lack MreB seem to rely on signal transduction by eukaryotic-type serine/threonine kinases (ESTKs) for maintaining correct shape<sup>236</sup>. For example, either overexpression or depletion of ESTKs locus *pknAB* in *Mycobacterium tuberculosis* led to narrow and overly elongated cells<sup>247</sup>. ESTKs fulfil a plethora of regulating functions in prokaryotic cells including stress response<sup>248</sup>, antibiotic resistance<sup>249</sup> and cross-talk between the divisome and autolysins<sup>250</sup>. It has been proposed that elongation in the absence of MreB can be triggered by ESTKs which cause a molecular shift from septal to peripheral PG synthesis<sup>251</sup>. If proven correct, such a mechanism constitutes an interesting alternative for peripheral PG synthesis in the absence of a MreB cytoskeleton. Compelling evidence towards this model was obtained by depleting StkP, the sole ESTK present in *S. pneumoniae*, which caused a shift from ovoid to rod cell shape, suggesting that peripheral cell wall synthesis was exceeding septal synthesis<sup>251</sup>.

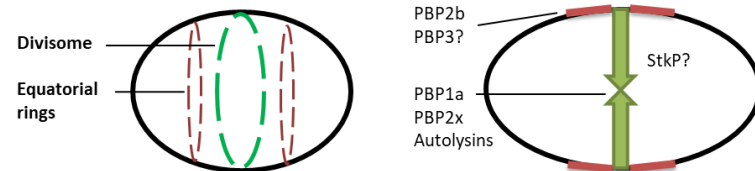
Another well studied case pertains to how *Caulobacter crescentus* requires a single protein to acquire its characteristic curved, crescent shape. *Caulobacter crescentin* is a cytoskeletal protein that forms mechanically rigid coiled-coil filaments<sup>252</sup>; knockout of the *creS* locus causes cells to lose the crescent shape and become regular

rods<sup>253</sup>. This is because crescentin filaments localise near the membrane, asymmetrically, on only one side of the cell (Fig. 6), and either mechanically induce concave curvature directly, or more likely, interfere locally with the directional motions of the MreB elongasome<sup>252,254</sup>.

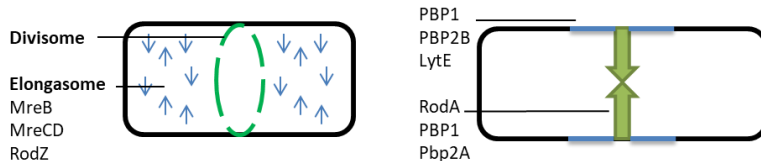
***Staphylococcus aureus***



***Streptococcus pneumoniae***



***Bacillus subtilis***



***Caulobacter crescentus***

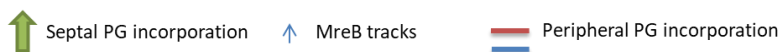


**Figure 6. Cell shape maintenance in prokaryotes requires spatial coordination of PG synthesis.** Deviation from the simplest cell shape – the

sphere (*S. aureus*) - to elongated ellipsoids (*S. pneumoniae*), cylindrical (*B. subtilis*) or crescent cell shape (*C. crescentus*) requires additional levels of regulation of PG synthesis. Left panels – structural elements known to be involved in directing PG incorporation in the cell: the divisome (present in most bacteria), the elongasome (in rods), equatorial rings marking previous division sites (in ovococci), and filaments of crescentin (in *Caulobacter*). Right Panels – cocci possess only one mode of PG incorporation, which takes place at the septum during division, and one PG synthesis machinery. Besides septal PG synthesis, ovococci and rods also incorporate PG at the side wall, leading to peripheral growth. While rods possess a machinery dedicated to lateral PG synthesis, coordinated by MreB patches moving circumferentially around the cell, ovococci may switch between the two modes via ESTK signalling. Similarly to rods, *C. crescentus* also possesses two machineries for PG incorporation, but the presence of bundles of crescentin on one side of the cell interferes locally with the elongasome, generating asymmetry. Some examples of PG synthases known or presumed to be part of each machinery are shown<sup>140,236,255,256</sup>.

*S. aureus* possesses 4 native PBPs, *S. pneumoniae* has 6 PBPs and the *E.coli* genome encodes for as much as 12 PBPs<sup>236</sup>. This could be interpreted as a trend where going from spheres to rods translates to an increased number of PBPs that are required to define shape. One could then speculate that rods have evolved from cocci, developing additional modes of PG synthesis to increase the complexity of their cell wall. While the Last Common Ancestor (LCA) from which all bacteria descend from was likely spherical, all evidence suggests that modern cocci such as *S. aureus* descend from rods. The deepest branches of the prokaryotic tree are composed exclusively of rods<sup>230,257</sup>, and coccus-to-rod transitions have never been observed, either phylogenetically or experimentally.



Conversely, rod-to-sphere differentiation events seem prevalent in bacteria and fundamentally tied to nutrient availability. *E. coli* cells become smaller and more spheroidal through expression of late stage BolA and the RpoS sigma factor<sup>258,259</sup>, while *Arthrobacter* and *Acinetobacter* spp. transition from rod to cocci when entering stationary phase<sup>260</sup>. *S. aureus* possesses at least two homologs of proteins that are part of the rod elongasome, MreC and MreD, which are essential for viability in *B. subtilis*<sup>261</sup>, *E.coli*<sup>262</sup> and *C. crescentus*<sup>263</sup>. Knockout mutation of either of the corresponding genes led to no observable phenotypes or loss of viability in *S. aureus* COL<sup>264</sup>, while in another study deletion of either *mreD* or *mreCD* in *S. aureus* SH1000 caused modest alterations in cell volume and shape<sup>265</sup>. Deletion of *divIVA*, which is required for division site selection in rods<sup>266</sup>, similarly did not impair normal cell division<sup>267</sup>. These data suggest that such elements may constitute vestigial DNA of a rod-shaped ancestor from which *S. aureus* evolved from.

## **Brief Overview**

In order to produce this dissertation I focused on investigating the interplay between PG synthesis and cell morphology in *S. aureus*. Specifically, I wanted to explore the possibility that these bacteria require peptidoglycan incorporation all around the cell surface during certain stages of the cell cycle in order to maintain their correct shape. I also aimed to determine how the PG synthesis machinery of *S. aureus* is recruited specifically to the divisome, when it is time for the cells to divide. Furthermore, in order to identify possible targets for pathogen-specific drug design, I wanted to examine the importance of crossbridge formation towards the structural stability of the *S. aureus* wall. Finally, throughout my studies I also focused on understanding the mechanisms of activity of new molecules with potential to become useful alternatives for therapy against bacterial infections.

## References

- 1 Donoghue, P. C. & Antcliffe, J. B. Early life: Origins of multicellularity. *Nature* **466**, 41-42, doi:10.1038/466041a (2010).
- 2 Schopf, J. W. Disparate rates, differing fates: tempo and mode of evolution changed from the Precambrian to the Phanerozoic. *Proc Natl Acad Sci U S A* **91**, 6735-6742 (1994).
- 3 Glud, R. N. *et al.* High rates of microbial carbon turnover in sediments in the deepest oceanic trench on Earth. *Nature Geoscience* **6**, 284, doi:10.1038/ngeo1773 (2013).
- 4 Ball, M. M. *et al.* Bacteria recovered from a high-altitude, tropical glacier in Venezuelan Andes. *World J Microbiol Biotechnol* **30**, 931-941, doi:10.1007/s11274-013-1511-1 (2014).
- 5 Druce, R. G. & Thomas, S. B. An ecological study of the psychrotrophic bacteria of soil, water, grass and hay. *J Appl Bacteriol* **33**, 420-435 (1970).
- 6 Danovaro, R. *et al.* A submarine volcanic eruption leads to a novel microbial habitat. *Nat Ecol Evol* **1**, 144, doi:10.1038/s41559-017-0144 (2017).
- 7 Setlow, P. Spores of *Bacillus subtilis*: their resistance to and killing by radiation, heat and chemicals. *J Appl Microbiol* **101**, 514-525, doi:10.1111/j.1365-2672.2005.02736.x (2006).
- 8 von Dohlen, C. D., Kohler, S., Alsop, S. T. & McManus, W. R. Mealybug beta-proteobacterial endosymbionts contain gamma-proteobacterial symbionts. *Nature* **412**, 433-436, doi:10.1038/35086563 (2001).
- 9 Peterson, J. *et al.* The NIH Human Microbiome Project. *Genome Res* **19**, 2317-2323, doi:10.1101/gr.096651.109 (2009).
- 10 Yoon, M. Y., Lee, K. & Yoon, S. S. Protective role of gut commensal microbes against intestinal infections. *J Microbiol* **52**, 983-989, doi:10.1007/s12275-014-4655-2 (2014).
- 11 Reinoso Webb, C., Kobozev, I., Furr, K. L. & Grisham, M. B. Protective and pro-inflammatory roles of intestinal bacteria. *Pathophysiology* **23**, 67-80, doi:10.1016/j.pathophys.2016.02.002 (2016).
- 12 Clarke, G. *et al.* Minireview: Gut microbiota: the neglected endocrine organ. *Mol Endocrinol* **28**, 1221-1238, doi:10.1210/me.2014-1108 (2014).
- 13 Koren, O. *et al.* Human oral, gut, and plaque microbiota in patients with atherosclerosis. *Proc Natl Acad Sci U S A* **108 Suppl 1**, 4592-4598, doi:10.1073/pnas.1011383107 (2011).
- 14 Qin, J. *et al.* A metagenome-wide association study of gut microbiota in type 2 diabetes. *Nature* **490**, 55-60, doi:10.1038/nature11450 (2012).
- 15 Bercik, P. *et al.* The intestinal microbiota affect central levels of brain-derived neurotrophic factor and behavior in mice. *Gastroenterology* **141**, 599-609, 609.e591-593, doi:10.1053/j.gastro.2011.04.052 (2011).
- 16 Diaz Heijtz, R. *et al.* Normal gut microbiota modulates brain development and behavior. *Proc Natl Acad Sci U S A* **108**, 3047-3052, doi:10.1073/pnas.1010529108 (2011).

- 17 Sender, R., Fuchs, S. & Milo, R. Are We Really Vastly Outnumbered? Revisiting the Ratio of Bacterial to Host Cells in Humans. *Cell* **164**, 337-340, doi:10.1016/j.cell.2016.01.013 (2016).
- 18 Lawn, S. D. & Zumla, A. I. Tuberculosis. *Lancet* **378**, 57-72, doi:10.1016/S0140-6736(10)62173-3 (2011).
- 19 Fleming, A. On the antibacterial action of cultures of a penicillium, with special reference to their use in the isolation of *B. influenzae*. 1929. *Bull World Health Organ* **79**, 780-790 (2001).
- 20 Quinn, R. Rethinking antibiotic research and development: World War II and the penicillin collaborative. *Am J Public Health* **103**, 426-434, doi:10.2105/AJPH.2012.300693 (2013).
- 21 Chambers, H. F. & DeLeo, F. R. Waves of resistance: *Staphylococcus aureus* in the antibiotic era. *Nat Rev Micro* **7**, 629-641, doi:http://www.nature.com/nrmicro/journal/v7/n9/supplinfo/nrmicro2200\_S1.html (2009).
- 22 Grundmann, H., Aires-De-Sousa, M., Boyce, J. & Tiemersma, E. Emergence and resurgence of methicillin-resistant *Staphylococcus aureus* as a public-health threat. *Lancet* **368**, 874-885 (2006).
- 23 Rhomberg, P. R., Fritsche, T. R., Sader, H. S. & Jones, R. N. Clonal occurrences of multidrug-resistant Gram-negative bacilli: report from the Meropenem Yearly Susceptibility Test Information Collection Surveillance Program in the United States (2004). *Diagn Microbiol Infect Dis* **54**, 249-257, doi:10.1016/j.diagmicrobio.2005.10.010 (2006).
- 24 Nacheha, J. B. & Chaisson, R. E. Tuberculosis drug resistance: a global threat. *Clin Infect Dis* **36**, S24-30, doi:10.1086/344657 (2003).
- 25 Theuretzbacher, U. Accelerating resistance, inadequate antibacterial drug pipelines and international responses. *Int J Antimicrob Agents* **39**, 295-299, doi:10.1016/j.ijantimicag.2011.12.006 (2012).
- 26 Gorwitz, R. *et al.* Changes in the prevalence of nasal colonization with *Staphylococcus aureus* in the United States, 2001-2004. *J Infect Dis* **197**, 1226-1234 (2008).
- 27 Kluytmans, J., van Belkum, A. & Verbrugh, H. Nasal carriage of *Staphylococcus aureus*: epidemiology, underlying mechanisms, and associated risks. *Clin Microbiol Rev* **10**, 505-520 (1997).
- 28 Wenzel, R. & Perl, T. The significance of nasal carriage of *Staphylococcus aureus* and the incidence of postoperative wound infection. *J Hosp Infect* **31**, 13-24 (1995).
- 29 Kazakova, S. *et al.* A clone of methicillin-resistant *Staphylococcus aureus* among professional football players. *N Engl J Med* **352**, 468-475 (2005).
- 30 Lowy, F. *Staphylococcus aureus* infections. *N Engl J Med* **339**, 520-532 (1998).
- 31 Muto, C. *et al.* SHEA guideline for preventing nosocomial transmission of multidrug-resistant strains of *Staphylococcus aureus* and enterococcus. *Infect Control Hosp Epidemiol* **24**, 362-386 (2003).
- 32 Miller, L. & Diep, B. Clinical practice: colonization, fomites, and virulence: rethinking the pathogenesis of community-associated methicillin-resistant *Staphylococcus aureus* infection. *Clin Infect Dis* **46**, 752-760 (2008).

- 33 Barber, M. & Rozwadowska-Dowzenko, M. Infection by penicillin-resistant staphylococci. *Lancet* **2**, 641-644 (1948).
- 34 Abraham, E. P. & Chain, E. An enzyme from bacteria able to destroy penicillin. 1940. *Rev Infect Dis* **10**, 677-678 (1988).
- 35 Enright, M. C. *et al.* The evolutionary history of methicillin-resistant *Staphylococcus aureus* (MRSA). *Proc Natl Acad Sci U S A* **99**, 7687-7692, doi:10.1073/pnas.122108599 (2002).
- 36 Ubukata, K., Nonoguchi, R., Matsuhashi, M. & Konno, M. Expression and inducibility in *Staphylococcus aureus* of the *mecA* gene, which encodes a methicillin-resistant *S. aureus*-specific penicillin-binding protein. *J Bacteriol* **171**, 2882-2885 (1989).
- 37 Katayama, Y. *et al.* Identification in methicillin-susceptible *Staphylococcus hominis* of an active primordial mobile genetic element for the staphylococcal cassette chromosome *mec* of methicillin-resistant *Staphylococcus aureus*. *J Bacteriol* **185**, 2711-2722 (2003).
- 38 Holden, M. *et al.* Complete genomes of two clinical *Staphylococcus aureus* strains: evidence for the rapid evolution of virulence and drug resistance. *Proc Natl Acad Sci U S A* **101**, 9786-9791 (2004).
- 39 Kuroda, M. *et al.* Whole genome sequencing of methicillin-resistant *Staphylococcus aureus*. *Lancet* **357**, 1225-1240 (2001).
- 40 Wu, S., de Lencastre, H. & Tomasz, A. Recruitment of the *mecA* gene homologue of *Staphylococcus sciuri* into a resistance determinant and expression of the resistant phenotype in *Staphylococcus aureus*. *J Bacteriol* **183**, 2417-2424 (2001).
- 41 Hartman, B. & Tomasz, A. Low-affinity penicillin-binding protein associated with beta-lactam resistance in *Staphylococcus aureus*. *J Bacteriol* **158**, 513-516 (1984).
- 42 Pinho, M., de Lencastre, H. & Tomasz, A. An acquired and a native penicillin-binding protein cooperate in building the cell wall of drug-resistant staphylococci. *Proc Natl Acad Sci U S A* **98**, 10886-10891 (2001).
- 43 Sharma, V., Hackbarth, C., Dickinson, T. & Archer, G. Interaction of native and mutant *MecI* repressors with sequences that regulate *mecA*, the gene encoding penicillin binding protein 2a in methicillin-resistant staphylococci. *J Bacteriol* **180**, 2160-2166 (1998).
- 44 McKinney, T., Sharma, V., Craig, W. & Archer, G. Transcription of the gene mediating methicillin resistance in *Staphylococcus aureus* (*mecA*) is corepressed but not coinduced by cognate *mecA* and beta-lactamase regulators. *J Bacteriol* **183**, 6862-6868 (2001).
- 45 Kleven MR, M. M., Nadle J, Petit S, Gershman K, Ray S. Vol. 298 71 (JAMA, 2007).
- 46 Boyce, J. *et al.* Methicillin-resistant *Staphylococcus aureus* (MRSA): a briefing for acute care hospitals and nursing facilities. The AHA Technical Panel on Infections Within Hospitals. *Infect Control Hosp Epidemiol* **15**, 105-115 (1994).
- 47 Laupland, K., Ross, T. & Gregson, D. *Staphylococcus aureus* bloodstream infections: risk factors, outcomes, and the influence of methicillin resistance in Calgary, Canada, 2000-2006. *J Infect Dis* **198**, 336-343 (2008).

- 48 Li, M. *et al.* Evolution of virulence in epidemic community-associated methicillin-resistant *Staphylococcus aureus*. *Proc Natl Acad Sci U S A* **106**, 5883-5888 (2009).
- 49 Moran, G. *et al.* Methicillin-resistant *S. aureus* infections among patients in the emergency department. *N Engl J Med* **355**, 666-674 (2006).
- 50 Vandenesch, F. *et al.* Community-acquired methicillin-resistant *Staphylococcus aureus* carrying Panton-Valentine leukocidin genes: worldwide emergence. *Emerg Infect Dis* **9**, 978-984 (2003).
- 51 Li, M. *et al.* Evolution of virulence in epidemic community-associated methicillin-resistant *Staphylococcus aureus*. *Proc Natl Acad Sci U S A* **106**, 5883-5888 (2009).
- 52 Kennedy, A. *et al.* Epidemic community-associated methicillin-resistant *Staphylococcus aureus*: recent clonal expansion and diversification. *Proc Natl Acad Sci U S A* **105**, 1327-1332 (2008).
- 53 Chambers, H. Community-associated MRSA--resistance and virulence converge. *N Engl J Med* **352**, 1485-1487 (2005).
- 54 Liu, C. *et al.* Clinical practice guidelines by the infectious diseases society of america for the treatment of methicillin-resistant *Staphylococcus aureus* infections in adults and children: executive summary. *Clin Infect Dis* **52**, 285-292, doi:10.1093/cid/cir034 (2011).
- 55 van Wageningen, A. M. *et al.* Sequencing and analysis of genes involved in the biosynthesis of a vancomycin group antibiotic. *Chem Biol* **5**, 155-162 (1998).
- 56 Hiramatsu, K. *et al.* Dissemination in Japanese hospitals of strains of *Staphylococcus aureus* heterogeneously resistant to vancomycin. *Lancet* **350**, 1670-1673 (1997).
- 57 CDC. *Staphylococcus aureus* resistant to vancomycin--United States, 2002. *MMWR Morb Mortal Wkly Rep* **51**, 565-567 (2002).
- 58 Bishburg, E. & Bishburg, K. Minocycline--an old drug for a new century: emphasis on methicillin-resistant *Staphylococcus aureus* (MRSA) and *Acinetobacter baumannii*. *Int J Antimicrob Agents* **34**, 395-401 (2009).
- 59 Gales, A. *et al.* Emergence of linezolid-resistant *Staphylococcus aureus* during treatment of pulmonary infection in a patient with cystic fibrosis. *Int J Antimicrob Agents* **27**, 300-302 (2006).
- 60 Hirschwerk, D., Ginocchio, C., Bythrow, M. & Condon, S. Diminished susceptibility to daptomycin accompanied by clinical failure in a patient with methicillin-resistant *Staphylococcus aureus* bacteremia. *Infect Control Hosp Epidemiol* **27**, 315-317 (2006).
- 61 Pader, V. *et al.* *Staphylococcus aureus* inactivates daptomycin by releasing membrane phospholipids. *Nat Microbiol* **2**, 16194, doi:10.1038/nmicrobiol.2016.194 (2016).
- 62 Ling, L. L. *et al.* A new antibiotic kills pathogens without detectable resistance. *Nature* **517**, 455-459, doi:10.1038/nature14098 (2015).
- 63 Fernandes, P. Antibacterial discovery and development--the failure of success? *Nat Biotechnol* **24**, 1497-1503, doi:10.1038/nbt1206-1497 (2006).

- 64 Fernandes, P. & Martens, E. Antibiotics in late clinical development. *Biochem Pharmacol* **133**, 152-163, doi:10.1016/j.bcp.2016.09.025 (2017).
- 65 Zhanel, G. G., Walkty, A. J. & Karlowsky, J. A. Fidaxomicin: A novel agent for the treatment of *Clostridium difficile* infection. *Can J Infect Dis Med Microbiol* **26**, 305-312 (2015).
- 66 Zhanel, G. G. *et al.* New lipoglycopeptides: a comparative review of dalbavancin, oritavancin and telavancin. *Drugs* **70**, 859-886, doi:10.2165/11534440-000000000-00000 (2010).
- 67 Lapuebla, A. *et al.* Activity of Imipenem with Relebactam against Gram-Negative Pathogens from New York City. *Antimicrob Agents Chemother* **59**, 5029-5031, doi:10.1128/AAC.00830-15 (2015).
- 68 Fernandes, P., Martens, E., Bertrand, D. & Pereira, D. The solithromycin journey-It is all in the chemistry. *Bioorg Med Chem* **24**, 6420-6428, doi:10.1016/j.bmc.2016.08.035 (2016).
- 69 Kim, E. J., Shin, W. H., Kim, K. S. & Han, S. S. Safety pharmacology of DW-224a, a novel fluoroquinolone antibiotic agent. *Drug Chem Toxicol* **27**, 295-307, doi:10.1081/DCT-200039708 (2004).
- 70 Li, C. R. *et al.* *In vivo* antibacterial activity of MRX-I, a new oxazolidinone. *Antimicrob Agents Chemother* **58**, 2418-2421, doi:10.1128/AAC.01526-13 (2014).
- 71 Pucci, M. J. & Bush, K. Investigational antimicrobial agents of 2013. *Clin Microbiol Rev* **26**, 792-821, doi:10.1128/CMR.00033-13 (2013).
- 72 Höltje, J. & Heidrich, C. Enzymology of elongation and constriction of the murein sacculus of *Escherichia coli*. *Biochimie* **83**, 103-108 (2001).
- 73 Nanninga, N. Morphogenesis of *Escherichia coli*. *Microbiol Mol Biol Rev* **62**, 110-129 (1998).
- 74 Vollmer, W., Blanot, D. & de Pedro, M. Peptidoglycan structure and architecture. *FEMS Microbiol Rev* **32**, 149-167 (2008).
- 75 Glauner, B., Höltje, J. & Schwarz, U. The composition of the murein of *Escherichia coli*. *J Biol Chem* **263**, 10088-10095 (1988).
- 76 Navarre, W. & Schneewind, O. Surface proteins of gram-positive bacteria and mechanisms of their targeting to the cell wall envelope. *Microbiol Mol Biol Rev* **63**, 174-229 (1999).
- 77 Boneca, I. G., Huang, Z. H., Gage, D. A. & Tomasz, A. Characterization of *Staphylococcus aureus* cell wall glycan strands, evidence for a new beta-N-acetylglucosaminidase activity. *J Biol Chem* **275**, 9910-9918 (2000).
- 78 Atrih, A., Bacher, G., Allmaier, G., Williamson, M. P. & Foster, S. J. Analysis of peptidoglycan structure from vegetative cells of *Bacillus subtilis* 168 and role of PBP 5 in peptidoglycan maturation. *J Bacteriol* **181**, 3956-3966 (1999).
- 79 Schleifer, K. & Kandler, O. Peptidoglycan types of bacterial cell walls and their taxonomic implications. *Bacteriol Rev* **36**, 407-477 (1972).
- 80 Swenson, J. & Neuhaus, F. Biosynthesis of peptidoglycan in *Staphylococcus aureus*: incorporation of the Nepsilon-Ala-Lys moiety into the peptide subunit of nascent peptidoglycan. *J Bacteriol* **125**, 626-634 (1976).
- 81 Maillard, A. *et al.* Structure-based site-directed mutagenesis of the UDP-MurNAC-pentapeptide-binding cavity of the FemX alanyl transferase from *Weissella viridescens*. *J Bacteriol* **187**, 3833-3838 (2005).

- 82 Bouhss, A., Trunkfield, A. E., Bugg, T. D. & Mengin-Lecreux, D. The biosynthesis of peptidoglycan lipid-linked intermediates. *FEMS Microbiol Rev* **32**, 208-233, doi:10.1111/j.1574-6976.2007.00089.x (2008).
- 83 Filipe, S., Severina, E. & Tomasz, A. The role of *murMN* operon in penicillin resistance and antibiotic tolerance of *Streptococcus pneumoniae*. *Microb Drug Resist* **7**, 303-316 (2001).
- 84 Lapidot, A. & Irving, C. Dynamic structure of whole cells probed by nuclear Overhauser enhanced nitrogen-15 nuclear magnetic resonance spectroscopy. *Proc Natl Acad Sci U S A* **74**, 1988-1992 (1977).
- 85 Lapidot, A. & Irving, C. Comparative in vivo nitrogen-15 nuclear magnetic resonance study of the cell wall components of five Gram-positive bacteria. *Biochemistry* **18**, 704-714 (1979).
- 86 Hayhurst, E. J., Kailas, L., Hobbs, J. K. & Foster, S. J. Cell wall peptidoglycan architecture in *Bacillus subtilis*. *Proc Natl Acad Sci U S A* **105**, 14603-14608, doi:10.1073/pnas.0804138105 (2008).
- 87 Koch, A. L. Orientation of the peptidoglycan chains in the sacculus of *Escherichia coli*. *Res Microbiol* **149**, 689-701 (1998).
- 88 Koch, A. L. Length distribution of the peptidoglycan chains in the sacculus of *Escherichia coli*. *J Theor Biol* **204**, 533-541, doi:10.1006/jtbi.2000.2039 (2000).
- 89 Dmitriev, B. *et al.* Tertiary structure of bacterial murein: the scaffold model. *J Bacteriol* **185**, 3458-3468 (2003).
- 90 Dmitriev, B., Toukach, F., Holst, O., Rietschel, E. & Ehlers, S. Tertiary structure of *Staphylococcus aureus* cell wall murein. *J Bacteriol* **186**, 7141-7148 (2004).
- 91 Vollmer, W. & Höltje, J. The architecture of the murein (peptidoglycan) in gram-negative bacteria: vertical scaffold or horizontal layer(s)? *J Bacteriol* **186**, 5978-5987 (2004).
- 92 Gan, L., Chen, S. & Jensen, G. Molecular organization of Gram-negative peptidoglycan. *Proc Natl Acad Sci U S A* **105**, 18953-18957 (2008).
- 93 Turner, R. D., Hurd, A. F., Cadby, A., Hobbs, J. K. & Foster, S. J. Cell wall elongation mode in Gram-negative bacteria is determined by peptidoglycan architecture. *Nat Commun* **4**, 1496, doi:10.1038/ncomms2503 (2013).
- 94 Kim, S. J., Singh, M., Preobrazhenskaya, M. & Schaefer, J. *Staphylococcus aureus* peptidoglycan stem packing by rotational-echo double resonance NMR spectroscopy. *Biochemistry* **52**, 3651-3659, doi:10.1021/bi4005039 (2013).
- 95 Kim, S. J., Chang, J. & Singh, M. Peptidoglycan architecture of Gram-positive bacteria by solid-state NMR. *Biochim Biophys Acta* **1848**, 350-362, doi:10.1016/j.bbamem.2014.05.031 (2015).
- 96 Monteiro, J. M. *et al.* Peptidoglycan synthesis drives an FtsZ-treadmilling-independent step of cytokinesis. *Nature*, doi:10.1038/nature25506 (2018).
- 97 van Heijenoort, J. Assembly of the monomer unit of bacterial peptidoglycan. *Cell Mol Life Sci* **54**, 300-304 (1998).
- 98 Rogers, H. J., Perkins, H. R. & Ward, J. B. *Microbial cell walls and membranes*. (Chapman and Hall, 1980).
- 99 Eschenburg, S., Kabsch, W., Healy, M. & Schonbrunn, E. A new view of the mechanisms of UDP-N-acetylglucosamine enolpyruvyl transferase (MurA)



- and 5-enolpyruvylshikimate-3-phosphate synthase (AroA) derived from X-ray structures of their tetrahedral reaction intermediate states. *J Biol Chem* **278**, 49215-49222 (2003).
- 100 Skarzynski, T. *et al.* Structure of UDP-N-acetylglucosamine enolpyruvyl transferase, an enzyme essential for the synthesis of bacterial peptidoglycan, complexed with substrate UDP-N-acetylglucosamine and the drug fosfomycin. *Structure* **4**, 1465-1474 (1996).
- 101 Munoz, E., Ghuysen, J. & Heymann, H. Cell walls of *Streptococcus pyogenes*, type 14. C polysaccharide-peptidoglycan and G polysaccharide-peptidoglycan complexes. *Biochemistry* **6**, 3659-3670 (1967).
- 102 Tipper, D., Strominger, J. & Ensign, J. Structure of the cell wall of *Staphylococcus aureus*, strain Copenhagen. VII. Mode of action of the bacteriolytic peptidase from Myxobacter and the isolation of intact cell wall polysaccharides. *Biochemistry* **6**, 906-920 (1967).
- 103 Tipper, D., Katz, W., Strominger, J. & Ghuysen, J. Substituents on the alpha-carboxyl group of D-glutamic acid in the peptidoglycan of several bacterial cell walls. *Biochemistry* **6**, 921-929 (1967).
- 104 Nathenson, S. G., Strominger, J. L. & Ito, E. Enzymatic synthesis of the peptide in bacterial uridine nucleotides. iv. purification and properties of D-glutamic acid-adding enzyme. *J Biol Chem* **239**, 1773-1776 (1964).
- 105 Ito, E. & Strominger, J. L. Enzymatic synthesis of the peptide in bacterial uridine nucleotides. VII. Comparative biochemistry. *J Biol Chem* **248**, 3131-3136 (1973).
- 106 Swenson, J. & Neuhaus, F. Biosynthesis of peptidoglycan in *Staphylococcus aureus*: incorporation of the Nepsilon-Ala-Lys moiety into the peptide subunit of nascent peptidoglycan. *J Bacteriol* **125**, 626-634 (1976).
- 107 Skarzynski, T. *et al.* Structure of UDP-N-acetylglucosamine enolpyruvyl transferase, an enzyme essential for the synthesis of bacterial peptidoglycan, complexed with substrate UDP-N-acetylglucosamine and the drug fosfomycin. *Structure* **4**, 1465-1474 (1996).
- 108 Lambert, M. P. & Neuhaus, F. C. Mechanism of D-cycloserine action: alanine racemase from *Escherichia coli* W. *J Bacteriol* **110**, 978-987 (1972).
- 109 Prosser, G. A. & de Carvalho, L. P. Reinterpreting the mechanism of inhibition of *Mycobacterium tuberculosis* D-alanine:D-alanine ligase by D-cycloserine. *Biochemistry* **52**, 7145-7149, doi:10.1021/bi400839f (2013).
- 110 Ikeda, M., Wachi, M., Jung, H., Ishino, F. & Matsushashi, M. The *Escherichia coli mraY* gene encoding UDP-N-acetylmuramoyl-pentapeptide: undecaprenyl-phosphate phospho-N-acetylmuramoyl-pentapeptide transferase. *J Bacteriol* **173**, 1021-1026 (1991).
- 111 Mengin-Lecreux, D., Texier, L., Rousseau, M. & van Heijenoort, J. The *murG* gene of *Escherichia coli* codes for the UDP-N-acetylglucosamine: N-acetylmuramyl-(pentapeptide) pyrophosphoryl-undecaprenol N-acetylglucosamine transferase involved in the membrane steps of peptidoglycan synthesis. *J Bacteriol* **173**, 4625-4636 (1991).

- 112 Kopp, U., Roos, M., Wecke, J. & Labischinski, H. Staphylococcal peptidoglycan interpeptide bridge biosynthesis: a novel antistaphylococcal target? *Microb Drug Resist* **2**, 29-41 (1996).
- 113 Berger-Bächli, B., Strässle, A., Gustafson, J. & Kayser, F. Mapping and characterization of multiple chromosomal factors involved in methicillin resistance in *Staphylococcus aureus*. *Antimicrob Agents Chemother* **36**, 1367-1373 (1992).
- 114 Berger-Bächli, B. & Tschierske, M. Role of fem factors in methicillin resistance. *Drug Resist Updat* **1**, 325-335 (1998).
- 115 Schneider, T. *et al.* In vitro assembly of a complete, pentaglycine interpeptide bridge containing cell wall precursor (lipid II-Gly5) of *Staphylococcus aureus*. *Mol Microbiol* **53**, 675-685 (2004).
- 116 Ehlert, K., Schröder, W. & Labischinski, H. Specificities of FemA and FemB for different glycine residues: FemB cannot substitute for FemA in staphylococcal peptidoglycan pentaglycine side chain formation. *J Bacteriol* **179**, 7573-7576 (1997).
- 117 Rohrer, S., Ehlert, K., Tschierske, M., Labischinski, H. & Berger-Bächli, B. The essential *Staphylococcus aureus* gene *fmhB* is involved in the first step of peptidoglycan pentaglycine interpeptide formation. *Proc Natl Acad Sci U S A* **96**, 9351-9356 (1999).
- 118 Münch, D. *et al.* Identification and *in vitro* analysis of the GatD/MurT enzyme-complex catalyzing lipid II amidation in *Staphylococcus aureus*. *PLoS Pathog* **8**, e1002509, doi:10.1371/journal.ppat.1002509 (2012).
- 119 Figueiredo, T. A. *et al.* Identification of genetic determinants and enzymes involved with the amidation of glutamic acid residues in the peptidoglycan of *Staphylococcus aureus*. *PLoS Pathog* **8**, e1002508, doi:10.1371/journal.ppat.1002508 (2012).
- 120 Sham, L. T. *et al.* Bacterial cell wall. MurJ is the flippase of lipid-linked precursors for peptidoglycan biogenesis. *Science* **345**, 220-222, doi:10.1126/science.1254522 (2014).
- 121 Meeske, A. J. *et al.* MurJ and a novel lipid II flippase are required for cell wall biogenesis in *Bacillus subtilis*. *Proc Natl Acad Sci U S A* **112**, 6437-6442, doi:10.1073/pnas.1504967112 (2015).
- 122 Ruiz, N. Bioinformatics identification of MurJ (MviN) as the peptidoglycan lipid II flippase in *Escherichia coli*. *Proc Natl Acad Sci U S A* **105**, 15553-15557 (2008).
- 123 Mohammadi, T. *et al.* Identification of FtsW as a transporter of lipid-linked cell wall precursors across the membrane. *EMBO J* **30**, 1425-1432, doi:10.1038/emboj.2011.61 (2011).
- 124 Mohammadi, T. *et al.* Specificity of the transport of lipid II by FtsW in *Escherichia coli*. *J Biol Chem* **289**, 14707-14718, doi:10.1074/jbc.M114.557371 (2014).
- 125 Meeske, A. J. *et al.* SEDS proteins are a widespread family of bacterial cell wall polymerases. *Nature* **537**, 634-638, doi:10.1038/nature19331 (2016).

- 126 Hakulinen, J. K. *et al.* MraY-antibiotic complex reveals details of  
tunicamycin mode of action. *Nat Chem Biol* **13**, 265-267,  
doi:10.1038/nchembio.2270 (2017).
- 127 Brandish, P. E. *et al.* Modes of action of tunicamycin, liposidomycin B, and  
mureidomycin A: inhibition of phospho-N-acetylmuramyl-pentapeptide  
translocase from *Escherichia coli*. *Antimicrob Agents Chemother* **40**, 1640-1644  
(1996).
- 128 Stone, K. J. & Strominger, J. L. Mechanism of action of bacitracin:  
complexation with metal ion and C 55 -isoprenyl pyrophosphate. *Proc Natl  
Acad Sci U S A* **68**, 3223-3227 (1971).
- 129 Mann, P. A. *et al.* Murgocil is a highly bioactive staphylococcal-specific  
inhibitor of the peptidoglycan glycosyltransferase enzyme MurG. *ACS Chem  
Biol* **8**, 2442-2451, doi:10.1021/cb400487f (2013).
- 130 Koyama, N. *et al.* The nonantibiotic small molecule cyslabdan enhances the  
potency of  $\beta$ -lactams against MRSA by inhibiting pentaglycine interpeptide  
bridge synthesis. *PLoS One* **7**, e48981, doi:10.1371/journal.pone.0048981  
(2012).
- 131 Huber, J. *et al.* Chemical genetic identification of peptidoglycan inhibitors  
potentiating carbapenem activity against methicillin-resistant *Staphylococcus  
aureus*. *Chem Biol* **16**, 837-848, doi:10.1016/j.chembiol.2009.05.012 (2009).
- 132 Lee, W. *et al.* The Mechanism of Action of Lysobactin. *J Am Chem Soc* **138**,  
100-103, doi:10.1021/jacs.5b11807 (2016).
- 133 Lovering, A. L., de Castro, L. H., Lim, D. & Strynadka, N. C. Structural  
insight into the transglycosylation step of bacterial cell-wall biosynthesis.  
*Science* **315**, 1402-1405, doi:10.1126/science.1136611 (2007).
- 134 Goffin, C. & Ghuysen, J. M. Multimodular penicillin-binding proteins: an  
enigmatic family of orthologs and paralogs. *Microbiol Mol Biol Rev* **62**, 1079-  
1093 (1998).
- 135 Heaslet, H., Shaw, B., Mistry, A. & Miller, A. A. Characterization of the  
active site of *S. aureus* monofunctional glycosyltransferase (Mtg) by site-  
directed mutation and structural analysis of the protein complexed with  
moenomycin. *J Struct Biol* **167**, 129-135, doi:10.1016/j.jsb.2009.04.010 (2009).
- 136 Fuda, C., Fisher, J. & Mobashery, S. Beta-lactam resistance in *Staphylococcus  
aureus*: the adaptive resistance of a plastic genome. *Cell Mol Life Sci* **62**, 2617-  
2633 (2005).
- 137 Waxman, D. & Strominger, J. Penicillin-binding proteins and the  
mechanism of action of beta-lactam antibiotics. *Annu Rev Biochem* **52**, 825-  
869 (1983).
- 138 Pootoolal, J., Neu, J. & Wright, G. Glycopeptide antibiotic resistance. *Annu  
Rev Pharmacol Toxicol* **42**, 381-408 (2002).
- 139 Sauvage, E., Kerff, F., Terrak, M., Ayala, J. A. & Charlier, P. The penicillin-  
binding proteins: structure and role in peptidoglycan biosynthesis. *FEMS  
Microbiol Rev* **32**, 234-258, doi:10.1111/j.1574-6976.2008.00105.x (2008).
- 140 Scheffers, D. J. & Pinho, M. G. Bacterial cell wall synthesis: New insights  
from localisation studies. *Microbiol. Mol. Biol. Rev.* **69**, 585-607,  
doi:10.1128/MMBR.69.4.585-607.2005 (2005).

- 141 Wada, A. & Watanabe, H. Penicillin-binding protein 1 of *Staphylococcus aureus* is essential for growth. *J Bacteriol* **180**, 2759-2765 (1998).
- 142 Pereira, S. F., Henriques, A. O., Pinho, M. G., de Lencastre, H. & Tomasz, A. Role of PBP1 in cell division of *Staphylococcus aureus*. *J. Bacteriol.* **189**, 3525-3531, doi:10.1128/JB.00044-07 (2007).
- 143 Reed, P. *et al.* *Staphylococcus aureus* Survives with a Minimal Peptidoglycan Synthesis Machine but Sacrifices Virulence and Antibiotic Resistance. *PLoS Pathog* **11**, e1004891, doi:10.1371/journal.ppat.1004891 (2015).
- 144 de Jonge, B. & Tomasz, A. Abnormal peptidoglycan produced in a methicillin-resistant strain of *Staphylococcus aureus* grown in the presence of methicillin: functional role for penicillin-binding protein 2A in cell wall synthesis. *Antimicrob Agents Chemother* **37**, 342-346 (1992).
- 145 Murakami, K., Fujimura, T. & Doi, M. Nucleotide sequence of the structural gene for the penicillin-binding protein 2 of *Staphylococcus aureus* and the presence of a homologous gene in other staphylococci. *FEMS Microbiol Lett* **117**, 131-136 (1994).
- 146 Leski, T. A. & Tomasz, A. Role of penicillin-binding protein 2 (PBP2) in the antibiotic susceptibility and cell wall cross-linking of *Staphylococcus aureus*: evidence for the cooperative functioning of PBP2, PBP4, and PBP2A. *J. Bacteriol.* **187**, 1815-1824, doi:10.1128/JB.187.5.1815-1824.2005 (2005).
- 147 Pinho, M. G. & Errington, J. Recruitment of penicillin-binding protein PBP2 to the division site of *Staphylococcus aureus* is dependent on its transpeptidation substrates. *Mol. Microbiol.* **55**, 799-807, doi:10.1111/j.1365-2958.2004.04420.x (2005).
- 148 Pinho, M. G., de Lencastre, H. & Tomasz, A. Cloning, characterization, and inactivation of the gene *pbpC*, encoding penicillin-binding protein 3 of *Staphylococcus aureus*. *J Bacteriol* **182**, 1074-1079 (2000).
- 149 Wyke, A. W., Ward, J. B., Hayes, M. V. & Curtis, N. A. A role in vivo for penicillin-binding protein-4 of *Staphylococcus aureus*. *Eur J Biochem* **119**, 389-393 (1981).
- 150 Loskill, P. *et al.* Reduction of the peptidoglycan crosslinking causes a decrease in stiffness of the *Staphylococcus aureus* cell envelope. *Biophys J* **107**, 1082-1089, doi:10.1016/j.bpj.2014.07.029 (2014).
- 151 Memmi, G., Filipe, S., Pinho, M., Fu, Z. & Cheung, A. *Staphylococcus aureus* PBP4 Is Essential for beta-Lactam Resistance in Community-Acquired Methicillin-Resistant Strains. *Antimicrob. Agents. Chemother.* **52**, 3955-3966, doi:10.1128/AAC.00049-08 (2008).
- 152 Atilano, M. *et al.* Teichoic acids are temporal and spatial regulators of peptidoglycan cross-linking in *Staphylococcus aureus*. *Proc. Natl. Acad. Sci. U S A* **107**, 18991-18996, doi:10.1073/pnas.1004304107 (2010).
- 153 Pinho, M., de Lencastre, H. & Tomasz, A. An acquired and a native penicillin-binding protein cooperate in building the cell wall of drug-resistant staphylococci. *Proc Natl Acad Sci U S A* **98**, 10886-10891 (2001).
- 154 Pinho, M. G., Filipe, S. R., de Lencastre, H. & al., e. Complementation of the essential peptidoglycan transpeptidase function of penicillin-binding protein 2 (PBP2) by the drug resistance protein PBP2A in *Staphylococcus*

- aureus*. *J. Bacteriol.* **183**, 6525-6531, doi:10.1128/jb.183.22.6525-6531.2001 (2001).
- 155 Vollmer, W., Joris, B., Charlier, P. & Foster, S. Bacterial peptidoglycan (murein) hydrolases. *FEMS Microbiol Rev* **32**, 259-286, doi:10.1111/j.1574-6976.2007.00099.x (2008).
- 156 Weidel, W. & Pelzer, H. Bagshaped macromolecules--a new outlook on bacterial cell walls. *Adv Enzymol Relat Subj Biochem* **26**, 193-232 (1964).
- 157 Shockman, G. D., Daneo-Moore, L., Kariyama, R. & Massidda, O. Bacterial walls, peptidoglycan hydrolases, autolysins, and autolysis. *Microb Drug Resist* **2**, 95-98, doi:10.1089/mdr.1996.2.95 (1996).
- 158 Pooley, H. M. Turnover and spreading of old wall during surface growth of *Bacillus subtilis*. *J Bacteriol* **125**, 1127-1138 (1976).
- 159 Goodell, E. W. & Schwarz, U. Cleavage and resynthesis of peptide cross bridges in *Escherichia coli* murein. *J Bacteriol* **156**, 136-140 (1983).
- 160 Höltje, J. V. Molecular interplay of murein synthases and murein hydrolases in *Escherichia coli*. *Microb Drug Resist* **2**, 99-103 (1996).
- 161 Pooley, H. M. & Shockman, G. D. Relationship between the location of autolysin, cell wall synthesis, and the development of resistance to cellular autolysis in *Streptococcus faecalis* after inhibition of protein synthesis. *J Bacteriol* **103**, 457-466 (1970).
- 162 Koch, A. L. & Doyle, R. J. Inside-to-outside growth and turnover of the wall of gram-positive rods. *J Theor Biol* **117**, 137-157 (1985).
- 163 Oshida, T. *et al.* A *Staphylococcus aureus* autolysin that has an N-acetylmuramoyl-L-alanine amidase domain and an endo-beta-N-acetylglucosaminidase domain: cloning, sequence analysis, and characterization. *Proc. Natl. Acad. Sci. U S A* **92**, 285-289 (1995).
- 164 Sugai, M. *et al.* Identification of endo-beta-N-acetylglucosaminidase and N-acetylmuramyl-L-alanine amidase as cluster-dispersing enzymes in *Staphylococcus aureus*. *J. Bacteriol.* **177**, 1491-1496 (1995).
- 165 Oshida, T. & Tomasz, A. Isolation and characterization of a *Tn551*-autolysis mutant of *Staphylococcus aureus*. *J Bacteriol* **174**, 4952-4959 (1992).
- 166 Baba, T. & Schneewind, O. Targeting of muralytic enzymes to the cell division site of Gram-positive bacteria: repeat domains direct autolysin to the equatorial surface ring of *Staphylococcus aureus*. *EMBO J* **17**, 4639-4646, doi:10.1093/emboj/17.16.4639 (1998).
- 167 Sugai, M. *et al.* Localized perforation of the cell wall by a major autolysin: atl gene products and the onset of penicillin-induced lysis of *Staphylococcus aureus*. *J Bacteriol* **179**, 2958-2962 (1997).
- 168 Schlag, M. *et al.* Role of staphylococcal wall teichoic acid in targeting the major autolysin Atl. *Mol Microbiol* **75**, 864-873, doi:10.1111/j.1365-2958.2009.07007.x (2010).
- 169 García, P., González, M. P., García, E., López, R. & García, J. L. LytB, a novel pneumococcal murein hydrolase essential for cell separation. *Mol Microbiol* **31**, 1275-1281 (1999).
- 170 Heidrich, C., Ursinus, A., Berger, J., Schwarz, H. & Höltje, J. V. Effects of multiple deletions of murein hydrolases on viability, septum cleavage, and

- sensitivity to large toxic molecules in *Escherichia coli*. *J Bacteriol* **184**, 6093-6099 (2002).
- 171 Garcia, D. L. & Dillard, J. P. AmiC functions as an N-acetylmuramyl-L-alanine amidase necessary for cell separation and can promote autolysis in *Neisseria gonorrhoeae*. *J Bacteriol* **188**, 7211-7221, doi:10.1128/JB.00724-06 (2006).
- 172 Klöckner, A. *et al.* AmiA is a penicillin target enzyme with dual activity in the intracellular pathogen *Chlamydia pneumoniae*. *Nat Commun* **5**, 4201, doi:10.1038/ncomms5201 (2014).
- 173 Egan, A. J. & Vollmer, W. The physiology of bacterial cell division. *Ann N Y Acad Sci* **1277**, 8-28, doi:10.1111/j.1749-6632.2012.06818.x (2013).
- 174 Tamames, J., González-Moreno, M., Mingorance, J., Valencia, A. & Vicente, M. Bringing gene order into bacterial shape. *Trends Genet* **17**, 124-126 (2001).
- 175 Haeusser, D. P. & Margolin, W. Splitsville: structural and functional insights into the dynamic bacterial Z ring. *Nat Rev Microbiol* **14**, 305-319, doi:10.1038/nrmicro.2016.26 (2016).
- 176 Erickson, H. P. & Osawa, M. Cell division without FtsZ--a variety of redundant mechanisms. *Mol Microbiol* **78**, 267-270 (2010).
- 177 Kalman, S. *et al.* Comparative genomes of *Chlamydia pneumoniae* and *C. trachomatis*. *Nat Genet* **21**, 385-389, doi:10.1038/7716 (1999).
- 178 Pilhofer, M. *et al.* Characterization and evolution of cell division and cell wall synthesis genes in the bacterial phyla Verrucomicrobia, Lentisphaerae, Chlamydiae, and Planctomycetes and phylogenetic comparison with rRNA genes. *J Bacteriol* **190**, 3192-3202, doi:10.1128/JB.01797-07 (2008).
- 179 Lindås, A. C., Karlsson, E. A., Lindgren, M. T., Ettema, T. J. & Bernander, R. A unique cell division machinery in the Archaea. *Proc Natl Acad Sci U S A* **105**, 18942-18946, doi:10.1073/pnas.0809467105 (2008).
- 180 den Blaauwen, T., Hamoen, L. W. & Levin, P. A. The divisome at 25: the road ahead. *Curr Opin Microbiol* **36**, 85-94, doi:10.1016/j.mib.2017.01.007 (2017).
- 181 Sang, Y., Tao, J. & Yao, Y. [Regulation of the Z ring positioning in bacterial cell division--a review]. *Wei Sheng Wu Xue Bao* **53**, 321-327 (2013).
- 182 Wu, L. J. & Errington, J. Nucleoid occlusion and bacterial cell division. *Nat Rev Microbiol* **10**, 8-12, doi:10.1038/nrmicro2671 (2011).
- 183 Raskin, D. M. & de Boer, P. A. Rapid pole-to-pole oscillation of a protein required for directing division to the middle of *Escherichia coli*. *Proc Natl Acad Sci U S A* **96**, 4971-4976 (1999).
- 184 Woldringh, C. L., Mulder, E., Huls, P. G. & Vischer, N. Toporegulation of bacterial division according to the nucleoid occlusion model. *Res Microbiol* **142**, 309-320 (1991).
- 185 Veiga, H., Jorge, A. M. & Pinho, M. G. Absence of nucleoid occlusion effector Noc impairs formation of orthogonal FtsZ rings during *Staphylococcus aureus* cell division. *Mol. Microbiol.* **80**, 1366-1380, doi:10.1111/j.1365-2958.2011.07651.x (2011).

- 186 Wu, L. J. & Errington, J. Coordination of cell division and chromosome segregation by a nucleoid occlusion protein in *Bacillus subtilis*. *Cell* **117**, 915-925, doi:10.1016/j.cell.2004.06.002 (2004).
- 187 Bernhardt, T. G. & de Boer, P. A. SlmA, a nucleoid-associated, FtsZ binding protein required for blocking septal ring assembly over Chromosomes in *E. coli*. *Mol Cell* **18**, 555-564, doi:10.1016/j.molcel.2005.04.012 (2005).
- 188 Wu, L. J. *et al.* Noc protein binds to specific DNA sequences to coordinate cell division with chromosome segregation. *EMBO J* **28**, 1940-1952, doi:10.1038/emboj.2009.144 (2009).
- 189 Tonthat, N. K. *et al.* Molecular mechanism by which the nucleoid occlusion factor, SlmA, keeps cytokinesis in check. *EMBO J* **30**, 154-164, doi:10.1038/emboj.2010.288 (2011).
- 190 Fleurie, A. *et al.* MapZ marks the division sites and positions FtsZ rings in *Streptococcus pneumoniae*. *Nature* **516**, 259-262, doi:10.1038/nature13966 (2014).
- 191 Willemse, J., Borst, J. W., de Waal, E., Bisseling, T. & van Wezel, G. P. Positive control of cell division: FtsZ is recruited by SsgB during sporulation of *Streptomyces*. *Genes Dev* **25**, 89-99, doi:10.1101/gad.600211 (2011).
- 192 Tzagoloff, H. & Novick, R. Geometry of cell division in *Staphylococcus aureus*. *J. Bacteriol.* **129**, 343-350 (1977).
- 193 Monahan, L. G., Liew, A. T., Bottomley, A. L. & Harry, E. J. Division site positioning in bacteria: one size does not fit all. *Front Microbiol* **5**, 19, doi:10.3389/fmicb.2014.00019 (2014).
- 194 Jun, S. & Mulder, B. Entropy-driven spatial organization of highly confined polymers: lessons for the bacterial chromosome. *Proc Natl Acad Sci U S A* **103**, 12388-12393, doi:10.1073/pnas.0605305103 (2006).
- 195 Yamada, S. *et al.* An autolysin ring associated with cell separation of *Staphylococcus aureus*. *J. Bacteriol.* **178**, 1565-1571 (1996).
- 196 Turner, R. D. *et al.* Peptidoglycan architecture can specify division planes in *Staphylococcus aureus*. *Nat. Commun.* **1**, 26, doi:10.1038/ncomms1025 (2010).
- 197 Pichoff, S. & Lutkenhaus, J. Tethering the Z ring to the membrane through a conserved membrane targeting sequence in FtsA. *Mol Microbiol* **55**, 1722-1734, doi:10.1111/j.1365-2958.2005.04522.x (2005).
- 198 Pichoff, S., Shen, B., Sullivan, B. & Lutkenhaus, J. FtsA mutants impaired for self-interaction bypass ZipA suggesting a model in which FtsA's self-interaction competes with its ability to recruit downstream division proteins. *Mol Microbiol* **83**, 151-167, doi:10.1111/j.1365-2958.2011.07923.x (2012).
- 199 Szwedziak, P., Wang, Q., Freund, S. M. & Löwe, J. FtsA forms actin-like protofilaments. *EMBO J* **31**, 2249-2260, doi:10.1038/emboj.2012.76 (2012).
- 200 Loose, M. & Mitchison, T. J. The bacterial cell division proteins FtsA and FtsZ self-organize into dynamic cytoskeletal patterns. *Nat Cell Biol* **16**, 38-46, doi:10.1038/ncb2885 (2014).
- 201 Ishikawa, S., Kawai, Y., Hiramatsu, K., Kuwano, M. & Ogasawara, N. A new FtsZ-interacting protein, YlmF, complements the activity of FtsA

- during progression of cell division in *Bacillus subtilis*. *Mol Microbiol* **60**, 1364-1380, doi:10.1111/j.1365-2958.2006.05184.x (2006).
- 202 Levin, P. A., Kurtser, I. G. & Grossman, A. D. Identification and  
characterization of a negative regulator of FtsZ ring formation in *Bacillus*  
*subtilis*. *Proc Natl Acad Sci U S A* **96**, 9642-9647 (1999).
- 203 Jorge, A. M., Hoiczky, E., Gomes, J. P. & Pinho, M. G. EzrA contributes to  
the regulation of cell size in *Staphylococcus aureus*. *PLoS One* **6**, e27542,  
doi:10.1371/journal.pone.0027542 (2011).
- 204 Steele, V. R., Bottomley, A. L., Garcia-Lara, J., Kasturiarachchi, J. & Foster, S.  
J. Multiple essential roles for EzrA in cell division of *Staphylococcus aureus*.  
*Mol Microbiol* **80**, 542-555, doi:10.1111/j.1365-2958.2011.07591.x (2011).
- 205 Gueiros-Filho, F. J. & Losick, R. A widely conserved bacterial cell division  
protein that promotes assembly of the tubulin-like protein FtsZ. *Genes Dev*  
**16**, 2544-2556, doi:10.1101/gad.1014102 (2002).
- 206 Errington, J., Daniel, R. A. & Scheffers, D. J. Cytokinesis in bacteria.  
*Microbiol Mol Biol Rev* **67**, 52-65, doi:10.1128/MMBR.67.1.52-65.2003 (2003).
- 207 Gamba, P., Veening, J. W., Saunders, N. J., Hamoen, L. W. & Daniel, R. A.  
Two-step assembly dynamics of the *Bacillus subtilis* divisome. *J Bacteriol* **191**,  
4186-4194, doi:10.1128/JB.01758-08 (2009).
- 208 Daniel, R. A., Noirot-Gros, M. F., Noirot, P. & Errington, J. Multiple  
interactions between the transmembrane division proteins of *Bacillus subtilis*  
and the role of FtsL instability in divisome assembly. *J Bacteriol* **188**, 7396-  
7404, doi:10.1128/JB.01031-06 (2006).
- 209 Buddelmeijer, N. & Beckwith, J. A complex of the *Escherichia coli* cell  
division proteins FtsL, FtsB and FtsQ forms independently of its localisation  
to the septal region. *Mol Microbiol* **52**, 1315-1327, doi:10.1111/j.1365-  
2958.2004.04044.x (2004).
- 210 Daniel, R. A., Harry, E. J. & Errington, J. Role of penicillin-binding protein  
PBP 2B in assembly and functioning of the division machinery of *Bacillus*  
*subtilis*. *Mol Microbiol* **35**, 299-311 (2000).
- 211 Bottomley, A. L. *et al.* *Staphylococcus aureus* DivIB is a peptidoglycan-binding  
protein that is required for a morphological checkpoint in cell division. *Mol*  
*Microbiol*, doi:10.1111/mmi.12813 (2014).
- 212 Kaimer, C., González-Pastor, J. E. & Graumann, P. L. SpoIIIE and a novel  
type of DNA translocase, SftA, couple chromosome segregation with cell  
division in *Bacillus subtilis*. *Mol Microbiol* **74**, 810-825, doi:10.1111/j.1365-  
2958.2009.06894.x (2009).
- 213 Crozat, E., Rousseau, P., Fournes, F. & Cornet, F. The FtsK family of DNA  
translocases finds the ends of circles. *J Mol Microbiol Biotechnol* **24**, 396-408,  
doi:10.1159/000369213 (2014).
- 214 Bath, J., Wu, L. J., Errington, J. & Wang, J. C. Role of *Bacillus subtilis* SpoIIIE  
in DNA transport across the mother cell-prespore division septum. *Science*  
**290**, 995-997 (2000).
- 215 Möll, A. & Thanbichler, M. FtsN-like proteins are conserved components of  
the cell division machinery in proteobacteria. *Mol Microbiol* **72**, 1037-1053,  
doi:10.1111/j.1365-2958.2009.06706.x (2009).



- 216 Gerding, M. A., Ogata, Y., Pecora, N. D., Niki, H. & de Boer, P. A. The trans-  
envelope Tol-Pal complex is part of the cell division machinery and  
required for proper outer-membrane invagination during cell constriction in  
E. coli. *Mol Microbiol* **63**, 1008-1025, doi:10.1111/j.1365-2958.2006.05571.x  
(2007).
- 217 Bernhardt, T. G. & de Boer, P. A. The *Escherichia coli* amidase AmiC is a  
periplasmic septal ring component exported via the twin-arginine transport  
pathway. *Mol Microbiol* **48**, 1171-1182 (2003).
- 218 Müller, P. *et al.* The essential cell division protein FtsN interacts with the  
murein (peptidoglycan) synthase PBP1B in *Escherichia coli*. *J Biol Chem* **282**,  
36394-36402, doi:10.1074/jbc.M706390200 (2007).
- 219 Lutkenhaus, J. FtsN--trigger for septation. *J Bacteriol* **191**, 7381-7382,  
doi:10.1128/JB.01100-09 (2009).
- 220 Li, Z., Trimble, M. J., Brun, Y. V. & Jensen, G. J. The structure of FtsZ  
filaments in vivo suggests a force-generating role in cell division. *EMBO J*  
**26**, 4694-4708, doi:10.1038/sj.emboj.7601895 (2007).
- 221 Balasubramanian, M. K., Srinivasan, R., Huang, Y. & Ng, K. H. Comparing  
contractile apparatus-driven cytokinesis mechanisms across kingdoms.  
*Cytoskeleton (Hoboken)* **69**, 942-956, doi:10.1002/cm.21082 (2012).
- 222 Amir, A., Babaeipour, F., McIntosh, D. B., Nelson, D. R. & Jun, S. Bending  
forces plastically deform growing bacterial cell walls. *Proc Natl Acad Sci U S  
A* **111**, 5778-5783, doi:10.1073/pnas.1317497111 (2014).
- 223 Buss, J. *et al.* A multi-layered protein network stabilizes the *Escherichia coli*  
FtsZ-ring and modulates constriction dynamics. *PLoS Genet* **11**, e1005128,  
doi:10.1371/journal.pgen.1005128 (2015).
- 224 Bisson-Filho, A. W. *et al.* Treadmilling by FtsZ filaments drives  
peptidoglycan synthesis and bacterial cell division. *Science* **355**, 739-743,  
doi:10.1126/science.aak9973 (2017).
- 225 Yang, X. *et al.* GTPase activity-coupled treadmilling of the bacterial tubulin  
FtsZ organizes septal cell wall synthesis. *Science* **355**, 744-747,  
doi:10.1126/science.aak9995 (2017).
- 226 Coltharp, C. & Xiao, J. Beyond force generation: Why is a dynamic ring of  
FtsZ polymers essential for bacterial cytokinesis? *Bioessays* **39**, 1-11,  
doi:10.1002/bies.201600179 (2017).
- 227 Surovtsev, I. V., Morgan, J. J. & Lindahl, P. A. Kinetic modeling of the  
assembly, dynamic steady state, and contraction of the FtsZ ring in  
prokaryotic cytokinesis. *PLoS Comput Biol* **4**, e1000102,  
doi:10.1371/journal.pcbi.1000102 (2008).
- 228 Lan, G., Wolgemuth, C. W. & Sun, S. X. Z-ring force and cell shape during  
division in rod-like bacteria. *Proc Natl Acad Sci U S A* **104**, 16110-16115,  
doi:10.1073/pnas.0702925104 (2007).
- 229 Glauner, B. & Höltje, J. V. Growth pattern of the murein sacculus of  
*Escherichia coli*. *J Biol Chem* **265**, 18988-18996 (1990).
- 230 Young, K. D. The selective value of bacterial shape. *Microbiol Mol Biol Rev*  
**70**, 660-703, doi:10.1128/MMBR.00001-06 (2006).

- 231 Young, K. D. Bacterial shape: two-dimensional questions and possibilities. *Annu Rev Microbiol* **64**, 223-240, doi:10.1146/annurev.micro.112408.134102 (2010).
- 232 Höltje, J. V. Growth of the stress-bearing and shape-maintaining murein sacculus of *Escherichia coli*. *Microbiol Mol Biol Rev* **62**, 181-203 (1998).
- 233 Henriques, A., Glaser, P., Piggot, P. & Moran, C. J. Control of cell shape and elongation by the *rodA* gene in *Bacillus subtilis*. *Mol Microbiol* **28**, 235-247 (1998).
- 234 Tamaki, S., Matsuzawa, H. & Matsuhashi, M. Cluster of *mrdA* and *mrdB* genes responsible for the rod shape and mecillinam sensitivity of *Escherichia coli*. *J Bacteriol* **141**, 52-57 (1980).
- 235 Spratt, B. G. Distinct penicillin binding proteins involved in the division, elongation, and shape of *Escherichia coli* K12. *Proc Natl Acad Sci U S A* **72**, 2999-3003 (1975).
- 236 Pinho, M. G., Kjos, M. & Veening, J. W. How to get (a)round: mechanisms controlling growth and division of coccoid bacteria. *Nat Rev Microbiol* **11**, 601-614, doi:10.1038/nrmicro3088 (2013).
- 237 Pinho, M. & Errington, J. Dispersed mode of *Staphylococcus aureus* cell wall synthesis in the absence of the division machinery. *Mol Microbiol* **50**, 871-881, doi:10.1046/j.1365-2958.2003.03719.x (2003).
- 238 Kuru, E. *et al.* *In situ* probing of newly synthesized peptidoglycan in live bacteria with fluorescent D-amino acids. *Angew. Chem. Int Ed. Engl.* **51**, 12519-12523, doi:10.1002/anie.201206749 (2012).
- 239 Zapun, A., Vernet, T. & Pinho, M. G. The different shapes of cocci. *FEMS Microbiol Rev* **32**, 345-360, doi:10.1111/j.1574-6976.2007.00098.x (2008).
- 240 Morlot, C., Zapun, A., Dideberg, O. & Vernet, T. Growth and division of *Streptococcus pneumoniae*: localisation of the high molecular weight penicillin-binding proteins during the cell cycle. *Mol Microbiol* **50**, 845-855 (2003).
- 241 Tsui, H. T. *et al.* Pbp2x localizes separately from Pbp2b and other peptidoglycan synthesis proteins during later stages of cell division of *Streptococcus pneumoniae* D39. *Mol Microbiol* **94**, 21-40, doi:10.1111/mmi.12745 (2014).
- 242 Typas, A., Banzhaf, M., Gross, C. A. & Vollmer, W. From the regulation of peptidoglycan synthesis to bacterial growth and morphology. *Nat Rev Microbiol* **10**, 123-136, doi:10.1038/nrmicro2677 (2011).
- 243 den Blaauwen, T., de Pedro, M. A., Nguyen-Distèche, M. & Ayala, J. A. Morphogenesis of rod-shaped sacculi. *FEMS Microbiol Rev* **32**, 321-344, doi:10.1111/j.1574-6976.2007.00090.x (2008).
- 244 Garner, E. C. *et al.* Coupled, circumferential motions of the cell wall synthesis machinery and MreB filaments in *B. subtilis*. *Science* **333**, 222-225, doi:10.1126/science.1203285 (2011).
- 245 Domínguez-Escobar, J. *et al.* Processive movement of MreB-associated cell wall biosynthetic complexes in bacteria. *Science* **333**, 225-228, doi:10.1126/science.1203466 (2011).

- 246 van Teeffelen, S. *et al.* The bacterial actin MreB rotates, and rotation depends  
on cell-wall assembly. *Proc Natl Acad Sci U S A* **108**, 15822-15827,  
doi:10.1073/pnas.1108999108 (2011).
- 247 Kang, C. M. *et al.* The Mycobacterium tuberculosis serine/threonine kinases  
PknA and PknB: substrate identification and regulation of cell shape. *Genes  
Dev* **19**, 1692-1704, doi:10.1101/gad.1311105 (2005).
- 248 Absalon, C. *et al.* CpgA, EF-Tu and the stressosome protein YezB are  
substrates of the Ser/Thr kinase/phosphatase couple, PrkC/PrpC, in *Bacillus  
subtilis*. *Microbiology* **155**, 932-943, doi:10.1099/mic.0.022475-0 (2009).
- 249 Beltramini, A. M., Mukhopadhyay, C. D. & Pancholi, V. Modulation of cell  
wall structure and antimicrobial susceptibility by a *Staphylococcus aureus*  
eukaryote-like serine/threonine kinase and phosphatase. *Infect Immun* **77**,  
1406-1416, doi:10.1128/IAI.01499-08 (2009).
- 250 Hardt, P. *et al.* The cell wall precursor lipid II acts as a molecular signal for  
the Ser/Thr kinase PknB of *Staphylococcus aureus*. *Int J Med Microbiol* **307**, 1-  
10, doi:10.1016/j.ijmm.2016.12.001 (2017).
- 251 Beilharz, K. *et al.* Control of cell division in *Streptococcus pneumoniae* by the  
conserved Ser/Thr protein kinase StkP. *Proc Natl Acad Sci U S A* **109**, E905-  
913, doi:10.1073/pnas.1119172109 (2012).
- 252 Kim, J. S. & Sun, S. X. Morphology of *Caulobacter crescentus* and the  
Mechanical Role of Crescentin. *Biophys J* **96**, L47-49,  
doi:10.1016/j.bpj.2009.02.010 (2009).
- 253 Ausmees, N., Kuhn, J. R. & Jacobs-Wagner, C. The bacterial cytoskeleton: an  
intermediate filament-like function in cell shape. *Cell* **115**, 705-713 (2003).
- 254 Dye, N. A. & Shapiro, L. The push and pull of the bacterial cytoskeleton.  
*Trends Cell Biol* **17**, 239-245, doi:10.1016/j.tcb.2007.03.005 (2007).
- 255 Strobel, W., Möll, A., Kiekebusch, D., Klein, K. E. & Thanbichler, M.  
Function and localisation dynamics of bifunctional penicillin-binding  
proteins in *Caulobacter crescentus*. *J Bacteriol* **196**, 1627-1639,  
doi:10.1128/JB.01194-13 (2014).
- 256 Goley, E. D. *et al.* Assembly of the *Caulobacter* cell division machine. *Mol  
Microbiol* **80**, 1680-1698, doi:10.1111/j.1365-2958.2011.07677.x (2011).
- 257 Siefert, J. L. & Fox, G. E. Phylogenetic mapping of bacterial morphology.  
*Microbiology* **144 ( Pt 10)**, 2803-2808, doi:10.1099/00221287-144-10-2803 (1998).
- 258 Lange, R. & Hengge-Aronis, R. Growth phase-regulated expression of *bolA*  
and morphology of stationary-phase *Escherichia coli* cells are controlled by  
the novel sigma factor sigma S. *J Bacteriol* **173**, 4474-4481 (1991).
- 259 Santos, J. M., Freire, P., Vicente, M. & Arraiano, C. M. The stationary-phase  
morphogene *bolA* from *Escherichia coli* is induced by stress during early  
stages of growth. *Mol Microbiol* **32**, 789-798 (1999).
- 260 James, G. A., Korber, D. R., Caldwell, D. E. & Costerton, J. W. Digital image  
analysis of growth and starvation responses of a surface-colonizing  
*Acinetobacter* sp. *J Bacteriol* **177**, 907-915 (1995).
- 261 Leaver, M. & Errington, J. Roles for MreC and MreD proteins in helical  
growth of the cylindrical cell wall in *Bacillus subtilis*. *Mol Microbiol* **57**, 1196-  
1209, doi:10.1111/j.1365-2958.2005.04736.x (2005).

- 262 Kruse, T., Bork-Jensen, J. & Gerdes, K. The morphogenetic MreBCD proteins of *Escherichia coli* form an essential membrane-bound complex. *Mol Microbiol* **55**, 78-89, doi:10.1111/j.1365-2958.2004.04367.x (2005).
- 263 Dye, N. A., Pincus, Z., Theriot, J. A., Shapiro, L. & Gitai, Z. Two independent spiral structures control cell shape in *Caulobacter*. *Proc Natl Acad Sci U S A* **102**, 18608-18613, doi:10.1073/pnas.0507708102 (2005).
- 264 Tavares, A. C., Fernandes, P. B., Carballido-López, R. & Pinho, M. G. MreC and MreD Proteins Are Not Required for Growth of *Staphylococcus aureus*. *PLoS One* **10**, e0140523, doi:10.1371/journal.pone.0140523 (2015).
- 265 García-Lara, J. *et al.* Supramolecular structure in the membrane of *Staphylococcus aureus*. *Proc Natl Acad Sci U S A* **112**, 15725-15730, doi:10.1073/pnas.1509557112 (2015).
- 266 Marston, A. L., Thomaidis, H. B., Edwards, D. H., Sharpe, M. E. & Errington, J. Polar localisation of the MinD protein of *Bacillus subtilis* and its role in selection of the mid-cell division site. *Genes Dev* **12**, 3419-3430 (1998).
- 267 Pinho, M. & Errington, J. A *divIVA* null mutant of *Staphylococcus aureus* undergoes normal cell division. *FEMS Microbiol Lett* **240**, 145-149 (2004).

# Chapter II

---

Cell shape dynamics during the  
staphylococcal cell cycle

### Author contributions

J. M. Monteiro and P.B. Fernandes performed all experiments shown, except SEM imaging of *S. aureus*, which was done by A. C. Tavares and PALM imaging of PBP4-PAmcherry, which was done by A. R. Pereira. Strains COL $\Delta$ atl, COL $\Delta$ sle1 and NCTC $\Delta$ lytM were constructed by F. Vaz; strains COL $\Delta$ sle1pBCBover and COL $\Delta$ sle1pSle1 were constructed by H. Veiga; strains BCBPM120 and BCBPM138 were constructed by P. M. Pereira.

### Acknowledgments

We thank Suckjoon Jun (UCSD), Adriano Henriques (ITQB) and Nathalie Reichmann (ITQB) for critically reading the manuscript. We thank T. Meylheuc from the Microscopy and Imaging Platform MIMA2 (INRA, France) for SEM observations, Rut Carballido-López and Arnaud Chastanet (Micalis Institute, INRA Jouy-en-Josas) for support for SEM observations and assistance with the preparation of the SEM samples, Luis Morgado (ITQB) for schematics in Fig. 5.

This chapter contains data published in:

**Monteiro JM\***, Fernandes PB\*, Vaz F, Pereira AR, Tavares AC, Ferreira MT, Pereira PM, Veiga H., Kuru E, VanNieuwenhze MS, Brun YV, Filipe SR and Pinho MG. Cell shape dynamics during the staphylococcal cell cycle. *Nature Communications* **6**, 8055, doi:10.1038/ncomms9055 (2015)

\*J.M.M. and P.B.F. contributed equally to this work

## **Abstract**

*Staphylococcus aureus* is an aggressive pathogen and a model organism to study cell division in sequential orthogonal planes in spherical bacteria. However, the small size of staphylococcal cells has impaired analysis of changes in morphology during the cell cycle. Here we use super-resolution microscopy and determine that *S. aureus* cells are not spherical throughout the cell cycle, but elongate during specific time windows, through peptidoglycan synthesis and remodelling. Both peptidoglycan hydrolysis and turgor pressure are required during division for reshaping the flat division septum into a curved surface. In this process, the septum generates less than one hemisphere of each daughter cell, a trait we show is common to other cocci. Therefore, cell surface scars of previous divisions do not divide the cells in quadrants, generating asymmetry in the daughter cells. Our results introduce a need to reassess the models for division plane selection in cocci.

## Introduction

Staphylococci are spherical organisms that divide sequentially in three orthogonal planes over three consecutive division cycles<sup>1,2</sup>. This mode of division is less common in bacterial cells than equatorial division, observed in many genera. Division in three planes implies that cells retain information about the positioning of the two preceding divisions in order to divide with precision. Given that this spatial information varies with each division, it cannot be encoded by DNA<sup>3</sup>. Peptidoglycan, the major component of the bacterial cell wall, has been proposed to encode epigenetic information in the form of protuberant, ring-like structures that mark previous division planes and are used by *Staphylococcus aureus* to divide accurately in sequential perpendicular planes<sup>3</sup>.

Orientation of division planes is merely one of the distinctive features of the staphylococcal cell cycle. *S. aureus* has been proposed to have only one cell wall synthesis machine, which incorporates peptidoglycan mostly at the division septum<sup>4,5</sup>, while rod-shaped bacteria such as *Escherichia coli* or *Bacillus subtilis* have two major cell wall synthesis machines, one for incorporation of new peptidoglycan at the division septum and another for elongation of the lateral wall<sup>4</sup>. Accordingly, *S. aureus* has only four native Penicillin-Binding Proteins (PBPs 1-4), described to localize at the septum, while *E. coli* and *B. subtilis* have 12 and 16 PBPs, respectively, which localize at the septum or at the lateral wall<sup>4</sup>. PBPs are enzymes involved in the last



steps of peptidoglycan biosynthesis, which catalyse the polymerization of the glycan strands, as well as their crosslinking via peptide stems. Given that an elongation-specific machinery seems to be absent in *S. aureus*, increase of the cell surface area required for growth has been attributed to a process of reshaping the flat septum into curved hemispheres of the two daughter cells, which occurs immediately after splitting of the mother cell during division<sup>2</sup>. Reshaping of the flat septum, resulting in doubling of the external surface area of peptidoglycan, could theoretically occur in the absence of synthesis, if accompanied by changes in the angle of the glycan chains with respect to the peptide chains<sup>6</sup>. Alternatively, increase of the surface area could be driven by hydrolysis of peptidoglycan bonds catalysed by specific autolysins. At least 13 genes of the *S. aureus* genome encode known or putative peptidoglycan hydrolases, although the products of only three of these genes (*atl*, *sle1* and *lytM*) have been characterized. Of these genes, *atl* encodes the major autolysin in *S. aureus*, which is involved in the separation of the daughter cells after division<sup>7,8</sup>. Interestingly, orthogonal rings of Atl can be observed by immunoelectron microscopy at the surface of *S. aureus* cells, similar to scars of previous divisions<sup>9</sup>, confirming that information regarding the localisation of previous, orthogonal, division planes can be present at the cell surface.

*S. aureus* is an aggressive pathogen and one of the most important nosocomial bacteria causing antibiotic-resistant infections.

Despite its clinical relevance, the small size of staphylococcal cells (with a  $\sim 1 \mu\text{m}$  diameter, only four times larger than the diffraction limit of resolution of conventional light microscopy) has impaired a detailed analysis of its cell cycle and of the morphological changes that occur as *S. aureus* grows and divides. This lack of knowledge extends to the cell cycle of other cocci as well. Therefore detailed characterization of the mode of growth and division of *S. aureus* has implications for the global understanding of the cell cycle of cocci. Here, we have used super-resolution microscopy to analyse the dynamics of cell shape and size during the cell cycle of *S. aureus*. We found that, contrary to current thinking, *S. aureus* cells elongate before dividing. Furthermore, we show that the division septum generates less than one hemisphere of each daughter cell and therefore scars of previous divisions do not mark quadrants of the cell. Our results suggest that the models for division plane selection in cocci should be re-examined.

## Experimental Procedures

### Bacterial growth conditions

Strains and plasmids used in this study are listed in Table 1. *S. aureus* strains were grown in tryptic soy broth (TSB, Difco) with aeration at 37 °C or on tryptic soy agar (TSA, Difco) at 30 °C or 37 °C. For microscopy experiments, overnight cultures of *S. aureus* strains were diluted 1:200 in fresh TSB medium and allowed to grow at 37 °C until an OD<sub>600nm</sub> of approximately 0.5. Cells were then harvested and resuspended in the same medium. *Escherichia coli* and *Sporosarcina ureae* strains were grown in Luria-Bertani broth (LB, Difco) with aeration, or LB agar (LA, Difco) at 37 °C or 30 °C, respectively. Antibiotics ampicillin (Amp) and erythromycin (Ery) were added to the media at a final concentration of 100 µg ml<sup>-1</sup> and 10 µg ml<sup>-1</sup>, respectively, when necessary. 5-Bromo-4-chloro-3-indolyl β-D-galactopyranoside (X-gal) was used at 100 µg ml<sup>-1</sup>. Expression of PBP4 from plasmid pBCBPM115 was induced with cadmium chloride (1 µM). Expression of Sle1 from plasmid pSle1 was induced with IPTG (1 mM) in the presence of 10 µg ml<sup>-1</sup> of chloramphenicol.

**Table 1. Bacterial strains and plasmids used in this study**

Strains	Description	Source or reference
<i>Escherichia coli</i>		
DC10B	$\Delta dcm$ in the DH10B background; Dam methylation only	10
<i>Staphylococcus aureus</i>		
COL	HA-MRSA	11
NCTC8325-4	MSSA strain	R. Novick
RN4220	Restriction-deficient derivative of NCTC8325-4	R. Novick
COL $\Delta pbpD$	<i>pbp4</i> in-frame deletion mutant of parental strain COL	12
COLpPBP4-YFP	COL encoding a C-terminal YFP fusion to PBP4 at the native locus	13
COL $\Delta atl$	$\Delta atl$ in-frame deletion mutant of parental strain COL	This study
COL $\Delta sle1$	$\Delta sle1$ in-frame deletion mutant of parental strain COL	This study
COL $\Delta sle1$ pBCBover	COL $\Delta sle1$ with pBCBover	This study
COL $\Delta sle1$ pSle1	COL $\Delta sle1$ complemented with pSle1	This study
COL $walKRi$	COL strain with WalKR operon under the control of the IPTG inducible Pspac promoter; Ery <sup>r</sup>	This study
NCTC $\Delta lytM$	$\Delta lytM$ in-frame deletion mutant of parental strain NCTC8325-4	This study
NCTC $\Delta sle1$	$\Delta sle1$ in-frame deletion mutant of parental strain NCTC8325-4	This study
NCTC $\Delta pbpD::pbpD$ -PAmCherry	NCTC strain with the <i>pbpD</i> gene substituted by the <i>pbpD</i> -PAmCherry photoactivable derivative	This study
BCBPM120	COL $\Delta pbpD$ with pCNX	This study
BCBPM138	COL $\Delta pbpD$ with pBCBPM115, encoding PBP4 under the control of P <sub>Cad</sub>	This study
<i>Sporosarcina ureae</i> SL6708	Derivative of <i>S. ureae</i> ATCC 1388	14

**Table 1. Bacterial strains and plasmids used in this study (cont.)**

Plasmids	Description	Source or reference
pMAD	<i>E. coli-S. aureus</i> shuttle vector with a thermosensitive origin of replication for Gram-positive bacteria; Amp <sup>r</sup> Ery <sup>r</sup> <i>lacZ</i>	15
pMUTIN4	Integrative vector for <i>S. aureus</i> encoding IPTG inducible P <sub>spac</sub> promoter; Amp <sup>r</sup> , Ery <sup>r</sup>	16
pCN34	Vector containing the aphA-3 kanamycin resistance cassette	17
pCN51	Shuttle vector containing a cadmium inducible P <sub>cad</sub> promoter; Amp <sup>R</sup> Ery <sup>R</sup>	17
pCNX	Shuttle vector containing a cadmium inducible P <sub>cad</sub> promoter; Amp <sup>R</sup> Kan <sup>R</sup>	This study
pGC2	<i>E. coli/S. aureus</i> shuttle vector, Amp <sup>r</sup> Cm <sup>r</sup>	18
pDH88	<i>B. subtilis</i> with P <sub>spac</sub> promoter and <i>lacI</i>	19
pBAD/HisB-PAmCherry1	Plasmid encoding the sequence of the photoactivable PAmCherry1 protein	20
pΔ <i>atl</i>	pMAD derivative with the up- and downstream regions of <i>atl</i>	21
pΔ <i>lytM</i>	pMAD derivative with the up- and downstream regions of <i>lytM</i>	This study
pΔ <i>sle1</i>	pMAD derivative with the up- and downstream regions of <i>sle1</i>	This study
pBCBover	pGC2 derivative containing P <sub>spac</sub> promoter and <i>lacI</i>	This study
pSle1	pBCBover encoding Sle1 under the control of P <sub>spac</sub> promoter	This study
p <i>walkR</i>	pMUTIN4 derivative containing the ribosome binding site and 5' end of <i>walkR</i>	This study
pBCBRP007	pCNX derivative containing P <sub>cad</sub> -RBS- <i>pbpD</i> -7aaLinker-PAmCherry; Amp <sup>R</sup> Kan <sup>R</sup>	This study

**Table 1. Bacterial strains and plasmids used in this study (cont.)**

Plasmids	Description	Source or reference
pBCBRP008	pMAD derivative containing truncated <i>pbpD-7aa-PAmCherry</i> -Downstream region; Amp <sup>R</sup> Ery <sup>R</sup>	This study
pBCBPM115	pCNX encoding PBP4 under the control of P <sub>cad</sub>	This study

### Construction of *S. aureus* mutants

The full sequences of each primer used to construct mutants are in Table 2.

**Table 2. Oligonucleotides used in this study**

Primer name	Sequence (5'-3')
P1_Sle1	CATGCCATGGGCAAGTAGATGCACAACAAACTG
P2_Sle1	CATTATATATTTATATACGTAAGACTTTATTTAAAATCCTCCTC TTGCTTAAC
P3_Sle1	GTTAAGCAAGAGGAGGATTTTAAATAAAGTCTTACGTATATA AATATATAATG
P4_Sle1	TGGAGATCICAGCGGTACTTGTGATC
P1_lytM	CATGCCATGGGCAATGAAGCAGGTACATTTG
P2_lytM	GCAACTGGGATTTTCTGTATTAGTATAAAACATCCTCCATTA AAG
P3_lytM	CTTTAATGGAGGATGTTTTATACTAATACAGAAAATCCCAAGT TGC
P4_lytM	TGGAGATCIGGAGCGTAAGTATGATGATAG
yycF fw EcoRI	GCGCGCGAATTCTATTAATGATTTAAGAAAAGAGG
yycF stop rv BamHI	CGCGCGCGGATCCCTAGCCACGTTTTTTAATAGAATATGCC
P1pbp4pCNX	GGATCCAGGAGGTACCTTATGAAAAATTTAATATC
P2pbp4pCNX	CACCATGCTAGCGGCGCGCGGTACCTTTTCTTTTCTAAAT AAACGATTGATTA
P3pbp4pCNX	AGGTACCCGGCGCGCCGCTAGCATGGTGTGAGCAAGGGCGAGG A
P4pbp4pCNX	GCCTAAGAATTCTTACTTGTACAGCTCGTCCATGC
P1pMADpbp4PAmCherry	GATATCGGATCCACAGTCAATGACGAACAAAG
P2pMADpbp4PAmCherry	GTCCGTTTTAGTATGTTTTACTTGTACAGCTCGTCCATGCCG
P3pMADpbp4PAmCherry	TGGACGAGCTGTACAAGTAAAACATACTAAAAACGGACAAG TTGC
P4pMADpbp4PAmCherry	ATGGTACCCGGGACAAGTAACGATGAAGATTTAATAG
Pspac_pDH88_P9_XhoI_SalI	GCTGCGCTGTCGACGTTACCTCGAGTTCTACACAGCCCAGTC CAGAC

**Table 2. Oligonucleotides used in this study**

Primer name	Sequence (5'-3')
Pspac_pDH88_SpeI_P10	GTTAACAAAGACTAGTATGCTCTAGAAACCCGGGAAAAGC
Pspac_pDH88_SpeI_P11	CTAGAGCATACTAGTCTTTGTAACTTAGATCTTTATCG
Pspac_pDH88_P12_XhoI_EcoRI	GCTGAATTCGATGCCCTCGAGCTGATCCTAACTCACATTAATT GCG
Sle1_FW_XmaI	TACTCCCCGGGGCAAGAGGAGGATTTTAAAGTGC
Sle1_RV_XbaI	GCTGCTCTAGATTAGTGAATATATCTATAATTATTTAC
PBP4pCadP1BamFW	CGCAGGATCCAGGAGGTACCTTATGAAAAATTTAATATCTATT ATC
pCADPBP4wt_EcoREV	GCGTGAATTCCTTAGGTACCTTATTTCTTTTCTAAATAAAC

Underlined sequences correspond to restriction sites

The COL $\Delta$ *atl*, COL $\Delta$ *sle1* and NCTC $\Delta$ *lytM* null mutants were constructed using the pMAD vector<sup>15</sup> containing the upstream and downstream regions of each gene of interest, to allow recombination and integration of the plasmids into the chromosome, followed by their excision with the genes to be deleted. Briefly, upstream and downstream regions of *sle1* and *lytM* were amplified by PCR, using primers P1\_*sle1*/P2\_*sle1* and P3\_*sle1*/P4\_*sle1*, P1\_*lytM*/P2\_*lytM* and P3\_*lytM*/P4\_*lytM*, respectively. The PCR fragments encoding the upstream and downstream regions of each gene were joined by overlap PCR using the pairs of primers P1\_*Sle1*/P4\_*Sle1* and P1\_*lytM* and P4\_*lytM*. The resulting fragments were digested with *NcoI* and *BglIII* (Fermentas) and cloned into the pMAD vector, giving plasmids p $\Delta$ *sle1* and p $\Delta$ *lytM*, which were propagated in *E. coli* DC10B and the inserts were sequenced. The plasmids, as well as p $\Delta$ *atl*<sup>21</sup>, were then electroporated into *S. aureus* RN4220 strain at 30 °C, using Ery and X-gal selection, and transduced into COL or NCTC8325-4 using phage 80 $\alpha$ . The integration of the plasmids into the chromosome and their

excision was done as previously described<sup>22</sup>. Gene deletions were confirmed by PCR and sequencing of the amplified fragment.

For complementation of COL $\Delta$ *sle1*, plasmid pBCBover was constructed by introducing a DNA fragment containing the *Pspac* promoter, a multiple cloning site and the *lacI* gene into the *S. aureus* replicative vector pGC2<sup>18</sup>. For that, two DNA fragments, one containing the *Pspac* coding sequence and HindIII, SmaI, and XbaI restriction sites and a second one encompassing a BglII restriction site upstream of the *lacI* gene, were amplified from pDH88 plasmid<sup>19</sup> by using respectively the pair of primers Pspac\_pDH88\_P9\_XhoI\_Sall / Pspac\_pDH88\_SpeI\_P10 and Pspac\_pDH88\_SpeI\_P11 / Pspac\_pDH88-P12-XhoI-EcoRI. These two PCR products were then joined in a second PCR, using primers Pspac-pDH88\_P9\_XhoI\_Sall and Pspac\_pDH88-P12-XhoI-EcoRI, to originate a 1743bp fragment in which a SpeI restriction site was introduced between XbaI and BglII restriction sites. The resulting fragment was restricted with Sall and EcoRI, cloned into the pGC2 vector and sequenced. The pSle1 plasmid was constructed by cloning the entire *sle1* coding sequence downstream of *Pspac* promoter in pBCBover. For that, a 1024bp DNA fragment containing *sle1* gene and its upstream RBS site was amplified from NCTC8325-4 genome using primers Sle1\_FW\_XmaI and Sle1\_RV\_XbaI, digested with SmaI and XbaI and cloned into pBCBover. The insert was then sequenced. Both pBCBover and pSle1 plasmids were electroporated into RN4220 (selection with 10  $\mu$ g ml<sup>-1</sup> chloramphenicol) and subsequently transduced, using phage 80 $\alpha$ , to



strain COL $\Delta$ sle1, generating strains COL $\Delta$ sle1pBCBover and COL $\Delta$ sle1pSle1 respectively.

Construction of an *S. aureus* COL mutant with *yycFG* (also known as *walkR*) under the control of the IPTG-inducible Pspac promoter was done using the pMUTIN4 plasmid<sup>16</sup>. A 518-bp fragment containing the ribosome binding site and 5' end of *yycF* (*walkR*) was amplified using primers *yycF\_fw\_EcoRI* and *yycF\_stop\_rv\_BamHI*. The DNA fragment was then digested with *EcoRI* and *BamHI*, cloned into pMUTIN4 giving plasmid *pwalkR*, which was propagated in *E. coli* DC10B and the insert was sequenced. Plasmid *pwalkR* was then electroporated into *S. aureus* RN4220 at 37 °C, using erythromycin selection, and transduced into COL using phage 80 $\alpha$ . Integration of the plasmid occurred through a single crossover event, placing the *walkR* operon under the control of the Pspac promoter.

To study PBP4 localisation in *S. aureus* NCTC8325-4 by PALM, we replaced the *pbpD* gene, encoding PBP4, for a gene encoding a photoactivatable derivative (*pbpD-PAmCherry*). For that purpose, *pbpD* was cloned fused to *PAmCherry1*<sup>20</sup> in the backbone of pCNX. The pCNX plasmid was constructed by substituting the *erm* erythromycin resistance cassette of the pCN51 plasmid<sup>17</sup> by the *aphA-3* kanamycin cassette from pCN34<sup>17</sup>, using *ApaI* and *XhoI* restriction sites. To clone *pbpD-PAmCherry* into pCNX, a fragment encompassing a ribosomal binding site, the *pbpD* gene lacking the stop codon and

seven codons encoding an amino acid linker was amplified using NCTC8325-4 genomic DNA as template and primers P1pbp4pCNX and P2pbp4pCNX. A fragment encompassing *PAmCherry1* was amplified from the pBAD/HisB-*PAmCherry1* plasmid<sup>20</sup> using P3pbp4pCNX and P4pbp4pCNX primers. The two fragments were joined by overlap PCR, digested with *Bam*HI and *Eco*RI, ligated into the pCNX plasmid generating plasmid pBCBRP007, and the insert was sequenced. We then replaced the *pbpD* gene from its native locus in the *S. aureus* genome by the *pbpD-PAmCherry* fusion. For this purpose two DNA fragments were amplified, one encompassing a truncated *pbpD* (last 999 bp), a sequence encoding a 7 amino acid linker and *PAmCherry1* amplified from the pBCBRP007 plasmid using primers P1pMADpbp4PAmCherry and P2pMADpbp4PAmCherry and a second DNA fragment of 1,000 bp corresponding to the region downstream of *pbpD* amplified from the NCTC8325-4 genome, using primers P3pMADpbp4PAmCherry and P4pMADpbp4PAmCherry. The two fragments were joined by overlap PCR using primers P1pMADpbp4PAmCherry and P4pMADpbp4PAmCherry, digested with *Bam*HI and *Xma*I restriction enzymes and cloned into pMAD, generating pBCBRP008. Correct sequence of the insert was confirmed and the pBCBRP008 plasmid was electroporated into RN4220 and subsequently transduced to NCTC8325-4 strain using phage 80 $\alpha$ . Integration and excision of pBCBRP008 from the genome was performed as previously described<sup>22</sup>; colonies in which *pbpD* had

been replaced by the *pbpD-PAmCherry* were identified by PCR and the strain was named NCTC $\Delta$ *pbpD::pbpD-PAmCherry*.

To complement COL $\Delta$ *pbpD* with a plasmid encoding PBP4, the 1.3 Kb *pbp4* gene was PCR amplified from NCTC8325-4 genomic DNA using primers PBP4pCadP1BamFW and pCADPBP4wt\_EcoREV and cloned into the pCNX replicative plasmid, under the control of a cadmium inducible promoter, using *BamHI* and *EcoRI* sites, generating plasmid pBCBPM115. Plasmids pCNX and pBCBPM115 were electroporated into RN4220 and then transduced into COL $\Delta$ *pbpD*, giving rise to strains BCBPM120 (COL $\Delta$ *pbpD*pCNX) and BCBPM138 (COL $\Delta$ *pbpD*pPBP4).

### **Scanning electron microscopy**

Exponentially growing *S. aureus* COL cells<sup>11</sup> were harvested by centrifugation, resuspended in fixative solution (2.5% glutaraldehyde in 0.2 M sodium cacodylate buffer, pH 7.4), deposited on glass discs (Marienfeld) and kept for 1 week at 4 °C. The fixative solution was subsequently removed and the cells were washed three times with sodium cacodylate. The sample was progressively dehydrated by immersion in a graded series of ethanol (50% - 100%) and then mounted on aluminum stubs with carbon adhesive discs (Agarscientific). The sample was critical-point dried under CO<sub>2</sub> and sputter coated with gold-palladium (Polaron SC7640) for 200 s at 10 mA. SEM observations were performed using secondary electron images (2 kV) with a Hitachi S4500 instrument at the Microscopy and

Imaging Platform (Micalis, B2HM, Massy, France) of the INRA research center of Jouy-en-Josas (France).

### **Super-resolution Structured Illumination Microscopy (SIM)**

SIM imaging was performed using a Plan-Apochromat 63x/1.4 oil DIC M27 objective, in an Elyra PS.1 microscope (Zeiss). Images were acquired using either 3 or 5 grid rotations, with 34  $\mu\text{m}$  grating period for the 561 nm laser (100 mW), 28  $\mu\text{m}$  period for 488 nm laser (100 mW) and 23  $\mu\text{m}$  period for 405 nm laser (50 mW). Images were acquired using a Pco.edge 5.5 camera and reconstructed using ZEN software (black edition, 2012, version 8.1.0.484) based on a structured illumination algorithm<sup>23</sup>, using synthetic, channel specific Optical Transfer Functions (OTFs) and noise filter settings ranging from -6 to -8.

### **Fast time-lapse imaging of *S. aureus***

A 2  $\mu\text{l}$  aliquot of an exponentially growing culture of *S. aureus* was placed on an agarose pad in TSB. Cells were imaged at 2 ms intervals for a total time of 10 seconds, using a Pco.edge 5.5 camera and a Plan-Apochromat 100x /1.46 NA Oil DIC ELYRA objective in an Elyra PS.1 microscope (Zeiss).

### **Labelling and imaging of *S. aureus***

For time-lapse experiments *S. aureus* cells were incubated with the membrane dye Nile Red (Invitrogen) at a final concentration of 10  $\mu\text{g ml}^{-1}$ , for 5 minutes at 37 °C, with agitation (550 rpm).

Subsequently, the cells were placed on an agarose pad containing 50% TSB in Phosphate Buffer Saline (PBS) and imaged during growth by SIM. Image sets were acquired every 3 minutes, for a total period of 1 hour, using 2% of 561 nm laser power and 50 ms exposure times. Measurements were performed on reconstructed super-resolution images using ZEN software.

To determine the fraction of old/new cell wall in *S. aureus*, cells were stained with either a wheat germ agglutinin Alexa Fluor 488 conjugate (WGA-488, Invitrogen) or fluorescent D-amino acid HADA<sup>24,25</sup> at a final concentration of 2  $\mu\text{g ml}^{-1}$  and 250  $\mu\text{M}$ , respectively. The cells were incubated at 37°C with agitation for 5 minutes or 30 minutes for WGA-488 or HADA, respectively. Unbound dye was removed from the media by washing cells with TSB and cells were then incubated with Nile Red (10  $\mu\text{g ml}^{-1}$ ) for 5 minutes at room temperature and placed on an agarose pad containing 50% TSB in PBS. Cells showing uniform WGA-488 or HADA staining were imaged by SIM at 0, 3, 6, 30 and 60 minutes, using 2% 561 nm laser with 50 ms exposure for Nile Red, 3% 488 nm laser with 50 ms exposure for WGA-488 and 20% 405 nm laser with 100 ms exposure for HADA.

To evaluate localisation of peptidoglycan synthesis activity, *S. aureus* cells grown to an  $\text{OD}_{600\text{nm}}$  of approximately 0.5 were labelled with fluorescent D-amino acid NADA (250  $\mu\text{M}$ ) for 20 minutes at 37 °C, 550 rpm. Cells were then washed with PBS, placed on an agarose

pad and visualized by SIM, using 10% 488 nm laser, 100 ms exposure. For pulse labeling experiments, *S. aureus* cells were incubated with either HADA or its L-enantiomer HALA<sup>24</sup> for 5 min at 37°C, 550 rpm and then imaged as described above.

*S. aureus* cell wall labelling with vancomycin was performed by incubating the cells for 2 minutes at room temperature with a mixture containing equal amounts of vancomycin (Sigma) and a BODIPY FL conjugate of vancomycin (Van-FL, Molecular Probes) to a final concentration of 0.8  $\mu\text{g ml}^{-1}$ . Cells were visualized by SIM, using 2% 488 nm laser, 100 ms exposure.

### **Labelling and imaging of *Sporosarcina ureae***

To determine the fraction of old/new cell wall in *S. ureae* by time lapse microscopy, cells from cultures at  $\text{OD}_{600}\sim 0.5$  were stained with WGA-488 at a final concentration of 6  $\mu\text{g.ml}^{-1}$ . The cells were incubated at 30°C with agitation for 10 minutes. Unbound dye was removed from the medium by washing cells with LB. Cells were then incubated with Nile Red (10  $\mu\text{g ml}^{-1}$ ) for 5 minutes at room temperature and placed on an agarose pad containing 50% LB in PBS. Cells showing uniform WGA-488 labeling were imaged by SIM at 0, 15, 30, 45 and 60 minutes, using 2% 561 nm laser with 50 ms exposure for Nile Red, 3% 488 nm laser with 50 ms exposure for WGA-488.

### **Photoactivated Localisation Microscopy (PALM)**

To observe PBP4-PAmCherry single molecules by PALM, an overnight culture of NCTC $\Delta$ *pbpD::pbpD-mCherryPA* was diluted 1/200 in TSB and incubated at 37 °C. At mid-exponential phase ( $OD_{600nm}$  0.6), 1 ml of culture was harvested by centrifugation and washed with 1 ml of PBS. Cells were re-suspended in 20  $\mu$ l of PBS and 1  $\mu$ l was placed on a thin layer of 1.2% agarose in PBS mounted on a gene frame. Image sequences for PALM analysis were obtained using a Zeiss Elyra PS.1 microscope with a 100x 1.46NA objective, additional magnification of 1.6X, equipped with an EMCCD camera (Andor - iXon DU897) using Zeiss ZEN software. For an initial bleach of auto-fluorescent molecules and unwanted pre-activated fluorophores, the sample was first imaged with a 561 nm laser at  $\sim 0.76$  kW cm<sup>-2</sup> and 33 ms exposure for 2,000 frames. After bleaching, the continuous activation and imaging of PAmCherry molecules was performed for 8,000 frames by simultaneously irradiating the sample with a 405 nm laser at  $\sim 1.9$  W cm<sup>-2</sup> and a 561 nm laser at  $\sim 0.76$  kW cm<sup>-2</sup>, using 33 ms of exposure time. To maintain a stable density of fluorophores photo activating in each frame and compensate the depletion of PAmCherry molecules during the course of the experiment, the intensity of the 405 nm laser was increased until  $\sim 38$  W cm<sup>-2</sup>. Post-processing of the last 8,000 frames was performed using the ZEN software where an *xy* 2D-Gaussian fit was applied to the individually resolvable sub-diffraction molecules present in each frame (mask of 9 pixels with a minimum signal to noise ratio of 6).

## Hyperosmotic shock

Cells were grown in TSB until an OD<sub>600nm</sub> of approximately 0.5 and then incubated for 30 minutes at 37 °C with agitation (700 rpm) in the presence of NADA (250 µM). The cells were harvested, washed once with 50 mM Tris-HCl buffer pH=7.5 containing a saturating concentration of NaCl (4.96 M) and incubated for 15 minutes at 37 °C. Cells were pelleted and placed on an agarose pad containing the same medium used to perform the hyperosmotic shock and imaged by SIM.

## Calculation of cell dimensions

To calculate the volume of each cell, an ellipse was fitted to the border limits of the cellular membrane of Nile Red labelled cells, overlaying the membrane dye signal. Subsequently, the shorter and longer axes were measured, coinciding with the septum and the axis perpendicular to it, respectively. The volume of the cell was obtained by an approximation to the volume of a prolate spheroid (equation 1) where  $a$  and  $b$  correspond to the longer and shorter semi-axes, respectively.

$$(1) V = \frac{4}{3} \pi a b^2$$

Cell surface area was calculated using the Knud Thomsen approximation<sup>26</sup> (equation 2) to calculate the surface area of ellipsoids, where  $a$  corresponds to the longer semi-axis and  $b$  and  $c$



correspond to shorter semi-axes, which are identical in the case of *S. aureus* cells.

$$(2) S \approx 4\pi \left[ \frac{1}{3} \times (ab^{1.6}ac^{1.6}bc^{1.6}) \right]^{1/1.6}$$

To evaluate cellular symmetry and identify “D” shaped cells, cells in Phase 1 of the cell cycle were selected and an ellipse was fit to the cell borders corresponding to the old cell wall. The ellipse centre was defined as the middle point of the longer axis and the distances from this point (along a perpendicular axis) to new peripheral cell wall and old peripheral cell wall were calculated (see Fig. 8d). Symmetry was assessed by the ratio between the distance from the centre to the old cell wall and the distance from the centre to the new cell wall. A cell was considered as asymmetric when this ratio was more than 1.33, *i.e.* when the distance from the cell centre to the new cell wall was less than 75% of the distance to the old cell wall.

### Calculation of fluorescence ratio in NADA labelled cells

NADA labelled *S. aureus* cells were observed using a Zeiss Axio Observer microscope equipped with a Photometrics CoolSNAP HQ2 camera (Roper Scientific) and Metamorph 7.5 software (Molecular Devices). To quantitatively assess D-amino acid incorporation, the fluorescence signal at the septum and at the peripheral cell wall was determined for 50 cells with fully formed septa. A fluorescence ratio (FR) for septal versus peripheral cell wall signals was determined as previously described<sup>27</sup>.

## Statistical analysis

Statistical analyses were done using GraphPad Prism 6 (GraphPad Software). Unpaired student's t-tests were used to evaluate the differences in cellular volume and shape between cell cycle stages and between the initial and final stages of each phase, as well as to compare fluorescence ratios between peripheral and septal wall signal intensity. One-way ANOVA was used to compare old/new cell wall fraction at different time points. *P*-values  $\leq 0.05$  were considered as significant for all analysis performed and were indicated with asterisks: \**P*  $\leq 0.05$ , \*\**P*  $\leq 0.01$  and \*\*\**P*  $\leq 0.001$ .

## **Results**

### ***S. aureus* cells elongate during the cell cycle**

To follow morphology dynamics during the cell cycle of *S. aureus*, cells of wild-type strain COL were labelled with the membrane dye Nile Red, placed on an agarose pad containing growth medium and imaged during growth at room temperature by Super-Resolution Structured Illumination Microscopy (SIM) (Fig. 1a). During the initial phase of the cell cycle (here referred to as Phase 1), prior to initiation of division septum formation, cells were approximately spherical in shape, as determined by calculating the ratio between the longer axis of the cell (perpendicular to the division septum) and the shorter axis (coincident with the septum) and then became slightly elongated (Fig. 1c, Fig. 2 and Table 3). In a second stage (Phase 2), cells initiated and completed the synthesis of the division septum and did not significantly elongate. Finally, during the last stage of the cell cycle (Phase 3), cells with a complete septum elongated further, before splitting into two daughter cells. Splitting was accompanied by fast reshaping of the flat septum to become approximately one hemisphere of each daughter cell.

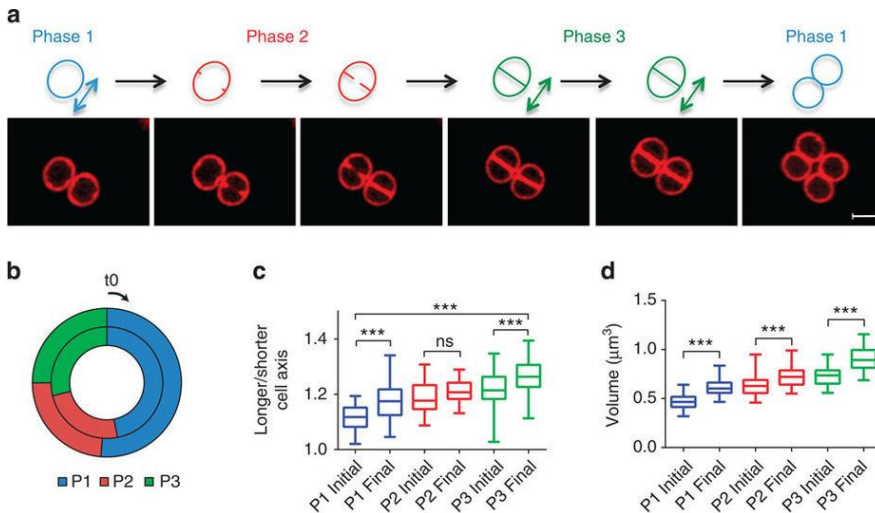


**Figure 1. Morphological changes during the cell cycle of *Staphylococcus aureus*.** (a) *S. aureus* COL cells were stained with membrane dye Nile Red and imaged by SIM for 60 min, at 3 min intervals. Phase 1 (P1) cells have recently divided and have not initiated synthesis of the septum. Phase 2 (P2) cells are undergoing septum synthesis. Phase 3 (P3) cells have a complete septum and are going to split into two daughter cells. Coloured arrows indicate periods of cell elongation. The time interval between panels was 6 min. Scale bar, 1  $\mu\text{m}$ . (b) Duration of each phase of the cell cycle (represented as a fraction of the duplication time) was measured in individual cells imaged by SIM while growing at room temperature on agarose slides containing growth medium (inner circumference); or after growing in liquid culture, at 37  $^{\circ}\text{C}$ , and placed on the microscopy slide just before imaging (outer circumference). (c) Elongation of *S. aureus* cells during the cell cycle was evaluated by calculating the ratio of the longer to the shorter axis of each cell.  $n=40$  cells for each phase. (d) Cell volume was measured at the beginning and at the end of each phase of the cell cycle. Cells increased their volume continuously throughout the cell cycle.  $n=40$  for each phase. Data in (c,d) were collected from two independent experiments and are represented as box-and-whisker plots where boxes correspond to the first to third quartiles, lines inside the boxes indicate the median and ends of whiskers represent the minimum and maximum of all data. Statistical analysis was performed using the unpaired  $t$  test (\*\* $P < 0.001$ ; ns, not significant).

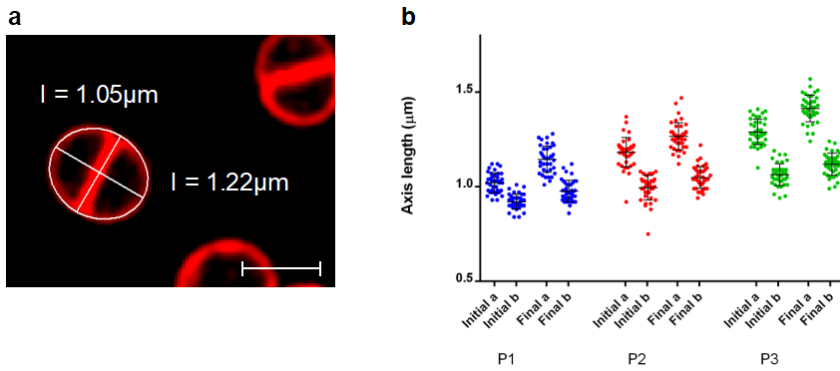


**Figure 2. Size measurements of *S. aureus* cells imaged by SIM during the cell cycle.** (a) The shape of *S. aureus* cells was approximated to a prolate spheroid and superimposition of an ellipse was used to measure the longer and shorter cellular axes during the different phases of growth. Scale bar =  $1 \mu\text{m}$  (b) Scatter plot of the measurements of the longer (a) and shorter (b) axes of *S. aureus* cells when starting (Initial) and finishing (Final) each of the three growth phases defined in Fig. 1.

**Table 3: Average ratio of longer/shorter axes of *S. aureus* cells upon initiation and completion of the three phases of the cell cycle.**

Strain	P1		P2		P3	
	Initial	Final	Initial	Final	Initial	Final
COL	$1.11 \pm 0.04$	$1.17 \pm 0.06$	$1.19 \pm 0.05$	$1.21 \pm 0.04$	$1.22 \pm 0.06$	$1.27 \pm 0.05$
COL $\Delta$ <i>pbpD</i>	$1.13 \pm 0.09$	$1.17 \pm 0.07$	$1.20 \pm 0.06$	$1.23 \pm 0.05$	$1.22 \pm 0.04$	$1.28 \pm 0.06$
COL $\Delta$ <i>atl</i>	$1.13 \pm 0.07$	$1.14 \pm 0.05$ (**)	$1.15 \pm 0.06$ (**)	$1.17 \pm 0.06$ (***)	$1.17 \pm 0.06$ (**)	$1.23 \pm 0.05$ (*)
COL $\Delta$ <i>sle1</i>	$1.19 \pm 0.08$ (***)	$1.20 \pm 0.08$	$1.19 \pm 0.06$	$1.19 \pm 0.06$	$1.20 \pm 0.07$	$1.23 \pm 0.10$

\*  $p \leq 0.05$ , \*\*  $p \leq 0.01$ , \*\*\*  $p \leq 0.001$  mutants vs. parental strain COL (n=40 cells for each strain)

Although we were able to observe cells undergoing complete cell cycles by SIM imaging, we noticed a delay in growth, when compared to cells on the same slide that were not exposed to laser light. Photodamage is cumulative and therefore could cause an increasing bias towards longer duration of growth phases over the course of the experiment. In order to overcome this limitation, all quantitative analyses were only performed on the first complete growth phase of each cell (i.e., in cells observed finishing the previous phase and starting the next phase), and not on the entire cell cycle. Using this approach we measured the duration of each growth phase of the *S. aureus* cell cycle (Fig. 1b). Cells spent approximately half of the cell cycle in Phase 1 ( $47\pm 9\%$ ), with the other half being spent in septum synthesis (Phase 2,  $24\pm 7\%$ ) and the final elongation step (Phase 3,  $29\pm 6\%$ ), with a cell cycle duration of  $66 \pm 9$  minutes. Because the cells analysed by this method were growing at room temperature on growth medium containing agarose pads, on the microscope stage, we independently confirmed the length of each phase by growing *S. aureus* cells in liquid culture with aeration at  $37^\circ\text{C}$ , labelling cell membranes and immediately observing them by SIM. The percentage of cells observed in each phase should be proportional to the fraction of the cell cycle spent in that stage. Fig. 1b shows that similar results for the duration of Phases 1-3 were obtained by both methods.

Interestingly, at the timescale of this experiment, we never observed intermediate stages in the process of cell splitting and

reshaping of the flat septum into a curved surface, implying that these events are likely to be extremely fast. In order to verify this assumption, we imaged cells growing on an agarose pad, at 2 ms intervals (Fig. 3a). *S. aureus* cells divided into two daughter cells in the interval between two acquisitions, indicating that splitting takes less than 2 ms (n=10). The spatial and temporal resolution of these images does not allow us to determine if (i) splitting and septum reshaping occur simultaneously, as one could expect if remodelling of the flat septum did not require any enzymatic activity and resulted solely from the increased turgor pressure imposed upon the septum as it splits and becomes exposed to the external milieu, or (ii) splitting and septum reshaping are two consecutive processes. We reasoned that if the latter hypothesis was correct, we should be able to capture intermediates in the division process in which the septum had already split but remained flat. For this purpose we fixed cells during exponential growth and imaged them using Scanning Electron Microscopy (SEM) (Fig. 3b). In agreement with previous data<sup>9</sup>, we observed recently divided cells in which the previous septum was seen as a smooth flat surface, indicating that septum splitting and reshaping are likely to be sequential events.

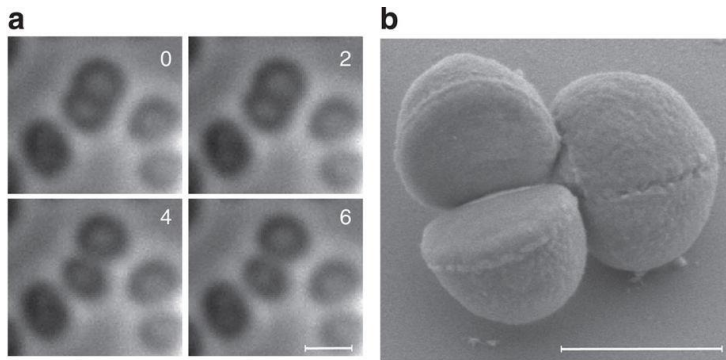


**Figure 3. Splitting of *S. aureus* cells occurs on the millisecond timescale.** (a) Dividing *S. aureus* cells were imaged on an agarose pad, acquiring frames every 2 ms, showing that splitting of the mother cell occurs in <2 ms (between the 2 ms and the 4 ms frame). Time is indicated in milliseconds. Scale bar, 1  $\mu\text{m}$ . (b) To capture intermediate stages in the splitting process, *S. aureus* cells were fixed with glutaraldehyde during growth and imaged by SEM. The cell on the left has just divided in two daughter cells. The previous division septum is seen as a smooth flat surface indicating that septum splitting and reshaping into a curved hemisphere are likely to be sequential events. Note that cells with flat septa were not as rare as could be expected given the speed of the splitting process. It is therefore possible that the cell treatment required for SEM stabilizes this stage. Scale bar, 750 nm.

### **The septum gives less than one hemisphere of each daughter cell**

Previous descriptions of the *S. aureus* cell cycle suggested that cell wall synthesis occurred mainly, if not only, at the division septum<sup>5</sup>. Furthermore, it was assumed that the “new” cell wall material from the septum of the mother cell formed one complete hemisphere of each of the daughter cells, while the other hemisphere was made of “old” cell wall material originating from the peripheral wall of the mother cell. However, we observed that just prior to



splitting, at the end of Phase 3, the mother cell has an ellipsoid shape, with a semi-major axis of  $0.70 \pm 0.04 \mu\text{m}$  (perpendicular to the septum) and two semi-minor axes of  $0.55 \pm 0.03 \mu\text{m}$  (equivalent to the radius of the septum), resulting in a septal surface area of  $0.95 \mu\text{m}^2$ . After splitting, at the beginning of Phase 1, each daughter cell has semi-major and semi-minor axes of  $0.52 \pm 0.03 \mu\text{m}$  and  $0.46 \pm 0.03 \mu\text{m}$ , respectively. Therefore, the total surface area of each daughter cell is  $\sim 2.89 \mu\text{m}^2$  (see Experimental Procedures for Knud Thomsen approximation used for calculations), of which  $0.95 \mu\text{m}^2$ , or  $\sim 33\%$ , should be composed of new cell wall material, originating from the septum of the mother cell. The remaining  $\sim 67\%$  of the cell surface should be composed of “old” cell wall material, originating from one hemisphere of the mother cell, i.e., the distribution of old and new cell wall material should not be 50% of each, as previously assumed<sup>3,5,6</sup> (Fig. 4a). To determine whether the mode of *S. aureus* growth was consistent with these assumptions, cells were labelled with a green fluorescent derivative of wheat germ agglutinin (WGA-488), a lectin which labels *N*-acetylglucosamine residues present in peptidoglycan and in wall teichoic acids. Importantly, WGA labels the cell wall present at the cell surface (peripheral wall) but does not diffuse into (and therefore does not label) the division septum. Cells were next washed to remove unbound WGA-488, and stained with the membrane dye Nile Red, which diffuses through the septum and therefore labels the entire membrane of the cell. Finally, cells were placed on an agarose pad containing growth medium and imaged by

SIM during growth (Fig. 4b). Cells whose surface was completely labelled by WGA-488 were selected for analysis and both the perimeter of each cell, as well as the fraction of the cell surface made of old cell wall (WGA-488 labelled), were measured. In agreement with our model, we found that after splitting of the mother cell, each daughter cell had  $61.3 \pm 3.3\%$  ( $n=30$ ) of its surface labelled by WGA-488, i.e., made of old cell wall, clearly showing that the flat septum, even after reshaping, does not contribute to half of the cell surface (Fig. 4c).

These results were confirmed in a second experiment, similar to the one described above, in which cells were labelled with HADA instead of WGA-488. HADA is a blue fluorescent derivative of 3-amino-D-alanine that can be incorporated in the pentapeptide chain of peptidoglycan<sup>24</sup>. Selected cells whose entire surface was labelled with HADA at time zero were followed during growth for 60 minutes (Fig. 4d). Similar to the results obtained with WGA-488 labelling, upon splitting of the mother cell,  $62.5 \pm 3.4\%$  of the surface of each daughter cell was labelled with HADA.

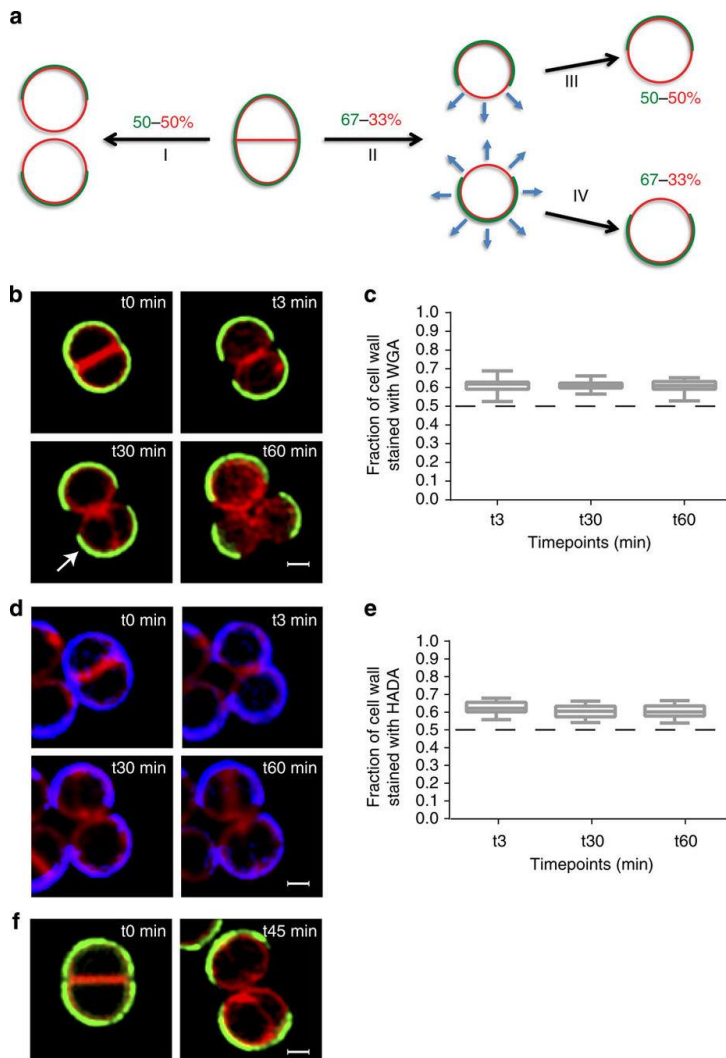


**Figure 4. Asymmetrical inheritance of cell wall material during *S. aureus* cell division.** (a) Schematic representation of the possible modes of division and growth of *S. aureus*. Peripheral cell wall of the mother cell is represented in green and cell membrane is represented in red. Upon division of the mother cell, the new cell wall material, derived from the previous septum, may constitute 50% of the surface of each daughter cell, if the surface area of the flat septum increases as it becomes curved (I), or 33%, if there is no increase in the surface area of septum material (II). In the latter case, the cell can then grow by peptidoglycan synthesis and/or autolysis either at the site of the new cell wall material only (III) or throughout the entire cell surface (IV).

(IV). **(b)** *S. aureus* COL cells were labelled for 5 min with peripheral cell wall dye WGA-488 (green), washed and stained with membrane dye Nile Red. Cells were placed on an agarose pad and resumed growth at room temperature. Upon division, the old cell wall preserved the green WGA-488 signal. Cells were imaged by SIM at 3, 30 and 60 min after splitting. The cell indicated by the arrow underwent a second round of division. **(c)** The fraction of WGA-488-labelled cell wall (green) relative to cell perimeter (red) remained above 0.60 during the cell cycle,  $n=30$ . No statistically significant variation was found ( $P>0.05$ ). **(d)** An experiment equivalent to that described in panel **(b)** was done using cell wall dye HADA instead of WGA-488. **(e)** The fraction of cell wall labelled with HADA (blue) relative to the cell perimeter (red), decreased slightly during the first 30 min but remained above 0.60 during the cell cycle,  $n=30$ . ( $P=0.03$ ). **(f)** The cell wall of *Sporosarcina ureae* was labelled with WGA-488, washed, labelled with Nile Red and imaged by SIM. Panels show the same cell before and after division, indicating that old cell wall material (green) constitutes more than half of the daughter cells surface. Contrast of individual channels was adjusted on merged images. Scale bars, 0.5  $\mu\text{m}$ . Data in **(c,e)** are represented as box-and-whisker plots where boxes correspond to the first to third quartiles, lines inside the boxes indicate the median and ends of whiskers represent the minimum and maximum of all data. Statistical analysis was performed using one-way analysis of variance.

Careful inspection of SEM images of *S. aureus* cells confirms that the “old” cell wall constitutes more than 50% of the surface of each daughter cell (Fig. 5). Cell wall material which is at least one generation old has been described as having an irregular, rough appearance, while newly synthesized cell wall, resulting directly from the septum of the mother cell, has a smoother appearance with concentric rings<sup>3,28</sup>, with a clear border separating the two types of cell surface<sup>29</sup>. These borders, seen in Fig. 5 and denoted in blue in the

schematic representation of the cells, are clearly not placed at mid cell, reinforcing the idea that more than half of the surface of *S. aureus* cells is at least one generation old.

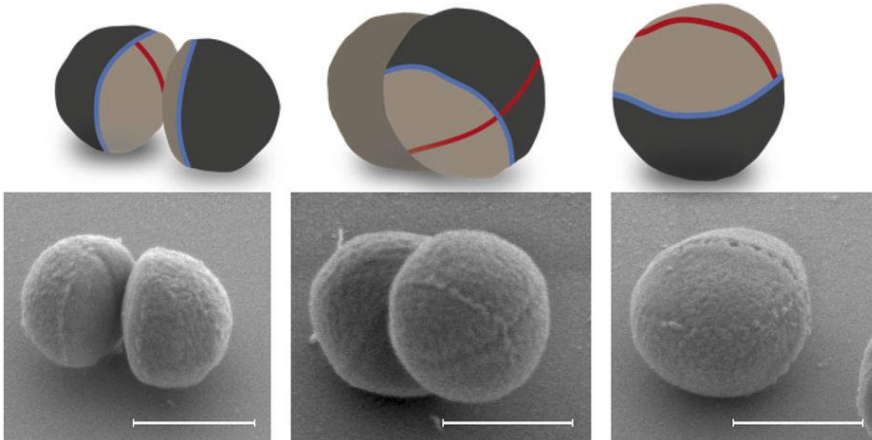


**Figure 5. Scars of previous divisions do not mark cell quadrants.** SEM images of *S. aureus* COL cells showing an asymmetric scar (blue line in scheme) corresponding to the previous division site and a fissure located in the middle of the cell (red line), presumably corresponding to the next division site. The new cell wall (light brown), resulting from septal material from the mother cell, which has a smooth surface immediately after division (first panel), occupies less than half of the total surface. Scale bars, 600 nm.

We then asked if this mode of division of spherical cells, in which the division septum of the mother cell generates less than one hemisphere of each daughter cells was restricted to *S. aureus* or common to other cocci. Labelling of peripheral cell walls in *Sporosarcina ureae* with WGA-488 showed that division of spherical cells from this organism also results in daughter cells with a fraction of approximately 60% of the surface made of “old” cell wall (Fig. 4f).

### ***S. aureus* grows by remodelling the entire cell surface**

The fact that cell wall synthesis in staphylococci occurred mainly, if not exclusively, at the division septum<sup>5</sup>, led to the suggestion that *S. aureus* does not enlarge during the cell cycle and that the conversion of the flat division septum into one hemisphere of each daughter cell accounted for the doubling in volume required for cell division to take place<sup>3,5,6</sup>. Importantly, the diffraction limit of resolution of conventional light microscopy (~250 nm)<sup>30,31</sup> impaired, until now, detection of size variations in the range of those required for the doubling of *S. aureus* cell volume (see discussion). These variations can, however, be observed by SIM, which improves the lateral xy resolution to approximately 110 nm<sup>32</sup>. Using this technique, we observed that staphylococcal cells increased in volume during the entire cell cycle, from a volume of  $0.47 \pm 0.07 \mu\text{m}^3$  at the beginning of Phase 1 to a volume of  $0.91 \pm 0.12 \mu\text{m}^3$  at the end of Phase 3 (Fig. 1d and Table 4). If enlargement of *S. aureus* cells was due mainly to the remodelling of the flat septum into a hemisphere, the volume increase should be essentially restricted to the process of splitting and reshaping of the septum. On the contrary, we have observed that there is no significant increase in volume when staphylococcal cells divide, i.e., that each of the two daughter cells has approximately half of the volume of the Phase 3 mother cell (Fig. 1d). Furthermore, the largest and fastest increase in volume occurs during Phase 3 ( $\Delta\text{volume} = 0.16 \pm 0.07 \mu\text{m}^3$  at a rate of  $0.009 \pm 0.003 \mu\text{m}^3 \text{min}^{-1}$ , Table 4), during which there is no reshaping of the flat septum, clearly

indicating that other mechanisms must be involved with the enlargement of *S. aureus* cells.

**Table 4. Average volume ( $\mu\text{m}^3$ ) of *S. aureus* cells upon initiation and completion of the three phases of the cell cycle.**

Strain	P1		P2		P3	
	Initial	Final	Initial	Final	Initial	Final
COL	0.47±0.07	0.62±0.08	0.63±0.10	0.72±0.10	0.73±0.10	0.91±0.12
COL $\Delta$ <i>pbpD</i>	0.40±0.08 (***)	0.59±0.10	0.61±0.08	0.69±0.09	0.70±0.07	0.86±0.11
COL $\Delta$ <i>atl</i>	0.46±0.07	0.66±0.10	0.68±0.10(*)	0.79±0.10(**)	0.82±0.13 (***)	0.97±0.16
COL $\Delta$ <i>se1</i>	0.48±0.07	0.55±0.06 (***)	0.55±0.07 (***)	0.64±0.09 (***)	0.63±0.09 (***)	0.98±0.17 (*)

\*  $P \leq 0.05$ , \*\*  $P \leq 0.01$ , \*\*\*  $P \leq 0.001$  mutants vs. parental strain COL (n=40 cells for each strain)

Next we wondered if enlargement of cells occurred via remodelling only of the material derived from the previous septum or via remodelling of the entire cell surface (Fig. 4a). In the former case, the percentage of “new” cell wall should increase during the course of the cell cycle, eventually reaching half of the total cell surface, while in the latter case the ratio of new to old cell wall observed immediately after splitting of the mother cell (~39% to ~61%, respectively, Fig. 4b) should be maintained over the cell cycle. Therefore, following the growth of cells in which the “old” cell wall was labelled with WGA-488 should allow us to determine how *S.*

*aureus* cells enlarge. The perimeter of WGA-488 labelled cells increased from  $3.08 \pm 0.17 \mu\text{m}$  to  $3.40 \pm 0.21 \mu\text{m}$  after 60 minutes on the slide, confirming that cells were growing. Under these conditions, the fraction of cell wall labelled by WGA-488 remained at  $60.6 \pm 3.2\%$ , even in cells that were already initiating the next round of division (Fig. 4b and c). Similar results were obtained with HADA labelled cells, in which the fraction of labelled cell wall remained at  $60.5 \pm 3.8\%$  after 60 minutes (Fig. 4d and e), indicating that cell enlargement was due to remodelling of the entire cell surface and not exclusively of the septal material.

### ***S. aureus* enlarges via peptidoglycan synthesis and autolysis**

Enlargement of bacterial cells can occur via synthesis of new peptidoglycan, autolysis of old peptidoglycan, or a combination of both processes. We have previously observed that peptidoglycan synthesis occurred mostly at the division septum<sup>5</sup>. Given that we have now shown that growth of staphylococcal cells occurs via remodelling of the entire cell surface, we considered the possibility that enlargement was mainly due to autolytic activity. However, autolysis without synthesis would lead to a thinning and/or increase in the porosity of the old peptidoglycan mesh over consecutive generations. Since approximately 60% of old cell wall is transmitted to daughter cells in each cell division, staphylococcal cells would have regions of the surface a few generations old, which were necessarily submitted to the enlargement process multiple times.



Thinning of these regions due to peptidoglycan autolysis without synthesis could therefore endanger the integrity of the bacterial cell. Making use of newly available tools to study peptidoglycan synthesis and to image protein localisation, we revisited the question regarding the localisation of peptidoglycan synthesis in *S. aureus*. *S. aureus* cells were labelled with HADA, which can be incorporated by PBPs in the pentapeptide chain of peptidoglycan<sup>24</sup>. Cells in growth phases 2 and 3, i.e., cells with partial or complete septa, showed labelling mostly at the septum, in agreement with previous reports showing that the majority of PBP activity takes place at the septum<sup>4,5,33</sup>. However, peripheral signal was also observable (Fig. 6a). Labelling around the entire cell surface was even more noticeable in Phase 1 cells, lacking a division septum (Fig. 6a, arrows).

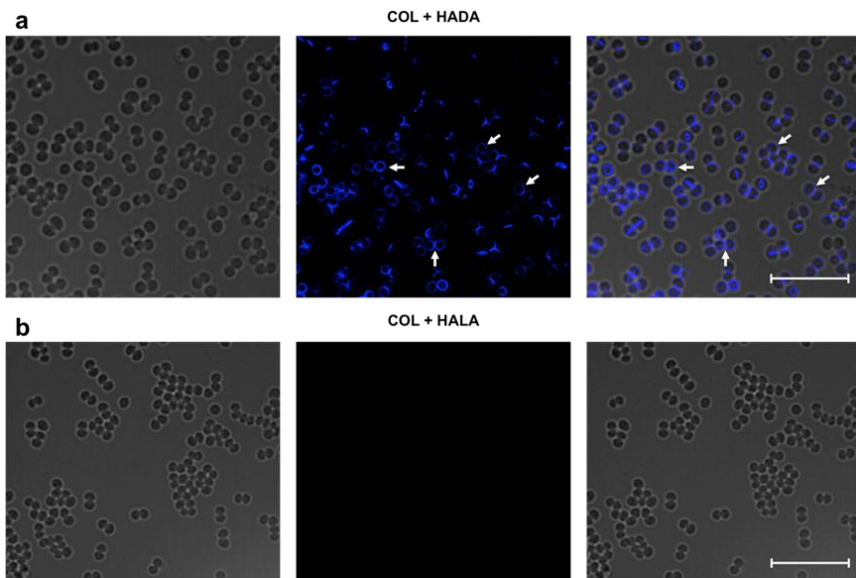


**Figure 6.** Fluorescent D-amino acid HADA is incorporated at the peripheral wall of *S. aureus* cells. *S. aureus* COL cells were labelled for 5

minutes with HADA, a fluorescent derivative of 3-amino-D-alanine that can be incorporated in the pentapeptide chain of peptidoglycan (a) or its L-enantiomer HALA that should not be incorporated into the peptidoglycan (b), used as a control for non-specific binding. Cells were then imaged by SIM, showing that the peripheral walls of cells in phase 1 (examples indicated by white arrows) were labelled by HADA but not by HALA. Scale bars = 10  $\mu$ m

We then asked which of the four native *S. aureus* PBPs had peripheral activity. Given that PBP1 and PBP2 are essential proteins in MSSA strains and therefore cannot be depleted<sup>34,35</sup>, *S. aureus* mutants lacking PBP3 and PBP4 were initially tested. For this purpose, we used a green fluorescent variant of HADA, NADA. COL $\Delta$ *pbpD* cells, lacking PBP4, were virtually devoid of NADA labelling away from the septum (Fig. 7b), when compared to COL (Fig. 7a), showing that this protein is the main enzyme responsible for the peripheral signal. Complementation of COL $\Delta$ *pbpD* with a plasmid-encoded PBP4 resulted in recovery of the peripheral signal (Fig. 7c and d). A comparison of the ratio of the septal versus peripheral fluorescence signal in the COL parental strain ( $7.91 \pm 0.42$ ) and COL $\Delta$ *pbpD* ( $18.7 \pm 0.76$ ) confirmed that incorporation of D-alanine labelled analogues was essentially absent from the peripheral wall of the mutant lacking PBP4 (Fig. 7e). In agreement, localisation of a fluorescent derivative of PBP4 showed that although this protein is mainly localized at the septum, as we have previously reported<sup>36</sup>, peripheral fluorescent signal could also be observed (Fig. 7f). Quantification by PhotoActivated Localisation Microscopy (PALM)

showed that  $26 \pm 11\%$  of the total PBP4 molecules (fused to photoactivatable mCherry) in phase 3 cells are present at the peripheral membrane (Fig. 7g).

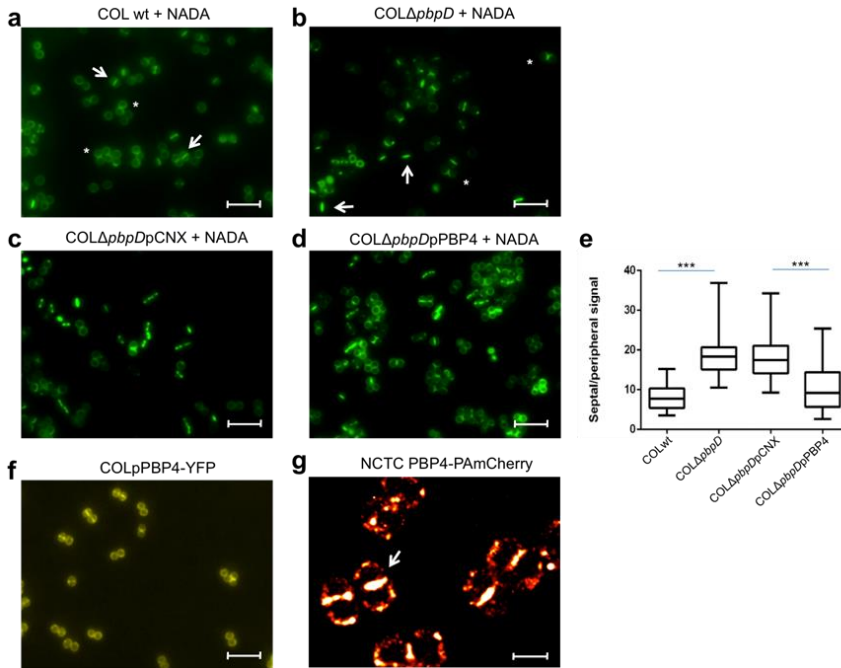


**Figure 7. PBP4 is active at the division septum and at the peripheral wall.**

(a) *S. aureus* COL cells were incubated for 20 minutes with NADA and imaged by wide-field fluorescence microscopy. Cells with partial (Phase 2) or complete (Phase 3) septa (arrows) showed labelling mostly at the septum, although some fluorescent signal could also be observed at the peripheral cell surface. Cells without septa (Phase 1, asterisks) showed NADA incorporation at the peripheral cell wall. Scale bar = 5  $\mu\text{m}$ . (b) COLΔpbpD cells, lacking PBP4 were imaged as described above. NADA incorporation at the peripheral cell surface was virtually absent both in cells undergoing septation (arrows) and in newly split cells (asterisk), indicating that PBP4 is responsible for the majority of peripheral NADA incorporation. Scale bar = 5  $\mu\text{m}$ . (c,d) Strain COLΔpbpD was complemented with empty pCNX vector (c) and pCNX encoding PBP4 under the control of *Pcad* (d), in the presence of cadmium chloride (1 $\mu\text{M}$ ), and imaged as above. NADA incorporation at

the peripheral cell surface was only observed in the strain complemented with PBP4. Scale bar = 5  $\mu\text{m}$ . **(e)** The intensity of the NADA fluorescence signal was measured at the septum and peripheral wall, in cells (n=50) with complete division septa, and the ratio between septal and peripheral signal was calculated for each cell. This ratio was significantly higher for COL $\Delta$ pbpD than for COL cells ( $18.7\pm 5.4$  vs  $7.9\pm 3.0$ ,  $P<0.001$ ) showing that the mutant lacking PBP4 is deficient in peripheral NADA incorporation. This ratio was also higher in COL $\Delta$ pbpD containing the empty vector pCNX than in the same strain complemented with plasmid-encoded PBP4 ( $18.2\pm 5.7$  vs  $10.2\pm 5.4$ ,  $P<0.001$ ). **(f)** Localisation of a YFP-tagged derivative of PBP4 in COL cells by wide-field fluorescence microscopy showing that a small fraction of PBP4 localizes at the cell periphery. Scale bar = 5  $\mu\text{m}$ . **(g)** PALM image showing PBP4-PAmCherry localisation in *S. aureus* NCTC8325-4 background. Cells (n=50) showing PBP4-PAmCherry in complete septa (white arrow) were used to quantify the number of PBP4 molecules (n=27533) present either at the peripheral membrane ( $26\pm 11\%$ ) or at the septa ( $74\pm 11\%$ ). Images are false coloured showing red to white increasing intensity range. Scale bar, 1  $\mu\text{m}$ .

Furthermore, the duration of Phase 1 is longer in COL $\Delta$ pbpD than in the parental strain COL (Fig. 8a) and the cell volume is smaller (Table 4), reinforcing the hypothesis that PBP4 is one of the proteins that have a role in peripheral peptidoglycan synthesis during this growth phase. In contrast, cell elongation is unaffected in COL $\Delta$ pbpD cells (Table 3), suggesting that additional proteins play a role in cell growth. We therefore evaluated the role of two major autolysins, Atl<sup>7</sup> and Sle1<sup>37</sup> in cell enlargement and elongation, as well as in septum remodelling, by deleting chromosomal *atl* or *sle1* genes of strain COL. The lack of Atl amidase and glucosaminidase activities led to larger cells which are less elongated when compared to the

parental strain COL (Tables 3 and 4), indicating that Atl autolytic activity is involved not only in cell separation, as previously shown<sup>8,9</sup>, but also in cell size homeostasis and shape maintenance. COL $\Delta$ *sle1* cells remain elongated throughout the entire cell cycle, which could result from increased stiffness of peptidoglycan in the absence of Sle1 amidase activity, possibly impairing correct reshaping of the cell following division. Furthermore, these cells have a longer Phase 3 than the parental strain COL (Fig. 8a), suggesting that cell splitting is impaired in this mutant.

Interestingly, we have observed the appearance, albeit at low frequency, of cells with the shape of the letter “D” in cultures of COL $\Delta$ *sle1* (Fig. 8b, arrows). These cells seem to be impaired in the process of reshaping of the flat septum, generated immediately after the splitting of the mother cell, into a curved hemisphere. D-shaped cells were never observed in the parental strain COL by SIM. This phenotype seems to be a consequence of defects in specific autolytic enzymes whose activity is required for the reshaping of the flat septum, since asymmetric cells were also identified at higher frequencies than in the parental strains in (i) an *sle1* deletion mutant in the background of a different *S. aureus* strain, namely NCTC8325-4 (Fig. 9b); (ii) an NCTC8325-4 mutant lacking LytM, an autolysin with glycylglycine endopeptidase activity<sup>38</sup> (Fig. 9c); (iii) a COL mutant depleted for the two-component system WalK/WalR (also known as YycG/YycF), which positively controls autolytic activity<sup>39</sup> (Fig. 9e).

Interestingly, although WalKR is essential in RN4220<sup>39</sup>, strain COL grows in its absence.

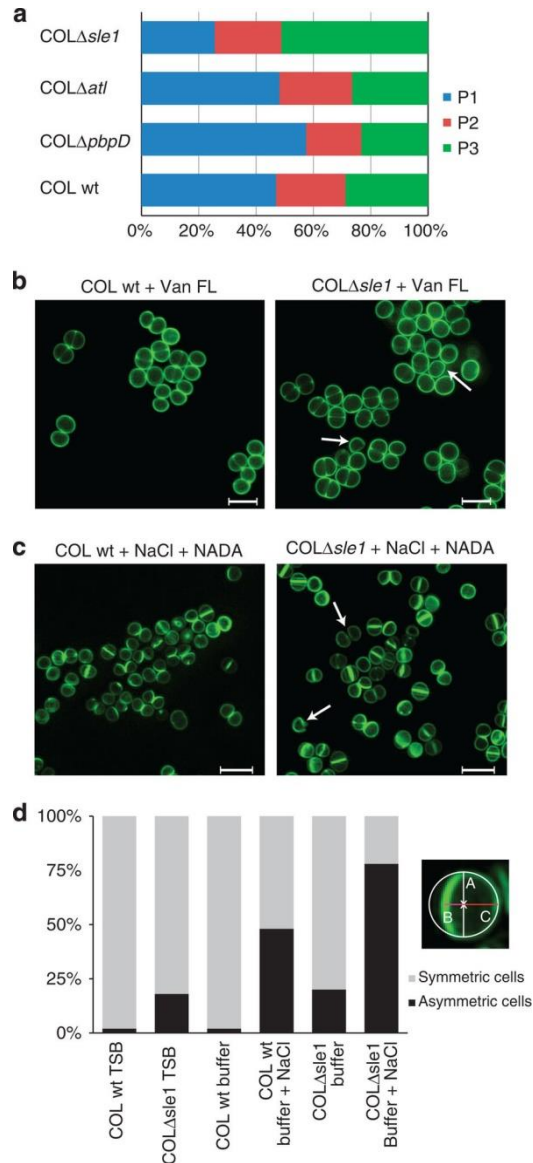


**Figure 8. Effect of impaired peptidoglycan synthesis or autolysis on the cell cycle and morphology of *S. aureus*.** (a) Duration of phases of the cell cycle of *S. aureus* mutants lacking peptidoglycan synthesis enzyme PBP4 (COL $\Delta$ pbpD, total duration of cell cycle 73 $\pm$ 10 min) or autolysins Atl

(COL $\Delta$ *atl*, 82 $\pm$ 8 min) and Sle1 (COL $\Delta$ *sle1*, 86 $\pm$ 15 min), compared with the parental strain COL (66 $\pm$ 9 min). Cells ( $n=40$  for each phase) were growing in solid medium and only cells that completed at least one growth phase during the time of the experiment were included in the analysis. Approximately 50% of COL $\Delta$ *pbpD* cells that initiated Phase 1 did not complete it (versus 20% of COL cells) and were not included in the analysis. **(b)** The cell wall of COL and COL $\Delta$ *sle1* was stained with Van-FL and imaged by SIM. Asymmetric cells with a shape close to a 'D' (white arrows) were observed, indicating that reshaping of the flat septum into a curved hemisphere following division was impaired in this mutant. **(c)** Exponentially growing COL and COL $\Delta$ *sle1* cells were stained with NADA, incubated for 15 min in saturating concentration of NaCl, placed on an agarose pad containing the same salt concentration and imaged by SIM. Cells with a shape close to a 'D' (examples indicated by white arrows) were observed at higher frequency in the mutant lacking Sle1 (right) than in the parental strain COL (left). Scale bars, 2  $\mu$ m. **(d)** Symmetry of cells depicted in panels **b** and **c** was assessed by fitting an ellipse to the cells ( $n=50$  for each class) and defining its centre (X) as the middle point of the shorter axis (A). The distances from X to new peripheral cell wall (B) and old peripheral cell wall (C) were calculated. Cells were considered as asymmetric (black bars) if the ratio C/B was more than 1.33 and symmetric (grey bars) when this ratio was  $\leq 1.33$ . wt, wild type.

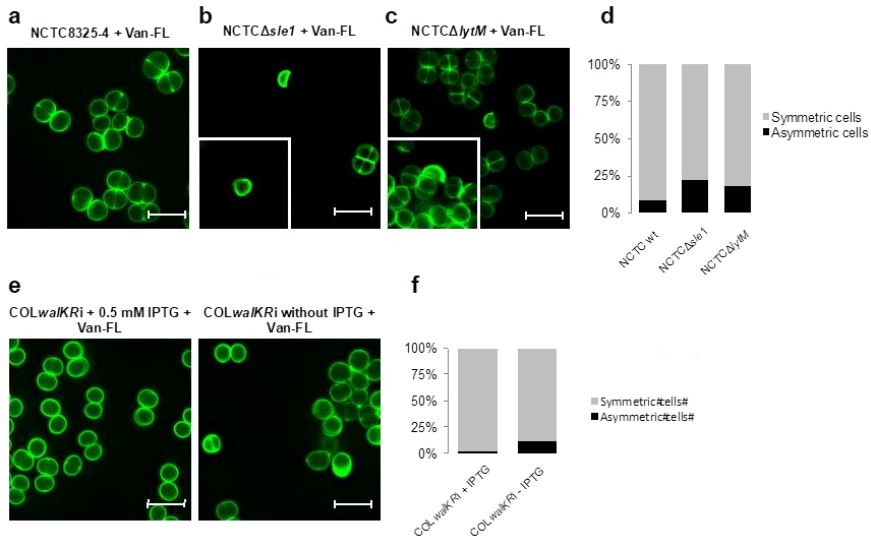


**Figure 9. Effect of impaired peptidoglycan autolysis on the morphology of *S. aureus*.** Cells of MSSA strain NCTC8325-4 (**a**), its mutant lacking autolysin Sle1 (NCTC $\Delta$ sle1, **b**), or lacking autolysin LytM (NCTC $\Delta$ lytM, **c**) were labelled with cell wall dye Van-FL and imaged by SIM, confirming the presence of D-shaped cells in the mutants. (**d**) Symmetry of cells depicted in panels “a” to “c” was assessed as described in Fig. 8d, showing an increase in the frequency of asymmetric cells in the two autolysin mutants. (**e**) Cells of MRSA strain COL with the two-component system *walkKR* (positive regulator of autolysins) placed under the control of the IPTG-inducible promoter *Pspac* (COLwalkKRi), were grown in the presence or in the absence of inducer, labelled with Van-FL and imaged by SIM, showing the presence of D-shaped cells. (**f**) Symmetry of cells depicted in panel “e” was assessed as described in Fig. 8d, showing an increase in the frequency of asymmetric cells upon depletion of the WalkR two-component system. Scale bars = 2  $\mu$ m

In order to determine if turgor pressure also had a role in driving the reshaping of the flat septum, we incubated COL and COL $\Delta$ sle1 in buffer containing saturating NaCl concentration. The decreased turgor pressure led to higher frequency of “D” shaped or asymmetric cells both in COL $\Delta$ sle1 and in parental strain COL, albeit



to lower levels in the parental strain (Fig. 8d). Strain COL $\Delta$ *sle1* complemented with a plasmid-encoded *Sle1* behaved as the parental strain COL (Fig. 10). These results suggest that the division septum requires the action of both autolytic enzymes and turgor pressure to change from a flat to a curved surface, although we cannot exclude the possibility that the effect of NaCl is due to an impact on the activity of autolysins.

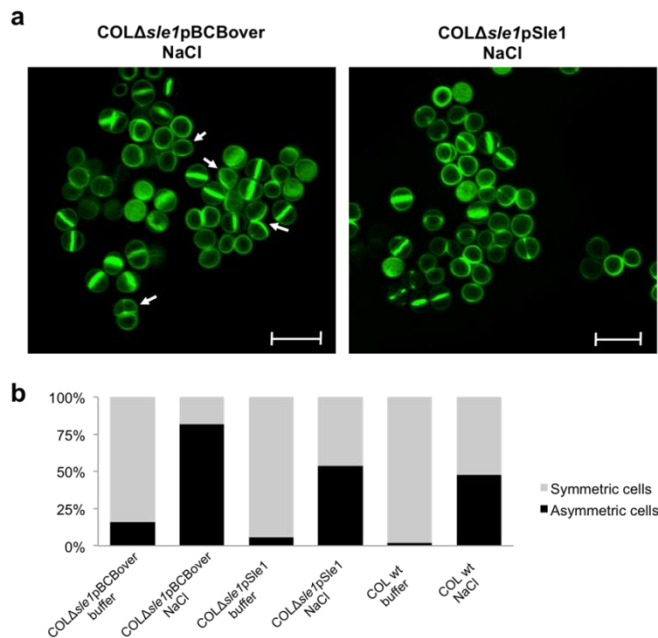


**Figure 10. Complementing of COL $\Delta$ *sle1* with plasmid-encoded *sle1*.** (a) Cells of COL $\Delta$ *sle1* strain were transformed with empty vector pBCBover (left) or the same vector encoding *sle1* under the control of IPTG inducible  $P_{spac}$  promoter (right) were labelled with NADA, incubated for 15 minutes in saturating concentration of NaCl, placed on an agarose pad containing the same salt concentration and imaged by SIM. Asymmetric cells with a shape close to a “D” (white arrows) were observed in higher frequency in the strain containing the empty vector. Scale bars = 2  $\mu$ m. (b) Symmetry of cells

## *Chapter II*

depicted in panel “a” was assessed as described in Fig 8d, showing that the phenotype of strain COL $\Delta$ *sle1* is complemented by the expression of *Sle1* from a plasmid.

## Discussion

Despite its importance as a clinical pathogen, the small size of *S. aureus* cells has impaired a detailed analysis of the morphological changes occurring during its cell cycle, given that size variations required to double the cell volume are close to the limit of resolution of conventional optical microscopy: *S. aureus* cells are approximately 1  $\mu\text{m}$  in diameter (or 0.52  $\mu\text{m}^3$  in volume). Approximating the cell shape to a sphere, an increase of the diameter to 1.26  $\mu\text{m}$  is sufficient to double cell volume. However, this 260 nm increase is close to the diffraction limit of resolution of conventional optical microscopy, which is  $\sim 250$  nm for most biocompatible fluorophores<sup>30,31</sup>.

The current model for *S. aureus* cell division postulates that cells do not significantly enlarge during the cell cycle and that the major variation in cell volume occurs upon splitting of the mother cell, when the flat septum is reshaped into a curved surface to generate one hemisphere of each daughter cell. This model was based on the fact that both incorporation of new peptidoglycan material and localisation of the major peptidoglycan synthesis enzymes, the PBPs, occurred mostly at the septum<sup>5,22,33,34,36</sup>, two observations that still hold true. However, here, by fast imaging of dividing *S. aureus* cells, we show that reshaping of the division septum is an extremely rapid process, on the timescale of less than two milliseconds, and therefore not compatible with a duplication of cellular volume and the consequent abrupt changes in concentrations of cellular contents. It is

therefore more likely that, similar to other bacteria, the volume of *S. aureus* cells gradually increases over the cell cycle, but these size variations are too small to be observable by conventional light microscopy.

Recent advances in fluorescence microscopy, specifically the introduction of super-resolution techniques, now allow an unprecedented level of detail in the analysis of bacterial cell morphology. Making use of SIM, with a lateral resolution of approximately 110 nm<sup>32</sup>, we measured variations of the volume of *S. aureus* cells and concluded that (i) cell volume increases gradually over the entire cell cycle and (ii) there is no substantial increase in cell volume due to reshaping of the flat septum, given that upon splitting of a mother cell, each newly generated daughter cell has approximately half of the mother cell's volume. Furthermore, and contrary to previous assumptions, the cell wall material resulting from the division septum of the mother cell (new cell wall) does not constitute half of the cell surface of each daughter cell, but approximately 33% (Fig. 11). Taken together, these observations suggest that other mechanisms besides septum reshaping are responsible for cell growth in *S. aureus*.

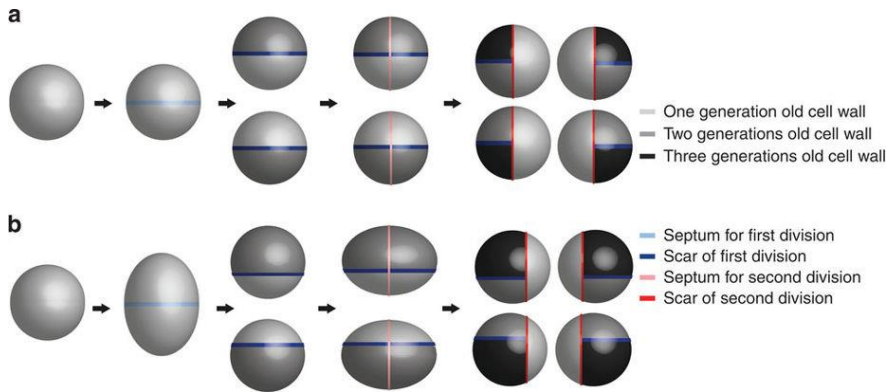


**Figure 11. Comparison of two models for *S. aureus* growth and division.** (a) Previous model which assumed that *S. aureus* cells remained approximately spherical over the cell cycle and that, on division, the cell wall material from the septum of the mother cell increased in cell surface area to constitute half (one hemisphere made of new cell wall) of the cell surface of each daughter cell. As a consequence, scars of previous divisions divided the cell in quadrants and formed T-junctions at the cell poles, which could be used as topological cues to direct cellular processes such as chromosome segregation. These scars were proposed to encode epigenetic information that could be used by *S. aureus* to determine orthogonal placement of division septum. (b) In the model proposed based on this work, *S. aureus* cells are approximately spherical at the beginning of the cell cycle and elongate as the cell cycle progresses. On division, there is no increase in the surface area of the previous septum, which becomes  $\sim 33\%$  of the surface area of each daughter cell. This asymmetry in the regions composed of new and old cell wall results in scars of previous divisions that do not divide cells in quadrants. Consequently, T-junctions of scars of two previous divisions are not located at the cell poles. Two consecutive divisions in orthogonal planes are depicted in panels (a,b).

Upon division of the mother cell, *S. aureus* cells could grow by (i) remodelling and enlarging only the new cell wall material or (ii) remodelling the entire cell surface. In the first case, the surface area corresponding to new cell wall material would be expected to expand

from 33% and eventually constitute half of the cell surface, while in the second case the 33/67 ratio of new/old cell wall would be maintained during the entire cell cycle. We have labelled peripheral cell wall with a lectin (WGA-488) as well as a fluorescent derivative of D-alanine (HADA) and confirmed that the latter hypothesis is correct.

Cell enlargement can occur by synthesis of new peptidoglycan material, autolysis of old peptidoglycan or a combination of both processes. The fact that the entire cell surface is enlarged during growth, but different sections of the surface vary in age, seems incompatible with the notion that peptidoglycan synthesis or autolysis alone are responsible for the increase in cell surface. If that were the case, then regions with different ages of the cell wall would have different thickness and/or porosity. By transmission electron microscopy, *S. aureus* peripheral cell wall seems homogeneous in thickness<sup>40</sup>. The porosity of new and old cell wall may be different, as the former shows a series of concentric rings while the latter appears as a network of fibers with a large number of empty spaces between them, perhaps resulting from autolytic activity<sup>28,41</sup>. However, if this autolytic activity would occur across the entire cell surface multiple times, i.e., over several generations, in the absence of peptidoglycan synthesis, holes in older regions of the cell surface would presumably become larger, possibly endangering the integrity of the cell.

It therefore seems likely that peptidoglycan synthesis has to occur across the cell surface, concomitantly with autolysis. In fact, we were able to detect peripheral PBP activity through the incorporation of fluorescent derivatives of 3-amino-D-alanine<sup>24</sup>, mediated mostly by PBP4, in agreement with recent data by Gautam et al.<sup>42</sup>. It is possible that other PBPs also have a role in peripheral peptidoglycan synthesis, which is not detected in our assay given that PBP4 is the main responsible for incorporation of exogenous peptidoglycan synthesis probes<sup>42,43</sup>. It is important to note that these probes may be incorporated by PBPs in an exchange reaction that occurs outside the cell, and therefore do not necessarily reflect the sites of incorporation of lipid-linked peptidoglycan precursors. It is possible that PBP4 activity is required, not (only) to incorporate new peptidoglycan precursor molecules, therefore increasing the amount of peptidoglycan material in the cell wall, but also to make new bonds in pre-existing material that was subjected to autolytic activity during cell expansion leading to an increased mechanical strength. In fact PBP4 was shown to be responsible for the very high levels of peptidoglycan crosslinking characteristic of *S. aureus*<sup>12,44</sup> and required to increase the stiffness of the cell envelope<sup>13</sup>.

Finally, we have also pondered over the question of the extremely fast process of septum reshaping into a curved hemisphere, namely if it was a purely mechanical process or if it required enzymatic activity. Previous reports using atomic force microscopy (AFM) imaging have shown the presence of perforation

holes around the bacterial circumference coincident with the outer edge of the division septum. These holes become larger, merge and form longer nicks in the peripheral wall as splitting of the septum proceeds<sup>41</sup>. These holes are most likely the result of activity of autolysins such as Atl, a protein required for cell separation, which localizes in rings at the division site<sup>8,9</sup>. Interestingly, Atl localizes exclusively at the external edge of the septum, not across the entire septal surface<sup>9</sup>, suggesting that its activity is only required at the initial steps of splitting. This would be in agreement with the suggestion by Matias and Beveridge that the septum of *S. aureus* has a middle zone that separates two adjacent septal cross walls<sup>45</sup>. Once the outer edge of the septum is cleaved by autolysins, cell separation could proceed through a merely mechanical process driven by turgor pressure on the two separate halves of the cross-wall, as no additional cleavage of peptidoglycan bonds would be required across the septum. The time required for splitting, which we have now shown to occur in less than two milliseconds, does indeed suggest a mechanical process, probably driven by turgor pressure, in agreement with our data showing that septum reshaping is impaired in high osmolarity conditions and with recent data published while this manuscript was under revision<sup>46</sup>. However, we have also shown that autolysins such as Sle1 and LytM have a role in reshaping of the flat septum, given that mutants lacking one of these proteins, particularly when exposed to medium with high osmolarity, generate daughter cells in which the previous septum remains flatter.



Nevertheless we cannot determine if Sle1 and LytM activities occur before or during splitting. Interestingly, Bailey and colleagues have recently shown that the new cell wall material in the flat septum is stiffer than the rest of the cell wall and becomes softer when fully expanded into a hemisphere<sup>47</sup>. Therefore, these authors suggest that reshaping of the flat septum cannot occur only through stretching (as this would require the flat septum to be thicker but softer than the rest of the cell wall), but instead requires partial degradation of the peptidoglycan by autolytic enzymes<sup>47</sup>.

The increase in resolution resulting from advances in super-resolution microscopy has allowed us to completely redefine the cell cycle of *S. aureus*, one of the most relevant bacterial pathogens, with important implications for current models of cell division in cocci. *S. aureus* cells divide in three orthogonal planes over three consecutive division cycles<sup>1,2</sup>, raising the question of how do the cells retain “memory” of the two previous planes of division, in order to define a third, perpendicular, division plane. Scars of previous divisions have been proposed to contain epigenetic information regarding the previous planes of division<sup>3</sup>. Junctions of these scars at the cell poles could be used as topological cues to drive chromosome segregation in an axis perpendicular to the next division plane<sup>48</sup>. The process of nucleoid occlusion, which prevents assembly of the divisome over the chromosome, would then restrict the localisation of the next division plane to a plane orthogonal to the two previous ones<sup>48</sup>. However, these models assume that scars of previous division planes

are placed precisely at the center of the cell (similar to the equator or meridians of earth, Fig. 11a), and therefore cross each other at poles of the cells. Our observation that lines dividing the *S. aureus* cell surface containing old/new cell wall material do not divide the cell in two equal parts (Fig. 11b), reopens the question of how staphylococci divide in orthogonal planes. Our findings may also be extended to other cocci which divide in orthogonal planes, such as *Sporosarcina*, and thus our observations described for *S. aureus* should have implications for the global understanding of cell division in other coccal bacteria.

## References

- 1 Tzagoloff, H. & Novick, R. Geometry of cell division in *Staphylococcus aureus*. *J. Bacteriol.* **129**, 343-350 (1977).
- 2 Pinho, M. G., Kjos, M. & Veening, J.-W. How to get (a)round: mechanisms controlling growth and division of coccoid bacteria. *Nat. Rev. Microbiol.* **11**, 601-614, doi:10.1038/nrmicro3088 (2013).
- 3 Turner, R. D. *et al.* Peptidoglycan architecture can specify division planes in *Staphylococcus aureus*. *Nat. Commun.* **1**, 26, doi:10.1038/ncomms1025 (2010).
- 4 Scheffers, D. J. & Pinho, M. G. Bacterial cell wall synthesis: New insights from localisation studies. *Microbiol. Mol. Biol. Rev.* **69**, 585-607, doi:10.1128/MMBR.69.4.585-607.2005 (2005).
- 5 Pinho, M. & Errington, J. Dispersed mode of *Staphylococcus aureus* cell wall synthesis in the absence of the division machinery. *Mol Microbiol* **50**, 871-881, doi:10.1046/j.1365-2958.2003.03719.x (2003).
- 6 Seligman, S. J. & Pincus, M. R. A model for the three-dimensional structure of peptidoglycan in staphylococci. *J. Theor. Biol.* **124**, 275-292 (1987).
- 7 Oshida, T. *et al.* A *Staphylococcus aureus* autolysin that has an N-acetylmuramoyl-L-alanine amidase domain and an endo-beta-N-acetylglucosaminidase domain: cloning, sequence analysis, and characterization. *Proc. Natl. Acad. Sci. U S A* **92**, 285-289 (1995).
- 8 Sugai, M. *et al.* Identification of endo-beta-N-acetylglucosaminidase and N-acetylmuramyl-L-alanine amidase as cluster-dispersing enzymes in *Staphylococcus aureus*. *J. Bacteriol.* **177**, 1491-1496 (1995).
- 9 Yamada, S. *et al.* An autolysin ring associated with cell separation of *Staphylococcus aureus*. *J. Bacteriol.* **178**, 1565-1571 (1996).
- 10 Monk, I. R., Shah, I. M., Xu, M., Tan, M. W. & Foster, T. J. Transforming the untransformable: application of direct transformation to manipulate genetically *Staphylococcus aureus* and *Staphylococcus epidermidis*. *mBio* **3**, doi:10.1128/mBio.00277-11 (2012).
- 11 Gill, S. R. *et al.* Insights on evolution of virulence and resistance from the complete genome analysis of an early methicillin-resistant *Staphylococcus aureus* strain and a biofilm-producing methicillin-resistant *Staphylococcus epidermidis* strain. *J. Bacteriol.* **187**, 2426-2438, doi:10.1128/JB.187.7.2426-2438.2005 (2005).
- 12 Memmi, G., Filipe, S., Pinho, M., Fu, Z. & Cheung, A. *Staphylococcus aureus* PBP4 Is Essential for beta-Lactam Resistance in Community-Acquired Methicillin-Resistant Strains. *Antimicrob. Agents. Chemother.* **52**, 3955-3966, doi:10.1128/AAC.00049-08 (2008).
- 13 Loskill, P. *et al.* Reduction of the peptidoglycan crosslinking causes a decrease in stiffness of the *Staphylococcus aureus* cell envelope. *Biophys. J.* **107**, 1082-1089, doi:10.1016/j.bpj.2014.07.029 (2014).
- 14 Zhang, L., Higgins, M. L. & Piggot, P. J. The division during bacterial sporulation is symmetrically located in *Sporosarcina ureae*. *Mol. Microbiol.* **25**, 1091-1098 (1997).

- 15 Arnaud, M., Chastanet, A. & Debarbouille, M. New vector for efficient allelic replacement in naturally nontransformable, low-GC-content, gram-positive bacteria. *Appl. Environ. Microbiol.* **70**, 6887-6891, doi:10.1128/AEM.70.11.6887-6891.2004 (2004).
- 16 Vagner, V., Dervyn, E. & Ehrlich, S. D. A vector for systematic gene inactivation in *Bacillus subtilis*. *Microbiology* **144**, 3097-3104 (1998).
- 17 Charpentier, E. *et al.* Novel cassette-based shuttle vector system for gram-positive bacteria. *Appl. Environ. Microbiol.* **70**, 6076-6085, doi:10.1128/AEM.70.10.6076-6085.2004 (2004).
- 18 Wu, S., de Lencastre, H., Sali, A. & Tomasz, A. A phosphoglucomutase-like gene essential for the optimal expression of methicillin resistance in *Staphylococcus aureus*: molecular cloning and DNA sequencing. *Microb Drug Resist* **2**, 277-286 (1996).
- 19 Henner, D. J. Inducible expression of regulatory genes in *Bacillus subtilis*. *Methods Enzymol* **185**, 223-228 (1990).
- 20 Subach, F. V. *et al.* Photoactivatable mCherry for high-resolution two-color fluorescence microscopy. *Nature methods* **6**, 153-159, doi:10.1038/nmeth.1298 (2009).
- 21 Atilano, M. L. *et al.* Bacterial autolysins trim cell surface peptidoglycan to prevent detection by the *Drosophila* innate immune system. *eLife* **3**, e02277, doi:10.7554/eLife.02277 (2014).
- 22 Pereira, P., Veiga, H., Jorge, A. & Pinho, M. Fluorescent Reporters for Studies of Cellular Localisation of Proteins in *Staphylococcus aureus*. *Appl. Environ. Microbiol.* **76**, 4346-4353, doi:10.1128/AEM.00359-10 (2010).
- 23 Heintzmann, R. & Cremer, C. G. Laterally modulated excitation microscopy: improvement of resolution by using a diffraction grating. *Proc. SPIE 3568, Optical Biopsies and Microscopic Techniques III*, 185 (1999).
- 24 Kuru, E. *et al.* In situ Probing of Newly Synthesized Peptidoglycan in Live Bacteria with Fluorescent D-Amino Acids. *Angew. Chem. Int Ed. Engl.* **51**, 12519-12523, doi:10.1002/anie.201206749 (2012).
- 25 Kuru, E., Tekkam, S., Hall, E., Brun, Y. V. & Van Nieuwenhze, M. S. Synthesis of fluorescent D-amino acids and their use for probing peptidoglycan synthesis and bacterial growth in situ. *Nat. Protoc.* **10**, 33-52, doi:10.1038/nprot.2014.197 (2015).
- 26 Xu, D. *et al.* The ellipsoidal area ratio: an alternative anisotropy index for diffusion tensor imaging. *Magn. Reson. Imaging* **27**, 311-323, doi:10.1016/j.mri.2008.07.018 (2009).
- 27 Pereira, P., Filipe, S., Tomasz, A. & Pinho, M. Fluorescence ratio imaging microscopy shows decreased access of vancomycin to cell wall synthetic sites in vancomycin-resistant *Staphylococcus aureus*. *Antimicrob Agents Chemother* **51**, 3627-3633, doi:10.1128/AAC.00431-07 (2007).
- 28 Amako, K., Umeda, A. & Murata, K. Arrangement of peptidoglycan in the cell wall of *Staphylococcus* spp. *J. Bacteriol.* **150**, 844-850 (1982).
- 29 Amako, K. & Umeda, A. Scanning electron microscopy of *Staphylococcus*. *J. Ultrastruct. Res.* **58**, 34-40 (1977).

- 30 Abbe, E. Beiträge zur Theorie des Mikroskops und der mikroskopischen  
Wahrnehmung. *Arch Mikrosk Anat* 9: 413–418. *Arch. Mikrosk. Anat.* **9**, 413–  
418 (1873).
- 31 Rayleigh, L. On the theory of optical images, with special reference to  
microscopy. *Philos. Mag.* **42**, 167-195 (1896).
- 32 Schermelleh, L., Heintzmann, R. & Leonhardt, H. A guide to super-  
resolution fluorescence microscopy. *J. Cell Biol.* **190**, 165-175,  
doi:10.1083/jcb.201002018 (2010).
- 33 Pinho, M. G. & Errington, J. Recruitment of penicillin-binding protein PBP2  
to the division site of *Staphylococcus aureus* is dependent on its  
transpeptidation substrates. *Mol. Microbiol.* **55**, 799-807, doi:10.1111/j.1365-  
2958.2004.04420.x (2005).
- 34 Pereira, S. F., Henriques, A. O., Pinho, M. G., de Lencastre, H. & Tomasz, A.  
Role of PBP1 in cell division of *Staphylococcus aureus*. *J. Bacteriol.* **189**, 3525-  
3531, doi:10.1128/JB.00044-07 (2007).
- 35 Pinho, M. G., Filipe, S. R., de Lencastre, H. & al., e. Complementation of the  
essential peptidoglycan transpeptidase function of penicillin-binding  
protein 2 (PBP2) by the drug resistance protein PBP2A in *Staphylococcus  
aureus*. *J. Bacteriol.* **183**, 6525-6531, doi:10.1128/JB.183.22.6525-6531.2001  
(2001).
- 36 Atilano, M. *et al.* Teichoic acids are temporal and spatial regulators of  
peptidoglycan cross-linking in *Staphylococcus aureus*. *Proc. Natl. Acad. Sci. U  
S A* **107**, 18991-18996, doi:10.1073/pnas.1004304107 (2010).
- 37 Kajimura, J. *et al.* Identification and molecular characterization of an N-  
acetylmuramyl-L-alanine amidase Sle1 involved in cell separation of  
*Staphylococcus aureus*. *Mol. Microbiol.* **58**, 1087-1101, doi:10.1111/j.1365-  
2958.2005.04881.x (2005).
- 38 Ramadurai, L., Lockwood, K. J., Nadakavukaren, M. J. & Jayaswal, R. K.  
Characterization of a chromosomally encoded glycylglycine endopeptidase  
of *Staphylococcus aureus*. *Microbiology* **145 ( Pt 4)**, 801-808 (1999).
- 39 Dubrac, S., Boneca, I. G., Poupel, O. & Msadek, T. New insights into the  
Walk/WalR (YycG/YycF) essential signal transduction pathway reveal a  
major role in controlling cell wall metabolism and biofilm formation in  
*Staphylococcus aureus*. *J. Bacteriol.* **189**, 8257-8269, doi:10.1128/JB.00645-07  
(2007).
- 40 Giesbrecht, P., Kersten, T., Maidhof, H. & Wecke, J. Staphylococcal cell wall:  
morphogenesis and fatal variations in the presence of penicillin. *Microbiol.  
Mol. Biol. Rev.* **62**, 1371-1414 (1998).
- 41 Touhami, A., Jericho, M. H. & Beveridge, T. J. Atomic force microscopy of  
cell growth and division in *Staphylococcus aureus*. *J. Bacteriol.* **186**, 3286-3295,  
doi:10.1128/JB.186.11.3286-3295.2004 (2004).
- 42 Gautam, S., Kim, T. & Spiegel, D. A. Chemical Probes Reveal an Extraseptal  
Mode of Cross-Linking in *Staphylococcus aureus*. *J Am Chem Soc*,  
doi:10.1021/jacs.5b02972 (2015).

- 43 Qiao, Y. *et al.* Detection of lipid-linked peptidoglycan precursors by exploiting an unexpected transpeptidase reaction. *J. Am. Chem. Soc.* **136**, 14678-14681, doi:10.1021/ja508147s (2014).
- 44 Leski, T. A. & Tomasz, A. Role of penicillin-binding protein 2 (PBP2) in the antibiotic susceptibility and cell wall cross-linking of *Staphylococcus aureus*: evidence for the cooperative functioning of PBP2, PBP4, and PBP2A. *J. Bacteriol.* **187**, 1815-1824, doi:10.1128/JB.187.5.1815-1824.2005 (2005).
- 45 Matias, V. R. & Beveridge, T. J. Native cell wall organization shown by cryo-electron microscopy confirms the existence of a periplasmic space in *Staphylococcus aureus*. *J. Bacteriol.* **188**, 1011-1021, doi:10.1128/JB.188.3.1011-1021.2006 (2006).
- 46 Zhou, X. *et al.* Bacterial division. Mechanical crack propagation drives millisecond daughter cell separation in *Staphylococcus aureus*. *Science* **348**, 574-578, doi:10.1126/science.aaa1511 (2015).
- 47 Bailey, R. G. *et al.* The Interplay between Cell Wall Mechanical Properties and the Cell Cycle in *Staphylococcus aureus*. *Biophys. J.* **107**, 2538-2545, doi:10.1016/j.bpj.2014.10.036 (2014).
- 48 Veiga, H., Jorge, A. M. & Pinho, M. G. Absence of nucleoid occlusion effector Noc impairs formation of orthogonal FtsZ rings during *Staphylococcus aureus* cell division. *Mol. Microbiol.* **80**, 1366-1380, doi:10.1111/j.1365-2958.2011.07651.x (2011).

## Chapter III

---

Recruitment of MurJ to the divisome  
directs peptidoglycan synthesis to the  
septum

### **Author contributions**

J. M. Monteiro performed all experiments shown except testing antibiotics on the cell cycle, which were performed by P. B. Fernandes. B. M. Saraiva developed tools for automatic cell analysis. N.T. Reichmann, P.B Fernandes, H. Veiga, A.C. Tavares, M. Santos, M.T. Ferreira and V. Macário contributed with either strains or plasmids.

### **Acknowledgments:**

We thank Rita Sobral (FCT-NOVA) for the construction of pSG-murF; Terry Roemer (Merck) for kindly providing DMPI and strains AS-022 and AS-185; Matthew DeLisa (Cornell) for pTRC99a-P7, Richard Novick (NYU) for pCN51, Simon Foster (The University of Sheffield) for antibodies against DivIB and DivIC, Adriano Henriques (ITQB-NOVA) for critical reading of the manuscript and Ludwig Krippahl (FCT-NOVA) for help with image analysis tools.

This chapter contains data published in:

**Monteiro JM\***, Pereira AR\*, Reichmann NT, Saraiva BM, Fernandes PB, Veiga H, Tavares AC, Santos M, Ferreira MT, Macário V, VanNieuhenhze MS, Filipe SR and Pinho MG. Peptidoglycan synthesis drives an FtsZ treadmilling-independent step of cytokinesis. *Nature* **22**;554(7693):528-532 (2018); doi: 10.1038/nature25506.

\*J.M.M. and A.R.P. contributed equally to this work



## **Abstract**

Survival of most bacteria depends on their ability to synthesize a robust cell wall to interface with the external *milieu*. Peptidoglycan (PG), the major component of the bacterial wall, is a macromolecule that envelops the cell in a tough but flexible mesh-like structure that can bear the mechanical stress resulting from high intracellular turgor. Bacilli and ovococcal species possess two distinct PG synthesis machineries, each dedicated exclusively to either cell elongation or septation. In contrast, coccoid bacteria like *Staphylococcus aureus* possess only one protein machinery that synthesizes PG, which has to be diverted from the periphery of the cell to the septum in preparation for division. The molecular cue that coordinates this transition has remained elusive. Here we investigated the localisation of most proteins involved in PG biosynthesis in *S. aureus* and showed that the putative lipid II flippase MurJ localizes exclusively to the septum during division. Furthermore, we determined that MurJ recruitment to the divisome is dependent on the assembly of the DivIB/DivIC/FtsL complex and drives PG incorporation to mid-cell. Our findings demonstrate an elegant mechanism by which the timely recruitment of a single protein to a precise location in the cell shifts the localisation of PG synthesis.

## Introduction

Biosynthesis of PG is a multi-enzymatic process that must be tightly coordinated with the cell cycle<sup>1</sup> (see Fig. 1a and General Introduction for a review). It starts in the cytoplasm with the synthesis of the UDP-N-acetylmuramyl-pentapeptide precursor, which is linked to lipid carrier bactoprenol and converted into lipid II at the inner face of the membrane. In *S. aureus*, lipid II is then further modified by the addition of a pentaglycine bridge and amidation, before being flipped across the membrane. The last steps of PG synthesis take place at the outer face of the membrane, where lipid II is incorporated into the growing PG network by transglycosylation and transpeptidation reactions catalysed mainly by penicillin-binding proteins (PBPs) (Fig. 1a). The identity of the lipid II flippase has been a matter of debate over the years. The most recent evidence points to MurJ, a member of the MOP (multidrug/oligosaccharidyl-lipid/polysaccharide) exporter superfamily, as the flippase in *Escherichia coli*<sup>2,3</sup>. Although strict MurJ homologs are exclusive to Gram-negative bacteria, in *S. aureus* the essential gene SAV1754 or SACOL1804 (which encodes a MOP protein that we have renamed MurJ) has been reported as a functional MurJ ortholog based on structural topology and genetic evidence<sup>4</sup>. An alternative protein suggested for the flippase function in *E. coli* is FtsW, a member of the SEDS (sporulation, elongation, division and synthesis) protein family. However, recent reports showed that SEDS family members are peptidoglycan transglycosylases that probably function together with

a cognate PBP during PG polymerization<sup>5,6</sup>. *S. aureus* encodes two SEDS proteins, SACOL1122 and SACOL2075 that show significant homology and similar genomic context to *Bacillus subtilis* SEDS proteins FtsW and RodA, respectively, as described before<sup>7</sup>.

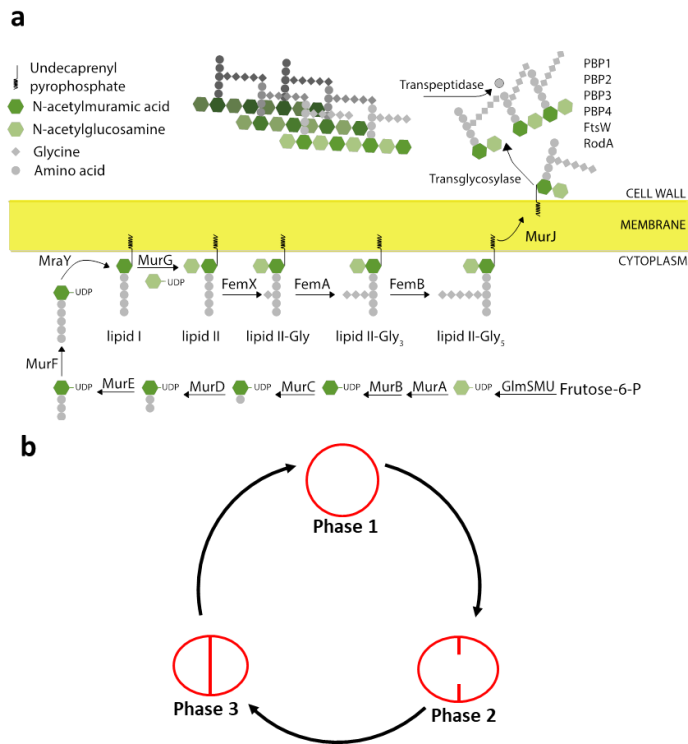


**Figure 1. PG synthesis and cell cycle schematics for *S. aureus*.** (a), Scheme of the peptidoglycan synthesis pathway in *S. aureus*. (b), Scheme of the *S. aureus* cell cycle. Phase 1 cells have not initiated septum synthesis; Phase 2 cells are undergoing septum synthesis; Phase 3 cells have a complete septum undergoing maturation in preparation for splitting.

The biochemical steps of PG synthesis are very similar in all bacteria. Therefore, different bacterial shapes are mainly determined

by the spatial and temporal regulation of PG synthesis, rather than by different chemical compositions of PG<sup>8</sup>. Rod-shaped bacteria, such as *Bacillus subtilis*, achieve their shape through the action of two PG synthesis machineries that incorporate PG at the septum and at the lateral wall, in processes coordinated by cytoskeletal proteins FtsZ and MreB, respectively<sup>9,10</sup>. Ovococcal species such as *Streptococcus pneumoniae* or *Lactococcus lactis* also have two dedicated machineries, but they both localise to the septum and function in succession<sup>8</sup>. In contrast, cocci like *S. aureus* possess a single PG synthesis machinery, which is active mainly at the septum during division<sup>11</sup>, but also incorporates PG at the cell periphery during initial stages of the cell cycle, i.e., in new born cells which have not initiated septum synthesis, as shown in Chapter II (cells in Phase 1 of the cell cycle, Fig. 1b)<sup>12</sup>. When synthesis of the division septum is initiated (Phase 2), PG synthesis is diverted from the cell periphery to the division site, by an unknown mechanism, where it continues to occur after septum closure (Phase 3), until the cell undergoes splitting, giving two identical daughter cells<sup>12</sup>. In this work, we aimed to identify the molecular cue that determines the shift of PG synthesis from the cell periphery to the septum in cocci.

## **Experimental Procedures**

### **Bacterial growth conditions**

Strains and plasmids used in this study are listed in Table 1. *S. aureus* strains were grown in tryptic soy broth (TSB, Difco) at 200 r.p.m with aeration at 37 °C or on tryptic soy agar (TSA, Difco) at 30 or 37°C. *E. coli* strains were grown in Luria–Bertani broth (Difco) with aeration, or Luria–Bertani agar (Difco) at 37 or 30°C. When necessary, antibiotics ampicillin (100 µg ml<sup>-1</sup>), erythromycin (10 µg ml<sup>-1</sup>), kanamycin (50 µg ml<sup>-1</sup>), neomycin (50 µg ml<sup>-1</sup>) or chloramphenicol (30 µg ml<sup>-1</sup>) were added to the media. 5-bromo-4-chloro-3-indolyl β-D-galactopyranoside (X-gal, Apollo Scientific) was used at 100 µg ml<sup>-1</sup>. Unless stated otherwise, isopropyl β-D-1-thiogalactopyranoside (IPTG, Apollo Scientific) was used at 0.1 mM to induce expression of constructs under the control of the *Pspac* promoter. Cadmium chloride (Sigma-Aldrich) was used at 0.1 µM when required to induce expression of constructs under the control of the *Pcad* promoter.

**Table 1. Strains and plasmids used in this study**

Strains	Description	Source or reference
<i>Escherichia coli</i>		
DC10B	$\Delta$ dcm in the DH10B background; Dam methylation only	13
DH5 $\alpha$	<i>recA endA1 gyrA96 thi-1 hsdR17 supE44 relA1 f80dlacZDM15</i>	Gibco-BRL
<i>Staphylococcus aureus</i>		
COL	HA-MRSA	14
RN4220	Restriction-deficient derivative of NCTC8325-4	15
ColMurB-GFP	COL <i>murB::murB-gfp</i> ; Ery <sup>r</sup>	This Work
ColMurD-GFP	COL <i>murD::murD-gfp</i> ; Ery <sup>r</sup>	This Work
ColMurF-GFP	COL <i>murF::murF-gfp</i> ; Ery <sup>r</sup>	This Work
ColMraY-sGFP	COL pCN- <i>mraYsgfp</i> ; Ery <sup>r</sup>	This Work
BCBMS001	RN4220 <i>murG::murG-gfp</i> ; Ery <sup>r</sup>	16
ColMurG-GFP	COL <i>murG::murG-gfp</i> ; Ery <sup>r</sup>	This Work
ColFemX-sGFP	COL <i>femX::femX-sgfp</i> ; Ery <sup>r</sup>	This Work
ColFemA-mCherry	COL <i>femA::femA-mcherry</i>	This Work
ColFemB-GFP	COL <i>femB::femB-gfp</i> ; Ery <sup>r</sup>	This Work
ColFtsW-mCherry	COL <i>ftsW::ftsW-mCherry</i>	This Work
ColFtsW-sGFP	COL <i>ftsW::ftsW-sgfp</i>	This Work
ColMurJ-mCherry	COL <i>murJ::murJ-mCherry</i>	This Work
ColMurJ-sGFP	COL <i>murJ::murJ-sgfp</i>	This Work
ColRodA-sGFP	COL <i>rodA::rodA-sgfp</i>	This Work
ColsGFP-PBP1	COL <i>pbpA::sgfp-pbpA</i>	This Work
BCBPM073	COL <i>pbpB::sgfp-pbpB</i>	17

*Recruitment of MurJ to the divisome directs peptidoglycan synthesis to the septum*

Strains	Description	Source or reference
ColGFP-PBP3	COL <i>pbpC::sgfp-pbpC</i>	This Work
COLpPBP4-YFP	COL <i>pbpD::pbpD-yfp</i> ; Kan <sup>r</sup>	18
BCBAJ020	COL <i>spa::Pspac-ftsZ-cfp</i>	17
ColFtsZ-mCherryi	COL <i>spa::Pspac-ftsZ-mcherry</i>	This Work
ColDltC-sGFPi	COL <i>spa::Pspac-dltC-sgfp</i>	This work
ColWZ	COL <i>ftsW::ftsW-mCherry, spa::Pspac-ftsZ-cfp</i>	This Work
ColWZpEPSA	COL <i>ftsW::ftsW-mCherry, spa::Pspac-ftsZ-cfp, pEPSA; Cm<sup>r</sup></i>	This Work
ColWZpAS-FtsL	COL <i>ftsW::ftsW-mCherry, spa::Pspac-ftsZ-cfp, pAS-185; Cm<sup>r</sup></i>	This Work
ColWZpAS-FtsA	COL <i>ftsW::ftsW-mCherry, spa::Pspac-ftsZ-cfp, pAS-022; Cm<sup>r</sup></i>	This Work
ColP1Z	COL <i>pbpA::sgfp-pbpA, spa::Pspac-ftsZ-mcherry</i>	This Work
ColP1ZpEPSA	COL <i>pbpA::sgfp-pbpA, spa::Pspac-ftsZ-mcherry, pEPSA; Cm<sup>r</sup></i>	This Work
ColP1ZpAS-FtsL	COL <i>pbpA::sgfp-pbpA, spa::Pspac-ftsZ-mcherry, pAS-185; Cm<sup>r</sup></i>	This Work
ColP1ZpAS-FtsA	COL <i>pbpA::sgfp-pbpA, spa::Pspac-ftsZ-mcherry, pAS-022; Cm<sup>r</sup></i>	This Work
ColJZ	COL <i>murJ::murJ-mCherry, spa::Pspac-ftsZ-cfp</i>	This Work
ColJZpEPSA	COL <i>murJ::murJ-mCherry, spa::Pspac-ftsZ-cfp, pEPSA; Cm<sup>r</sup></i>	This Work
ColJZpAS-FtsL	COL <i>murJ::murJ-mCherry, spa::Pspac-ftsZ-cfp, pAS-185; Cm<sup>r</sup></i>	This Work
ColJZpAS-DivIB	COL <i>murJ::murJ-mCherry, spa::Pspac-ftsZ-cfp, pAS-DivIB; Cm<sup>r</sup></i>	This Work
ColJZpAS-DivIC	COL <i>murJ::murJ-mCherry, spa::Pspac-ftsZ-cfp, pAS-DivIC; Cm<sup>r</sup></i>	This Work
ColZIB	COL <i>spa::Pspac-ftsZ-cfp, pCN-yfpDivIB; Kan<sup>r</sup></i>	This Work
ColZZ	COL <i>spa::Pspac-ftsZ-cfp, pCN-ftsZmch; Kan<sup>r</sup></i>	This Work
ColJIB	COL <i>murJ::murJ-mCherry, pCN-yfpDivIB; Kan<sup>r</sup></i>	This Work
ColWgZm	COL <i>ftsW::ftsW-sgfp, spa::Pspac-ftsZ-mcherry</i>	This Work
ColJgZm	COL <i>murJ::murJ-sgfp, spa::Pspac-ftsZ-mcherry</i>	This Work

### Chapter III

Strains	Description	Source or reference
ColWJ	COL <i>ftsW::ftsW-mCherry, murJ::murJ-sgfp</i>	This Work
ColWJpEPSA	COL <i>ftsW::ftsW-mCherry, murJ::murJ-sgfp</i> , pEPSA; Cm <sup>r</sup>	This Work
ColWJpAS-FtsL	COL <i>ftsW::ftsW-mCherry, murJ::murJ-sgfp</i> , pAS-185; Cm <sup>r</sup>	This Work
AS-022	RN4220 pAS-022; Cm <sup>r</sup>	19
AS-185	RN4220 pAS-185; Cm <sup>r</sup>	19

Plasmids	Description	Source or reference
pBCB4-chE	<i>S. aureus</i> integrative vector for N- and C-terminal mCherry fusions; Amp <sup>r</sup> Ery <sup>r</sup>	20
pTRC99a-P7	Vector containing <i>sgfp-p7</i> ; Amp <sup>r</sup>	21
pMUTINYFPKa n	Vector containing <i>yfp</i> ; Amp <sup>r</sup> Kan <sup>r</sup>	22
pSG5082	<i>S. aureus</i> integrative vector that allows for C-terminal <i>gfpmutP2</i> fusions; Amp <sup>r</sup> Ery <sup>r</sup>	23
pSG-murB	pSG5082 derivative containing a 3' fragment of <i>murB</i> ; Amp <sup>r</sup> Ery <sup>r</sup>	This work
pSG-murD	pSG5082 derivative containing a 3' fragment of <i>murD</i> ; Amp <sup>r</sup> Ery <sup>r</sup>	This work
pSG-murF	pSG5082 derivative containing a 3' fragment of <i>murF</i> ; Amp <sup>r</sup> Ery <sup>r</sup>	This work
pSG-femB	pSG5082 derivative containing a 3' fragment of <i>femB</i> ; Amp <sup>r</sup> Ery <sup>r</sup>	This work
pMAD	<i>E. coli-S. aureus</i> shuttle vector with a thermosensitive origin of replication for Gram positive bacteria; Amp <sup>r</sup> Ery <sup>r</sup> <i>lacZ</i>	24
pMAD- femAmch	pMAD derivative containing a <i>femA-mCherry</i> fusion and the downstream region of <i>femA</i> ; Amp <sup>r</sup> Ery <sup>r</sup>	This work
pMAD-ftsWmch	pMAD derivative containing an <i>ftsW-mCherry</i> fusion and the downstream region of <i>ftsW</i> ; Amp <sup>r</sup> Ery <sup>r</sup>	This work
pMAD-ftsWsgfp	pMAD derivative containing an <i>ftsW-sgfp</i> fusion and the downstream region of <i>ftsW</i> ; Amp <sup>r</sup> Ery <sup>r</sup>	This work
pMAD-murJmch	pMAD derivative containing a <i>murJ-mCherry</i> fusion and the downstream region of <i>murJ</i> ; Amp <sup>r</sup> Ery <sup>r</sup>	This work
pMAD-murJsgfp	pMAD derivative containing a <i>murJ-sgfp</i> fusion and the downstream region of <i>murJ</i> ; Amp <sup>r</sup> Ery <sup>r</sup>	This work
pMAD- rodAsgfp	pMAD derivative containing a <i>rodA-sgfp</i> fusion and the downstream region of <i>rodA</i> ; Amp <sup>r</sup> Ery <sup>r</sup>	This work



pMAD-sgfpPbp1	pMAD derivative containing an <i>sgfp-pbpA</i> fusion and the upstream region of <i>pbpA</i> , Amp <sup>r</sup> Ery <sup>r</sup>	This work
pMAD-sgfpPbp3	pMAD derivative containing an <i>sgfp-pbpC</i> fusion and the upstream region of <i>pbpC</i> , Amp <sup>r</sup> Ery <sup>r</sup>	This work
pBCB13	pMAD derivative with up- and downstream regions of the <i>spa</i> locus and <i>Pspac-lacI</i> , Amp <sup>r</sup> Ery <sup>r</sup> <i>lacZ</i>	20
pBCB13-ftsZmch	pBCB13 derivative containing an <i>ftsZ-mCherry</i> fusion; Amp <sup>r</sup> Ery <sup>r</sup>	This work
pBCB13-dltCsgfp	pBCB13 derivative containing a <i>dltC-sgfp</i> fusion; Amp <sup>r</sup> Ery <sup>r</sup>	This work
pCN51	Shuttle replicative vector containing the cadmium inducible <i>Pcad</i> promoter; Amp <sup>r</sup> Ery <sup>r</sup>	25
pCN-mraYsgfp	pCN51 derivative encoding a <i>MraY-sGFP</i> sandwich fusion; Amp <sup>r</sup> Ery <sup>r</sup>	This work
pCNX	Replicative vector containing the cadmium inducible <i>Pcad</i> promoter; Amp <sup>r</sup> Kan <sup>r</sup>	12
pCN-ftsZmch	pCNX derivative encoding an <i>FtsZ-mCherry</i> fusion; Amp <sup>r</sup> Kan <sup>r</sup>	This work
pCN-yfpDivIB	pCNX derivative encoding an <i>YFP-DivIB</i> fusion; Amp <sup>r</sup> Kan <sup>r</sup>	This work
pFAST3	<i>S. aureus</i> integrative vector that allows for C-terminal <i>sgfp</i> fusions; Amp <sup>r</sup> Ery <sup>r</sup>	26
pFAST-femX	pFAST3 derivative containing a 5' fragment of <i>femX</i> ; Amp <sup>r</sup> Ery <sup>r</sup>	This work
pEPSA5	<i>E.coli/S. aureus</i> shuttle replicative vector containing a xylose-inducible promoter T5X; Amp <sup>r</sup> Cm <sup>r</sup>	27
pAS-022	pEPSA5 derivative encoding a xylose inducible anti- <i>ftsA</i> antisense RNA fragment; Amp <sup>r</sup> Cm <sup>r</sup>	19
pAS-185	pEPSA5 derivative encoding a xylose inducible anti- <i>ftsL</i> antisense RNA fragment; Amp <sup>r</sup> Cm <sup>r</sup>	19
pAS-DivIB	pEPSA5 derivative encoding a xylose inducible anti- <i>divIB</i> antisense RNA fragment; Amp <sup>r</sup> Cm <sup>r</sup>	This work
pAS-DivIC	pEPSA5 derivative encoding a xylose inducible anti- <i>divIC</i> antisense RNA fragment; Amp <sup>r</sup> Cm <sup>r</sup>	This work

### Construction of *S. aureus* fluorescent strains

Cloning of fluorescent fusions in *S. aureus* was done using the following general strategy: plasmids were propagated in *E.coli* strains DC10B or DH5 $\alpha$  and purified from overnight cultures supplemented with the relevant antibiotics. Plasmids were then introduced into electrocompetent *S. aureus* RN4220 cells as described before<sup>28</sup> and

transduced to COL using phage 80 $\alpha$ <sup>29</sup>. Constructs were confirmed by PCR and sequencing of the amplified fragment. Table 2 describes the primers used in this study.

**Table 2. Oligonucleotides used in this work.**

Primer Name	Sequence (5'-3')
murBg_P1	atagg <u>tacc</u> atccgtgaaggtggtattcg
murBg_P2	caat <u>ctcgag</u> cgattccttggatgttacc
murDg_P1	caaggt <u>acca</u> agacaagtgatagagtcgg
murDg_P2	ggaact <u>cgag</u> ataagatgtaaatgggcac
murFg_P1	cgggt <u>tacc</u> acatatgcaagattagg
murFg_P2	gctgct <u>cgag</u> tgaatataagcattacc
femBg_P1	gtggt <u>tacc</u> gattccttgaactgatgag
femBg_P2	ccgt <u>ctcgag</u> ttctttaatttttacgtaattatcc
femAm_P1	ccgg <u>gaattc</u> gcaaatacggaaatgaatataactacgag
femAm_P2	agaaccagcagcggagccagccgactaaaaattctgtcttaac
femAm_P3	tccgctgctggtctgctgagttcatgattgtgagcaagg
femAm_P4	ttgataattccttcttagtacagctgctccatgccacc
femAm_P5	aagggaattatcaaaacatgaaattacagagtaactgttaccg
femAm_P6	cgcggg <u>atcc</u> tattttttaatttttacgtaattatc
ftsWm_P1	tat <u>ccggg</u> ttacaaccgacaattagcatatgcataatgag
ftsWm_P2	cctctccaccagaacctctccaccataaattgtcttcttatcaac
ftsWm_P3	aggagggtctggtggaggaggtctatgattacgaattcgagctcggctgct
ftsWm_P4	tactaaatattgctagtatttttactgtacagctcgtccatgccaccgg
ftsWm_P5	acgagctgtacaagtaaaaaatactagccaatatttagtacg
ftsWm_P6	ttagg <u>atcc</u> ttaccgccaccactgtggcttaatacattagc
ftsWg_P1	tat <u>ccggg</u> ttacaaccgacaattagcatatgcataatgag
ftsWg_P2	gctgctgct <u>tcgac</u> ggagcgccgaggaataaattgtcttcttatcaac
ftsWg_P3	gctgctgct <u>tcgac</u> agtaaaaggagaagaactttcac
ftsWg_P4	gctgctgct <u>tcgac</u> ttattgtatagttcatccatgccatg
ftsWg_P5	gctgctgct <u>tcgac</u> aaaaatactagccaatatttag
ftsWg_P6	ttagg <u>atcc</u> ttaccgccaccactgtggcttaatacattagc
murJm_P1	cggag <u>atc</u> ttggattactggagaaagcgtaagc
murJm_P2	accgactgcaccgcttcgtaaaaacctaactctacg
murJm_P3	agcggtgtagtcggtatgattgtgagcaagg
murJm_P4	cgccatggctgtacagctcgtccatg
murJm_P5	tgccatggcgtagagttaggttttacg

*Recruitment of MurJ to the divisome directs peptidoglycan synthesis to the septum*

<b>Primer Name</b>	<b>Sequence (5'-3')</b>
murJm_P6	cgggatccatacttctgcagtcttattg
murJg_P1	tactccccgggggatattccaaggtataaatc
murJg_P2	gctgcgctgtcgacggagcgccgcaggatcgtaaaacctaactctacgtc
murJg_P3	gctgcgctgtcgacagtaaaggagaagaactttcac
murJg_P4	gctgcgctgtcgacttattgtatagttcatccatgcatg
murJg_P5	gctgcgctgtcgacttaagacgtagagttagg
murJg_P6	tgaggatccgatttctgtcccactcccttacc
rodAg_P1	aatccgggtatcagacaaaattttattacatttttaggtgc
rodAg_P2	tcctccaccagaacctctccaccattacttttggatgggtataaatcgac
rodAg_P3	gaggaggttctggtggaggaggttctatgactagtagtaaggagaagaact
rodAg_P4	ctaaaatagttaaattagtcgactttgtatagttcatcc
rodAg_P5	ggatgaactatacaaaagtcgactaatttaaactattttgag
rodAg_P6	attggatccatgaaggagtgaaatgctatgact
gpbpA_P1	ccgagatctcagggttccaagaatag
gpbpA_P2	gttcttctcttaatttttgccttcgacattac
gpbpA_P3	gaagcaaaaaataaaggagaagaacttttactgg
gpbpA_P4	agagccacctccgcagaaccgctccaccgtcgactttgtatagttcatcc
gpbpA_P5	ggcgggttctggcggaggtggctctgcgaagcaaaaaataaaataaa
gpbpA_P6	cgggatcccaactccaagtcaccttaag
gpbpC_P1	cgagatctatgctgctagtagaaggtagcag
gpbpC_P2	ccttactcataactactctctattcaag
gpbpC_P3	gaggtaggtagttatgagtaaaggagaagaac
gpbpC_P4	agagccacctccgcagaaccgctccaccgtcgactttgtatagttcatcc
gpbpC_P5	ggcgggttctggcggaggtggctctttaaagaactaaagaaaaaac
gpbpC_P6	cgggatcccatttttatcatttggatc
iftsZm_P1	tactccccggggccaataaaactaggagg
iftsZm_P2	ggaggcgccgcaggaacgtctgttcttctgaac
iftsZm_P3	gacgttctgcgccctccgctatcattaaagagttcatg
iftsZm_P4	ccgctcgagttactgtacagctctcc
idltCg_P1	gccccgggaaaaataaggaggaaaaaaatggaatttagagaacaag
idltCg_P2	cgggccgtcgtaactcttaatgcttc
idltCg_P3	gccccggcgccgcccagtaaaaggagaagaactttcac
idltCg_P4	ccggtcaggttaatggtgatgatggtgatggc
mraYg_P1	gcgccccgggcaagaatggctacattaaattag
mraYg_P2	aatgttatatgtaaaatcctaaaagtccaacaacataatg
mraYg_P3	gattttaccatataacattatgagtaaaggagaagaac
mraYg_P4	cacttagcagggtgtcactttgtatagttcatcc
mraYg_P5	aacctgctaaagtttatgggagatacaggtagc

Primer Name	Sequence (5'-3')
mraYg_P6	gcgcg <u>ccccggg</u> gtaatgcactccaatccataaac
ftsZm_pCNX_P1	cg <u>ggatc</u> caaaaaataaggaggaaaaaaatgtagaattgacaaggattt
ftsZm_pCNX_P2	gcc <u>gaattc</u> tacttgtagactcgtccatgcc
ydivIB_pCNX_P1	gcgcg <u>ccccggg</u> tgattaactttataaggagg
ydivIB_pCNX_P2	ctccgccagaaccgctccacctttatataattcatcc
ydivIB_pCNX_P3	gcggttctggcggagggtgctctatggatgataaaacg
ydivIB_pCNX_P4	gcg <u>ggatc</u> cttaattattcttacttgattgtttgtaattttgttaaaacgc
femXg_P1	cg <u>gggtacc</u> cgcttggtttaagcgaggg
femXg_P2	cgcgctc <u>gagtt</u> tcgttttaattacgag
ASdivIB_P1	gcgcg <u>gaattc</u> tgattcgctttgtcgcttacg
ASdivIB_P2	gcg <u>ggatc</u> catgattctacagactctaattg
ASdivIC_P1	gcgcg <u>gaattc</u> ttttgttctttgaaactgtg
ASdivIC_P2	gcg <u>ggatc</u> cattggagggtgacaagcaatg

Underlined sequences correspond to restriction sites

The ColMurB-GFP, ColMurD-GFP, ColMurF-GFP and ColFemB-GFP strains were constructed using the pSG5082 vector<sup>30</sup>. Briefly, DNA fragments with approximately 500 bp spanning the 3' ends (minus stop codons) of the *murB*, *murD*, *murF* and *femB* genes from COL were amplified using primer pairs murBg\_P1/murBg\_P2; murDg\_P1/murDg\_P2; murFg\_P1/murFg\_P2 and femBg\_P1/femBg\_P2, respectively. Fragments were digested with *KpnI* and *XhoI* restriction enzymes and cloned into pSG5082 upstream and in frame with *gfpmutP2*, originating plasmids pSG-murB, pSG-murD, pSG-murF and pSG-femB. These plasmids were then electroporated to RN4220, where they integrated in the genome by a single homologous recombination event and subsequently transduced to COL. Resulting strains contain the corresponding fluorescent fusions in each gene's native locus under the control of its

native promoter, followed by the pSG5082 backbone and a truncated copy of the gene. The strategy to construct ColFemX-sGFP was essentially the same, except that the pFAST3<sup>31</sup> vector was used instead of pSG5082. A *femX* fragment was amplified from COL DNA with primers femXg\_P1 and femXg\_P2, digested with *KpnI/XhoI* and cloned into pFAST3 upstream and in frame with *sgfp*, giving pFAST-femX, which was electroporated into RN4220 and transduced into COL. Strain ColMurG-GFP was obtained by transducing the *murG-gfp* construct from BCBMS001<sup>32</sup> into COL.

Strains ColFemA-mCherry, ColFtsW-mCherry, ColMurJ-mCherry, ColRodA-sGFP, ColsGFP-PBP1 and ColsGFP-PBP3 were constructed by allelic replacement strategies using the pMAD vector. In each case three DNA fragments (F1, F2 and F3 – see Table 3) containing overhangs complementary with adjacent fragments were amplified from COL DNA and joined by overlap PCR, giving F1-F2-F3 fusion constructs. The full constructs were then amplified by PCR using up- and downstream primers (P1 and P6 in each case), digested with the corresponding restriction enzymes and cloned into pMAD. Integration and excision of the pMAD derivatives in COL by a double recombination event, leading to allelic exchange, was performed as described before<sup>24</sup>. The relevant information for the cloning steps for each strain is described in Table 3.

**Table 3. Cloning strategies for the construction of strains using pMAD.**

Strain	F1		F2		F3		Cut	Plasmid
	Primer Pair	Temp Region	Primer Pair	Temp Region	Primer Pair	Temp Region		
ColFemA-mCherry	femAm_P1/ femAm_P2	COL 3' <i>femA</i> + linker	femAm_P3/ femAm_P4	pBCB4- che <i>mCherry</i>	femAm_P5/ femAm_P6	COL downstream <i>femA</i>	EcoRI/ BamHI	pMAD- femAmch
ColFtsW-mCherry	ftsWm_P1/ ftsWm_P2	COL 3' <i>ftsW</i> + linker	ftsWm_P3/ ftsWm_P4	pBCB4- che <i>mCherry</i>	ftsWm_P5/ ftsWm_P6	COL downstream <i>ftsW</i>	SmaI/ BamHI	pMAD- ftsWmch
ColFtsW-sGFP	ftsWg_P1/ ftsWg_P2	COL 3' <i>ftsW</i> + linker	ftsWg_P3/ ftsWg_P4	pTRC99 a-P7 <i>sgfp</i>	ftsWg_P5/ ftsWg_P6	COL downstream <i>ftsW</i>	SmaI/ BamHI	pMAD- ftsWgfp
ColMurJ-mCherry	murJm_P1/ murJm_P2	COL 3' <i>murJ</i> + linker	murJm_P3/ murJm_P4	pBCB4- che <i>mCherry</i>	murJm_P5/ murJm_P6	COL downstream <i>murJ</i>	BglIII/ BamHI	pMAD- murJmch
ColMurJ-sGFP	murJg_P1/ murJg_P2	COL 3' <i>murJ</i> + linker	murJg_P3/ murJg_P4	pTRC99 a-P7 <i>sgfp</i>	murJg_P5/ murJg_P6	COL downstream <i>murJ</i>	SmaI/ BamHI	pMAD- murJgfp
ColRodA-sGFP	rodAg_P1/ rodAg_P2	COL 3' <i>rodA</i> region + linker	rodAg_P3/ rodAg_P4	pTRC99 a-P7 <i>sgfp</i>	rodAg_P5/ rodAg_P6	COL downstream <i>rodA</i>	SmaI/ BamHI	pMAD- rodAsgfp
ColsGFP-PBP1	gpbpA_P1/ gpbpA_P2	COL upstream <i>pbpA</i>	gpbpA_P3/ gpbpA_P4	pTRC99 a-P7 <i>sgfp</i> +linker	gpbpA_P5/ gpbpA_P6	COL 5' <i>pbpA</i>	BglIII/ BamHI	pMAD- sgfpPbp1
ColsGFP-PBP3	gpbpC_P1/ gpbpC_P3	COL upstream <i>pbpC</i>	gpbpC_P3/ gpbpC_P5	pTRC99 a-P7 <i>sgfp</i> +linker	gpbpC_P5/ gpbpC_P6	COL 5' <i>pbpC</i>	BglIII/ BamHI	pMAD- sgfpPbp3

Temp – template DNA used in the PCR reaction.

In order to obtain strains ColFtsW-sGFP and ColMurJ-sGFP, plasmids pMAD-ftsWsgfp and pMAD-murJsgfp were first constructed. For pMAD-ftsWsgfp, three fragments (F1, F2 and F3), each flanked by restriction sites, were introduced into pMAD. F1, containing the 3' end of *ftsW* minus the stop codon, was amplified from NCTC8325-4 DNA with primers ftsWg\_P1/ftsWg\_P2 and digested with *SmaI/SalI*; F2, containing *sgfp*, was amplified from

pTRC99a-P7 with primers *ftsWg\_P3/ftsWg\_P4* and digested with *Sall*; F3, containing the downstream region of *ftsW*, was amplified from NCTC8325-4 DNA and digested with *Sall/BamHI*. Fragments were then sequentially cloned into pMAD (F1, followed by F3 and finally by F2) using the adjacent restriction sites, giving pMAD-*ftsWsgfp*. For pMAD-*murJsgfp* the same strategy was used. F1, containing the 3' end of *murJ* minus the stop codon, was amplified from COL DNA using primers *murJg\_P1/murJg\_P2* and digested with *SmaI/Sall*; F2, containing *sgfp*, was amplified from pTRC99a-P7 using primers *murJg\_P3/murJg\_P4* and digested with *Sall*; F3, containing the last 26bp of *murJ* and its downstream region, was amplified from COL DNA using primers *murJg\_P5/murJg\_P6* and digested with *Sall/BamHI*. Fragments were cloned into pMAD resulting in plasmid pMAD-*murJsgfp*. Plasmids pMAD-*ftsWsgfp* and pMAD-*murJsgfp* were then electroporated to RN4220, transduced to COL and following allelic replacement strains ColFtsW-sGFP and ColMurJ-sGFP were obtained.

Strain ColFtsZ-mCherryi was constructed using the pBCB13 plasmid<sup>20</sup>, a derivative of pMAD that allows allelic exchanges in the *spa* locus. Briefly, a DNA fragment containing the Ribosome Binding Site (RBS), the *ftsZ* gene without its stop codon and a 5 amino acid linker was amplified by PCR from COL with primers *iftsZm\_P1/iftsZm\_P2*. A second fragment containing *mCherry* was amplified from pBCB4che using primers *iftsZm\_P3/iFtsZm\_P4*. The two fragments were joined by overlap PCR using primers

iftsZm\_P1/iftsZm\_P4 and the resulting construct was digested with *SmaI/XhoI* and cloned into pBCB13, downstream of the *Pspac* promoter, giving pBCB13-ftsZmch. Similarly, to construct strain ColDltC-sGFPi a DNA fragment containing an RBS, the *dltC* gene without stop codon and a two amino acid linker was amplified by PCR from COL with primers idltCg\_P1 and idltCg\_P2. A second fragment containing *sgfp* was amplified from pTRC99a-P7 using primers idltCg\_P3/idltCg\_P4. The two fragments were joined by overlap PCR using primers idltCg\_P1/idltCg\_P4 and the resulting construct was digested with *SmaI/XhoI* and cloned into pBCB13 downstream of the *Pspac* promoter, giving pBCB13-dltCsgfp. Following transduction to COL, plasmids integration/excision at the *spa* locus was performed as described before<sup>24</sup>.

Strain ColMraY-sGFP was constructed using the pCN51 replicative plasmid to express an MraY-sGFP sandwich fusion. Briefly, three DNA fragments (F1, F2 and F3) with overhangs were amplified in order to construct a fusion with *sgfp* inserted within the *mraY* coding sequence, between codons 220 and 221. F1, containing an RBS and the first 660 bp of *mraY*, was amplified from COL DNA using primers mraYg\_P1/mraYg\_P2; F2, containing *sgfp* minus the stop codon, was amplified from pTRC99a-P7 with primers mraYg\_P3/mraYg\_P4; F3, containing the last 306 bp of *mraY*, was amplified from COL using primers mraYg\_P5 and mraYg\_P6. The three fragments were joined by overlap PCR and digested with *SmaI* and cloned into pCN51, resulting in pCN-mraYsgfp.



Strains ColWZ and ColJZ were constructed by transducing plasmids pMAD-ftsWmch and pMAD-murJmch, respectively, into BCBAJ020. ColP1Z was constructed by transducing pMAD-sgfpPbp1 into ColFtsZ-mCherryi. Strains ColWgZm and ColJgZm were constructed by transducing plasmids pMAD-ftsWsgfp and pMAD-murJsgfp, respectively, into ColFtsZ-mCherryi. Strain ColWJ was obtained by transducing pMAD-murJsgfp to ColFtsW-mCherry. In each case, allelic replacement was performed as described above. In order to construct ColZZ, an *ftsZ-mCherry* fusion was amplified from genomic DNA of ColFtsZ-mCherryi with primers ftsZm\_pCNX\_P1 and ftsZm\_pCNX\_P2, digested with *Bam*HI/*Eco*RI and cloned in pCNX downstream of the *Pcad* promoter, giving plasmid pCN-ftsZmch. This plasmid was then electroporated into RN4220 and transduced to BCBAJ020, giving strain ColZZ.

To study co-localisation between DivIB with FtsZ or MurJ, an *yfp-divIB* fusion was constructed and cloned into pCNX. Briefly, a fragment containing *yfp* minus the stop codon and a 3' terminal overhang was amplified from pMUTINYFPKan<sup>22</sup> with primers ydivIB\_pCNX\_P1/ydivIB\_pCNX\_P2. A second fragment containing the full *divIB* gene with a 5' overhang was amplified from COL DNA with primers ydivIB\_pCNX\_P3/ydivIB\_pCNX\_P4. The two fragments were then joined by overlap PCR, digested with *Sma*I/*Kpn*I and cloned into pCNX downstream of *Pcad*, giving plasmid pCN-yfpDivIB. This plasmid was transduced to BCBAJ020 and ColMurJ-mCherry, giving strains ColZIB and ColJIB, respectively.

### **Construction of *S. aureus* strains containing antisense RNA vectors**

To construct strains carrying antisense RNA vectors, 250 bp fragments of *divIB* or *divIC* genes were amplified from COL DNA with primer pairs ASdivIB\_P1/ASdivIB\_P2 and ASdivIC\_P1/AS\_DivIC\_P2, respectively, digested with *EcoRI/BamHI* and cloned in antisense direction into pEPSA5, relative to the xylose inducible T5X promoter, giving pAS-DivIB and pAS-DivIC. These plasmids were then transduced into ColJZ, giving ColJZpAS-DivIB and ColJZpAS-DivIC respectively. Additionally, phage lysates were obtained from AS-022 and AS-185 strains<sup>33</sup> carrying antisense RNA pEPSA vectors pAS-022 and pAS-185 targeting *ftsA* and *ftsL*, respectively. pAS-022 was transduced to ColWZ and ColP1Z, giving strains ColWZpAS-FtsA and ColP1ZpAS-FtsA. pAS-185 was transduced to ColJZ, ColWZ, ColP1Z and ColWJ, giving strains ColJZpAS-FtsL, ColWZpAS-FtsL, ColP1ZpAS-FtsL and ColWJpAS-FtsL, respectively. Control strains for these experiments were obtained by transducing the empty vector pEPSA5 into ColJZ, ColWZ, ColP1Z and ColWJ, giving strains ColJZpEPSA, ColWZpEPSA, ColP1ZpEPSA and ColWJpEPSA, respectively.

### **Growth curves of *S. aureus* strains**

Overnight cultures of COL strains encoding fluorescent derivatives of PG synthesis enzymes were back-diluted to OD<sub>600nm</sub> 0.02 in TSB and grown at 37°C for 11 hours with OD<sub>600nm</sub>

measurements taken every hour. Doubling times were calculated for each strain during exponential growth phase.

### **Minimum inhibitory concentration (MIC) assays**

MICs of relevant antimicrobial compounds were determined by broth microdilution in sterile 96-well plates. The medium used was TSB, containing a series of two-fold dilutions of each compound. Cultures of *S. aureus* strains and mutants were added at a final density of  $5 \times 10^5$  CFU ml<sup>-1</sup> to each well. Wells were reserved in each plate for sterility control (no cells added) and cell viability (no compound added). Plates were aerobically incubated at 37°C. Endpoints were assessed visually after 24 and 48 h. All assays were done in triplicate.

### **Western Blotting**

*S. aureus* strains ColJZpEPSA, ColJZpAS-DivIB and ColJZpAS-DivIC were grown overnight, back-diluted 1:200 in fresh TSB and incubated at 37°C until an OD<sub>600nm</sub> of approximately 0.2. At this point, xylose was added to the medium at 4% to allow the expression of the antisense RNA fragments. After 1 hour of antisense expression, cells were harvested and broken with glass beads in a FastPrep FP120 cell disrupter (Thermo Electro Corporation). Samples were centrifuged to remove unbroken cells and debris and total protein content of the clarified lysates was determined using the Bradford method and bovine serum albumin as a standard (BCA Protein Assay Kit, Pierce). Equal amounts of total protein from each

sample were separated on 10% SDS-PAGE at 80V and then transferred to Hybond-P PVDF membrane (GE Healthcare) using a Semi-dry transfer cell (Biorad), according to standard western blotting techniques. Membranes were cut to separate PBP2A region from DivIB or DivIC region. DivIB and DivIC proteins were detected using specific polyclonal antibodies at 1:5000 and 1:10000 dilutions, respectively. PBP2A was detected using the antibody from a Slidex MRSA detection kit (Biomérieux) at 1:500 dilution. Protein bands were visualised using the ECL Prime Detection Reagents (GE Healthcare), following manufacturer's instructions.

### ***S. aureus* imaging by fluorescence microscopy**

Super-resolution Structured Illumination Microscopy (SIM) imaging was performed using an Elyra PS.1 microscope (Zeiss) with a Plan-Apochromat 63x/1.4 oil DIC M27 objective. SIM images were acquired using five grid rotations, unless stated otherwise, with 34  $\mu\text{m}$  grating period for the 561 nm laser (100 mW), 28  $\mu\text{m}$  period for 488 nm laser (100 mW) and 23  $\mu\text{m}$  period for 405 nm laser (50 mW). Images were captured using a Pco.edge 5.5 camera and reconstructed using ZEN software (black edition, 2012, version 8.1.0.484) based on a structured illumination algorithm, using synthetic, channel specific optical transfer functions and noise filter settings ranging from -6 to -8. Wide-field fluorescence microscopy was performed using a Zeiss Axio Observer microscope with a Plan-Apochromat 100x/1.4 oil Ph3 objective. Images were acquired with a Retiga R1 CCD camera

(QImaging) using Metamorph 7.5 software (Molecular Devices). For fluorescence microscopy experiments, unless stated otherwise, overnight cultures of *S. aureus* strains were back-diluted 1:200 in fresh media with appropriate inducers and allowed to grow until  $OD_{600nm} \sim 0.6$  before being harvested and washed with phosphate buffer saline (PBS). Cells were then placed on microscope slides covered with a thin layer of agarose (1% in PBS) and imaged by SIM or wide-field microscopy.

To assess if MurJ localisation was dependent on interaction with its substrate, strain ColMurJ-mCherry was grown until  $OD_{600nm}$  of 0.4 and incubated with 3-{1-[(2,3-Dimethylphenyl)methyl]piperidin-4-yl}-1-methyl-2-pyridin-4-yl-1H-indole (DMPI, gift from Merck) at  $3 \mu\text{g ml}^{-1}$  for 30 minutes and then imaged by wide-field fluorescence microscopy as described above. For antisense RNA experiments, strains were grown until  $OD_{600nm}$  of 0.1-0.2 at which point expression of the antisense RNA fragments was induced with xylose (Apollo Scientific) at a final concentration of 4% for 1 hour. Cells were then harvested and washed with PBS to remove xylose, mounted on microscope slides as described above and imaged by wide-field fluorescence microscopy. Assays were done in triplicate. To evaluate localisation of peptidoglycan synthesis activity, *S. aureus* cells were given a pulse of fluorescent D-amino-acid HADA<sup>34</sup> ( $250 \mu\text{M}$ ) for 1 min and then washed two times with PBS. Cells were then placed on an agarose pad and visualised by wide-field microscopy. Assays were done in triplicate. To label *S. aureus*

membranes, cells were incubated with Nile Red (Invitrogen) at a final concentration of  $10 \mu\text{g ml}^{-1}$  for 5 minutes at room temperature, washed with PBS and then mounted on microscope slides.

### **HADA incorporation microscopy assay**

To assess if MurJ activity was required for HADA incorporation, strains COL and ColDltC-sGFPi (which expresses a cytoplasmic DltC-sGFP fusion and therefore can be easily distinguished from COL under the microscope) were grown to an  $\text{OD}_{600\text{nm}}$  of 0.4 at which point each culture was separated into two flasks and either DMPI ( $3 \mu\text{g ml}^{-1}$  in DMSO) or DMSO (0.2 % final concentration) were added to the cultures. Following 25 minutes of incubation, HADA ( $500 \mu\text{M}$ ) was added to each culture for 5 minutes. Cells were then harvested, washed twice with PBS (supplemented with DMPI when applicable) and DMSO-treated COL cells were mixed with DMPI-treated ColDltC-sGFPi cells. To exclude the possibility that the expression of DltC-sGFP affected the results, a reverse experiment was performed where cells of DMSO-treated ColDltC-sGFPi were mixed with DMPI-treated COL. These mixtures of two strains were then imaged by fluorescence microscopy as described above.

### **Inhibition of the cell cycle assays**

An overnight culture of strain COL was back-diluted 1:200 and grown until  $\text{OD}_{600\text{nm}} \sim 0.4$  at which point either DMPI<sup>35</sup> ( $3 \mu\text{g ml}^{-1}$ ), PC190723<sup>36</sup> ( $2.5 \mu\text{g ml}^{-1}$ ), oxacillin ( $1000 \mu\text{g ml}^{-1}$ , Sigma-Aldrich) or

DMSO (0.2 %) were added to the medium. Cells were then grown for 30 minutes with each inhibitor, harvested and labelled with Nile Red, as described above, before being imaged by SIM. Cells were sorted into each phase of the cell cycle (Phase 1, Phase 2 or Phase 3), as previously described<sup>12</sup>. Assays were done in triplicate.

### **Automatic cell imaging analysis**

Analysis of phase-contrast and fluorescence images was performed using in-house developed software eHooke. For cell segmentation, eHooke uses phase-contrast images and applies the isodata algorithm<sup>37</sup> for automatic thresholding to find a pixel intensity value that separates the pixels corresponding to the background from those corresponding to cells. Using this threshold, the software then creates a binary mask which is used to compute the Euclidean Distances<sup>38</sup> of each pixel in order to find the centres of individual regions inside the mask. The software then expands those centres to define individual cell regions using the watershed algorithm<sup>39</sup>. In order to measure cell areas and volumes, eHooke first defines each individual cell region, computes the area by counting the number of pixels inside the region and the volume by measuring the long and short axes of the cell. Cell volume is then derived assuming a prolate spheroid shape as described before<sup>12</sup>.

To calculate fluorescent ratios (FR) between septal and membrane signal, eHooke was used to define the different regions of

the cell, namely membrane, cytoplasm and septum in images obtained by wide-field fluorescence microscopy. The membrane is defined by dilating the outline of the cell towards its inside. To separate the septum from the cytoplasm the software uses the isodata algorithm<sup>37</sup> to find the brightest region inside the cell. This region is then defined as the septum. To measure the median fluorescence, only the 25% brightest pixels of the septum were considered, in order to remove possible misidentified pixels from the measurement. Only cells with a closed septum were selected for measurements. FR values were then calculated according to the equation:

$$FR = \frac{\text{Median(Septum)} - \text{Background}}{\text{Median(Membrane)} - \text{Background}}$$

In order to measure the Pearson's Correlation Coefficient (PCC) between two fluorescent proteins in a strain, images of each fluorescence channel were aligned and loaded side-by-side in eHooke. Following automatic cell segmentation, cells showing an FtsZ signal at the septum were selected for PCC measurements. The pixels corresponding to each cell were isolated and PCC values between channels were then calculated using the following equation, adapted from <sup>40</sup>:  $PCC = \frac{\sum_i (X_i - \bar{X})(Y_i - \bar{Y})}{\sqrt{\sum_i (X_i - \bar{X})^2} \sqrt{\sum_i (Y_i - \bar{Y})^2}}$ , where  $X_i$  and  $Y_i$  correspond to each pixel intensity for two fluorescence channels and  $\bar{X}$  and  $\bar{Y}$  correspond to the mean intensities of those channels.

### **Code availability**



*Recruitment of MurJ to the divisome directs peptidoglycan synthesis to the septum*

Code is available online at Github:  
<https://github.com/BacterialCellBiologyLab/Bruno-Saraiva-2017>.

### **Statistical Analysis**

Statistical analyses were done using GraphPad Prism 6 (GraphPad Software). Unpaired student's *t*-tests were used to evaluate the differences of cellular volumes as well as to compare fluorescence ratios between peripheral and septal wall signal intensity. Mann-Whitney *U* tests were used to compare differences between PCC non-normal distributions obtained in co-localisation experiments. *P* values  $\leq 0.05$  were considered as significant for all analysis performed and were indicated with asterisks: \* $P \leq 0.05$ , \*\* $P \leq 0.01$  and \*\*\* $P \leq 0.001$ .

## Results

### Localisation of peptidoglycan synthesis proteins during division

We posited that the molecular cue for septal PG synthesis could be the recruitment of a key protein involved in PG biosynthesis to mid-cell during the assembly of the divisome. Therefore, we determined the localisation of most proteins that are involved in PG synthesis in *S. aureus*. We constructed a set of strains in the background of MRSA COL, expressing fluorescent derivatives of MurB, MurD, MurF, MraY, MurG, FemX, FemA, FemB, FtsW, MurJ, RodA, PBP1, PBP2<sup>17</sup>, PBP3 and PBP4<sup>20</sup> (see Fig. 2 and Table 4). All fluorescent fusions were expressed from their native locus under the control of their native promoter, as the sole copy of the gene in the cell, with the exception of MraY-sGFP. Most of these proteins are either essential to cell viability or auxiliary factors required for oxacillin resistance<sup>41,42</sup>. As growth rates and minimum inhibitory concentration (MICs) to oxacillin and D-cycloserine were similar to the parental strain COL (except for MraY-sGFP), fluorescent derivatives of PG synthesis enzymes seemed functional (Table 4). Despite several attempts, we were unable to construct a strain harbouring a functional fluorescent fusion to MraY. Thus, despite the inherent limitations, we used a strain expressing the native MraY protein from the native locus, and an sGFP sandwich MraY fusion (see methods) as a second copy, expressed from replicative plasmid pCN51, under the control of a cadmium-inducible promoter. Live

cells of all strains expressing fluorescent fusions of PG synthesis enzymes were imaged by Super Resolution Structured Illumination Microscopy (SIM) (Fig. 2a).

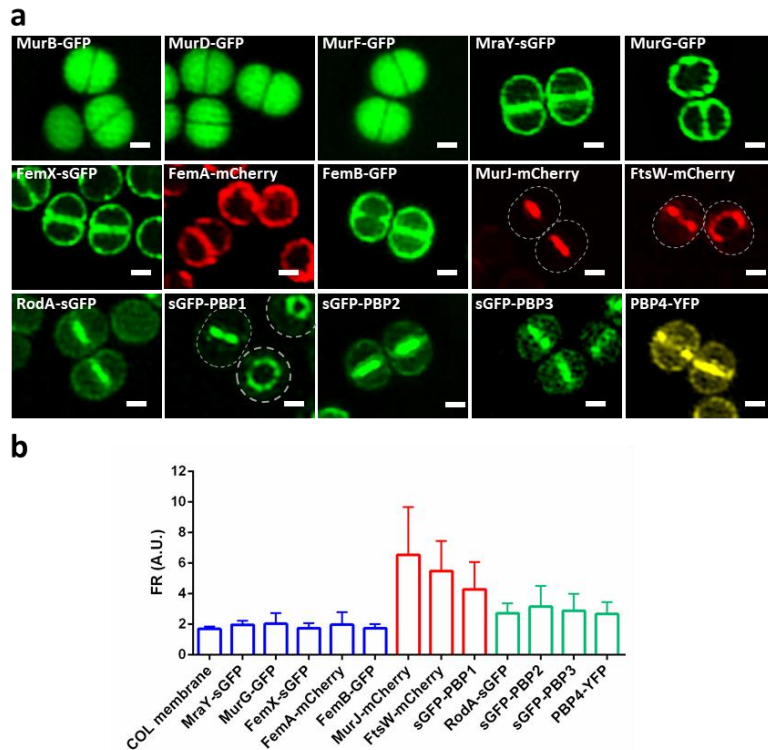


**Figure 2. Localisation of PG synthesis proteins during division in *S. aureus*** (a), Structured Illumination Microscopy (SIM) images of *S. aureus* cells expressing fluorescent derivatives of PG synthesis proteins. Scale bars, 0.5  $\mu$ m. (b), Fluorescence ratios (FR) between fluorescence signal at the septum versus the peripheral membrane measured in cells with a complete septum (Phase 3). Blue bars: membrane proteins with FR~2, similar to Nile Red staining of COL membrane, expected as the septum contains two membranes versus one in the cell periphery. Green bars: septal enriched proteins with  $2.5 < FR < 3.5$ . Red bars: septal proteins with  $FR > 4$ . Data are represented as column graphs where the height of the column is the mean and whiskers are standard deviation.

**Table 4. Strains used to study localisation of peptidoglycan synthesis in *Staphylococcus aureus*.**

Strain	Gene	Protein	Tag	Function	Doubling (min)	Oxa MIC ( $\mu\text{g/ml}$ )
ColMurB-GFP	<i>murB</i>	MurB	GFP	Reduction of UDP-N-acetylenolpyruvoyglucosamine	35	500
ColMurD-GFP	<i>murD</i>	MurD	GFP	Addition of D-glutamate to UDP-MurNAc-L-ala	37	500
ColMurF-GFP	<i>murF</i>	MurF	GFP	Addition of D-ala-D-ala to UDP-MurNAc-tripeptide	33	250
ColMraY-sGFP	<i>mraY</i>	MraY	sGFP	Transfer of UDP-MurNAc-pentapeptide to undecaprenyl phosphate	37	250
ColMurG-GFP	<i>murG</i>	MurG	GFP	Transfer of GlcNAc to undecaprenyl-pyrophosphoryl-MurNAc-pentapeptide	35	500
ColFemX-sGFP	<i>femB</i>	FemX	sGFP	Transfer of gly to lys moiety in lipid II	35	500
ColFemA-mCherry	<i>femA</i>	FemA	mCh	Transfer of 2 gly to lipid II-Gly	34	500
ColFemB-GFP	<i>femB</i>	FemB	GFP	Transfer of 2 gly to lipid II-gly <sub>3</sub>	36	500
ColFtsW-mCherry	<i>ftsW</i>	FtsW	mCh	Putative transglycosylase - inferred by homology	36	500
ColMurJ-mCherry	<i>murJ</i>	MurJ	mCh	Putative lipid II membrane translocase - inferred by homology	35	1000
ColRodA-sGFP	<i>rodA</i>	RodA	sGFP	Putative transglycosylase - inferred by homology	35	1000
ColsGFP-PBP1	<i>pbpA</i>	PBP1	sGFP	Transpeptidase	33	250
BCBPM073	<i>pbpB</i>	PBP2	sGFP	Bifunctional transglycosylase and transpeptidase	36	1000
ColsGFP-PBP3	<i>pbpC</i>	PBP3	sGFP	Peptidoglycan transpeptidase	34	500

ColpPBP4- YFP	<i>pbpD</i>	PBP4	YFP	Peptidoglycan transpeptidase	35	500
COL	---	---	---	---	36	500

As expected MurB, MurD and MurF fusions, which act on cytoplasmic PG precursors, showed cytoplasmic localisation. Also consistent with their substrate localisation, the remaining fusions localized to the membrane, including FemXAB proteins which do not have canonical membrane-targeting domains. Given that during septum synthesis most PG synthesis activity occurs at that place<sup>11</sup>, we were expecting all membrane PG synthesis enzymes in dividing cells to be greatly enriched at the septum. However, MraY, MurG, and the FemXAB proteins were evenly distributed throughout the membrane (including the septum) suggesting that the key step for spatial regulation of PG synthesis was not the synthesis of lipid I or lipid II, as could perhaps be expected. Only later steps, namely those catalysed by FtsW, MurJ and RodA, as well as PBPs 1-4, seemed enriched at the septum. This was confirmed using an in-house developed software – eHooke - to measure the fluorescence ratio (FR) of septal versus peripheral membrane fluorescence signal in cells (n>400 cells for each strain) imaged by wide-field fluorescence microscopy. Membrane-bound PG synthesis proteins fell into three classes: Class 1 (Fig. 2b, blue bars and Table 5) included MraY, MurG, FemX, FemA and FemB proteins which were dispersed over the entire membrane and had FR values close to 2, similar to membrane

dye Nile Red; Class 2 (Fig. 2b, green bars and Table 5) included RodA, PBP2, PBP3 and PBP4, which were enriched at the septum ( $2.5 < FR < 3.5$ ) but could also be observed at the peripheral membrane; Class 3 (Fig. 2b, red bars and Table 5) included PBP1, FtsW and MurJ, seen as septal proteins for which virtually no signal could be observed in the peripheral membrane during septum synthesis ( $FR > 4$ ). These data suggested that the first steps in PG synthesis that occur specifically at the septum are those catalyzed by the hypothetical lipidII flippase MurJ, the hypothetical transglycosylase FtsW and/or the transpeptidase PBP1.

**Table 5. Fluorescent ratios between septal and peripheral signal measured for PG synthesis proteins.**

	FR 25% (A.U.)
COL NR	1.70±0.16 (n = 439)
MraY-sGFP	1.96±0.27 (n = 533)
MurG-GFP	2.03±0.70 (n = 516)
FemX-sGFP	1.96±0.27 (n = 533)
FemA-mCherry	1.97±0.81 (n = 513)
FemB-GFP	1.74±0.27 (n = 622)
MurJ-mCherry	6.54±3.12 (n = 503)
FtsW-mCherry	5.47±1.97 (n = 517)
sGFP-PBP1	4.28±1.80 (n = 503)
RodA-sGFP	2.73±0.64 (n = 689)
sGFP-PBP2	3.16±1.35 (n = 1321)
sGFP-PBP3	2.88±1.11 (n = 488)
PBP4-YFP	2.68±0.77 (n = 516)

In order to clarify which protein(s) was responsible for directing PG synthesis to the septum, newly synthesised PG was labelled with the fluorescent D-amino acid HADA, which is specifically incorporated into PG<sup>34</sup>, in a strain expressing both FtsW-mCherry (which co-localises with PBP1, see below) and MurJ-sGFP. HADA incorporation appeared to co-localise with both proteins in cells in Phase 1 of the cell cycle and in most Phase 2 cells (Fig. 4a; see Fig. 1b for cell cycle phases). However, MurJ/HADA septal co-localisation was more frequent than FtsW/HADA co-localisation (88% vs 70% of cells, N=200), as cells with septal FtsW but peripheral MurJ had peripheral HADA incorporation (see asterisk in Fig. 4a). This suggested that septal PG synthesis was dependent on the presence of MurJ. If this was the case, preventing MurJ recruitment to mid-cell should abolish septal PG synthesis. We therefore investigated the mechanism of MurJ localisation so that we could selectively prevent its septal recruitment, while maintaining correct FtsW/PBP1 septal localisation.

We initially tested if MurJ, PBP1 or FtsW were recruited to the septum through substrate recognition, i.e. through affinity to an intermediate of PG biosynthesis. This mechanism of localisation has been observed for PBP2<sup>43</sup>. To deplete PG precursors from the cells, we treated ColsGFP-PBP1, ColFtsW-mCherry and ColMurJ-mCherry with different PG synthesis inhibitors, namely D-cycloserine, oxacillin and tunicamycin and used strain BCBPM073<sup>17</sup>, which expresses sGFP-PBP2, as a control. As expected, treatment with the three

antibiotics led to the delocalisation of sGFP-PBP2 throughout the cell membrane. On the contrary, localisation of sGFP-PBP1, FtsW-mCherry, or MurJ-mCherry was unaffected (Fig. 3), showing that these proteins do not localise via substrate recognition.

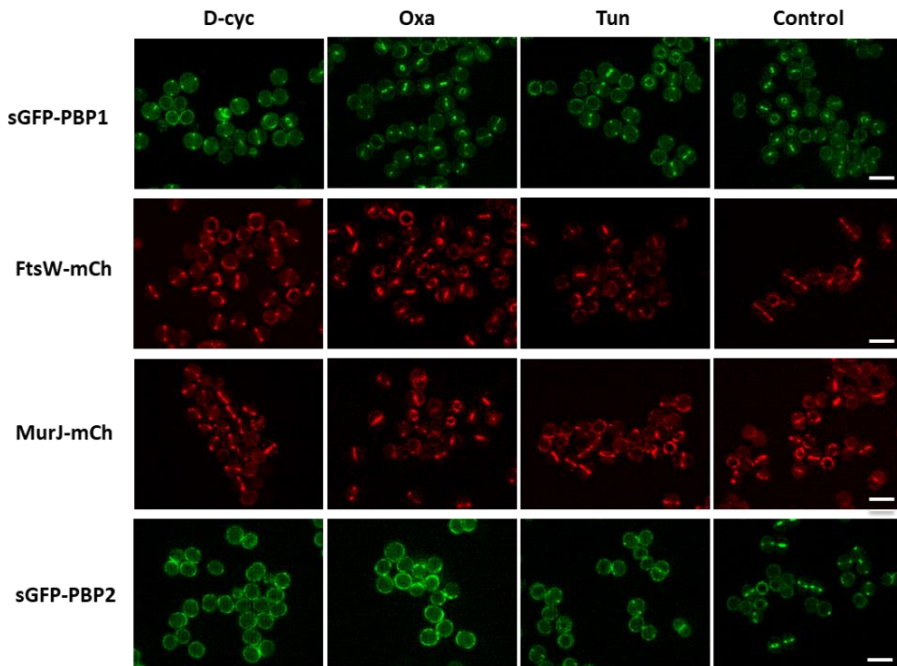


**Figure 3. PBP1, FtsW and MurJ recruitment to the septum is independent of peptidoglycan intermediates.** COL strains harbouring sGFP-PBP1, FtsW-mCherry, MurJ-mCherry or sGFP-PBP2 functional fusions were treated with PG synthesis inhibitors D-cycloserine, oxacillin or tunicamycin at 10X MIC for each compound for 30 minutes before being imaged by SR-SIM. Scale bars = 2  $\mu$ m. D-cyc, D-cycloserine; Oxa, oxacillin; Tun, tunicamycin.

An alternative mechanism for recruitment of these proteins to the septum could be protein-protein interaction with divisome components. For that purpose, we determined the timings of MurJ, FtsW and PBP1 arrival to the septum, as localisation of divisome



proteins is often dependent on the presence of earlier localising proteins<sup>44,45</sup>.

### **Order of arrival of peptidoglycan synthesis proteins to mid-cell**

In *B. subtilis* divisome assembly is a two-step process, with proteins such as FtsA, ZapA and EzrA arriving very early, concomitantly with FtsZ followed, after a time delay, by a second group of proteins including DivIB, DivIC, FtsL, GpsB, DivIVA, FtsW or PBP2B<sup>46</sup>. While describing the hierarchy of divisome assembly in *S. aureus* was beyond the scope of this work, we wanted to assess the time of recruitment of *S. aureus* PBP1, FtsW and MurJ to the septum, to determine which protein arrives first. This was done by comparing their localisation with that of FtsZ. We also compared the localisation of DivIB with FtsZ, as a control for later arrival to the divisome. For that purpose we constructed a set of strains expressing FtsZ-CFP or FtsZ-mCherry fusions together with a second fluorescent fusion, either sGFP-PBP1, FtsW-mCherry, MurJ-mCherry or YFP-DivIB (Fig. 4b). These strains were imaged by wide-field microscopy and cells showing FtsZ localisation at mid-cell were selected for analysis. Co-localisation between each fusion pair was determined by measuring Pearson's Correlation Coefficient (PCC) values between the fluorescence signals in the two channels, as we reasoned that proteins arriving to the septum exactly at the same time should have a PCC close to 1 and this value should decrease for proteins that arrive to

the septum at later stages of divisome assembly. As a positive control for co-localisation we constructed a strain expressing two fusions of the same protein with two different tags – FtsZ-CFP and FtsZ-mCherry (Fig. 4b).

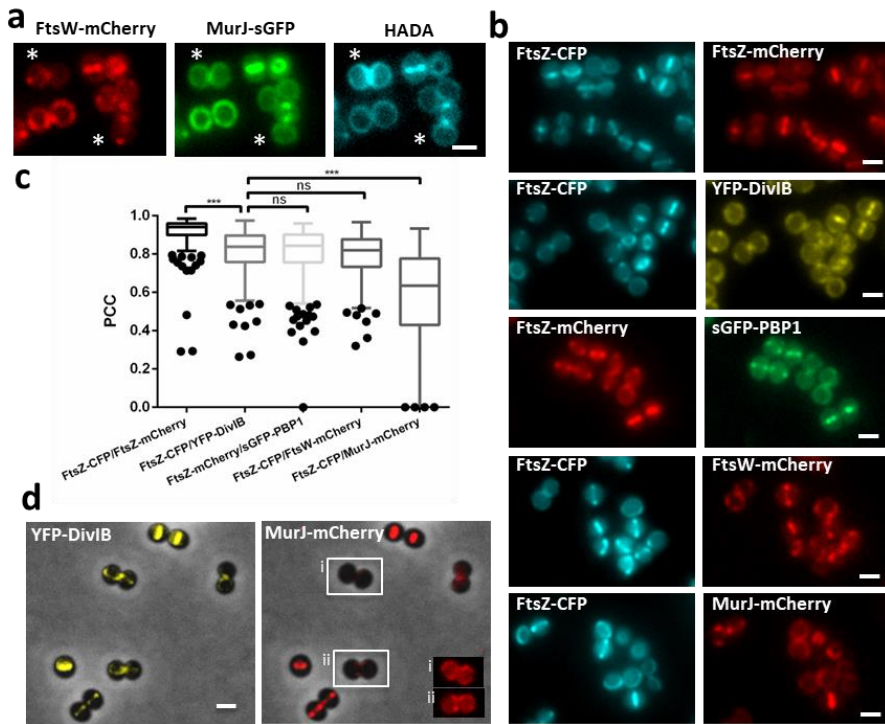


**Figure 4. Hierarchy of arrival of key PG synthesis proteins to the divisome.** (a), PG synthesis in strain ColWJ was labelled with HADA. Asterisk shows cell with septal FtsW and peripheral MurJ and HADA labelling. (b), Fluorescence microscopy images of strains (from top) ColZZ (positive control), ColZIB, ColP1Z, ColWZ and ColJZ. (c), Pearson's correlation coefficient (PCC) for pairs of fluorescent proteins expressed in the same strain. PCC=1 would indicate perfect co-localisation. Negative PCC values are represented as 0. Data are represented as box-and-whisker plots where boxes correspond to the first to third quartiles, lines inside the boxes indicate the median, ends of whiskers and outliers follow a Tukey representation. Statistical analysis was performed using a two-sided Mann-

Whitney *U* test (\*\**P*<0.001; ns, not significant). **(d)**, Fluorescence microscopy images of strain ColJIB. Cells with septal YFP-DivIB localisation but MurJ-mCherry still not at the septum (peripheral) are highlighted in insets i and ii, where the brightness of fluorescence signal was increased to allow visualisation of MurJ localisation. Scale bars, 1  $\mu$ m.

**Table 6. Pearson’s Correlation Coefficient values between fluorescent protein pairs.**

Strain Name	Protein 1	Protein 2	PCC
COLZZ	FtsZ-CFP	FtsZ-mCherry	0.92±0.07, N = 312
COLZIB	FtsZ-CFP	YFP-DivIB	0.81±0.11, N = 391
COLP1Z	FtsZ-CFP	sGFP-PBP1	0.81±0.13, N = 337
COLWZ	FtsZ-CFP	FtsW-mCherry	0.80±0.11, N = 330
COLJZ	FtsZ-CFP	MurJ-mCherry	0.59±0.24, N = 334
COLWgZc	FtsZ-mCherry	FtsW-sGFP	0.83±0.10, N = 136
COLJgZc	FtsZ-mCherry	MurJ-sGFP	0.62±0.23, N = 139
COLJZpAS-FtsL	FtsZ-CFP	MurJ-mCherry	0.44±0.34, N = 227
COLJZpEPSA	FtsZ-CFP	MurJ-mCherry	0.61±0.27, N = 300

Co-localisation between FtsZ-CFP and YFP-DivIB was significantly lower than between control pair FtsZ-CFP and FtsZ-mCherry (*P*<0.001), suggesting that DivIB arrives to the divisome later than FtsZ as expected, possibly during a second stage of assembly. Co-localisation between FtsZ-mCherry and sGFP-PBP1 and between FtsZ-CFP and FtsW-mCherry was not significantly different from FtsZ-CFP and YFP-DivIB, suggesting that PBP1 and FtsW are recruited to the divisome at approximately the same time as DivIB. In contrast, the FtsZ-CFP and MurJ-mCherry PCC was much lower than for the pairs above, indicating that MurJ arrives to the divisome at a later stage than DivIB, PBP1 and FtsW (Fig. 4c and Table 6). It is unlikely that the nature of each individual fluorescent tag used could

influence the co-localisation results as tagging the pairs FtsZ/FtsW and FtsZ/MurJ with different fluorescent proteins, did not alter the results (Fig. 5 and Table 6). To confirm that MurJ arrives to the divisome later than DivIB, we looked at a strain expressing YFP-DivIB and MurJ-mCherry. A subpopulation (20%, N = 200) of cells of this strain showing YFP-DivIB septal localisation had MurJ-mCherry dispersed around the membrane (Fig. 4d, insets) suggesting later arrival, while every cell with septal MurJ-mCherry had septal YFP-DivIB localisation.

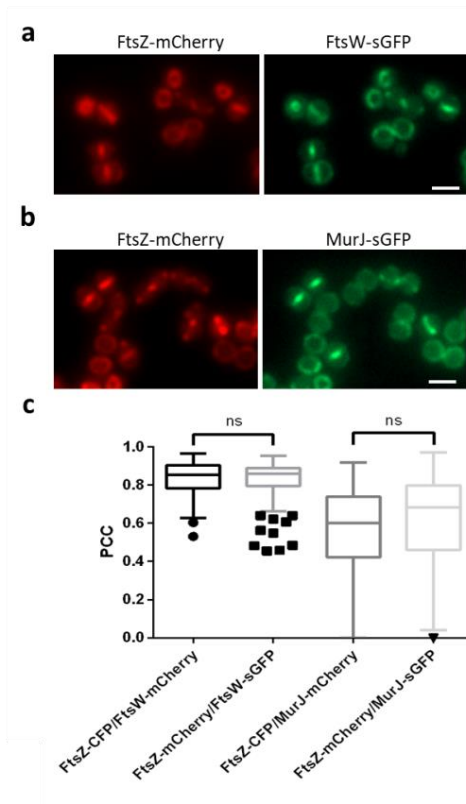


**Figure 5. Switching fluorescent tags has no effect on protein co-localisation data.** COL strains expressing FtsZ-mCherry/FtsW-sGFP (a) or

FtsZ-mCherry/MurJ-sGFP **(b)** were compared to strains expressing FtsZ-CFP/FtsW-mCherry or FtsZ-CFP/MurJ-mCherry, respectively (described in Fig. 4b and c). Scale bars, 2  $\mu$ m. **(c)**, Pearson's correlation coefficient (PCC) values between fluorescence channels for each protein fusion pair were calculated for cells showing septal FtsZ localisation. Negative PCC values are represented as 0. Data are represented as box-and-whisker plots where boxes correspond to the first to third quartiles, lines inside the boxes indicate the median and ends of whiskers and outliers follow a Tukey representation. Statistical analysis was performed using a two-sided Mann-Whitney *U* test (ns, not significant).

Our data therefore indicates that PBP1 and FtsW arrive to the divisome before MurJ. This was surprising since MurJ is likely the flippase of the PG precursor and therefore its activity should precede, and be required for, both transglycolysation (a predicted function of FtsW) and transpeptidation (performed by PBP1)<sup>47</sup>. This inconsistency could be explained if PBP1 had a second function during cell division in addition to its transpeptidase activity as previously suggested<sup>47</sup>, which could be required early in divisome assembly.

### **MurJ recruitment to the divisome triggers peptidoglycan incorporation at mid-cell**

As shown above, arrival of PBP1/FtsW to the divisome seems to occur approximately at the same time as DivIB, while arrival of MurJ seems to occur after DivIB and therefore could theoretically be dependent on the presence of the DivIB/DivIC/FtsL sub-complex. In order to test this, we depleted expression of DivIB, DivIC and FtsL

using antisense RNA fragments expressed from pEPSA-based plasmids<sup>19</sup> (Table 7) and determined the effect of the absence of the corresponding proteins on the recruitment of MurJ to the septum. Given that inhibition of divisome assembly causes the enlargement of *S. aureus* cells<sup>11,48</sup>, we assessed the efficiency of each antisense RNA by the increase in cell volume (Fig. 6a) and by Western blot (Fig. 7). Upon expression of the antisense RNA targeting *divIB*, *divIC* or *ftsL*, we observed a reduction in septal co-occurrence between FtsZ-CFP and MurJ-mCherry (Fig. 6c), with the appearance of large cells where FtsZ-CFP was properly localized to the septum but MurJ-mCherry appeared dispersed throughout the cell surface (Fig. 6c, arrows).

**Table 7. Sequences encoding RNA antisense fragments targeting divisome genes.**

Antisense RNA name	Original Designation	Target gene	DNA sequence encoding antisense RNA (5'-3')	Reference
AS-FtsA	AS-022	<i>ftsA</i>	tatcttgatctgaagcagaatcatagaatgcatgaccatattggtgttaac ttttcagcagtttcataagaagtgttaatccttgtagcaatcgtctgtaat atcacgacctgccatttcgatagaatcagcatcactaattcaccgcttcat aaaaagcaactgcgtaacgtctccaccaatcaat	19
AS-FtsL	AS-185	<i>ftsL</i>	Cttttctacagccattataaattgctccttatttaagtattcagctacacgta atttcgcgcttcgtctctgttattgtcatctaaactctctctgtagcgtaat cggtttacgalttaacacgcttaacttaggtgatatgctctgtgataactg gtaatcctctgggtacctctggaccttttcataattctggaacacctgtttaca taaacgatcttctaaagaatggaagtgattaccgaaactcctgcatctact ttcaactcaatcgcttggcttctattgaatctcaaaagctgacaattcatcg tttactgcaatcgtagtcttgaataactcgttttcaggatgctcgcccttt ctcttgcttttcaggaataacctctttataatgcaactaattct	19
AS-DivIB	N/A	<i>divIB</i>	tggattcgctttgctgcttacgtcttaactccgctttctcaagtgtaatg gctttaattggtgtacttacttttctgctttttctgtagctttctctcaatcaatc gagtcgctatttggctttaggagctgattgaggtgttctggtgctgactga aattacatcgattcatttggctgcaatttctgattatatactataatcctcat tttcaatattagctgctgataatcat	This work

Antisense RNA name	Original Designation	Target gene	DNA sequence encoding antisense RNA (5'-3')	Reference
AS-DivIC	N/A	<i>divIC</i>	tttgtgctttgaaactgtctcttgcctttcgcctctgtgcatcaatc attgcatgttttggacaacaagcaagattgataaacaacaattatcgc aagtaatacgcgccgaaatactgtaatacgcctacgaacaacacgcat catttttgacgtgttttctctctctcctcgcgacgtgactgalttctatg ttctactttatttcaatgcttgcactccaat	This work

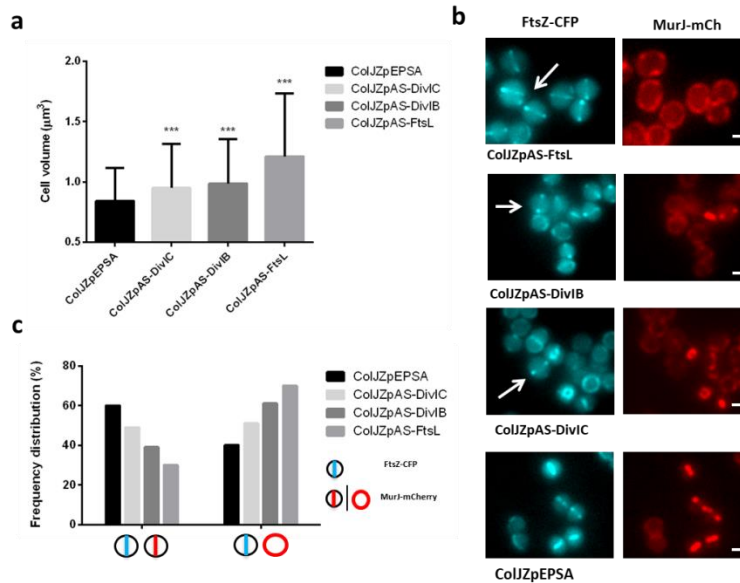


**Figure 6. MurJ recruitment to the divisome is dependent on the assembly of DivIB/DivIC/FtsL complexes.** (a), Cell volumes in populations of *S. aureus* strains treated with antisense RNA fragments targeting divisome genes *divIB* (ColJzpAS-DivIB, N = 279), *divIC* (ColJzpAS-DivIC, N = 379) or *ftsL* (ColJzpAS-FtsL, N = 361), when compared to untreated control (ColJzpEPSA, N = 421). (b) Localisation of FtsZ-CFP and MurJ-mCherry in cells treated with antisense RNA. Large cells were observed where FtsZ-CFP was localized to the division septum but MurJ-mCherry was dispersed throughout the cell surface (white arrows). (c), Frequency of FtsZ-CFP and MurJ-mCherry colocalisation in cells treated with antisense RNA when compared to untreated cells (N = 200 for each strain). Ellipses crossed with colored lines represent septal localisation. Colored ellipses represent

peripheral localisation. Scale bars = 1  $\mu\text{m}$ . Data in (a) are represented as column bar graphs where the height of the bar corresponds to the mean and end of whisker corresponds to standard deviation. Statistical analysis was performed using the unpaired t-test (\*\* $P < 0.001$ ).

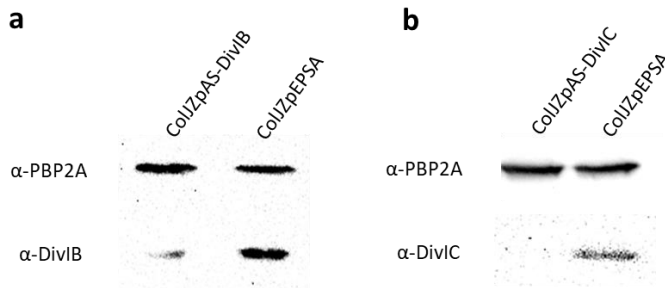


**Figure 7. Antisense RNA fragments targeting the DivIB/DivIC/FtsL complex decreased protein expression.** (a), Western blot showing total protein extracts of ColJZpAS-DivIB following 1 hour of antisense induction and control ColJZpEPSA probed with antibodies against either PBP2A (loading control - upper bands) or DivIB (lower bands). (b), Western blot showing total protein extracts of ColJZpAS-DivIC following 1 hour of antisense induction and control ColJZpEPSA probed with antibodies against either PBP2A (loading control – upper bands) or DivIC (lower bands).

These results suggest that recruitment of MurJ to the divisome is dependent on the presence of the DivIB/DivIC/FtsL complex, and that lack of any of these proteins impairs MurJ septal localisation. However, in all strains, large cells constituted only a sub-population. It is likely that antisense RNA expression did not completely deplete DivIB/DivIC/FtsL in every cell and/or did not have an effect in cells where the complex was already assembled. This could be the reason for the presence of cells with correctly localized MurJ.



Contrasting with MurJ, FtsW and PBP1 localisation was not dependent on the DivIB/DivIC/FtsL complex. Septal recruitment of FtsW-mCherry or sGFP-PBP1 was observed even in very large cells with open FtsZ-CFP rings, implying that destabilization of the complex had no effect on FtsW or PBP1 recruitment to the divisome (Fig. 8c and d). In contrast, inhibition of divisome assembly at a very early step, namely by depletion of FtsA, caused FtsW and PBP1 de-localisation, concomitant with FtsZ de-localisation (Fig. 8e and f).

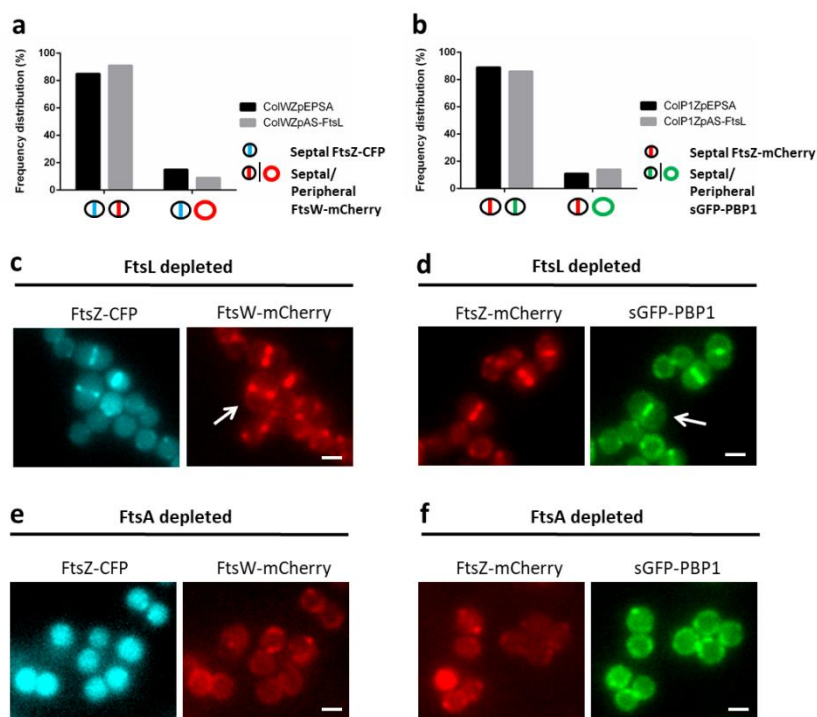


**Figure 8.** FtsW and PBP1 recruitment to the divisome is independent of DivIB/DivIC/FtsL complexes. Strains ColWZpAS-FtsL and ColP1ZpAS-FtsL, harbouring FtsZ-CFP/FtsW-mCherry and FtsZ-mCherry/sGFP-PBP1 fluorescent fusion pairs, respectively, were depleted of FtsL expression

using antisense RNA and imaged by wide-field fluorescence microscopy. **(a)**, Frequency of FtsZ-CFP and FtsW-mCherry co-occurrence in ColWZpAS-FtsL when compared to control ColWZpEPSA (N=200 for each). **(b)**, Frequency of FtsZ-mCherry and sGFP-PBP1 co-occurrence in ColP1ZpAS-FtsL and in control ColP1ZpEPSA (N=200 for each). Very large FtsL-depleted cells were observed where either FtsW-mCherry **(c)** or sGFP-PBP1 **(d)** co-localised with the FtsZ fusion at the septum (arrows). **(e,f)**, Inhibition of divisome assembly at an early stage by depletion of FtsA expression in either ColWZpAS-FtsA or ColP1ZpAS-FtsA prevented the recruitment of FtsW-mCherry **(e)** or sGFP-PBP1 **(f)** to the septum, concomitant with FtsZ destabilisation. Scale bars, 1  $\mu$ m.

Having a tool to specifically delocalise MurJ (but not PBP1 or FtsW) allowed us to test if this protein was required for septal PG synthesis. Therefore, we introduced plasmid pAS-185, encoding antisense RNA against FtsL in order to delocalize MurJ (but not FtsW). Induction of the FtsL antisense RNA, followed by a short pulse of HADA, revealed that HADA was only incorporated at the septum when MurJ-sGFP was present at the septum as well (Fig. 9a, asterisks and 9b). Strikingly, large cells of ColWJpAS-FtsL (Fig. 9a, arrows and 9b) with FtsW-mCherry correctly localized to the division plane but MurJ-sGFP dispersed around the cell surface, incorporated HADA throughout the cell periphery, indicating that recruitment of MurJ to the divisome by the DivIB/DivIC/FtsL complex is necessary for septal HADA insertion. Finally, we showed that inhibiting MurJ activity using DMPI<sup>4</sup>, a MurJ inhibitor that does not prevent its recruitment to the divisome (Fig. 10a), drastically reduced HADA incorporation (i.e. PG synthesis) at the septum (Fig. 10d and e). Our

data strongly indicates that MurJ is likely the molecular cue directing PG synthesis specifically to the septum during division.

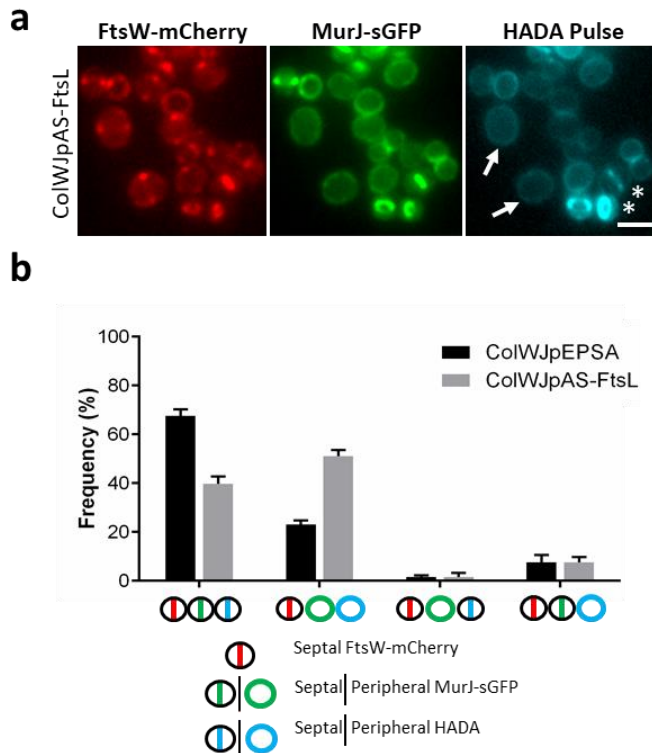


**Figure 9. MurJ recruitment to the divisome is required for PG incorporation at mid-cell. (a)** HADA septal incorporation in FtsL-depleted cells was only observed in cells with septal MurJ-sGFP (asterisks). Septal FtsW-mCherry was not sufficient to ensure HADA septal incorporation (arrows). Scale bar, 2  $\mu$ m. **(b)**, Co-localisation between FtsW-mCherry, MurJ-sGFP and HADA labelling in FtsL-depleted (ColWJpAS-FtsL) or control (ColWJpEPSA) cells with septal FtsW-mCherry (N=100 cells for each strain, in each of the three biological repeats).

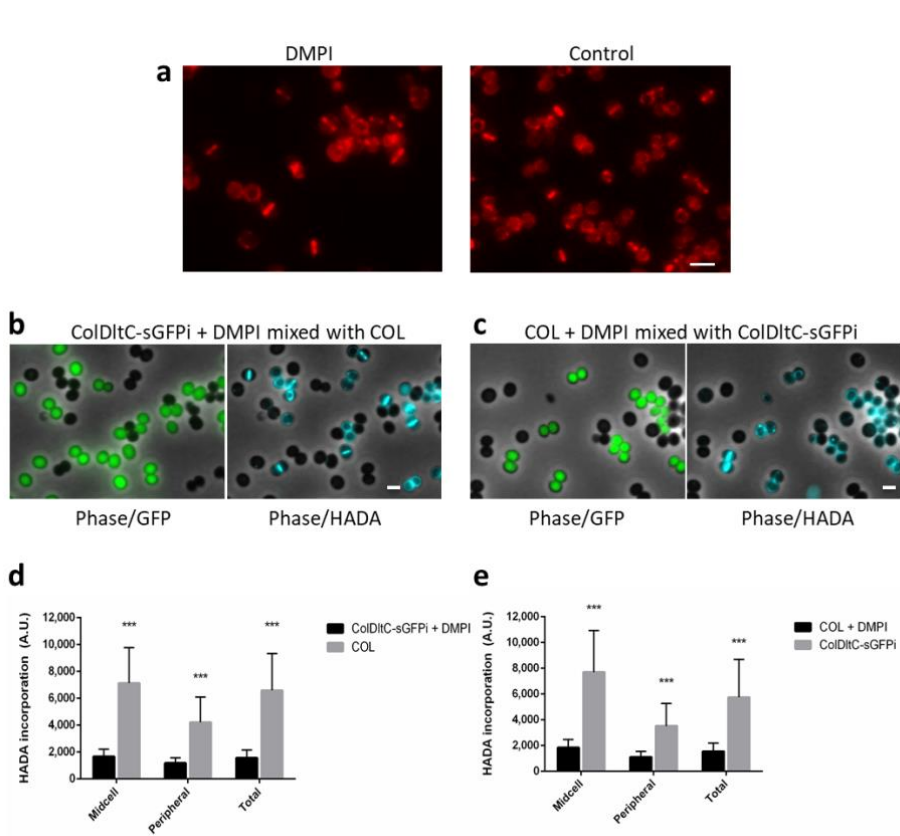


**Figure 10. Inhibition of MurJ activity does not prevent its recruitment to mid-cell but impairs PG synthesis.** (a), Fluorescence microscopy images of ColMurJ-mCherry cells grown in the presence (left) or absence (right) of DMPI for 30 minutes at 2X MIC. Scale bar, 2  $\mu$ m. **b,c** Fluorescence microscopy images showing mixed cultures of either (b) DMPI-treated ColDltC-sGFPi cells mixed with COL cells or (c) DMPI-treated COL cells mixed with ColDltC-sGFPi cells, following incubation with HADA. The two cultures, which can be easily distinguished due to GFP expression in ColDltC-sGFPi, were mixed on the same slide to decrease fluorescence variation of HADA signal due to imaging conditions. Phase contrast/GFP channel overlays are shown on the left and phase contrast/HADA channel overlays are shown on the right. Scale bars, 1  $\mu$ m. **d, e** HADA fluorescence signal measured at the mid-cell (Mid-cell), the periphery (Peripheral) or over the entire cell (Total) of DMPI-treated ColDltC-sGFPi cells mixed with COL

cells **(d)** or DMPI-treated COL cells mixed with ColDltC-sGFPi cells **(e)**. Images in a-c are representative of three biological replicates. Data in (d,e) are represented as column plots (N=100 for each column) where the height of the column is the mean and the whiskers indicate standard deviation. Statistical analysis was performed using two-sided unpaired t-tests (\*\*\*,  $P < 0.001$ ).

Given these findings, we would expect MurJ to be essential for the transition from Phase 1 to Phase 2 during the cell cycle, i.e, to initiation of septum synthesis. Therefore, preventing MurJ recruitment to the septum or inhibiting its activity should lead to the accumulation of Phase 1 cells, unable to progress to Phase 2. Phase 2 cells, which are synthesizing the septum, may also be halted by lack of MurJ, as translocation of the PG precursor across the membrane is essential for PG synthesis to occur. However, Phase 3 cells, which have a complete septum, may be able to split and progress to Phase 1, which would lead to a decrease of this population upon MurJ inhibition (Fig. 11a-(i)).

We treated *S. aureus* cells with DMPI, which inhibits MurJ<sup>4</sup>, for the duration of one cell cycle and characterized the distribution of cells in the three phases of the cell cycle. For comparison we also tested other inhibitors, namely PC190723<sup>17</sup> (targets FtsZ) and oxacillin (inhibits PG transpeptidation catalysed by PBPs). We reasoned that treatment with PC190723 would lead to cell cycle arrest at Phase 1, as FtsZ is essential for assembly of the divisome (Fig. 11a-(ii)), while oxacillin would lead to cell cycle arrest at P2 because most of the PG is synthesized during that phase (Fig. 11a-(iii)). COL cells were

treated with 2X MIC of each compound for the duration of a cell cycle (30 minutes), labelled with membrane dye Nile Red and imaged by SIM (Fig. 11b). Consistent with previous data<sup>12</sup>, in the absence of inhibitors approximately half (58%) of the cells were in Phase 1, with the other half split evenly between Phase 2 (21%) and Phase 3 (21%). Inhibition of MurJ by DMPI resulted in the accumulation of Phase 1 cells (70%), indicating that MurJ is crucial to entry in Phase 2. In contrast, incubation with oxacillin led to a decrease in the proportion of cells in Phase 1 (36%) concomitant with an increase of the proportion of cells in P2 (37%), suggesting that PBP activity is critical for the completion of Phase 2 (Fig. 11c).

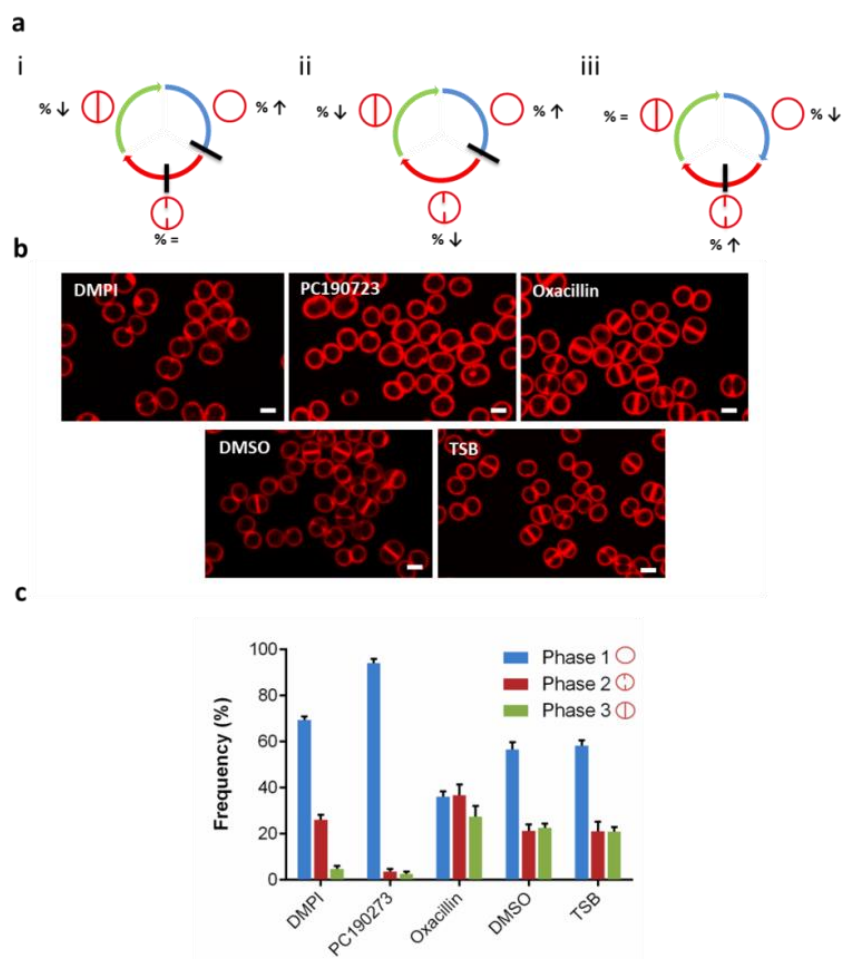


**Figure 11. Inhibition of MurJ leads to cell cycle arrest at Phase 1.** (a), Representation of the effect of antibiotics on the cell cycle. (i) If an inhibitor of the cell cycle blocks the transition from P1 to P2 as well as the progression of P2 then the fraction of the cell population in P2 should remain the same while the fraction in P1 should increase. (ii) If the transition from P1 to P2 is blocked then the cell population should be enriched in P1. (iii) In case an inhibitor blocks the progression of P2, then the fraction of the cell population in P2 should increase (b), SIM images of Nile Red stained COL cells treated with DMPI (inhibits MurJ), PC190723 (inhibits FtsZ), oxacillin (inhibits PBP), DMSO or TSB (mock controls) for the duration of a cell cycle (30 min). Scale bars, 2  $\mu$ m. (c), COL cells treated with inhibitors were sorted into each

### *Chapter III*

cell cycle phase based on Nile Red staining and the frequency of each phase in the cell population was expressed as a percentage of the total cells measured. N = 1415 for DMPI, N = 1226 for PC190273, N = 1652 for Oxacillin, N = 1542 for DMSO and N = 1876 TSB control cells.



## **Discussion**

The spatial and temporal coordination of PG synthesis is of the utmost importance to the bacterial cell. Unlike rod-shaped and ovococcal species that have two dedicated machineries to synthesise peripheral and septal PG, cocci like *S. aureus* make do with just one. Its sole machinery has to work in two locations, shifting its activity from the periphery of the cell to the middle when it is time to build the septum. The timing of the shift has to be precise, perfectly synchronized with the cell cycle, as premature septation could have disastrous consequences for the cell. In this work we have identified that the molecular cue that signals this transition from peripheral to septal synthesis is the recruitment of the MurJ translocase to the divisome.

We propose a model where the *S. aureus* PG synthesis machinery continuously incorporates PG at the periphery of the cell during initial stages of the cell cycle. In preparation for division and following Z-ring assembly, the DivIB/DivIC/FtsL complex recruits MurJ to the divisome, which ensures that translocation of lipid II occurs exclusively at mid-cell. Substrate affinity<sup>43</sup> then diverts PBP2 from the periphery to the mid-cell, where it incorporates lipid II into the growing PG network (Fig. 12). This mechanism forgoes the need for an additional dedicated multi-protein machinery for PG synthesis.

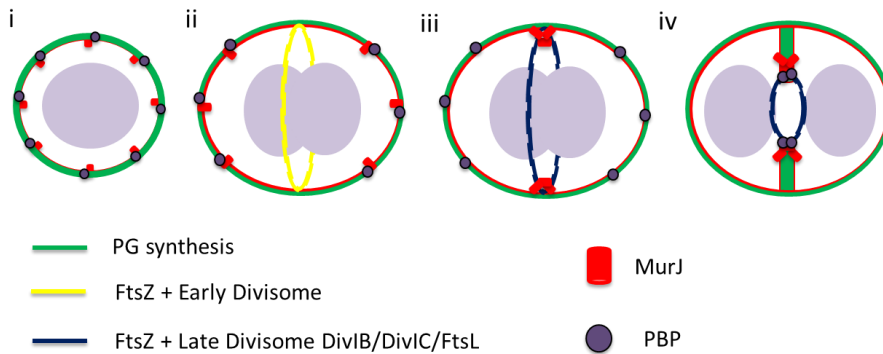


**Figure 12. Proposed model for how recruitment of MurJ to the divisome directs PG synthesis to mid-cell.** (i), Cells in Phase 1 of the cell cycle (before septal synthesis is initiated) incorporate new PG all around the cell periphery. (ii), In preparation for division, FtsZ and early components of the divisome assemble at mid-cell. (iii), The DivIB/DivIC/FtsL complex recruits MurJ to the divisome, which initiates specific translocation of lipid II at mid-cell (iv), The major PG synthase PBP2 accumulates at mid-cell via substrate affinity to translocated lipid II, initiating major PG incorporation at mid-cell, together with the other PBPs.

The requirement for an assembled DivIB/DivIC/FtsL complex for the recruitment of MurJ and, by extension, PG synthesis to the septum, is interesting because these proteins seemingly do not have an enzymatic activity, despite being widely conserved in bacteria that have cell walls<sup>49</sup>. It has been suggested that DivIB, DivIC and FtsL in Gram-positives and their orthologues FtsQ, FtsB and FtsL in Gram-negatives function as a checkpoint system that mediates between Z-ring formation and PG synthesis<sup>44</sup>. Furthermore, assembly of this complex at the septum in *E. coli* seems to be dependent on the prior recruitment of the multifunctional DNA translocase FtsK<sup>50</sup>, which has

been shown to have an important role in synchronizing segregation of the chromosomes with cell division in bacteria<sup>51-53</sup>. Having MurJ recruitment to the septum dependent on the assembly of the DivIB/DivIC/FtsL complex could be a topological cue to ensure that DNA segregation is occurring prior to septum synthesis, avoiding the premature bisection of the nucleoid.

## References

- 1 Scheffers, D. J. & Pinho, M. G. Bacterial cell wall synthesis: New insights from localisation studies. *Microbiol. Mol. Biol. Rev.* **69**, 585-607, doi:10.1128/MMBR.69.4.585-607.2005 (2005).
- 2 Ruiz, N. Bioinformatics identification of MurJ (MviN) as the peptidoglycan lipid II flippase in *Escherichia coli*. *Proc Natl Acad Sci U S A* **105**, 15553-15557 (2008).
- 3 Sham, L. T. *et al.* Bacterial cell wall. MurJ is the flippase of lipid-linked precursors for peptidoglycan biogenesis. *Science* **345**, 220-222, doi:10.1126/science.1254522 (2014).
- 4 Huber, J. *et al.* Chemical genetic identification of peptidoglycan inhibitors potentiating carbapenem activity against methicillin-resistant *Staphylococcus aureus*. *Chem Biol* **16**, 837-848, doi:10.1016/j.chembiol.2009.05.012 (2009).
- 5 Meeske, A. J. *et al.* MurJ and a novel lipid II flippase are required for cell wall biogenesis in *Bacillus subtilis*. *Proc Natl Acad Sci U S A* **112**, 6437-6442, doi:10.1073/pnas.1504967112 (2015).
- 6 Meeske, A. J. *et al.* SEDS proteins are a widespread family of bacterial cell wall polymerases. *Nature* **537**, 634-638, doi:10.1038/nature19331 (2016).
- 7 Steele, V. R., Bottomley, A. L., Garcia-Lara, J., Kasturiarachchi, J. & Foster, S. J. Multiple essential roles for EzrA in cell division of *Staphylococcus aureus*. *Mol Microbiol* **80**, 542-555, doi:10.1111/j.1365-2958.2011.07591.x (2011).
- 8 Pinho, M. G., Kjos, M. & Veening, J. W. How to get (a)round: mechanisms controlling growth and division of coccoid bacteria. *Nat Rev Microbiol* **11**, 601-614, doi:10.1038/nrmicro3088 (2013).
- 9 Chastanet, A. & Carballido-Lopez, R. The actin-like MreB proteins in *Bacillus subtilis*: a new turn. *Front Biosci (Schol Ed)* **4**, 1582-1606 (2012).
- 10 Young, K. D. Bacterial shape: two-dimensional questions and possibilities. *Annu Rev Microbiol* **64**, 223-240, doi:10.1146/annurev.micro.112408.134102 (2010).
- 11 Pinho, M. & Errington, J. Dispersed mode of *Staphylococcus aureus* cell wall synthesis in the absence of the division machinery. *Mol Microbiol* **50**, 871-881, doi:10.1046/j.1365-2958.2003.03719.x (2003).
- 12 Monteiro, J. M. *et al.* Cell shape dynamics during the staphylococcal cell cycle. *Nat Commun* **6**, 8055, doi:10.1038/ncomms9055 (2015).
- 13 Monk, I. R., Shah, I. M., Xu, M., Tan, M. W. & Foster, T. J. Transforming the untransformable: application of direct transformation to manipulate genetically *Staphylococcus aureus* and *Staphylococcus epidermidis*. *MBio* **3**, doi:10.1128/mBio.00277-11 (2012).
- 14 Gill, S. R. *et al.* Insights on evolution of virulence and resistance from the complete genome analysis of an early methicillin-resistant *Staphylococcus aureus* strain and a biofilm-producing methicillin-resistant *Staphylococcus epidermidis* strain. *J. Bacteriol.* **187**, 2426-2438, doi:10.1128/JB.187.7.2426-2438.2005 (2005).
- 15 Nair, D. *et al.* Whole-genome sequencing of *Staphylococcus aureus* strain RN4220, a key laboratory strain used in virulence research, identifies

- mutations that affect not only virulence factors but also the fitness of the strain. *J Bacteriol* **193**, 2332-2335, doi:10.1128/JB.00027-11 (2011).
- 16 Mann, P. A. *et al.* Murgocil is a highly bioactive staphylococcal-specific inhibitor of the peptidoglycan glycosyltransferase enzyme MurG. *ACS Chem Biol* **8**, 2442-2451, doi:10.1021/cb400487f (2013).
- 17 Tan, C. M. *et al.* Restoring methicillin-resistant *Staphylococcus aureus* susceptibility to  $\beta$ -lactam antibiotics. *Sci Transl Med* **4**, 126ra135, doi:10.1126/scitranslmed.3003592 (2012).
- 18 Loskill, P. *et al.* Reduction of the peptidoglycan crosslinking causes a decrease in stiffness of the *Staphylococcus aureus* cell envelope. *Biophys J* **107**, 1082-1089, doi:10.1016/j.bpj.2014.07.029 (2014).
- 19 Donald, R. G. *et al.* A *Staphylococcus aureus* fitness test platform for mechanism-based profiling of antibacterial compounds. *Chem Biol* **16**, 826-836, doi:10.1016/j.chembiol.2009.07.004 (2009).
- 20 Pereira, P., Veiga, H., Jorge, A. & Pinho, M. Fluorescent reporters for studies of cellular localisation of proteins in *Staphylococcus aureus*. *Appl. Environ. Microbiol.* **76**, 4346-4353, doi:10.1128/AEM.00359-10 (2010).
- 21 Fisher, A. C. & DeLisa, M. P. Laboratory evolution of fast-folding green fluorescent protein using secretory pathway quality control. *PLoS One* **3**, e2351, doi:10.1371/journal.pone.0002351 (2008).
- 22 Atilano, M. *et al.* Teichoic acids are temporal and spatial regulators of peptidoglycan cross-linking in *Staphylococcus aureus*. *Proc. Natl. Acad. Sci. U S A* **107**, 18991-18996, doi:10.1073/pnas.1004304107 (2010).
- 23 Pinho, M. & Errington, J. A *divIVA* null mutant of *Staphylococcus aureus* undergoes normal cell division. *FEMS Microbiol Lett* **240**, 145-149 (2004).
- 24 Arnaud, M., Chastanet, A. & Debarbouille, M. New vector for efficient allelic replacement in naturally nontransformable, low-GC-content, gram-positive bacteria. *Appl. Environ. Microbiol.* **70**, 6887-6891, doi:10.1128/AEM.70.11.6887-6891.2004 (2004).
- 25 Charpentier, E. *et al.* Novel cassette-based shuttle vector system for gram-positive bacteria. *Appl. Environ. Microbiol.* **70**, 6076-6085, doi:10.1128/AEM.70.10.6076-6085.2004 (2004).
- 26 Nair, D. R. *et al.* Characterization of a novel small molecule that potentiates  $\beta$ -lactam activity against gram-positive and gram-negative pathogens. *Antimicrob Agents Chemother* **59**, 1876-1885, doi:10.1128/AAC.04164-14 (2015).
- 27 Forsyth, R. A. *et al.* A genome-wide strategy for the identification of essential genes in *Staphylococcus aureus*. *Mol Microbiol* **43**, 1387-1400 (2002).
- 28 Kraemer, G. R. & Iandolo, J. J. High-frequency transformation of *Staphylococcus aureus* by electroporation. *Current Microbiology* **21**, 373-376, doi:10.1007/bf02199440 (1990).
- 29 Oshida, T. & Tomasz, A. Isolation and characterization of a Tn551-autolysis mutant of *Staphylococcus aureus*. *J Bacteriol* **174**, 4952-4959 (1992).
- 30 Pinho, M. G. & Errington, J. A *divIVA* null mutant of *Staphylococcus aureus* undergoes normal cell division. *FEMS Microbiology Letters* **240**, 145-149, doi:10.1016/j.femsle.2004.09.038 (2004).

- 31 Nair, D. R. *et al.* Characterization of a novel small molecule that potentiates  $\beta$ -lactam activity against gram-positive and gram-negative pathogens. *Antimicrob Agents Chemother* **59**, 1876-1885, doi:10.1128/aac.04164-14 (2015).
- 32 Mann, P. A. *et al.* Murgocil is a highly bioactive staphylococcal-specific inhibitor of the peptidoglycan glycosyltransferase enzyme MurG. *ACS Chem Biol* **8**, 2442-2451, doi:10.1021/cb400487f (2013).
- 33 Donald, R. G. *et al.* A *Staphylococcus aureus* fitness test platform for mechanism-based profiling of antibacterial compounds. *Chem Biol* **16**, 826-836, doi:10.1016/j.chembiol.2009.07.004 (2009).
- 34 Kuru, E. *et al.* In situ Probing of Newly Synthesized Peptidoglycan in Live Bacteria with Fluorescent D-Amino Acids. *Angew. Chem. Int Ed. Engl.* **51**, 12519-12523, doi:10.1002/anie.201206749 (2012).
- 35 Huber, J. *et al.* Chemical genetic identification of peptidoglycan inhibitors potentiating carbapenem activity against methicillin-resistant *Staphylococcus aureus*. *Chem Biol* **16**, 837-848, doi:10.1016/j.chembiol.2009.05.012 (2009).
- 36 Andreu, J. M. *et al.* The antibacterial cell division inhibitor PC190723 is an FtsZ polymer-stabilizing agent that induces filament assembly and condensation. *J Biol Chem* **285**, 14239-14246, doi:10.1074/jbc.M109.094722 (2010).
- 37 Velasco, F. Thresholding using the ISODATA clustering algorithm. *IEEE Transactions on Systems, Man and Cybernetics* **10**, 771-774, doi:10.1109/tsmc.1980.4308400 (1980).
- 38 Falcão, A. X., Stolfi, J. & de Alencar Lotufo, R. The image foresting transform: theory, algorithms, and applications. *IEEE Trans Pattern Anal Mach Intell* **26**, 19-29, doi:10.1109/tpami.2004.10012 (2004).
- 39 Roerdink, J. & Meijster, A. The Watershed Transform: Definitions, Algorithms and Parallelization Strategies. *Fundamenta Informaticae* **41**, 187-228 (2000).
- 40 Dunn, K. W., Kamocka, M. M. & McDonald, J. H. A practical guide to evaluating colocalisation in biological microscopy. *Am J Physiol Cell Physiol* **300**, C723-742, doi:10.1152/ajpcell.00462.2010 (2011).
- 41 Berger-Bächli, B., Strässle, A., Gustafson, J. & Kayser, F. Mapping and characterization of multiple chromosomal factors involved in methicillin resistance in *Staphylococcus aureus*. *Antimicrob Agents Chemother* **36**, 1367-1373 (1992).
- 42 De Lencastre, H. *et al.* Antibiotic resistance as a stress response: complete sequencing of a large number of chromosomal loci in *Staphylococcus aureus* strain COL that impact on the expression of resistance to methicillin. *Microb Drug Resist* **5**, 163-175 (1999).
- 43 Pinho, M. G. & Errington, J. Recruitment of penicillin-binding protein PBP2 to the division site of *Staphylococcus aureus* is dependent on its transpeptidation substrates. *Mol. Microbiol.* **55**, 799-807, doi:10.1111/j.1365-2958.2004.04420.x (2005).
- 44 Goehring, N. W., Gonzalez, M. D. & Beckwith, J. Premature targeting of cell division proteins to mid-cell reveals hierarchies of protein interactions involved in divisome assembly. *Mol Microbiol* **61**, 33-45 (2006).

- 45 Errington, J., Daniel, R. A. & Scheffers, D. J. Cytokinesis in Bacteria. *Microbiology and Molecular Biology Reviews* **67**, 52-65, doi:10.1128/mmbr.67.1.52-65.2003 (2003).
- 46 Gamba, P., Veening, J. W., Saunders, N. J., Hamoen, L. W. & Daniel, R. A. Two-step assembly dynamics of the *Bacillus subtilis* divisome. *J Bacteriol* **191**, 4186-4194, doi:10.1128/JB.01758-08 (2009).
- 47 Pereira, S. F., Henriques, A. O., Pinho, M. G., de Lencastre, H. & Tomasz, A. Role of PBP1 in cell division of *Staphylococcus aureus*. *J. Bacteriol.* **189**, 3525-3531, doi:10.1128/JB.00044-07 (2007).
- 48 Bottomley, A. L. *et al.* *Staphylococcus aureus* DivIB is a peptidoglycan-binding protein that is required for a morphological checkpoint in cell division. *Mol Microbiol*, doi:10.1111/mmi.12813 (2014).
- 49 Gonzalez, M. D., Akbay, E. A., Boyd, D. & Beckwith, J. Multiple interaction domains in FtsL, a protein component of the widely conserved bacterial FtsLBQ cell division complex. *J Bacteriol* **192**, 2757-2768, doi:10.1128/JB.01609-09 (2010).
- 50 Chen, J. C. & Beckwith, J. FtsQ, FtsL and FtsI require FtsK, but not FtsN, for co-localisation with FtsZ during *Escherichia coli* cell division. *Mol Microbiol* **42**, 395-413 (2001).
- 51 Bigot, S., Corre, J., Louarn, J. M., Cornet, F. & Barre, F. X. FtsK activities in Xer recombination, DNA mobilization and cell division involve overlapping and separate domains of the protein. *Mol Microbiol* **54**, 876-886, doi:10.1111/j.1365-2958.2004.04335.x (2004).
- 52 Dubarry, N., Possoz, C. & Barre, F. X. Multiple regions along the *Escherichia coli* FtsK protein are implicated in cell division. *Mol Microbiol* **78**, 1088-1100, doi:10.1111/j.1365-2958.2010.07412.x (2010).
- 53 Veiga, H. & G Pinho, M. *Staphylococcus aureus* requires at least one FtsK/SpoIIIE protein for correct chromosome segregation. *Mol Microbiol* **103**, 504-517, doi:10.1111/mmi.13572 (2017).





## Chapter IV

---

Building Bridges: the pentaglycine crosslinks in *S. aureus* peptidoglycan are required for cell integrity

**Author contributions**

J. M. Monteiro performed all experiments except for the glycine incorporation enzymatic assays, which were performed by D. Münch.

**Acknowledgments:**

I would like to thank Prof. Dr. Hans-Georg Sahl, Prof. Dr. Gabriele Bierbaum, Prof Dr. Tanja Schneider and all the members of the Pharmazeutische Mikrobiologie and IMMIP groups in Bonn University for hosting me, especially Daniela Münch for all the help with the *in vitro* lipid II experiments.

This chapter contains unpublished data.

## **Abstract**

Infections caused by multi-drug resistant bacteria constitute a major challenge to global public health. In particular, the prevalence of methicillin-resistant *Staphylococcus aureus* (MRSA) strains remains high in several parts of the world, urging the development of new and efficient countermeasures. *S. aureus* builds its cell wall using peptidoglycan (PG) layers crosslinked by pentaglycine bridges. Crossbridge synthesis is done by the Fem protein family of transferases: FemX adds the first glycine to PG precursor lipid II, FemA adds the second and the third and FemB adds the fourth and fifth glycines. FemA and FemB are exclusive to *S. aureus*, making these proteins interesting candidates for pathogen-specific drug design. In order to explore this possibility, we constructed a conditional mutant of the *femAB* operon in the background of community-acquired MRSA strain (CA-MRSA) MW2. Depletion of *femAB* expression was lethal, with cells appearing as pseudomulticellular forms that eventually lysed due to extensive membrane rupture. Furthermore, we investigated key residues present in the putative transferase pocket and the  $\alpha 6$  helix of FemA by site-directed mutagenesis. Expression of FemA point mutants KR180AA and Y315A, with wild-type FemB, failed to fully complement the depletion of *femAB*. Furthermore, we determined that transferase activity was lower in mutants KR180AA and Y315A when compared to wild-type FemA, using an *in vitro* lipid II assay.

*Chapter IV*

Our data implies that FemA would be a good target for the development of anti-staphylococcal therapies.

## **Introduction**

Decades of research into the discovery and development of antibiotics to treat bacterial infections have resulted in a wide variety of molecules that target diverse biosynthetic pathways required for cell viability. Nevertheless, heavy antibiotic misuse has progressively caused a surge of bacterial strains which have evolved resistance against multiple drugs<sup>1,2</sup>. Of particular note are methicillin-resistant *Staphylococcus aureus* (MRSA) strains, which cause invasive, often fatal, infections that are notoriously difficult to treat and can quickly spread, through contact between individuals or contact with contaminated surfaces<sup>3-5</sup>. Traditionally associated with debilitated or immunocompromised patients in healthcare settings, infections of highly virulent MRSA strains have also emerged in the communities (community acquired MRSA, CA-MRSA), affecting individuals without predisposing risk factors. Despite efforts to contain their spread, MRSA infections are now a global problem and account for >40% of nosocomial isolates in a variety of countries, including Southern Europe where the prevalence of MRSA is particularly high (2016 ECDC annual report). Bacterial resistance to antibiotics is poised to become the major public health challenge of the 21<sup>st</sup> century, with MRSA at the tip of the spear, prompting the need to develop new strategies effective against this (and other) pathogens.

Most of the widely used, and more potent, antibiotics target steps in the biosynthesis of peptidoglycan (PG), the core component

of the bacterial wall. PG is a macromolecule composed of glycan chains, where each unit is constituted of N-acetylmuramic acid (MurNAc) and N-acetylglucosamine (GlcNAc) sugars, with a stem peptide attached to MurNAc. Glycan chains are connected (crosslinked) through flexible species-specific peptide bridges, creating a mesh-like structure that envelops the cell<sup>6,7</sup>. The structural features of PG therefore confer both robustness and flexibility to the cell envelope, which are necessary to withstand high pressure derived from intracellular turgor<sup>8</sup>. During PG synthesis, both the incorporation of each monomer to the growing glycan chains (transglycosylation, TG) and the crosslinking between chains (transpeptidation, TP) are usually catalysed by penicillin-binding proteins (PBPs)<sup>9,10</sup>.

The ongoing wave of infectious MRSA strains is resistant to all classes of  $\beta$ -lactams currently in use (penicillins, cephalosporins, carbapenems), which irreversibly acylate the TPase site of PBPs<sup>1</sup>. In these strains, the major determinant of methicillin resistance is the acquired *mecA* gene, which encodes for PBP2A, an enzyme insensitive to  $\beta$ -lactam acylation<sup>11</sup>. However, high-level  $\beta$ -lactam resistance is in fact dependent on several elements, which were identified by transposon mutagenesis and termed *fem* (factor essential for methicillin resistance) or *aux* (auxiliary) genes<sup>12,13</sup>. Approximately 30 *fem/aux* determinants have been identified so far and most are housekeeping genes, involved in a variety of cellular processes and probably present in every *S. aureus* strain<sup>14</sup>. Three closely related

factors - *fmhB* and the co-transcribed *femA* and *femB* genes, encode for the FemX, FemA and FemB proteins, respectively, transferases which synthesise the pentaglycine bridges used to crosslink glycan chains in *S. aureus*<sup>15,16</sup>. During the inner membrane steps of PG synthesis (see General Introduction), the Fem proteins sequentially transfer five glycine residues to PG precursor lipid II using glycyl-charged tRNA molecules<sup>17</sup>. Importantly, *in vivo* and *in vitro* studies have shown that each Fem has strict substrate specificity: FemX adds the first glycine, FemA adds the second and the third and FemB adds the fourth and fifth glycines, and each Fem cannot substitute for another<sup>18,19</sup>. Although *fmhB* was shown to be an essential gene<sup>20</sup>, mutants carrying a *Tn551* inactivated *femA* or *femB* genes grew poorly but were viable, suggesting that *S. aureus* can survive with a PG composed of monoglycine crossbridges<sup>15,21</sup>. HPLC analysis of the PG composition in these mutants revealed an overall reduction, but not absence of crosslinked species and, importantly, monoglycyl-substituted oligomers were never found<sup>22</sup>. Moreover, the *Tn551* insertion in the *femA* gene occurred in the promoter region of the *femAB* operon, which led to a 90% decrease in *femAB* transcription, while *Tn551* insertion in the *femB* locus presumably led to the complete knockout of the gene<sup>21</sup>. These findings still raised questions of whether residual *femA* activity in the *femA* mutants was responsible for a minimal degree of crosslinking that would still ensure cell viability, or alternatively, whether strains had acquired compensatory mutations allowing for cell survival with shortened crossbridges.

A second study on the essentiality of *femAB* was done by Strandén and colleagues who constructed a *femAB* mutant, AS145, by allelic replacement of the *femAB* operon by a tetracycline resistance marker<sup>23</sup>. AS145 showed impaired growth, methicillin hypersusceptibility and drastically reduced crosslinking of glycan strands, when compared to the parental strain<sup>23,24</sup>. *Cis*-complementation of the *femAB* mutation in AS145 with wild-type *femAB* restored synthesis of the pentaglycine crossbridge and methicillin resistance, although the growth rates remained low<sup>25</sup>. Therefore the authors postulated that survival of AS145 required a compensatory or suppressor mutation which still remains unidentified<sup>25</sup>. Transcriptional analysis revealed that AS145 underwent severe metabolic adaptations to survive, including upregulation of membrane transporters associated with glycerol uptake (an osmoprotectant), upregulation of the arginine-deiminase pathway (an alternative for ATP production) and downregulation of nitrogen metabolism. Collectively these data suggested that *femAB* mutants adapted to survive with shortened crossbridges by drastically decreasing metabolic activity to alleviate internal turgor<sup>25</sup>.

FemA folds into a globular domain with two antiparallel coiled-coil helical arms extending into the solvent<sup>26</sup>. The globular domain contains a deep L-shaped channel proposed to be a binding cavity suitable for an extended conformation of the stem peptide moiety in lipid II-Gly<sub>1</sub>. If correct, an amino-acid charged tRNA molecule could then be held at the junction between the L-shaped



channel and the arms<sup>26</sup>, a mechanism similar to what was previously described for the *Tetrahymena termophyla* seryl-tRNA synthetase protein<sup>27</sup>. More recently, Maillard and colleagues performed site-directed mutagenesis on selected residues located in the putative substrate binding cavity of *Weissella viridescens* FemX, which is structurally similar to *S. aureus* FemA. In particular, substitution of Arg211 by methionine (corresponding to Arg220 in *S. aureus* FemA) led to a severe decrease in transferase activity, without affecting protein folding<sup>28</sup>, suggesting that this residue could be crucial for substrate binding.

The *femAB* operon and pentaglycine crossbridges are unique features of *S. aureus* among prokaryotes. This makes FemAB proteins potentially interesting targets for MRSA-specific drug design. In this work we wanted to investigate if full depletion of the *femAB* operon is lethal in an MRSA strain and to determine the phenotypic defects associated with lack of *femAB* expression. Furthermore, we wanted to identify key residues essential for FemA activity, towards the future development of a FemA inhibitor.

## Experimental Procedures

### Bacterial growth conditions

Strains and plasmids constructed for this study are listed in Table 1. *S. aureus* strains were grown in tryptic soy broth (TSB, Difco) at 200 r.p.m with aeration at 37 °C or on tryptic soy agar (TSA, Difco) at 30 or 37 °C. *Escherichia coli* strains were grown in Luria–Bertani broth (Difco) with aeration, or Luria–Bertani agar (Difco) at 37 or 30 °C. When necessary, antibiotics ampicillin (100 µg/ml), erythromycin (10 µg/ml), kanamycin (50 µg/ml), neomycin (50 µg/ml) or chloramphenicol (30 µg/ml) were added to the media. Unless stated otherwise, isopropyl β-D-1-thiogalactopyranoside (IPTG, Apollo Scientific) was used at 500 µM to induce expression of constructs under the control of the *Pspac* promoter. Cadmium chloride (Sigma-Aldrich) was used at 1 µM when required to induce expression of constructs under the control of the *Pcad* promoter.

*Building Bridges: the pentaglycine crosslinks in S. aureus peptidoglycan are required for cell integrity*

**Table 1 – Strains and plasmids used in this study.**

Strains	Description	Source or reference
<i>E. coli</i>		
DC10B	Δdcm in the DH10B background; Dam methylation only	29
BL21 (DE3)	B F <sup>-</sup> dcm ompT hsdS(rB <sup>-</sup> mB <sup>-</sup> ) gal λ(DE3)	Stratagene
BL21-FemX	BL21(DE3) expressing full length C-ter His-tagged FemX; Kan <sup>r</sup>	This work
BL21-GlyS	BL21(DE3) expressing full length C-ter His-tagged GlyS; Kan <sup>r</sup>	This work
BL21-FemA <sup>wt</sup>	BL21(DE3) expressing full length C-ter His-tagged FemA; Kan <sup>r</sup>	This work
BL21-FemA <sup>KR180AA</sup>	BL21(DE3) expressing mutant C-ter His-tagged FemA <sup>KR180AA</sup> ; Kan <sup>r</sup>	This work
BL21-FemA <sup>RF220AA</sup>	BL21(DE3) expressing mutant C-ter His-tagged FemA <sup>RF220AA</sup> ; Kan <sup>r</sup>	This work
BL21-FemA <sup>Y327A</sup>	BL21(DE3) expressing mutant C-ter His-tagged FemA <sup>Y327A</sup> ; Kan <sup>r</sup>	This work
<i>S. aureus</i>		
RN4220	Restriction-deficient derivative of NCTC8325-4	30
MW2	CA-MRSA; SCCmec type IV, ST1, pbla <sup>+</sup>	31
MW2-iFemAB	MW2 femAB::Pspac-femAB pMGPII; Ery <sup>r</sup> Cm <sup>r</sup>	This work
MW2pFemA <sup>wt</sup>	MW2 femAB::Pspac-femAB pMGPII pFemA <sup>wt</sup> ; Ery <sup>r</sup> Cm <sup>r</sup> Kan <sup>r</sup>	This work
MW2pFemA <sup>KR180AA</sup>	MW2 femAB::Pspac-femAB pMGPII pFemA <sup>KR180AA</sup> ; Ery <sup>r</sup> Cm <sup>r</sup> Kan <sup>r</sup>	This work
MW2pFemA <sup>RF220AA</sup>	MW2 femAB::Pspac-femAB pMGPII pFemA <sup>RF220AA</sup> ; Ery <sup>r</sup> Cm <sup>r</sup> Kan <sup>r</sup>	This work
MW2pFemA <sup>Y327A</sup>	MW2 femAB::Pspac-femAB pMGPII pFemA <sup>Y327A</sup> ; Ery <sup>r</sup> Cm <sup>r</sup> Kan <sup>r</sup>	This work

Plasmids	Description	Source or reference
pMUTIN4	<i>S. aureus</i> integrative vector containing an IPTG-inducible <i>Pspac</i> promoter; Amp <sup>r</sup> Ery <sup>r</sup>	32
pMGPII	<i>S. aureus</i> replicative plasmid containing <i>lacI</i> ; Amp <sup>r</sup> Cm <sup>r</sup>	33
pCNX	Replicative vector containing a cadmium inducible <i>Pcad</i> promoter; Amp <sup>r</sup> Kan <sup>r</sup>	34
pFemABi	pMUTIN4 derivative containing a <i>femA-femB</i> DNA fragment under <i>Pspac</i> ; Amp <sup>r</sup> Ery <sup>r</sup>	This work
pMADfemAmch	Vector containing a <i>femA-mCherry-STOP-femB</i> DNA fragment; Amp <sup>r</sup> Ery <sup>r</sup>	35
pFemAB <sup>wt</sup>	pCNX derivative expressing a FemA-mCherry fusion and FemB, both under the control of <i>Pcad</i> ; Amp <sup>r</sup> Kan <sup>r</sup>	This work
pFemA <sup>KR180AA</sup> B	pCNX derivative expressing a mutant FemA(K180A, R181A)-mCherry fusion and FemB, both under the control of <i>Pcad</i> ; Amp <sup>r</sup> Kan <sup>r</sup>	This work
pFemA <sup>RF220AA</sup> B	pCNX derivative expressing a mutant FemA(R220A, F224A)-mCherry fusion and FemB, both under the control of <i>Pcad</i> ; Amp <sup>r</sup> Kan <sup>r</sup>	This work
pFemA <sup>Y327A</sup> B	pCNX derivative expressing a mutant FemA(Y327A)-mCherry fusion and FemB, both under the control of <i>Pcad</i> ; Amp <sup>r</sup> Kan <sup>r</sup>	This work
pET-24b	<i>E. coli</i> replicative vector for the expression of proteins with a His <sub>6</sub> fusion at the C-terminus, under the <i>Pspac</i> promoter; Kan <sup>r</sup>	Novagen
pET-GlyS	pET-24b derivative encoding a GlyS-His <sub>6</sub> fusion; Kan <sup>r</sup>	19
pET-FemX	pET-24b derivative encoding a FemX-His <sub>6</sub> fusion; Kan <sup>r</sup>	19
pET-FemA <sup>wt</sup>	pET-24b derivative encoding a FemA-His <sub>6</sub> fusion; Kan <sup>r</sup>	This work
pET-FemA <sup>KR180AA</sup>	pET-24b derivative encoding a mutant FemA(K180A, R181A)-His <sub>6</sub> fusion; Kan <sup>r</sup>	This work
pET-FemA <sup>RF220AA</sup>	pET-24b derivative encoding a mutant FemA(R220A, F224A)-His <sub>6</sub> fusion; Kan <sup>r</sup>	This work
pET-FemA <sup>Y327A</sup>	pET-24b derivative encoding a mutant FemA(Y327A)-His <sub>6</sub> fusion; Kan <sup>r</sup>	This work

### Construction of *S. aureus* strains

In order to construct an *S. aureus* strain with the *femAB* operon under the control of an inducible promoter, a fragment containing the first 400 bp of *femA* was amplified from *S. aureus* MW2 DNA with primer pair spacfemab\_P1 EcoRI/spacfemab\_P2 BamHI (Table 2), cut

with EcoRI and BamHI restriction enzymes and cloned into pMUTIN4<sup>32</sup>, downstream of the *Pspac* promoter, giving plasmid pFemABi, which was sequenced. pFemABi was then propagated in DC10b cells, electroporated into electrocompetent RN4220 cells, and transduced (using phage 80 $\alpha$ ) to MW2, where it integrated in the *femAB* locus by homologous recombination. The resulting strain contains a truncated copy of *femA* under the control of the *femAB* native promoter, and the *femAB* operon under the control of *Pspac*. Multicopy plasmid pMGPII<sup>33</sup>, which encodes *Pspac* repressor LacI, was then transduced into this strain, giving rise to MW2-iFemAB

To construct *S. aureus* strains expressing mutated alleles of FemA-mCherry together with wild-type FemB, first *femA-mCherry-STOP* codon-*femB* was amplified from pMADfemAmch<sup>35</sup> using primers pcnfemab\_P1 BamHI and pcnfemab\_P2 EcoRI. This fragment was cut with BamHI and EcoRI and cloned into replicative vector pCNX, under the control of *Pcad*, giving plasmid pFemAB<sup>wt</sup>. pFemAB<sup>wt</sup> was then used as the template for site-directed mutagenesis. Primers fema\_kr180aa\_fw/ fema\_kr180aa\_rev were used to generate pFemA<sup>KR180AA</sup>, containing both K180A and R181A mutations; Primers fema\_rf220aa\_fw/fema\_rf220aa\_rev were used to generate pFemA<sup>RF220AA</sup>, containing both R220A and F224A mutations; and primers fema\_Y327a\_fw/fema\_Y327a\_rev were used to generate pFemA<sup>Y327A</sup>, containing an Y327A mutation (Table 2). Site-directed mutagenesis was performed with Phusion polymerase (Thermo Scientific) following manufacturer's instructions, and each plasmid

was sequenced to confirm the presence of the mutations. pFemAB<sup>wt</sup>, pFemA<sup>KR180AA</sup>, pFemA<sup>RF220AA</sup> and pFemA<sup>Y327A</sup> were propagated in DC10b, transformed to RN4220 and transduced to MW2-iFemAB, giving strains MW2pFemAB<sup>wt</sup>, MW2pFemA<sup>KR180AA</sup>, MW2pFemA<sup>RF220AA</sup> and MW2pFemA<sup>Y327A</sup>, respectively.

**Table 2. Oligonucleotides used in this study.**

Primer Name	Sequence (5'-3')
spacfemab_P1 EcoRI	GCGCGAATTCATGAAGTTTACAAATTTAACAGC
spacfemab_P2 BamHI	CGCGGGATCCTTATCAAAGAACCAATCATTACCAGCATTAC
pcnfemab_P1 BamHI	GCGCGGGATCCGCAAATACGGAAATGAAATTAATTAACG
pcnfemab_P2 EcoRI	CGCGCGGAATTCCTATTTCTTTAATTTTTTACGTAATTTATC
fema_kr180aa_fw	ATGGACTTAGAGCAGCAAACACGAAAAAAGTAAAAAAGAATG
fema_kr180aa_rev	TTTTCGTGTTTGCTGCTCTAAGTCCATCCATATTTTTAATGATG
fema_rf220aa_fw	GCTGATGCTGATGACAAAGCTTACTACAATCGCTTAAAAATATTAC
fema_rf220aa_rev	GTAGTAAGCTTTGTCATCAGCATCAGCAAAAGCTTTTGATTC
fema_Y327a_fw	GAAGTTGTTGCTTATGCTGGTGGTACATCAAATGCATTCC
fema_Y327a_rev	ACCAGCATAAGCAACAACCTCAAATGGATTGATAAAGAAG
femaexpress_P1 BamHI	CGCGCGGATCCATGAAGTTTACAAATTTAACGCTAAAGAGTTTG
femaexpress_P2 EcoRI	CGCGCGAATTCCTAAAAAATTCTGCTTTAACTTTTTTAAGTGC

Underlined sequences correspond to restriction sites

### Construction of *E. coli* strains

In order to construct protein expression vectors, primers femaexpress\_P1 BamHI and femaexpress\_P2 EcoRI (Table 2) were used to amplify the wild-type *femA* gene from pFemAB<sup>wt</sup> or *femA* mutant alleles from pFemA<sup>KR180AA</sup>, pFemA<sup>RF220AA</sup> and pFemA<sup>Y327A</sup>. The resulting fragments were digested with EcoRI and BamHI and cloned into pET-24b, giving plasmids pET-FemA<sup>wt</sup>, pET-FemA<sup>KR180AA</sup>, pET-FemA<sup>RF220AA</sup> and pET-FemA<sup>Y327A</sup>, respectively. These plasmids, along with pET-GlyS and pET-FemX were then propagated in DC10b and

transformed to BL21 (DE3) cells, giving strains BL21-FemA<sup>wt</sup>, BL21-FemA<sup>KR180AA</sup>, BL21-FemA<sup>RF220AA</sup>, BL21-FemA<sup>Y327A</sup>, BL21-GlyS and BL21-FemX, respectively.

### **Growth curves of *S. aureus* strains**

To assess whether the *femAB* operon is essential for viability, cells from an overnight culture of MW2 and MW2-iFemAB (supplemented with erythromycin and chloramphenicol and grown in the presence of IPTG at 500  $\mu$ M) were collected and washed three times with fresh TSB to remove IPTG. Cells were then back-diluted to OD<sub>600nm</sub> 0.001 in TSB supplemented with erythromycin and chloramphenicol and containing 0, 10, 25 or 500  $\mu$ M of IPTG (for MW2-iFemAB) and grown for 10 hours with OD<sub>600nm</sub> measurements taken every hour.

To evaluate morphological defects and peptidoglycan composition changes caused by the depletion of the *femAB* operon, overnight cultures of MW2 and MW2-iFemAB grown in TSB with 500  $\mu$ M of IPTG, erythromycin and chloramphenicol were back-diluted 1:500 in the same medium until the cultures reached an OD<sub>600</sub> of 0.7. At this point the cultures were washed three times to remove the IPTG and back-diluted 1:500 in fresh TSB with 0, 25 and 500  $\mu$ M of IPTG and growth was monitored. When growth of the non-induced culture was arrested (approximately 4 hours after incubation), cells were collected for microscopy or cell wall analysis (described below).

To assess the effects of FemA mutations on growth rates, peptidoglycan composition and fluorescence microscopy overnight cultures of MW2, MW2pFemAB<sup>wt</sup>, MW2pFemA<sup>KR180AA</sup>, MW2pFemA<sup>RF220AA</sup> and MW2pFemA<sup>Y327A</sup>, supplemented with erythromycin, chloramphenicol and kanamycin (when applicable, at the concentrations described above) plus 500  $\mu$ M of IPTG were harvested and washed to remove IPTG. Cells were then back-diluted to OD<sub>600nm</sub> 0.001 in the same medium without IPTG and CdCl<sub>2</sub> was added at 1  $\mu$ M, to drive the expression of either wild-type or mutant *femA* alleles from the pCNX-based plasmids.

### **Minimum inhibitory concentration (MIC) assays**

MICs of lysostaphin and oxacillin were determined by broth microdilution in sterile 96-well plates. The medium used was TSB, containing a series of two-fold dilutions of each compound. Cultures of *S. aureus* strains and mutants were added at a final density of  $\sim 5 \times 10^5$  CFU ml<sup>-1</sup> to each well. Wells were reserved in each plate for sterility control (no cells added) and cell viability (no compound added). Plates were incubated at 37°C. Endpoints were assessed visually after 48 h. All assays were done in triplicate.

### **Purification and analysis of *S. aureus* muropeptides**

Peptidoglycan was purified from exponentially-growing cultures of *S. aureus* as described by Filipe et al.<sup>36</sup>. Muropeptides were prepared from PG samples by digestion with mutanolysin (0.135 U/ $\mu$ g of PG, from Sigma-Aldrich) and analysed by reverse phase



HPLC using a Hypersil ODS (C18) column (Thermo-Fisher Scientific). Muropeptide species were eluted in 0.1 M sodium phosphate, pH 2.0, with a gradient of 5–30% methanol for 155 minutes and detected at 206 nm.

### **S. aureus imaging by fluorescence microscopy**

Super-resolution Structured Illumination Microscopy (SIM) imaging was performed using an Elyra PS.1 microscope (Zeiss) with a Plan-Apochromat 63x/1.4 oil DIC M27 objective. SIM images were acquired using five grid rotations, unless stated otherwise, with 34  $\mu\text{m}$  grating period for the 561 nm laser (100 mW), 28  $\mu\text{m}$  period for 488 nm laser (100 mW) and 23  $\mu\text{m}$  period for 405 nm laser (50 mW). Images were captured using a Pco.edge 5.5 camera and reconstructed using ZEN software (black edition, 2012, version 8.1.0.484) based on a structured illumination algorithm, using synthetic, channel specific optical transfer functions and noise filter settings ranging from -6 to -8.

To evaluate defects in cell morphology, cells were incubated with membrane dye Nile Red (10  $\mu\text{g}/\text{ml}$ , Invitrogen), Hoechst 33342 (10  $\mu\text{g}/\text{ml}$ , Invitrogen) and a mixture containing equal amounts of vancomycin (Sigma) and a BODIPY FL conjugate of vancomycin (Van-FL, Molecular Probes) to a final concentration of 0.8  $\mu\text{g}/\text{ml}$ , for 5 minutes at room temperature. Subsequently, cells were washed with phosphate buffer saline (PBS), mounted on microscope slides covered with a thin layer of 1% agarose in PBS and imaged by SIM.

### **Overexpression and purification of recombinant His-tagged proteins**

Recombinant proteins were purified essentially as described by Rohrer et al.<sup>37</sup>, with some modifications. Single colonies of BL21 (DE3) expression strains were isolated from LA plates with kanamycin and used to inoculate LB (1 L) containing kanamycin. Cultures were grown to an OD<sub>600nm</sub> of approximately 0.6 at which point IPTG was added (final concentration 1 mM) and incubated for 3 hours with shaking (150 rpm) at 30 °C. Cells were harvested by centrifugation and washed with 50 mM sodium phosphate buffer (pH 7.5) containing 300 mM NaCl and 20% glycerol. Afterwards, cells were suspended in the same buffer, containing PMSF (final concentration, 0.1 mM) and lysozyme (final concentration, 1 mg/mL), and incubated on ice for 30 min. Cells were then disrupted three times in an ultrasonicator and centrifuged for 30 min at 4°C to precipitate cell debris. The resulting supernatant was purified by affinity chromatography using a Ni-NTA column (Qiagen), following manufacturer's instructions. Protein concentration was assessed using a BCA Protein Assay Kit (Pierce).

### **Synthesis and purification of lipid II and lipid II-Gly<sub>1</sub>**

Lipid II was prepared by reacting undecaprenyl phosphate (Larodan), UDP-MurNAc-pentapeptide from *Staphylococcus simulans*, UDP-GlcNAc (Sigma) and membrane proteins of *Micrococcus luteus* as previously described<sup>19,38</sup>. Monoglycyl lipid II was synthesised by reacting lipid I with tRNA preparations, in the presence of enzymes

FemX and GlyS, according to the method described by Schneider *et al.*<sup>19</sup>. Lipid intermediates were extracted from reaction mixtures with an equal volume of butanol/pyridine acetate (2:1; vol:vol; pH 4.2). Extracts were then purified by anion-exchange chromatography using a Hi-Trap DEAE FF-agarose column (Amersham Biosciences) by reverse-phase HPLC and eluted in a linear gradient from chloroform–methanol–water (2:3:1) to chloroform–methanol–300 mM ammonium bicarbonate (2:3:1). The fractions containing lipid species were identified by thin layer chromatography with chloroform–methanol–water–ammonia (88:48:10:1) as solvent<sup>39</sup>. The concentration of purified lipids was calculated by measuring inorganic phosphates released after the treatment with perchloric acid, as described previously<sup>40</sup>.

### **FemA enzymatic activity assay**

In order to compare the activity of wild-type FemA to selected FemA mutants, enzymatic reactions were performed as described previously<sup>19</sup>. Briefly, 100  $\mu$ l reactions were prepared containing 2.5 nmol of lipid II-Gly<sub>1</sub>, 10  $\mu$ g of glycyl-tRNA synthetase (GlyS), 25  $\mu$ g of tRNA, 2 mM ATP and 50 nmol [<sup>14</sup>C]-glycine in Tris buffer (100 mM Tris-HCl, 20 mM MgCl<sub>2</sub>, pH 7.5, and 0.8% Triton X-100). Then 2.7  $\mu$ g of wild-type FemA or FemA mutant protein was added and the reaction mixtures were incubated for 30, 60 or 90 minutes at 30 °C. Lipid intermediates were then extracted and analysed by thin layer chromatography, as described above. Finally, the amount of [<sup>14</sup>C]-

glycine transferred to lipid II-Gly<sub>1</sub> was quantified using phosphoimaging in a STORM system (GE Healthcare). Enzymatic assays were done in triplicate.

### **Identification of FemA residues involved in tRNA binding**

Identification of FemA residues which could bind glycyI-charged tRNA was performed using DP-Bind<sup>41,42</sup> (<http://lcg.rit.albany.edu/dp-bind/>), a sequence-based web server which predicts DNA/RNA binding domains in proteins based on biochemical proteins of amino acids and evolutionary information. Probability maps were generated using PSI-BLAST position-specific scoring matrix (PSSM) and three distinct machine learning methods that use evolutionary information: support vector machine (PSSM-SVM), kernel logistic regression (PSSM-KLR), and penalized logistic regression (PSSM-PLR). FemA residues K180 and R181 were identified as DNA-binding domains based on strict consensus between the three methods. SwissPdb viewer/Deep view<sup>43</sup> (<http://www.expasy.org/spdbv/>) was used to evaluate the structure of FemA, using file 1LRZ (doi: [10.2210/pdb1LRZ/pdb](https://doi.org/10.2210/pdb1LRZ/pdb)) deposited in the RCSB PDB by Benson et. al.<sup>26</sup>.

## **Results and Discussion**

### **The *femAB* operon is essential for the viability of *S. aureus***

*S. aureus femAB* null mutants have been previously constructed<sup>21,22,44,45</sup>. Inactivation of *femAB* led to altered cell morphology, but cells survived, suggesting that this operon is not essential for cell viability. However, complementation of *femAB* deficient mutants with intact *femAB* copies did not restore normal bacterial growth, suggesting the presence of compensatory mutations and/or metabolic adaptations that allowed for survival<sup>25</sup>. In order to evaluate the essentiality of *femAB* as well as phenotypes resulting from *femAB* depletion in a background without the existence of compensatory mutations, we decided to construct a conditional *femAB* mutant. The *femAB* operon of the clinically relevant CA-MRSA strain MW2 was placed under the control of the IPTG inducible *Pspac* promoter. As the *Pspac* promoter is known to be leaky<sup>46</sup>, several copies of the *lacI* repressor gene were provided to decrease the basal transcription of *femAB*. The resulting strain was named MW2-iFemAB.

Growth of MW2-iFemAB in liquid medium supplemented with IPTG at 0, 10, 25 and 500  $\mu$ M was followed for 10 hours. In the presence of 500  $\mu$ M of IPTG, growth of the conditional mutant was similar to the parental strain MW2, therefore this concentration of inducer was used in subsequent assays. The growth rate of MW2-iFemAB decreased with decreasing IPTG concentrations and,

surprisingly, no bacterial growth was observed in the absence of IPTG, indicating that this operon is essential for survival (Fig. 1a). To assess the effects on peptidoglycan composition due to loss of FemAB activity, we analysed the cell wall of MW2-iFemAB cells incubated with 500, 25 or 0  $\mu\text{M}$  of IPTG until bacterial growth was arrested in the non-induced culture (see Experimental Procedures). As expected, the muropeptide profiles (see Fig. 1c for peak assignment) in cells depleted of FemAB show a massive accumulation of peak 4, which was previously identified as the monomeric pentapeptide substituted with a single glycine residue<sup>47</sup>, the substrate of FemA (Fig.1b, [IPTG] 0  $\mu\text{M}$ ). This was in contrast to cells where FemAB was fully induced (Fig.1b, [IPTG] 500  $\mu\text{M}$ ), where the major monomeric form present was the pentaglycine substituted monomer (peak 5). Accordingly, the loss of FemAB also prevented the formation of pentaglycine crosslinked forms such as dimers (peak 11), trimers (peak 15), tetramers (peak 16) and higher order forms, which co-elute near the end of the run (Fig. 1b, arrow). Low FemAB expression levels, just enough to sustain bacterial growth ([IPTG] 25  $\mu\text{M}$ ), resulted in the presence of some pentaglycine crosslinked forms (peaks 11, 15, 16, etc.) and the accumulation of a previously identified species<sup>47</sup> with unknown chemical composition (peak 10), which could constitute a monoglycine substituted dimer. This degree of peptidoglycan structural organisation might be the minimum to ensure cell viability.

Building Bridges: the pentaglycine crosslinks in *S. aureus* peptidoglycan are required for cell integrity

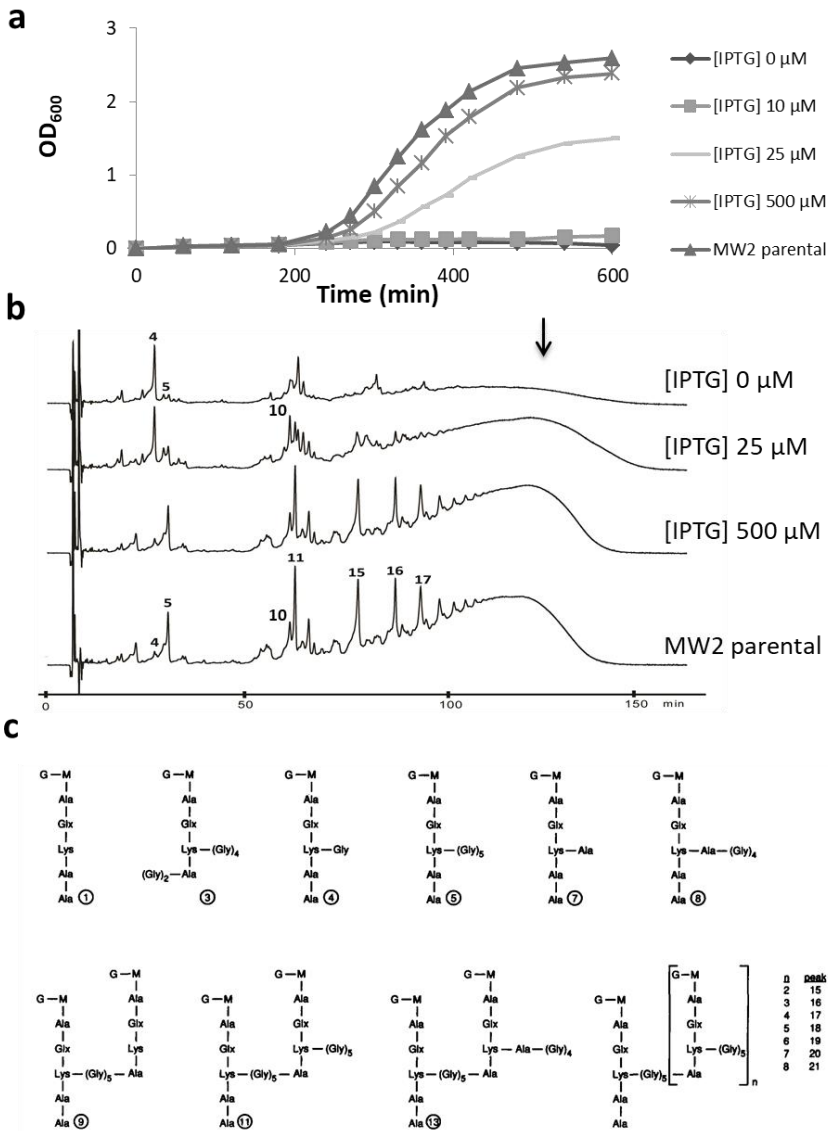


**Figure 1. *femAB* is essential for cell viability in *S. aureus*.** (a), Growth rates of MW2-*ifemAB* strain with IPTG-inducible *femAB* operon. In the presence of high IPTG concentrations ([IPTG] 500  $\mu$ M), growth was identical to the parental strain (MW2 parental). In the absence ([IPTG] 0  $\mu$ M) or with low concentrations of IPTG ([IPTG] 10  $\mu$ M), no cell growth was detected. (b), Muropeptide HPLC profiles of MW2-*iFemAB* induced with different levels of IPTG. Depletion of FemAB led to the accumulation of monomeric

pentapeptides substituted with one glycine (peak 4), in contrast to pentaglycine forms (peak 5) seen in fully induced ([IPTG] 500  $\mu$ M) or parental (MW2 parental) profiles. Loss of FemAB activity also impaired the formation of pentaglycine crosslinked forms such as di-, tri-, tetra- and pentamers (peaks 11, 15, 16 and 17, respectively) and higher order oligomers (black arrow). (c), Proposed structures of the peaks in PG muropeptide chromatographic analysis, according to de Jonge and Tomasz<sup>47</sup>. Muropeptides are numbered according to increasing retention times. G= N-acetylglucosamine; M = N-acetylmuramic acid.

### **Loss of FemAB activity leads to cellular lysis**

The morphology of cells depleted from FemAB was analysed by super resolution structured illumination microscopy (SIM). MW2-iFemAB was grown with or without IPTG (500  $\mu$ M). Immediately following growth arrest of the non-induced culture (Fig. 2a, black arrow), cells were stained with membrane dye FM 4-64, with peptidoglycan dye Van-FL (to show cell wall and septum positioning) and with DNA dye Hoechst 33342 (to give an indication of cell cycle phase). In the presence of IPTG, MW2-iFemAB cells divided normally with DNA segregation preceding the synthesis of a division septum at mid-cell (Fig. 2b, top panels), and cells containing multiple septa were not observed (Fig. 2c, left panel). In contrast, FemAB depleted cells often appeared as pseudomulticellular forms with two or more perpendicular septa, suggesting that the second round of division is starting before daughter cell separation is completed (Fig. 2c, right panel arrows). Furthermore, in FemAB depleted cells nucleoid morphology was altered, with cells containing



condensed DNA (Fig. 2b, bottom panels). Our results are in agreement with previous reports that suppressed *fem* mutants show irregular placement of cross walls and retarded cell separation<sup>21</sup>. This phenotype can be a consequence of either multiple septation or defective splitting.

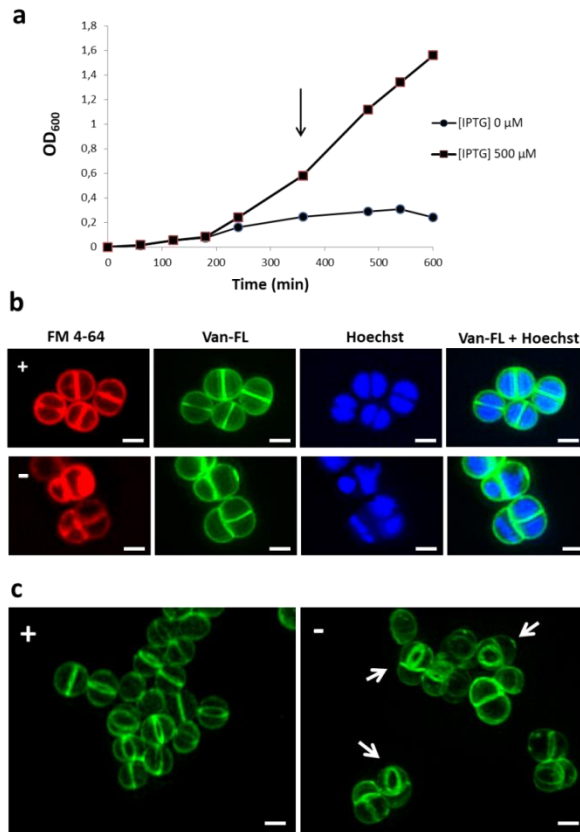


**Figure 2. Loss of FemAB activity inhibits daughter cell separation during division. (a),** Growth curves of MW2-iFemAB in the presence ([IPTG] 500 μM) or absence ([IPTG] 0 μM) of IPTG, to determine the timing of growth arrest in the non-induced condition (see Experimental Procedures). Cells were collected for SIM imaging at the indicated time point (black arrow). **(b),** SIM images of MW2-iFemAB cells growing in the presence (+) or absence (-) of IPTG and stained with membrane dye FM 4-64, peptidoglycan dye Van-

FL and DNA dye Hoechst 33342 (**c**), 3D-SIM images of MW2-iFemAB cells growing in the presence (+) or absence (-) of IPTG and stained with peptidoglycan dye Van-FL. IPTG-induced cells divide normally with DNA segregation preceding the synthesis of the division septum at mid-cell (Panel **b**, top row and Panel **c**, left column). In contrast, FemAB depleted cells often had condensed nucleoids (Panel **b**, bottom row) and appeared as pseudo multicellular forms with two perpendicular septa (Panel **c**, white arrows). Scale bars, 1  $\mu\text{m}$ .

When cells depleted of FemAB were incubated for longer periods, we noticed a decrease in culture density, suggesting cell lysis (Fig. 2a). We therefore imaged cells 2 hours after growth arrest and observed extensive membrane damage, characterized by holes, bulges and invaginations and the presence of anucleate cells (Fig. 3). These results suggest that the inability of *S. aureus* to survive with a shortened crossbridge structure, may be because the three-dimensional structure of a monoglycine crosslinked peptidoglycan does not confer sufficient robustness to bear the internal osmotic pressure, in the conditions tested, causing the cells to rupture. This is in agreement with data from Hübscher and colleagues<sup>25</sup>, which have shown by transcriptome analysis that *femAB* null mutant AS145 adapted to the *femAB* deficit by overhauling its metabolic pathways, probably to alleviate internal turgor<sup>25</sup>. It is also possible that monoglycine crossbridges are not suitable substrates for transpeptidation by *S. aureus* PBPs *in vivo* and thus crosslinking of glycan chains was stalled after FemAB depletion. This is in agreement with solid-state NMR data obtained by Kim et al.<sup>48</sup>, which indicates that monoglycyl crossbridges would be too short to connect the

glycan chains of the *S. aureus* PG, and that crosslinking with such a reduced bridge length would require a major rearrangement of the tertiary structure of PG<sup>48</sup>. In this way, the *femA* mutants generated in the past probably adapted to life with shortened crossbridges through changes in PG architecture. Accordingly, analysis of the average glycan chain length in *femAB* mutant AS145 revealed the presence of longer sugar chains when compared to parental strain BB903. *Cis*-complementation with a wild-type *femAB* copy did not restore normal glycan chain length in the *femAB* mutant, indicating that changes in PG structure was an adaptive response required for AS145 to survive with poorly crosslinked cell wall.

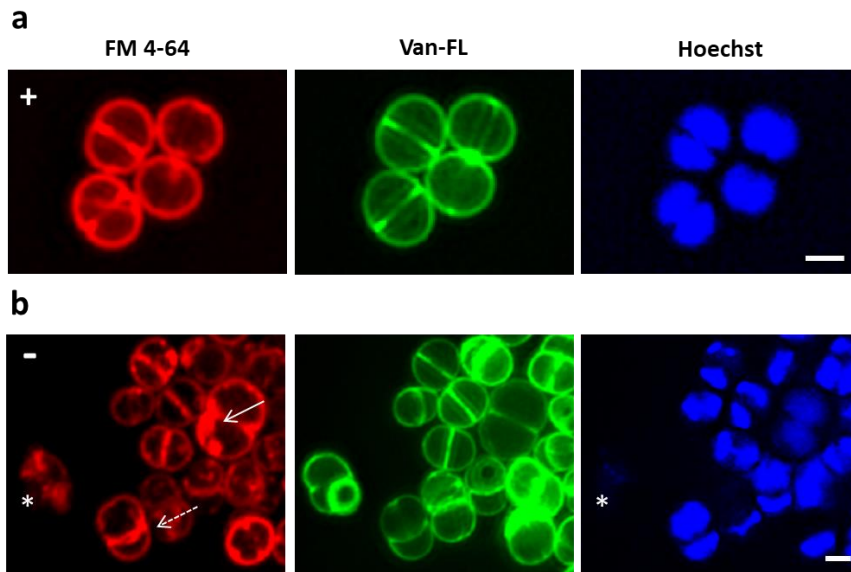


**Figure 3. FemAB depletion leads to cellular lysis.** MW2-iFemAB cells depleted of FemAB activity for a period of 2 hours following growth arrest were stained with membrane dye FM 4-64, peptidoglycan dye Van-FL and DNA dye Hoechst 33342 and imaged by SIM. FemAB depleted cells (b) show loss of membrane integrity characterized by holes (asterisk), bulges

(white arrow) and invaginations (dashed white arrow) as well as absence of DNA staining (asterisk), indicative of lysis, when compared to IPTG-induced cells (a). Scale bars, 1  $\mu\text{m}$ .

### Structure-based site directed mutagenesis of FemA

FemA is not only a good target for compounds that are synergistic with  $\beta$ -lactams<sup>49</sup> but also, as we show in this work, a lethal target by itself. As FemA is a protein unique to *S. aureus*, the development of anti-FemA compounds would be a potent tool for pathogen specific treatment strategies. To provide useful information for the studies of inhibitors of FemA, we identified putative key regions in the protein required for activity, based on the known crystal structure of FemA<sup>26</sup> and on homology to the FemX protein from *Weisella viridescens*<sup>28,50</sup>. We decided to focus on the putative transferase pocket (Fig. 4a – in blue) that contains Arg220, Phe224 (Fig. 4a – red circles) and Tyr327 (Fig.4a – orange circle), which are conserved across the Fem family. We also mined the sequence of FemA for regions which could bind DNA/RNA using DP-Bind<sup>41,42</sup>, in order to identify the putative tRNA-binding site. We found that the region with the highest probability corresponded to the  $\alpha$ 6 helix (aa 176-188) of FemA, rich in Lys/Arg residues with polar and charged sidechains exposed to the solvent<sup>26</sup>, which could stabilise the entering tRNA (Fig. 4a – in green). Specifically, amino acids Lys180 and Arg181 showed >96% probability of binding DNA/RNA in each of three individual prediction algorithms performed by DP-Bind (see

Experimental Procedures), and therefore we selected them for mutagenesis (Fig. 4b).

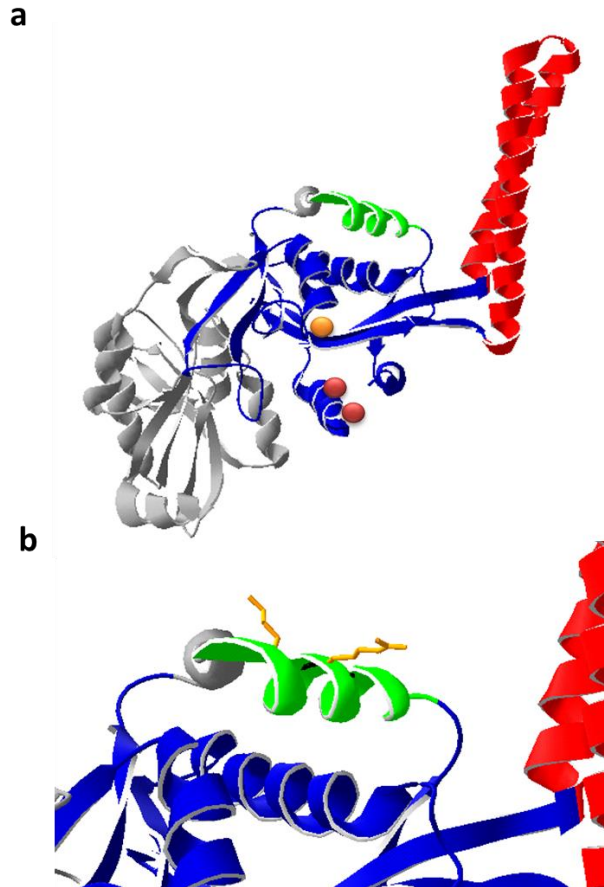


**Figure 4. Targeting FemA for site-directed mutagenesis.** (a), 3D representation of *S. aureus* FemA showing the globular subdomain 1B (in blue), proposed to fold into a channel suitable for binding of the dissacharide hexapeptide lipid substrate<sup>26</sup>. This channel contains amino acids Y327 (orange circle) and R220 and F224 (red circles), that were selected for mutagenesis. Binding of glycyl-charged tRNA is proposed to occur at the junction between the antiparallel coiled-coil arms (in red) and the globular domain (in blue)<sup>26</sup>. (b), Close-up view of the  $\alpha_6$  helix of FemA (in green), which is rich in polar and charged amino acids (Lys, Arg). Residues Lys180

and Arg181 (in yellow), containing positively charged side chains exposed to the solvent and predicted to bind DNA/RNA, were selected for mutagenesis.

To construct the FemA mutants we used the backbone of pFemAB<sup>wt</sup>, encoding *femAB*, and performed site-directed mutagenesis on selected residues of the *femA* gene and replaced them with alanines, thus generating pFemA<sup>RF220AA</sup>B and pFemA<sup>Y327A</sup>B, in order to target the transferase domain and pFemA<sup>KR180AA</sup>B to target the predicted tRNA binding helix. These expression plasmids were transformed into MW2-iFemAB, allowing us to deplete native *femAB* expression (in the absence of IPTG) and express mutant alleles (in the presence of cadmium).

We were able to complement the lack of *femAB* expression from the native locus by expressing *femAB* from pFemAB<sup>wt</sup> in the presence of cadmium (1  $\mu$ M), as assessed by growth rates, lysostaphin and oxacillin MICs, fluorescence microscopy and muropeptide profiles (Table 3). Expression of the catalytic site mutants FemA<sup>RF220AA</sup> and FemA<sup>Y327A</sup> caused a delay in entry into exponential phase (Fig. 5a) and a reduction of the pentaglycine substituted monomer content in peptidoglycan (Fig. 5b), although morphology was similar to wild-type and no significant differences in lysostaphin and oxacillin MICs were observed (Table 3). In contrast, the mutations in the  $\alpha$ 6 helix of FemA caused severe loss of FemA activity. The FemA<sup>KR180AA</sup> mutant showed a marked reduction in growth rate (Fig. 5a), increased lysostaphin and decreased oxacillin resistances and a pseudomulticellular morphology when observed by

microscopy (Table 3), similar to what was observed when depleting FemAB expression. Furthermore, analysis of the muuropeptide content in this mutant revealed a pronounced accumulation of monoglycyl substituted pentapeptides and concomitant reduction in pentaglycine crosslinked species (Fig. 5b and Table 3).

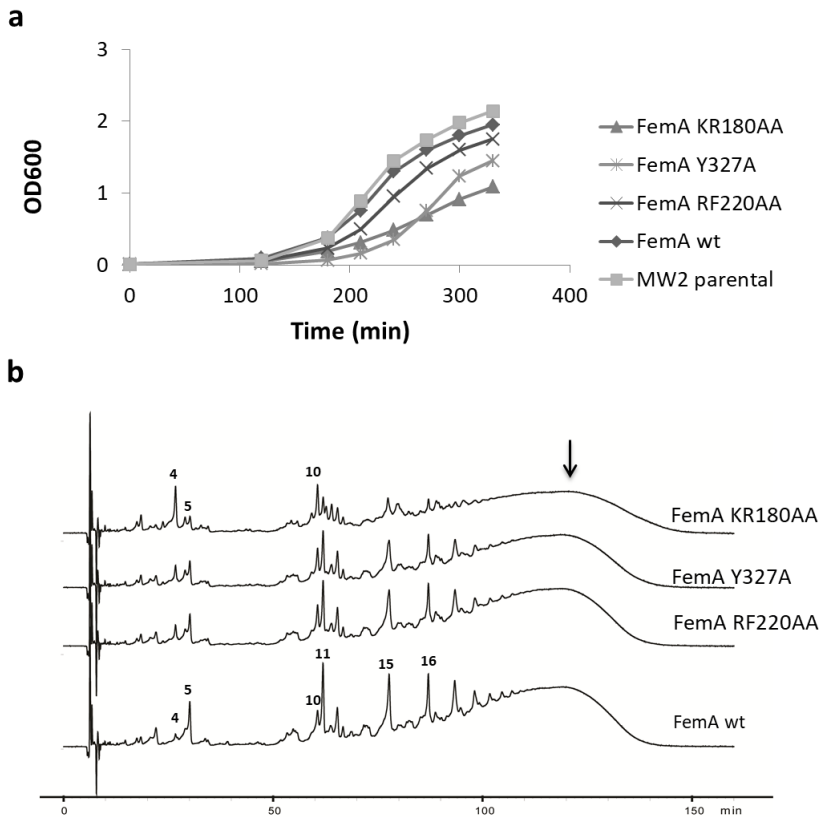


**Figure 5. Selected mutations decrease FemA activity *in vivo*.** MW2-iFemAB cells with ectopically expressed wild-type *femAB* (FemA wt) or *femAB* alleles with mutations in *femA* (encoding FemA KR180AA, FemA RF220AA and FemA Y327A) from a cadmium-inducible promoter *Pcad*. FemA activity was assessed by determining growth rates (a) and muuropeptide profiles (b). Expression of FemAB wt fully complemented the lack of native *femAB* activity, while expression of FemA<sup>KR180AA</sup> led to a pronounced growth defect

and accumulation of mono-glycine monomer species (peak 4) with concomitant reduction in higher-order pentaglycine crosslinked species (peaks 11, 15, 16 and arrow). We also observed the accumulation of peak 10 in this mutant, which could be a monoglycine substituted dimer. Expression of FemA<sup>Y327</sup> and FemA<sup>RF220</sup> mutants led to similar phenotypes, albeit to a lesser extent.

**Table 3. *In vivo* activity profiles of FemA mutants.**

	Doubling time (min)	MIC lysostaphin (µg/ml)	MIC oxacillin (µg/ml)	Morphology	Gly5/Gly1 monomer species fraction
MW2pFemA <sup>KR180AA</sup>	52	2,5	0,4	femA	1:3
MW2pFemA <sup>RF220AA</sup>	30	0,15	1,6	wt	2:1
MW2pFemA <sup>Y327A</sup>	27	0,08	0,8	wt	2:1
MW2pFemA <sup>wt</sup>	27	0,08	3,2	wt	6:1
Parental MW2	25	0,08	1,5	wt	6:1

Next we tested the activity of FemA mutants *in vitro*. For this purpose, we purified recombinant FemA<sup>wt</sup>, FemA<sup>KR180AA</sup>, FemA<sup>RF220AA</sup> and FemA<sup>Y327A</sup> with C-terminal histidine tags and synthesised the FemA substrate lipid II-Gly<sub>1</sub> *in vitro* (see Experimental Procedures). As recombinant FemA<sup>RF220AA</sup> was very unstable and readily precipitated, we could not use it for further assays. LipidII-Gly<sub>1</sub> was trapped in Triton X-100 micelles and incubated with either FemA<sup>wt</sup>, FemA<sup>KR180AA</sup> or FemA<sup>Y327A</sup> in the presence of [U-<sup>14</sup>C]-glycine charged tRNA. After 30, 60 or 90 minutes the lipid fraction was extracted and separated by thin layer chromatography and radioactive glycine transfer to lipid II-Gly<sub>1</sub> was measured. Both mutant forms FemA<sup>KR180AA</sup> and FemA<sup>Y327A</sup> transferred less [U-<sup>14</sup>C]-glycine to their substrate when compared to FemA<sup>wt</sup>, consistent with a reduction in



protein activity (Fig. 6). Taken together, *in vivo* and *in vitro* data show that the KR180AA and Y327A mutations caused a decrease in FemA transferase activity but did not impair the viability of *S. aureus*. This is in agreement with studies by Koyama and colleagues on the effects of cyclabdan, a molecule which partially inhibits FemA and does not impair growth <sup>49</sup>.

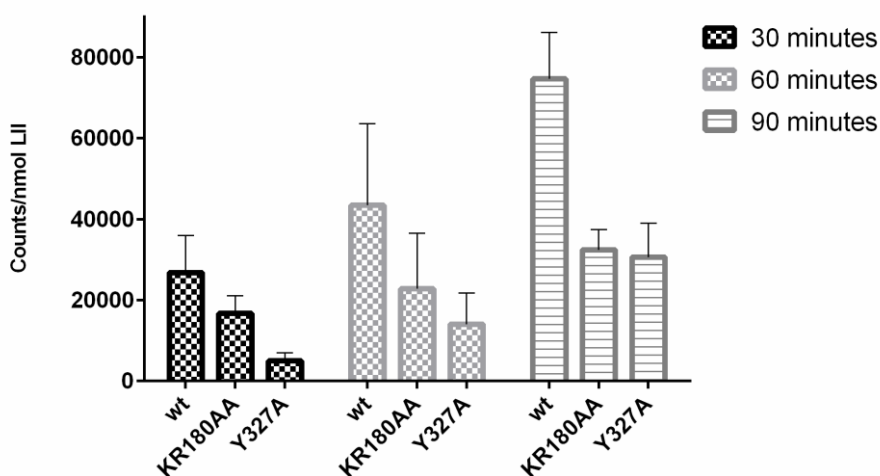


**Figure 6. FemA mutants show reduced activity *in vitro*.** Recombinant FemA<sup>wt</sup>, FemA<sup>KR180AA</sup> and FemA<sup>Y327A</sup> were incubated with lipid II-Gly<sub>1</sub> in the presence of [U-<sup>14</sup>C]-glycine charged tRNA, for either 30, 60 or 90 minutes. Both FemA<sup>KR180AA</sup> and FemA<sup>Y327A</sup> showed decreased [U-<sup>14</sup>C]-glycine transfer to lipid II-Gly<sub>1</sub> when compared to FemA<sup>wt</sup>. Columns denote mean values and error bars represent standard deviation from 3 independent measurements.

## Concluding remarks

The structural features of the staphylococcal peptidoglycan seem remarkably unique in nature, as pentaglycine crosslinks have not been observed outside of the genus. These long bridges likely confer high flexibility to *S. aureus* peptidoglycan which allows the cell to withstand intense internal turgor, as *femAB* mutants isolated in the past adapted to life with shortened crossbridges by drastically reducing metabolic activity<sup>25</sup>. Moreover, the nature and length of PG branching has been implicated in playing a role in resistance to  $\beta$ -lactams, not only in *S. aureus* but other bacteria<sup>23,44,51,52</sup>. It has been proposed that besides adaptation of metabolic pathways, previously isolated *femAB* mutants also contain compensatory or suppressor mutations that allow for survival with reduced cross bridges, however these remain uncharacterised<sup>25,45,53</sup>.

We have shown that at least in CA-MRSA strain MW2, depletion of the *femAB* operon is lethal, leading to the disruption of the cell envelope, causing cells to lyse. This suggests that monoglycyl-substituted mucopeptides are not valid substrates for transpeptidation *in vivo*, either because TPases fail to recognise them or because different *S. aureus* glycan strands are too far apart to be crosslinked via crossbridges with only one glycine. Nevertheless, these data indicate that inhibitors of FemA activity would be effective to treat MRSA infections, either acting on their own or in combination therapy with  $\beta$ -lactams that are already in use. Towards this

*Building Bridges: the pentaglycine crosslinks in S. aureus peptidoglycan are required for cell integrity*

possibility, we have identified specific residues present in the putative transferase and tRNA-binding domains of FemA which are important for protein activity and thus good candidate targets for future drug design.

## References

- 1 Chambers, H. F. & DeLeo, F. R. Waves of resistance: *Staphylococcus aureus* in the antibiotic era. *Nat Rev Micro* **7**, 629-641, doi:[http://www.nature.com/nrmicro/journal/v7/n9/supinfo/nrmicro2200\\_S1.html](http://www.nature.com/nrmicro/journal/v7/n9/supinfo/nrmicro2200_S1.html) (2009).
- 2 Grundmann, H., Aires-De-Sousa, M., Boyce, J. & Tiemersma, E. Emergence and resurgence of methicillin-resistant *Staphylococcus aureus* as a public-health threat. *LANCET* **368**, 874-885 (2006).
- 3 Wenzel, R. & Perl, T. The significance of nasal carriage of *Staphylococcus aureus* and the incidence of postoperative wound infection. *J Hosp Infect* **31**, 13-24 (1995).
- 4 Lowy, F. *Staphylococcus aureus* infections. *N Engl J Med* **339**, 520-532 (1998).
- 5 Miller, L. & Diep, B. Clinical practice: colonization, fomites, and virulence: rethinking the pathogenesis of community-associated methicillin-resistant *Staphylococcus aureus* infection. *Clin Infect Dis* **46**, 752-760 (2008).
- 6 Schleifer, K. & Kandler, O. Peptidoglycan types of bacterial cell walls and their taxonomic implications. *Bacteriol Rev* **36**, 407-477 (1972).
- 7 Swenson, J. & Neuhaus, F. Biosynthesis of peptidoglycan in *Staphylococcus aureus*: incorporation of the Nepsilon-Ala-Lys moiety into the peptide subunit of nascent peptidoglycan. *J Bacteriol* **125**, 626-634 (1976).
- 8 Vollmer, W., Blanot, D. & de Pedro, M. Peptidoglycan structure and architecture. *FEMS Microbiol Rev* **32**, 149-167 (2008).
- 9 Massova, I. & Mobashery, S. Kinship and diversification of bacterial penicillin-binding proteins and beta-lactamases. *Antimicrob Agents Chemother* **42**, 1-17 (1998).
- 10 Goffin, C. & Ghuysen, J. M. Multimodular penicillin-binding proteins: an enigmatic family of orthologs and paralogs. *Microbiol Mol Biol Rev* **62**, 1079-1093 (1998).
- 11 Ubukata, K., Nonoguchi, R., Matsuhashi, M. & Konno, M. Expression and inducibility in *Staphylococcus aureus* of the *mecA* gene, which encodes a methicillin-resistant *S. aureus*-specific penicillin-binding protein. *J Bacteriol* **171**, 2882-2885 (1989).
- 12 Berger-Bächi, B. Insertional inactivation of staphylococcal methicillin resistance by *Tn551*. *J Bacteriol* **154**, 479-487 (1983).
- 13 de Lencastre, H. & Tomasz, A. Reassessment of the number of auxiliary genes essential for expression of high-level methicillin resistance in *Staphylococcus aureus*. *Antimicrob Agents Chemother* **38**, 2590-2598 (1994).
- 14 De Lencastre, H. *et al.* Antibiotic resistance as a stress response: complete sequencing of a large number of chromosomal loci in *Staphylococcus aureus* strain COL that impact on the expression of resistance to methicillin. *Microb Drug Resist* **5**, 163-175 (1999).
- 15 Berger-Bächi, B., Barberis-Maino, L., Strässle, A. & Kayser, F. FemA, a host-mediated factor essential for methicillin resistance in *Staphylococcus aureus*: molecular cloning and characterization. *Mol Gen Genet* **219**, 263-269 (1989).

*Building Bridges: the pentaglycine crosslinks in S. aureus peptidoglycan are required for cell integrity*

- 16 Rohrer, S., Ehlert, K., Tschierske, M., Labischinski, H. & Berger-Bächi, B. The essential *Staphylococcus aureus* gene *fmhB* is involved in the first step of peptidoglycan pentaglycine interpeptide formation. *Proc Natl Acad Sci U S A* **96**, 9351-9356 (1999).
- 17 Matsuhashi, Y., Sawa, T., Takeuchi, T., Umezawa, H. & Nagatsu, I. Localisation of aminoglycoside 3'-phosphotransferase II on a cellular surface of R factor resistant *Escherichia coli*. *J Antibiot (Tokyo)* **29**, 1129-1130 (1976).
- 18 Ehlert, K., Schröder, W. & Labischinski, H. Specificities of FemA and FemB for different glycine residues: FemB cannot substitute for FemA in staphylococcal peptidoglycan pentaglycine side chain formation. *J Bacteriol* **179**, 7573-7576 (1997).
- 19 Schneider, T. *et al.* In vitro assembly of a complete, pentaglycine interpeptide bridge containing cell wall precursor (lipid II-Gly5) of *Staphylococcus aureus*. *Mol Microbiol* **53**, 675-685 (2004).
- 20 Tschierske, M. *et al.* Identification of three additional *femAB*-like open reading frames in *Staphylococcus aureus*. *FEMS Microbiol Lett* **171**, 97-102 (1999).
- 21 Henze, U., Sidow, T., Wecke, J., Labischinski, H. & Berger-Bächi, B. Influence of *femB* on methicillin resistance and peptidoglycan metabolism in *Staphylococcus aureus*. *J Bacteriol* **175**, 1612-1620 (1993).
- 22 de Jonge, B. *et al.* Altered muropeptide composition in *Staphylococcus aureus* strains with an inactivated *femA* locus. *J Bacteriol* **175**, 2779-2782 (1993).
- 23 Strandén, A., Ehlert, K., Labischinski, H. & Berger-Bächi, B. Cell wall monoglycine crossbridges and methicillin hypersusceptibility in a *femAB* null mutant of methicillin-resistant *Staphylococcus aureus*. *J Bacteriol* **179**, 9-16 (1997).
- 24 Schneewind, O., Fowler, A. & Faull, K. Structure of the cell wall anchor of surface proteins in *Staphylococcus aureus*. *Science* **268**, 103-106 (1995).
- 25 Hübscher, J. *et al.* Living with an imperfect cell wall: compensation of *femAB* inactivation in *Staphylococcus aureus*. *BMC Genomics* **8**, 307, doi:10.1186/1471-2164-8-307 (2007).
- 26 Benson, T. *et al.* X-ray crystal structure of *Staphylococcus aureus* FemA. *Structure* **10**, 1107-1115 (2002).
- 27 Dutnall, R., Tafrov, S., Sternglanz, R. & Ramakrishnan, V. Structure of the yeast histone acetyltransferase Hat1: insights into substrate specificity and implications for the Gcn5-related N-acetyltransferase superfamily. *Cold Spring Harb Symp Quant Biol* **63**, 501-507 (1998).
- 28 Maillard, A. *et al.* Structure-based site-directed mutagenesis of the UDP-MurNAc-pentapeptide-binding cavity of the FemX alanyl transferase from *Weissella viridescens*. *J Bacteriol* **187**, 3833-3838 (2005).
- 29 Monk, I. R., Shah, I. M., Xu, M., Tan, M. W. & Foster, T. J. Transforming the untransformable: application of direct transformation to manipulate genetically *Staphylococcus aureus* and *Staphylococcus epidermidis*. *MBio* **3**, doi:10.1128/mBio.00277-11 (2012).
- 30 Nair, D. *et al.* Whole-genome sequencing of *Staphylococcus aureus* strain RN4220, a key laboratory strain used in virulence research, identifies

- mutations that affect not only virulence factors but also the fitness of the strain. *J Bacteriol* **193**, 2332-2335, doi:10.1128/JB.00027-11 (2011).
- 31 Baba, T. *et al.* Genome and virulence determinants of high virulence community-acquired MRSA. *Lancet* **359**, 1819-1827 (2002).
- 32 Vagner, V., Dervyn, E. & Ehrlich, S. D. A vector for systematic gene inactivation in *Bacillus subtilis*. *Microbiology* **144**, 3097-3104 (1998).
- 33 Pinho, M. G., Filipe, S. R., de Lencastre, H. & Tomasz, A. Complementation of the essential peptidoglycan transpeptidase function of penicillin-binding protein 2 (PBP2) by the drug resistance protein PBP2A in *Staphylococcus aureus*. *J Bacteriol* **183**, 6525-6531, doi:10.1128/JB.183.22.6525-6531.2001 (2001).
- 34 Monteiro, J. M. *et al.* Cell shape dynamics during the staphylococcal cell cycle. *Nat Commun* **6**, 8055, doi:10.1038/ncomms9055 (2015).
- 35 Monteiro, J. M. *et al.* Peptidoglycan synthesis drives an FtsZ-treadmilling-independent step of cytokinesis. *Nature*, doi:10.1038/nature25506 (2018).
- 36 Filipe, S. R., Tomasz, A. & Ligoxygakis, P. Requirements of peptidoglycan structure that allow detection by the Drosophila Toll pathway. *EMBO Rep* **6**, 327-333, doi:10.1038/sj.embor.7400371 (2005).
- 37 Rohrer, S. & Berger-Bächi, B. Application of a bacterial two-hybrid system for the analysis of protein-protein interactions between FemABX family proteins. *Microbiology* **149**, 2733-2738 (2003).
- 38 Breukink, E. *et al.* Lipid II is an intrinsic component of the pore induced by nisin in bacterial membranes. *J Biol Chem* **278**, 19898-19903, doi:10.1074/jbc.M301463200 (2003).
- 39 Rick, P. D. *et al.* Characterization of the lipid-carrier involved in the synthesis of enterobacterial common antigen (ECA) and identification of a novel phosphoglyceride in a mutant of *Salmonella typhimurium* defective in ECA synthesis. *Glycobiology* **8**, 557-567 (1998).
- 40 Rouser, G., Fkeischer, S. & Yamamoto, A. Two dimensional thin layer chromatographic separation of polar lipids and determination of phospholipids by phosphorus analysis of spots. *Lipids* **5**, 494-496 (1970).
- 41 Hwang, S., Gou, Z. & Kuznetsov, I. B. DP-Bind: a web server for sequence-based prediction of DNA-binding residues in DNA-binding proteins. *Bioinformatics* **23**, 634-636, doi:10.1093/bioinformatics/btl672 (2007).
- 42 Kuznetsov, I. B., Gou, Z., Li, R. & Hwang, S. Using evolutionary and structural information to predict DNA-binding sites on DNA-binding proteins. *Proteins* **64**, 19-27, doi:10.1002/prot.20977 (2006).
- 43 Guex, N. & Peitsch, M. C. SWISS-MODEL and the Swiss-PdbViewer: an environment for comparative protein modeling. *Electrophoresis* **18**, 2714-2723, doi:10.1002/elps.1150181505 (1997).
- 44 Berger-Bächi, B., Strässle, A., Gustafson, J. & Kayser, F. Mapping and characterization of multiple chromosomal factors involved in methicillin resistance in *Staphylococcus aureus*. *Antimicrob Agents Chemother* **36**, 1367-1373 (1992).
- 45 Berger-Bächi, B. & Tschierske, M. Role of fem factors in methicillin resistance. *Drug Resist Updat* **1**, 325-335 (1998).

*Building Bridges: the pentaglycine crosslinks in S. aureus peptidoglycan are required for cell integrity*

- 46 Yansura, D. G. & Henner, D. J. Use of the *Escherichia coli* lac repressor and operator to control gene expression in *Bacillus subtilis*. *Proc Natl Acad Sci U S A* **81**, 439-443 (1984).
- 47 de Jonge, B. L., Chang, Y. S., Gage, D. & Tomasz, A. Peptidoglycan composition of a highly methicillin-resistant *Staphylococcus aureus* strain. The role of penicillin binding protein 2A. *J Biol Chem* **267**, 11248-11254 (1992).
- 48 Kim, S. J., Chang, J. & Singh, M. Peptidoglycan architecture of Gram-positive bacteria by solid-state NMR. *Biochim Biophys Acta* **1848**, 350-362, doi:10.1016/j.bbamem.2014.05.031 (2015).
- 49 Koyama, N. *et al.* The nonantibiotic small molecule cyslabdan enhances the potency of  $\beta$ -lactams against MRSA by inhibiting pentaglycine interpeptide bridge synthesis. *PLoS One* **7**, e48981, doi:10.1371/journal.pone.0048981 (2012).
- 50 Biarrotte-Sorin, S. *et al.* Crystal structures of *Weissella viridescens* FemX and its complex with UDP-MurNAc-pentapeptide: insights into FemABX family substrates recognition. *Structure* **12**, 257-267 (2004).
- 51 Filipe, S. & Tomasz, A. Inhibition of the expression of penicillin resistance in *Streptococcus pneumoniae* by inactivation of cell wall muropeptide branching genes. *Proc Natl Acad Sci U S A* **97**, 4891-4896 (2000).
- 52 Fiser, A., Filipe, S. & Tomasz, A. Cell wall branches, penicillin resistance and the secrets of the MurM protein. *Trends Microbiol* **11**, 547-553 (2003).
- 53 Ling, B. & Berger-Bächi, B. Increased overall antibiotic susceptibility in *Staphylococcus aureus* femAB null mutants. *Antimicrob Agents Chemother* **42**, 936-938 (1998).





# Chapter V

---

Characterising the mode of action of  
novel small molecules effective against  
MRSA

### Author contributions

J. M. Monteiro performed all fluorescence microscopy experiments and constructed the COLpPVra strain. The remaining experiments were done by members of the A. Cheung laboratory (Geisel School of Medicine at Dartmouth, Hanover, New Hampshire, USA) and Achillion Pharmaceuticals, (New Haven, Connecticut, USA).

### Acknowledgments

We thank T. Roemer and A. Cheung for facilitating the PC190723 and the DNAC-1 research, respectively. We thank A. Jorge for the BCBAJ020 strain and also thank Matthew P. DeLisa (Cornell University) for plasmid pTRC99a-P7.

This chapter contains data published in:

Tan CM\*, Therien AG\*, Lu J, Lee SH, Caron A, Gill CJ, Lebeau-Jacob C, Benton-Perdomo L, **Monteiro JM**, Pereira PM, Elsen NL, Wu J, Deschamps K, Petcu M, Wong S, Daigneault E, Kramer S, Liang L, Maxwell E, Claveau D, Vaillancourt J, Skorey K, Tam J, Wang H, Meredith TC, Sillaots S, Wang-Jarantow L, Ramtohum Y, Langlois E, Landry F, Reid JC, Parthasarathy G, Sharma S, Baryshnikova A, Lumb KJ, Pinho MG, Soisson SM and Roemer T. Restoring Methicillin-Resistant *Staphylococcus aureus* Susceptibility to  $\beta$ -Lactam Antibiotics. *Science Translational Medicine* **4**. 126ra35 (2012); doi: 10.1126/scitranslmed.3003592.

\* Contributed equally to this work.

and

Nair DR, **Monteiro JM**, Memmi G, Thanassi J, Pucci M, Scharzman J, Pinho MG and Cheung A. Characterization of a novel small molecule that potentiates  $\beta$ -lactam activity against Gram-positive and Gram-negative pathogens. *Antimicrobial Agents and Chemotherapy* **59**:1876–1885 (2015); doi:10.1128/AAC.04164-14.

## Abstract

The increasing prevalence of life-threatening infections caused by emerging drug-resistant bacteria constitutes a significant burden on global public health. There is a clear need for the development and characterisation of new antibiotics which can be effective alone or in combination with existing drugs on the market. Recent guidelines for antibacterial drug development from the Food and Drug Administration (FDA) clearly states that the mechanism of action of investigational drugs should be evaluated. Towards this end, cell biology tools provide a new way of studying the effects of antibiotics on bacterial cells. Here we describe the study of the mode of action of two novel molecules that are effective against methicillin-resistant *Staphylococcus aureus* (MRSA) – PC190723 and DNAC-1. The FtsZ-specific inhibitor PC190723 was shown to act synergistically with  $\beta$ -lactam antibiotics *in vitro* and *in vivo*. Using fluorescence microscopy we show that synergy between these agents is likely to be elicited by the concomitant delocalisation of their cognate drug targets (FtsZ and PBP2) in MRSA. DNAC-1 was identified in a loss-of-viability screen, using small molecules against MRSA. Treatment with DNAC-1 caused the disruption of cellular membrane structures and the appearance of mesosome-like projections into the cytosol, as assessed by fluorescence and transmission electron microscopy. Membrane permeation was accompanied by a rapid loss of membrane potential, as monitored by the use of the DiOC<sub>2</sub> (3,3'-diethyloxacarbocyanine iodide) dye. Furthermore, DNAC-1 inhibits staphylococcal cell wall

synthesis by preventing the polymerization of FtsZ at mid-cell and subsequent mislocalisation of peptidoglycan synthases PBP2 and PBP4.

## Introduction

After the discovery of penicillin,  $\beta$ -lactam antibiotics (and the broad-spectrum derivatives cephalosporins and carbapenems) significantly improved public health during the 20<sup>th</sup> century, and still constitute the most heavily used class of antibiotics<sup>1</sup>.  $\beta$ -lactam antibiotics target penicillin-binding proteins (PBPS), enzymes involved in peptidoglycan synthesis in bacteria, and have been the drugs of choice against bacterial infections for many decades due to low toxicity and relatively low dosage requirements for treatment, when compared to other classes<sup>1</sup>. Worryingly, drug resistance to  $\beta$ -lactams has consistently emerged in bacteria, appearing as early as one year following the introduction of a new antibiotic into the clinic<sup>2</sup>. Drug resistance has also emerged against other classes of antibiotics which are currently used, including drugs that target cell wall synthesis<sup>3</sup> (such as glycopeptides), DNA/RNA synthesis<sup>4</sup> (quinolones), protein synthesis<sup>5</sup> (macrolides) or that target the bacterial membrane<sup>6</sup> (daptomycin, nisin).

Infections caused by drug resistant bacteria are a major challenge to contemporary public health and, despite efforts to contain them, are predicted to escalate in the future<sup>2</sup>. Of significant note are infections caused by methicillin resistant *Staphylococcus aureus* (MRSA) strains, which are resistant to all classes of  $\beta$ -lactams<sup>3,7</sup>. Recently emerging MRSA isolates have also become resistant to last resort antibiotics, such as vancomycin and linezolid<sup>3</sup>.

*S. aureus* is a Gram positive bacterial human pathogen that can cause serious infections, including pneumonia, sepsis, osteomyelitis and endocarditis. Traditionally, MRSA infections were confined to hospitals and long-term care facilities (hospital-acquired MRSA [HA-MRSA] strains), where they affect debilitated patients. However, highly virulent and epidemiologically distinct MRSA strains that affect individuals without predisposing risk factors have appeared outside of the hospital, the so-called community-associated MRSA (CA-MRSA). Compounding this issue is a severe lack of new drugs introduced to the market, as large pharmaceutical companies have progressively abandoned the fields of antibiotic research and development for more profitable ventures, such as chemotherapy against cancer and chronic diseases<sup>8</sup>. A viable approach to circumvent bacterial resistance is towards the development of synergistic therapies, for example using a combination of an existing  $\beta$ -lactam with a second, novel, agent that potentiates its effect<sup>9</sup>. Synergistic therapy also has the benefit of allowing a lower dosage of the primary antibiotic, since its effect is augmented by the adjuvant<sup>10</sup>.

Since the development of new drugs is dwindling, it is imperative that a concerted effort is made towards better understanding the existing ones, as well as selectively searching for new efficient drugs that can either act alone or in combination with existing antibiotics. A vital part in the discovery and development of antibacterial drugs is the evaluation of the mechanism of action (MOA) of any given drug. In general terms, our knowledge of how

antibiotics induce bacterial cell death is focussed on identifying the essential cellular function that is disrupted by the primary target of a drug<sup>10</sup>. However, antibiotic mediated cell death is a multi-layered process, where the molecular interaction between drug and target is often merely the beginning. What follows is a cascade of alterations to the bacterial cell, which can include perturbations of biochemical pathways, disruption of cellular structures and the generation of toxic molecules<sup>10</sup>. For example, it has been shown that  $\beta$ -lactam induced cell lysis in *Streptococcus pneumoniae*<sup>11</sup> and *Escherichia coli*<sup>12</sup> is mediated by autolysins, hydrolases that cleave chemical bonds in peptidoglycan. As PG synthesis and degradation are concurrent processes during the bacterial cell cycle, inhibiting PG synthesis with a  $\beta$ -lactam creates an imbalance which leads to autolysin-driven degradation of the whole PG layer and subsequent lysis<sup>11</sup>.

This chapter contains data pertaining to the characterisation of the mode of action of two molecules that are potential candidates effective against MRSA, either alone or in combination with  $\beta$ -lactams – PC190723 and DNAC-1. We found that although these molecules have distinct chemical structures and different molecular targets in the *S. aureus* cell, both impair the proper assembly of the division machinery, which in turn prevents peptidoglycan synthesis at the septum.



## Experimental Procedures

### Bacterial growth conditions

Unless stated otherwise, *S. aureus* strains were grown in tryptic soy broth (TSB, Difco) at 200 r.p.m with aeration at 37 °C or 30 °C or on tryptic soy agar (TSA, Difco) at 30 or 37°C. *E. coli* strains were grown in Luria–Bertani broth (Difco) with aeration, or Luria–Bertani agar (Difco) at 37 or 30°C. When necessary, antibiotics ampicillin (100 µg/ml), erythromycin (10 µg/ml), kanamycin (50 µg/ml), neomycin (50 µg/ml) were added to the media. 5-bromo-4-chloro-3-indolyl β-D-galactopyranoside (X-gal, Apollo Scientific) was used at 100 µg/ml. Unless stated otherwise, isopropyl β-D-1-thiogalactopyranoside (IPTG, Apollo Scientific) was used at 0.1 mM to induce expression of constructs under the control of the *Pspac* promoter.

### Construction of *S. aureus* fluorescent strains

The primer sequences used to construct strains are described in Table 1. To construct an *S. aureus* COL strain where the native *pbpB* gene, encoding PBP2, was replaced by a *sfgfp-pbpB* fusion, we constructed a plasmid where we introduced the *sfgfp* gene, encoding the P5 superfolder GFP variant<sup>13</sup>, between the *recU* and the *pbpB* genes. For that purpose, we first amplified the upstream region of *pbpB* (primers BCBP5 and BCBP6) and the 5' region of the *pbpB* gene (primers BCBP7 and BCBP8). The *sfgfp* gene was amplified from

plasmid pTRC99a-P5<sup>13</sup> (primers BCBP9 and BCBP10). A sequence encoding a 12-amino acid linker was introduced between the *sfgfp* and the *pbpB* genes. The three fragments were joined by overlap polymerase chain reaction (PCR) in two steps and cloned into pBCBPM016, resulting in plasmid pBCBPM061. The pBCBPM016 plasmid is a derivative of the pMAD vector<sup>14</sup>, in which the erythromycin resistance cassette was replaced by a kanamycin resistance cassette obtained from the pDG792 plasmid<sup>15</sup>. Plasmid pBCBPM061 was sequenced, electroporated into *S. aureus* RN4220 strain and transduced into *S. aureus* COL strain with phage 80 $\alpha$ <sup>16</sup>. Insertion and excision of pBCBPM061 into the chromosome of COL were performed as previously described<sup>14</sup>. The replacement of the native *pbpB* gene by the *sfgfp-pbpB* gene fusion was confirmed by PCR (with primers BCBP11 and BCBP12). The resulting strain, named BCBPM073, expresses an sGFP fusion to PBP2, from its native chromosomal locus, under the control of its native promoter. To construct an *S. aureus* COL strain ectopically expressing an FtsZ-CFP fusion from the *spa* locus of the *S. aureus* chromosome, under the control of the *Pspac* promoter, we transduced the pBCBHV003 plasmid<sup>17</sup> into strain COL. Insertion and excision of pBCBHV003 into the chromosome of COL allowed the replacement of the *spa* gene by the *ftsZ-cfp* fusion, generating strain BCBAJ020.

In order to detect cell wall active compounds, we constructed a strain expressing a *vraSR* promoter fusion to *sfgfp*. Briefly, a 779-bp fragment encompassing the coding region of *sgfp-p7* was amplified

from pTRC99a-P7<sup>13</sup> using the primers sgfp P3 EcoRV and sgfp P2 NotI, digested with EcoRV and NotI, and used to replace the *gfpmutP2* gene in pSG5082<sup>18</sup>, giving pFAST3. An 844-bp fragment containing the *vraSR* promoter region was amplified from COL using the primers PvraSRP1KpnI and PvraSRP2XhoI, digested with KpnI and XhoI, and cloned into the KpnI/XhoI restriction sites of pFAST3, upstream of *sfgrp-p7*, resulting in pPvraS, as confirmed by DNA sequencing. pPvraSR was electroporated into the *S. aureus* RN4220 strain to enable chromosomal integration at the *vraSR* promoter by homologous recombination, as confirmed by PCR and sequencing; the resulting strain was named RNpPVra. Strain COLpPVra was obtained by transducing the integrated plasmid pPvraSR from RNpPVra to COL using phage 80 $\alpha$ , as previously described<sup>16</sup>.

**Table 1. Primer sequences used in this work**

Primer Name	Sequence (5'-3')
BCBP5	cgcg <del>gatccc</del> gtgtatgtttatcacgatgaaaa
BCBP6	tcatacgcggtcctcactttcatctaataatcaacttatcaac
BCBP7	cgcg <del>gatccc</del> ttgttagagctaccattatcaaca
BCBP8	actagtgggtggaggagggttctgggtggaggaggttctatgacggaaaacaaaggatcttctagcc
BCBP9	aaagtgaggaccgcgatgactagtagtaaaggagaagaac
BCBP10	agaacctctccaccagaacctcctcaccactagtgctgactttgtatagttcatccatgccatg
BCBP11	ggtggacgtggtatgtcac
BCBP12	tgaataatcatgaagcc
sgfp P3 EcoRV	gcg <del>cgatc</del> ataaggaggattcgtatgagtaaaggagaagaacttttc
sgfp P2 NotI	gcttag <del>cggccg</del> cttaatggtgatgatggtgatggtcactttgtatag
PvraSRP1KpnI	gctg <del>cgg</del> taccgggtctatttctgcgcc
PvraSRP2XhoI	gctg <del>cctcg</del> agacgttcaacatagttcataac

Underlined sequences correspond to restriction sites

### **Minimum inhibitory concentration (MIC) assays**

MICs of relevant antimicrobial compounds were determined by broth microdilution in sterile 96-well plates. The medium used was TSB, containing a series of two-fold dilutions of each compound. Cultures of *S. aureus* strains were added at a final density of  $5 \times 10^5$  CFU/ml to each well. Wells were reserved in each plate for sterility control (no cells added) and cell viability (no compound added). Plates were aerobically incubated at 37°C. Endpoints were assessed visually after 24 and 48 h. All assays were done in triplicate.

### **Fluorescence microscopy experiments with PC190723**

To analyse the mode of action of PC190723 by fluorescence microscopy, *S. aureus* strains BCBPM073 (expressing sGFP-PBP2) and BCBAJ020 (expressing FtsZ-CFP) were inoculated in TSB at 37°C for 18 hours. The cultures were then diluted 1:200 into fresh TSB supplemented with 0.1 mM IPTG when required and further incubated in the same conditions. At mid-exponential phase ( $OD_{600}$  0.6 to 0.8 nm), cultures were divided into pre-warmed flasks and either PC190723 or nalidixic acid (Sigma-Aldrich) were added at 1× or 10× the corresponding MIC values. Flasks to which no antibiotic was added were used as controls for the experiment. Bacterial cultures were then incubated for 30 min, after which aliquots were collected, pelleted, and washed with phosphate-buffered saline (PBS). Cells were mounted on a microscope slide covered with a thin film of 1% agarose in PBS and observed by fluorescence microscopy with a Zeiss

Axio observer Z1 microscope. Image acquisition was performed with a Photometrics CoolSNAP HQ2 camera (Roper Scientific) and MetaMorph 7.5 software (Molecular Devices).

### **Fluorescence microscopy experiments with DNAC-1**

To analyse the mode of action of DNAC-1 by fluorescence microscopy, we used strains expressing fluorescent fusions in the background of MRSA COL. BCBPM073 (expressing sGFP-PBP2), BCBPM162<sup>19</sup> (expressing PBP4-YFP), BCBAJ020 (expressing IPTG-inducible FtsZ-CFP from the *spa* locus) and COLpPVra (expressing a sGFP fusion to *PvraSR*) were incubated overnight in TSB supplemented with either erythromycin (10 µg/ml) or kanamycin (200 µg/ml), when required, at 37°C, back-diluted to fresh TSB and allowed to grow until mid-exponential phase (OD<sub>600</sub> ~0.6). In each case, the cultures were divided among five flasks, and DNAC-1 (in DMSO) was added at either 0.5× (2 µg/ml), 2× (8 µg/ml), or 10× MIC (40 µg/ml); the two remaining flasks were kept as controls with DMSO (0.2%) or TSB alone. The cultures were incubated for 15 min or 1 hour, after which the cells were pelleted, washed in PBS buffer, and mounted on microscope slides with pads of 1% agarose in PBS. To analyse the activation of the cell wall stress stimulon, a control with vancomycin at 2× MIC (6 µg/ml) was used. The displayed values were adjusted for each image for visualization purposes.

To assess morphology, COL cells were incubated with 2 µg/ml FM 4-64 [N-(3-triethylammoniumpropyl)-4-(p-

diethylaminophenyl-hexatrienyl) pyridinium dibromide], Bodipy FL-vancomycin (2  $\mu\text{g/ml}$ ), and Hoechst 33342 (4  $\mu\text{g/ml}$ ) (all from Molecular Probes) for 5 min at room temperature with shaking and washed before being imaged. To assess cell viability, cells were stained with propidium iodide (0.5  $\mu\text{g/ml}$ ; Invitrogen) as described above. The cells were imaged using a Zeiss Axio Observer microscope equipped with a Photometrics CoolSNAP HQ2 camera (Roper Scientific) and Metamorph 7.5 software (Molecular Devices), or by structured illumination microscopy (SIM) or laser wide-field microscopy in an Elyra PS.1 microscope (Zeiss) with a scientific complementary metal oxide semiconductor (sCMOS) camera and 5 grating rotations for each channel. SIM images were reconstructed and analysed with ZEN software (black edition, 2012; version 8.1.0.484). For the quantification of the signal of fluorescent derivatives of PBPs at the septum, five images were analysed per condition using ImageJ<sup>20</sup>. Only cells with a complete septum were analysed.

### **Macromolecular analysis of cell wall synthesis**

To assay for cell wall synthesis, we measured the incorporation of [<sup>3</sup>H]lysine into peptidoglycan in the presence of chloramphenicol (25  $\mu\text{g/ml}$  final concentration), which inhibits protein synthesis but allows peptidoglycan synthesis to continue, thus enabling us to judge pentapeptide synthesis of lipid II, a precursor of peptidoglycan, in the presence of DNAC-1 at 10 $\times$  MIC.

Ampicillin was used as a cell wall active antibiotic control. The effects of DNAC-1 and ampicillin on peptidoglycan synthesis were measured using the radiolabelled precursor [<sup>3</sup>H]lysine (2.5 µCi/ml final concentration) added to mid-exponential-phase cultures (~10<sup>8</sup> CFU/ml) of *S. aureus* strain ATCC 29213 in chemically defined medium, as previously described<sup>21</sup>. The radiolabelled precursor was added to the bacterial culture immediately before the antibiotics were added. The negative controls for the macromolecular assays consisted of all reaction components with no antibiotics added, with the resulting counts used as the 100% values. After an additional 20 min of incubation at 37°C in the presence or absence of antibiotics, the samples were removed for trichloroacetic acid precipitation and subsequent scintillation counter analyses to determine radioactive incorporation into the cell wall; the data were expressed as the percent inhibition of incorporation in comparison to a drug-free control.

### **Transmission electron microscopy**

*S. aureus* USA300 cells grown in MHC at 37°C were treated with either DNAC-1 (2× MIC) or DMSO for 90 min, washed twice with phosphate-buffered saline (PBS), and processed for electron microscopy (EM) by fixing with a 10× volume of 2% glutaraldehyde-tannic acid (GTA)–1% paraformaldehyde in 0.1 M Na-cacodylate buffer (pH 7.4), post-fixed in 1% OsO<sub>4</sub> in cacodylate buffer (pH 7.4), embedded, and serially dehydrated in ethanol. The samples were

sectioned and stained with uranyl acetate and imaged using a JEOL transmission electron microscope (TEM) 1010 at 100 kV and 20,000 $\times$  magnification. Thirty fields of each strain with nearly equatorial-cut surfaces were measured for cell wall thickness, and the results were expressed as the means  $\pm$  standard deviations. Statistical significance was determined using the Kruskal-Wallis test, with a *P* value of  $<0.05$  considered significant.

### **Membrane potential assays**

The carbocyanine dye DiOC2 (3,3'-diethyloxcarbocyanine iodide; Life Technologies) was used to assess membrane potential. *S. aureus* USA300 cultures were grown to the early exponential phase ( $OD_{620} = 0.3$ ) in MHB, incubated with 10  $\mu$ M DiOC2 in PBS with 1% glucose at 24 $^{\circ}$ C for 30 min in the dark, and then transferred to a 384-well plate. The cells were analysed using a plate reader, Tecan M1000 (excitation, 485 nm; emission, 680 nm). After establishing a baseline reading, either carbonyl cyanide *m*-chlorophenyl hydrazone (CCCP) (positive control) or DNAC-1 was added to the wells, and the drop in red fluorescence was monitored over time.



## Results

### PC190723 prevents correct Z ring placement

Chemical-genetic interaction networks have been used to predict compound synergy between cognate inhibitors of targets and their corresponding companion antibiotic<sup>22,23</sup>. These approaches have led to the identification of genes whose downregulation potentiates  $\beta$ -lactam activity against MRSA strains. Most  $\beta$ -lactam susceptibility determinants functionally participate in cell wall peptidoglycan biosynthesis (*glm*, *mur*, *mra*, *fem*, *pbp*, and SAV1754 genes), other aspects of cell wall biogenesis (*tarL*, *spsB*, and SAV1892), or wall stress signal transduction pathways (SAV1220)<sup>22-25</sup>. An additional group of  $\beta$ -lactam susceptibility determinants included components of the cell division Z ring, an ancestral tubulin-like macromolecular structure required for the assembly of the divisome. FtsZ is a self-activating guanosine triphosphatase (GTPase) that polymerizes into cytoskeletal Z ring filaments that localise to the future division site at the mid-cell early in the cell cycle<sup>26</sup>. Perturbations in Z ring assembly impair cell wall assembly<sup>27</sup>. PBP2, the target of several  $\beta$ -lactam antibiotics including oxacillin and imipenem, is itself delocalised from the septum in *S. aureus* upon genetic depletion of FtsZ<sup>28</sup>. Accordingly, the small-molecule PC190723, which targets the GTPase domain of FtsZ<sup>29,30</sup>, displayed synergy in combination with a wide variety of  $\beta$ -lactam antibiotics against MRSA. Importantly, PC190723 also produced strong microbiological activity as a single agent,

displaying a lower MIC<sub>90</sub> (0.5 µg/ml; minimum inhibitor concentration against 90% of clinical strain isolates tested) than the standard-of-care antibiotics linezolid and vancomycin (MIC<sub>90</sub> for both antibiotics is 2 µg/ml). PC190723 also has potent activity against linezolid-resistant, vancomycin intermediate resistant (VISA), and vancomycin-resistant (VRSA) *S. aureus*. PC190723 has been reported to have a bactericidal mode of action<sup>30</sup>, meaning that drug-treated cells rapidly lose viability rather than show arrested growth (that is, a bacteriostatic effect).

On the basis of the central role of FtsZ in cell division, and the prominent synergy between PC190723 and β-lactam antibiotics, we wondered if the mode of action of PC190723 involved the destabilisation of the assembly of the Z ring, which would prevent septal PG synthesis. To study localisation of FtsZ, we used a previously described fluorescent derivative of FtsZ [FtsZ–cyan fluorescent protein (FtsZ-CFP)]<sup>17</sup>. When expressed in MRSA COL, FtsZ-CFP correctly localised to the mid-cell and division septum (Fig. 1a)<sup>17,31</sup>. However, FtsZ-CFP localisation in MRSA COL was markedly altered in cells treated with PC190723 (at 10 times MIC for PC190723 - 10 µg/ml) for 30 min. FtsZ-CFP appeared as multiple rings and arcs without being specifically restricted to the future septum (Fig. 1a). MRSA COL bacteria treated with PC190723 also exhibited extensive enlargement as previously reported<sup>30</sup>, indicative of FtsZ-mediated disruption of localised cell wall synthesis at the septum<sup>28</sup>. Consistent with a direct effect of PC190723 on FtsZ localisation, similar

delocalisation of FtsZ-CFP was also observed in cells treated for 30 min with PC190723 at its MIC value of 1  $\mu\text{g/ml}$  (not shown). In a control experiment, bacteria treated with nalidixic acid (an antibiotic targeting DNA gyrase) under the same growth inhibitory conditions did not show altered FtsZ-CFP localisation (Fig. 2a). We also determined the localisation of PBP2 in PC190723-treated MRSA COL using a newly constructed functional superfolder green fluorescent protein (*sfgfp*)-*pbpB* fusion gene integrated at the native *pbpB* locus and regulated by its native promoter (see Experimental Procedures). sGFP-PBP2 correctly localised to the division septum in mock-treated cells in the same way as that observed for endogenous PBP2 protein<sup>28</sup> or for a previous GFP-PBP2 construct<sup>31</sup> (Fig. 1b). However, sGFP-PBP2 was extensively delocalised in cells treated with PC190723 at 1 $\times$  or 10 $\times$  MIC for 30 min (Fig. 1b), with discrete patches of sGFP-PBP2 accumulating throughout the plasma membrane. Like FtsZ-CFP, sGFP-PBP2 was correctly localised to the division site in MRSA COL cells treated with nalidixic acid (Fig. 2b). Collectively, these data demonstrate that FtsZ and PBP2 are delocalised from the division site of MRSA cells treated with PC190723. Because the proper function of FtsZ and PBP2 requires precise septum localisation to coordinate cell division and peptidoglycan biosynthesis, their extensive delocalisation in PC190723-treated cells provides insight into the molecular basis for the chemical synergy between compounds targeting these two proteins. Mechanistically, PC190723 and  $\beta$ -lactam antibiotics are likely to be synergistic against MRSA because of the

combined effects of (i) GTPase inhibition<sup>29,30</sup> and FtsZ delocalisation, and (ii) concomitant PBP2 delocalisation such that only a small amount of  $\beta$ -lactam antibiotic presumably is required to inactivate the residual and functional PBP2 enzyme localised at the septum.

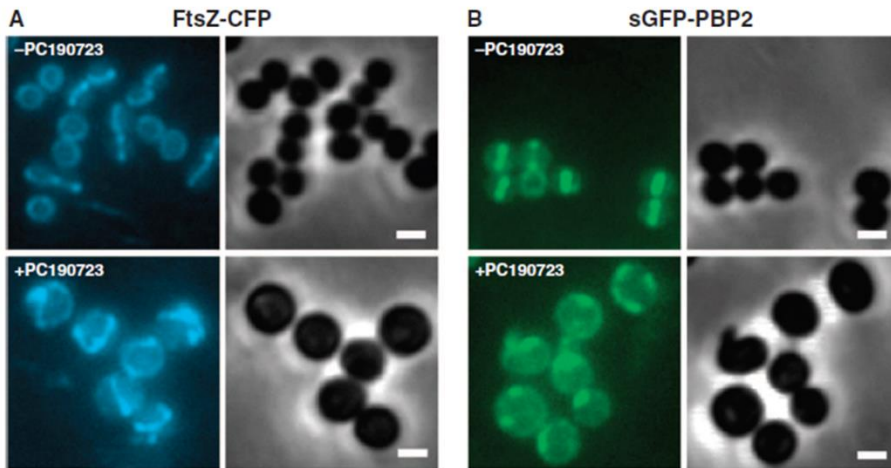


**Figure 1. Septal localisation of fluorescent derivatives of FtsZ and PBP2 is lost in PC190723-treated MRSA cells. (A)**, MRSA COL cells expressing FtsZ-CFP were grown in the absence (top panels) or presence of PC190723 (10  $\mu$ g/ml) (bottom panels) for 30 min and analysed by fluorescence microscopy. FtsZ-CFP localises to the division site in control cells but appears in multiple rings and arcs seen drug-treated cells. Right panels are companion phase-contrast images. **(B)**, MRSA COL cells expressing sGFP-PBP2 were grown in the absence (top panels) or presence (bottom panels) of PC190723 as described in (A) and similarly processed for fluorescence microscopy. sGFP-PBP2 localises at the division site in control cells but in broad patches of sGFP-PBP2 fluorescence around the cell periphery in drug-treated cells. Right panels are companion phase-contrast images. Scale bars, 1  $\mu$ m.

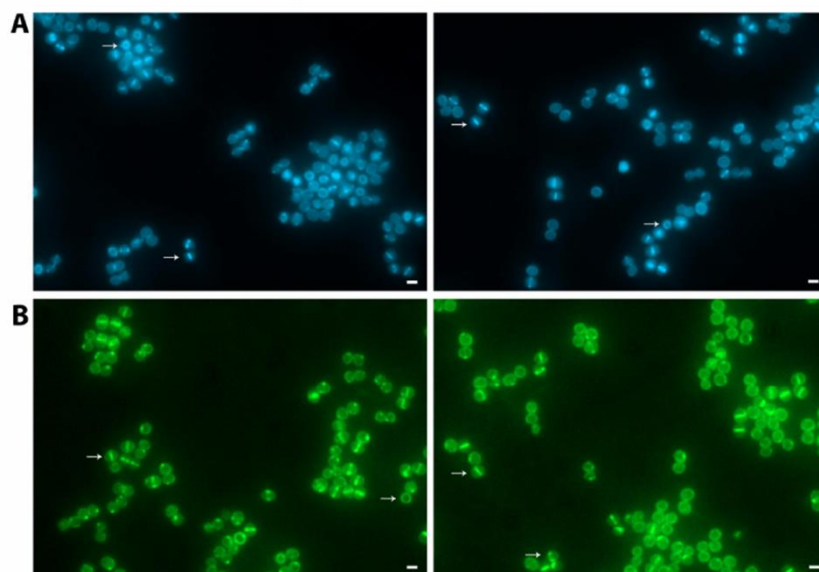


**Figure 2. Septal localisation of FtsZ-CFP and sGFP-PBP2 is unaltered in nalidixic acid-treated MRSA cells.** (A), MRSA COL cells expressing FtsZ-CFP were grown in the absence (left) or presence (right) of 100 µg/ml nalidixic acid (1X MIC) for 30 min and analysed by fluorescence microscopy. (B), MRSA COL cells expressing sGFP-PBP2 were identically grown in the absence (left) or presence (right) of nalidixic acid and analysed by fluorescence microscopy. Arrows indicate examples of FtsZ-CFP (A) and sGFP-PBP2 (B) localisation to the division site. Scale bar: 1 µm.

### **DNAC-1 impairs cell wall synthesis in MRSA**

A mechanistically unbiased viability screen was done at the New England Regional Centers of Excellence (NERCE) to identify small molecules that have an inhibitory activity either alone or in combination with a  $\beta$ -lactam<sup>32</sup>. One of the most promising compounds identified was DNAC-1 (Fig.3a), which had the lowest MIC (4 µg/ml) against CA-MRSA strain USA300. DNAC-1 was found

to potentiate the effects of different classes of antibiotics but is synergistic only with cell wall targeting antibiotics against MRSA<sup>32</sup>. Furthermore, DNAC-1 was shown to be bactericidal against MRSA on its own but was more effective in combination with oxacillin, as a combination of 4× MIC of DNAC-1 with 0.25× MIC of oxacillin led to the complete eradication of all viable cells in a culture of USA300 in 4 hours<sup>32</sup>. Based on the observed synergy between DNAC-1 and  $\beta$ -lactams, we decided to investigate if the mode of action DNAC-1 was related to the inhibition of cell wall synthesis. To this end, we used an assay which measures the incorporation of [<sup>3</sup>H]lysine into peptidoglycan in the presence of chloramphenicol (which inhibits protein synthesis) while allowing the incorporation of radiolabeled lysine into the pentapeptide of the peptidoglycan chain. Ampicillin was used as a positive control. As shown in Fig. 3, treatment with DNAC-1 led to a reduction in lysine incorporation into the nascent cell wall compared to the untreated control, at a level comparable to that with  $\beta$ -lactam antibiotic ampicillin.

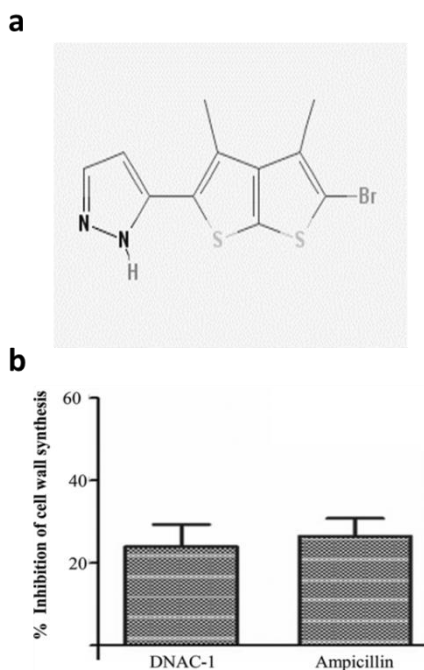


**Figure 3. Structure of DNAC-1 (a) and percent inhibition of cell wall biosynthesis of *S. aureus* by DNAC-1 (b), as measured by inhibition of radiolabeled lysine incorporation into nascent peptidoglycan.** In (b), bacteria were treated with either DNAC-1 or ampicillin (positive control) for 20 min in the presence of radioactive cell wall precursors. The data are presented as the percent inhibition compared to the untreated control.

To further assess the effect of DNAC-1 on cell wall morphology, USA300 cells were treated with DNAC-1 ( $2\times$  MIC) for 90 min, fixed, dehydrated, and observed under transmission electron microscopy (TEM). The cell wall thickness of the treated cells, evaluated in up to 30 different fields, was found to be increased compared to that of the untreated cells (Fig. 4), with mesosome-like invaginations<sup>16</sup> of the cell membrane into the cytosol along the cell periphery (Fig. 4a, centre) and along the septum (Fig. 4a, right).

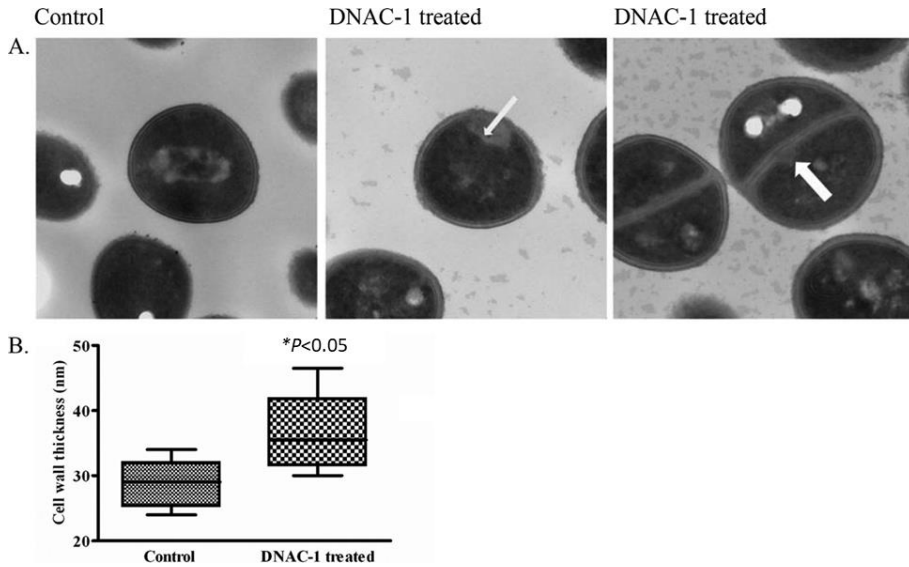


**Figure 4. Effect of DNAC-1 on cell wall, as observed by TEM.** USA300 cells were grown to mid-log phase and treated with DNAC-1 for 90 min or left untreated (control). The cells were then collected and processed for EM, as described in Experimental Procedures. **(A)**, Mesosome-like invaginations are seen both along the peripheral cell wall (arrow, center) and along the septum (arrow, right). **(B)**, DNAC-1-treated cells have a significantly thicker cell wall, as demonstrated in the box-and-whisker plot showing the standard deviation. The asterisk represents a statistically significant difference, at a  $P$  value  $<0.05$ , comparing the control to DNAC-1-treated cells.

### DNAC-1 causes mislocalisation of PBP2/4 and FtsZ

The results of the macromolecular synthesis assay and increased cell wall thickness in the TEM studies prompted us to question whether DNAC-1 affects the enzymes involved in cell wall synthesis. Accordingly, we examined the localisation of PBP2 and PBP4, both of which are known to be involved in cell wall synthesis and antibiotic resistance<sup>31,33</sup>. A lack of PBP4 activity is also known to



result in thickened cell walls<sup>34,35</sup>. To study localisation, we used MRSA COL strains expressing functional sGFP-PBP2 or PBP4-YFP fluorescent fusions<sup>9,33</sup>. Exposing actively growing cells to DNAC-1 at either 0.5× or 2× MIC for 15 min prevented the localisation of PBP2 and PBP4 to the septum, where they normally localise in dividing cells (Fig. 5a, left and centre). We quantified PBP localisation and saw that only 3% ( $n = 696$ ) of the DNAC-1-treated cells had PBP2 correctly localised at the septum versus 36% ( $n = 493$ ) of the untreated cells, while 13% ( $n = 652$ ) of the DNAC-1-treated cells had septal PBP4, compared to 27% ( $n = 591$ ) of the untreated cells. Since PBP2 localisation has been shown to depend on the polymerization of FtsZ at mid-cell<sup>28</sup>, we thus determined if the delocalisation of PBP2 upon DNAC-1 treatment was due to impaired Z ring formation. Accordingly, exposure of a strain containing CFP-tagged FtsZ<sup>9</sup> to 0.5× MIC of DNAC-1 for 15 min resulted in aberrant placement of FtsZ rings (Fig. 5a, right).

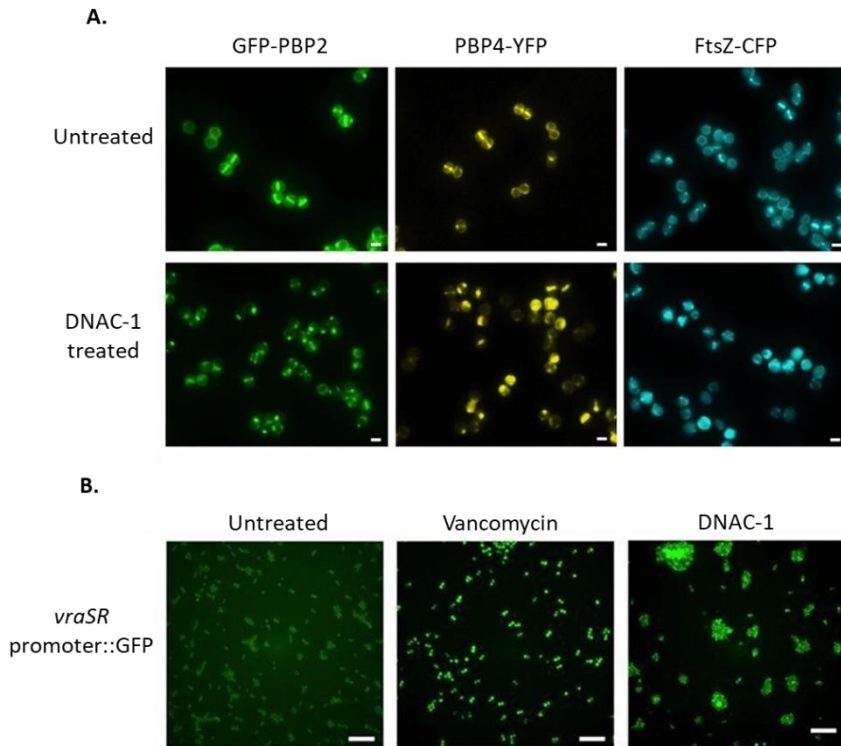


**Figure 5. Delocalisation of PBPs and FtsZ and activation of cell wall stress stimulon by DNAC-1. (A),** Localisation of PBP2, PBP4, and FtsZ was assessed using strains expressing either GFP-PBP2, PBP4-YFP, or FtsZ-CFP after treatment with 0.5× MIC of DNAC-1 for 15 min. Scale bars, 1  $\mu$ m. **(B),** Activation of the *vraSR* operon was tested using strains containing a *vraSR* promoter driving sfGFP expression. In the presence of 2× MIC of DNAC-1, the mean  $\pm$  standard deviation (SD) cell fluorescence was 3,594  $\pm$  1,344 arbitrary units (a.u.) ( $n = 468$ ), while in the presence of 2× MIC of vancomycin (positive control), the mean  $\pm$  SD cell fluorescence was 23,911  $\pm$  8,318 a.u. ( $n = 465$ ). The left panel corresponds to cells in the absence of antibiotics, which showed a mean  $\pm$  SD cell fluorescence of 2,196  $\pm$  447 a.u. ( $n = 511$ ). The  $P$  values were  $<0.0001$  between the DMSO control and vancomycin-treated cells and  $<0.05$  between the control and DNAC-1-treated cells. Scale bars, 10  $\mu$ m.

Cell wall-active compounds have also been known to trigger the cell wall stress stimulon (CWSS) by upregulating the *vraSR* operon<sup>36,37</sup>. To assess if DNAC-1 would trigger a CWSS response, we constructed a COL strain encoding a transcriptional fusion between the *vraSR* promoter and the gene encoding a fast-folding variant of GFP, *sfGFP*. We found that upon treatment with 2× MIC of DNAC-1 for 30 min, the sfGFP fluorescence signal in the cells was increased approximately 1.6 times compared to that with the mock-treated cells, indicating that the CWSS was triggered (Fig. 5b). However, the *vraSR* response to DNAC-1 was considerably weaker than the response triggered by vancomycin at 2× MIC (Fig. 5b, centre), a known activator of the cell wall stress stimulon<sup>37</sup>.

### **DNAC-1 disrupts the bacterial membrane**

The membrane disruption seen in the EM study prompted us to further examine the effect of DNAC-1 on the membrane. To reduce any artefacts that may have been introduced into samples during TEM processing, we employed super-resolution fluorescence microscopy of unfixed MRSA cells to investigate membrane defects. Within 15 min of exposure to DNAC-1 at 2× MIC, membrane staining of MRSA strain COL with FM 4-64 revealed numerous membrane spots and bulges into the cell cytosol compared to the untreated cells (Fig. 6a). These findings are in agreement with the mesosome-like structures visualized by TEM. No changes were observed in cell wall staining (Fig. 6b) using fluorescently labelled vancomycin. We also

monitored changes in membrane permeability with propidium iodide staining upon treatment with DNAC-1 at 2× MIC. The cells treated with DNAC-1 were rapidly permeabilised, as after 1 hour of exposure, ~55% of the bacterial cells showed propidium iodide staining, indicating a loss of cell membrane integrity (not shown).

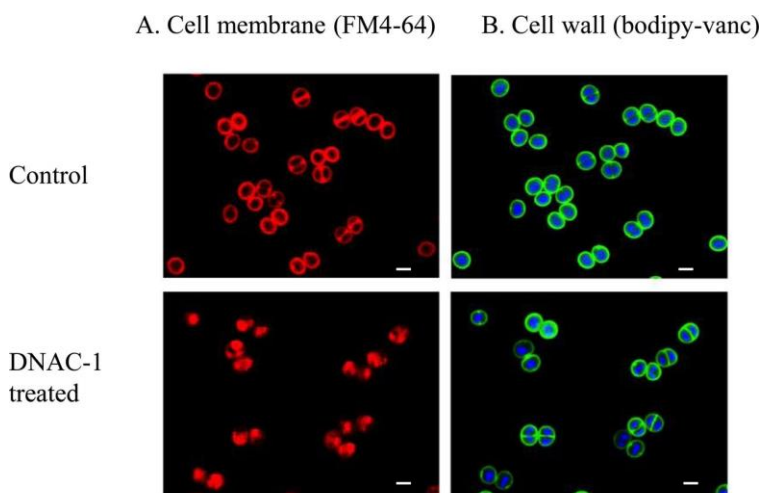


**Figure 6. Disruption of the cellular membrane integrity by DNAC-1.** Cells were either untreated (control) or treated with 2× MIC of DNAC-1 for 15 min and stained with FM 4-64 to visualize the membrane (A) and Bodipy-FL-vancomycin (green) to visualize the cell wall and Hoechst 33342 dye (blue) to see the DNA (B). DNAC-1 treated cells showed extensive membrane damage and condensation of the nucleoid. Scale bar, 1  $\mu$ m.

To investigate if DNAC-1 disrupts membrane potential, we used the dye DiOC<sub>2</sub>, which typically aggregates as a function of membrane potential. Upon treatment of USA300 with 2× to 8× MIC of DNAC-1 (8 to 32  $\mu$ g/ml), there was gradual dissipation of the membrane potential, as monitored by the loss of red fluorescence,

due to a loss of aggregation of DiOC<sub>2</sub> (Fig. 7). However, this decrease in membrane potential was less than that caused by the positive control, CCCP, a known proton translocator. Loss of cell viability paralleled the decrease in membrane potential, as confirmed by the colony forming units (CFU) counts at appropriate time points in the DNAC-1-treated cells compared with those of the untreated control (data not shown).

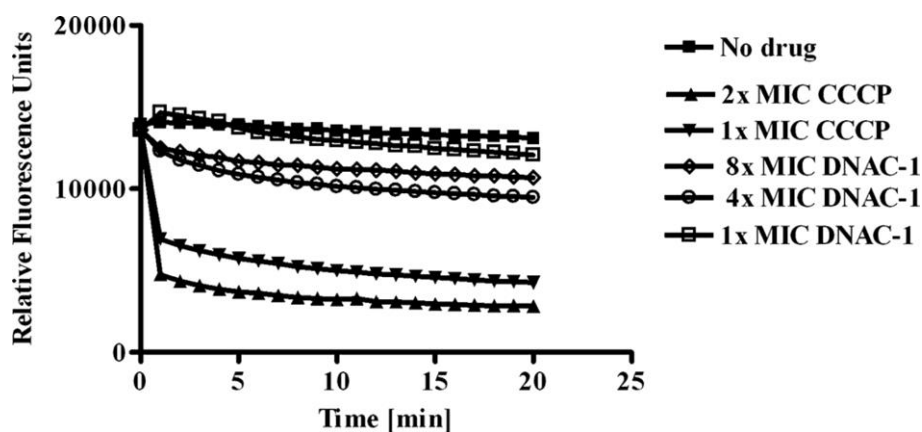


**Figure 7. DNAC-1 causes rapid membrane depolarization.** Actively growing USA300 cells were back-diluted, resuspended in PBS with glucose, and treated with DiOC<sub>2</sub> for 30 min in the dark at 25°C. A loss of fluorescence was monitored over time upon the addition of increasing concentrations of DNAC-1 (4×, 8×, and 16× MIC). CCCP was used as a positive control.

## Discussion

Resistance to last resort antibiotics vancomycin, daptomycin and linezolid is emerging in MRSA<sup>8</sup>. Despite this, large pharmaceutical companies have decreased investment in research and development of new antimicrobials, due to low financial returns. As the pharmaceutical pipeline is waning, understanding the activities of the few novel antibiotics that reach the market and the propensity of bacteria to evolve resistance against them is of the utmost importance. Therefore it is essential to investigate the mode of action of novel antibiotics, i.e. the effects that a certain inhibitor has on the viability of the bacterial cell as a whole<sup>10</sup>. This type of studies may also reveal previously unidentified relationships between biochemical pathways in the cell, which allows for more efficient future drug design<sup>38,39</sup>. Towards this goal, we have used a cell biology approach to contribute to the characterisation of the mode of action of two novel small molecules that are efficient against MRSA either on their own or in combination with commonly used  $\beta$ -lactam antibiotics.

Previous studies identified that the potent and selective FtsZ inhibitor PC190723 showed strong synergy against MRSA COL, specifically in combination with  $\beta$ -lactam imipenem. The molecular basis for this synergy is difficult to address, because FtsZ has a central role during the bacterial cell cycle, as it directly or indirectly recruits to the mid-cell most proteins that constitute the divisome<sup>26,40</sup>.

Consequently, inhibiting FtsZ activity with PC190723 disrupts all cell wall biogenesis processes including peptidoglycan synthesis, cross-linking and hydrolytic peptidoglycan degradation<sup>26,28,41,42</sup>. Nevertheless, it has been shown that the molecular targets of  $\beta$ -lactams, the PBPs, depend on the presence of FtsZ at mid-cell for recruitment<sup>28,43,44</sup>. Therefore we decided to investigate if PC190723 would prevent the correct assembly of the Z-ring at mid-cell with concomitant delocalisation of the major *S. aureus* PG synthase PBP2 in COL.

Treatment with PC190723 prevented correct FtsZ localisation, in accordance to what had been previously observed in *Bacillus subtilis*, although in these bacteria FtsZ appeared as multiple foci<sup>30</sup>, whereas we observed multiple rings and arcs of FtsZ in COL. Importantly, PBP2 was also delocalised in PC190273-treated cells. As  $\beta$ -lactam resistance in MRSA is mediated through the cooperation between PBP2 and  $\beta$ -lactam insensitive PBP2A<sup>45</sup>, PBP2 delocalisation in PC190723-treated cells is expected to result in deleterious effects to the cell. Therefore we postulate that the synergy between PC190723 and  $\beta$ -lactam antibiotics is partly due to the delocalisation of FtsZ which in turn prevents the recruitment of PBP2 to the septum, so that a substantially reduced concentration of the  $\beta$ -lactam is sufficient to inhibit any residual correctly localised PBP2. This synergy is likely amplified by a network of other factors. For example, mid-cell recruitment of MurJ, the enzyme likely responsible for translocating the peptidoglycan precursor lipid II across the membrane, also

requires the assembly of a functional FtsZ ring<sup>46</sup>. Because PBP2 localisation to the septum is also dependent on peptidoglycan precursor recognition<sup>31</sup>, FtsZ-mediated delocalisation of MurJ would similarly enhance  $\beta$ -lactam activity. The intricacies of chemical synergy between PC190723 and  $\beta$ -lactam antibiotics are highly complex but it is exactly the complexity of this network of interactions between FtsZ and downstream divisome components, including PBPs, which can be exploited towards developing combination strategies against MRSA.

The second compound studied, DNAC-1, was identified in a mechanistically unbiased screen to search for small molecules that work in conjunction with a  $\beta$ -lactam antibiotic, by the A. Cheung laboratory. DNAC-1 demonstrated potent inhibitory activity, not only in combination with  $\beta$ -lactams, but also on its own, against many Gram-positive bacteria, including MRSA. Moreover, DNAC-1 also potentiated the effects of ceftriaxone against resistant Gram-negative clinical isolates, suggesting it could be a viable option for broad spectrum antibiotic therapy. As DNAC-1 showed synergy with  $\beta$ -lactams we hypothesised that it could be inhibiting cell wall synthesis. Treatment with DNAC-1 resulted in decreased incorporation of radiolabelled lysine into nascent peptidoglycan and induced the cell wall stress response operon *vraSR* in MRSA COL, albeit to low levels, suggesting cell wall damage. Additionally, DNAC-1 also prevented the correct placement of the FtsZ ring at mid-cell, with concomitant delocalisation of PG synthases PBP2 and



PBP4, similarly to the effects observed following PC190723 treatment, as described above. However, in contrast to PC190723, we found that *S. aureus* cells exposed to DNAC-1 rapidly became permeabilised (within 15 minutes), as indicated by uniform propidium iodide staining throughout the cell population.

Because bactericidal activity due to cell wall synthesis inhibition is generally a slow process<sup>10</sup>, we wondered whether DNAC-1 would elicit direct membrane damage in cells. Accordingly, we noticed extensive membrane damage in treated cells, characterised by lipid bulges and invaginations, as seen in SIM images, and mesosome-like structures when cells observed by TEM, reminiscent of membrane disruption caused by cationic antimicrobial peptides<sup>47</sup>. Analysis of the cell membrane potential revealed a quick depolarization of the membrane, coinciding with a loss of viability. These data led us to suggest that DNAC-1 may exert a bimodal molecular mechanism on the bacterial membrane and cell wall, similarly to what has been described for daptomycin<sup>48</sup>.

We propose that the bactericidal effect of DNAC-1 occurs in two stages, in which the first stage involves permeabilisation of the membrane, followed by the inhibition of cell wall synthesis due to impaired divisome assembly and subsequent lack of recruitment of PG synthases, including PBP2 and PBP4. This model suggests that the combined use of a  $\beta$ -lactam and DNAC-1 would increase the antibacterial efficiency, by further decreasing PG synthesis. The

identification of the exact molecular target of DNAC-1 in the bacterial membrane would be an interesting pursuit, as it could reveal novel interactions between membrane and divisome components.

It is also possible that the rapid permeabilisation of the membrane by DNAC-1 is by itself sufficient to suspend all biochemical pathways in the cell, in which case the observed halt in divisome assembly comes as a consequence of a multitude of pathways failing. While DNAC-1 was shown to potentiate the effects of other classes of drugs, including those that affect DNA synthesis (norfloxacin, levofloxacin) and protein synthesis (tetracycline), synergy was only observed with cell wall active antibiotics<sup>32</sup>, which support a direct role for DNAC-1 in PG synthesis inhibition. Nevertheless, we cannot discard the possibility that this synergistic relationship is merely a result of facilitated access of DNAC-1 to its target in the membrane, due to the peptidoglycan layer being compromised. Alternatively, loss of proton motive force (PMF) following membrane depolarization triggered by DNAC-1 may indirectly lead to cellular death through impairment of essential cellular functions, as it has been shown that dissipation of the PMF alone is not bactericidal<sup>49</sup>. For example, it has been reported that in *B. subtilis* the acidification of the cell wall during growth regulates autolytic murein hydrolases<sup>50</sup>. In this way, loss of PMF may cause increased autolytic activity and consequent cell death due to degradation of the cell wall.

PC190723 and DNAC-1 are chemically distinct small molecules with different targets in the bacterial cell. Nevertheless both ultimately impair the assembly of the division machinery and consequently peptidoglycan synthesis at the septum, which has a bactericidal effect. PC190723 was well tolerated and highly efficient in combination with imipenem in a murine model of MRSA infection<sup>9</sup>. However, the frequency of resistance to PC190723 was very high, therefore it should not be considered a viable option for single agent therapy. DNAC-1 toxicity was assessed in cells of *Candida albicans*, cultured human bronchial epithelial cells and sheep erythrocytes, and did not perturb eukaryotic cell membranes at concentrations suitable for therapy<sup>32</sup>. As such, pending clinical trials both of these small molecules seem potentially viable options as therapeutic agents against MRSA, preferably in synergy with existing  $\beta$ -lactams.

The work described in this chapter demonstrates the usefulness of a cell biology approach, in combination with biochemical methods, in studies of antibiotic mode of action.

## References

- 1 Chambers, H. F. & DeLeo, F. R. Waves of resistance: *Staphylococcus aureus* in the antibiotic era. *Nat Rev Micro* **7**, 629-641, doi:[http://www.nature.com/nrmicro/journal/v7/n9/suppinfo/nrmicro2200\\_S1.html](http://www.nature.com/nrmicro/journal/v7/n9/suppinfo/nrmicro2200_S1.html) (2009).
- 2 Boucher, H. W. *et al.* Bad bugs, no drugs: no ESKAPE! An update from the Infectious Diseases Society of America. *Clin Infect Dis* **48**, 1-12, doi:10.1086/595011 (2009).
- 3 Grundmann, H., Aires-De-Sousa, M., Boyce, J. & Tiemersma, E. Emergence and resurgence of methicillin-resistant *Staphylococcus aureus* as a public-health threat. *Lancet* **368**, 874-885 (2006).
- 4 Correia, S., Poeta, P., Hébraud, M., Capelo, J. L. & Igrejas, G. Mechanisms of quinolone action and resistance: where do we stand? *J Med Microbiol* **66**, 551-559, doi:10.1099/jmm.0.000475 (2017).
- 5 Schroeder, M. R. & Stephens, D. S. Macrolide Resistance in *Streptococcus pneumoniae*. *Front Cell Infect Microbiol* **6**, 98, doi:10.3389/fcimb.2016.00098 (2016).
- 6 Pader, V. *et al.* *Staphylococcus aureus* inactivates daptomycin by releasing membrane phospholipids. *Nat Microbiol* **2**, 16194, doi:10.1038/nmicrobiol.2016.194 (2016).
- 7 Enright, M. C. *et al.* The evolutionary history of methicillin-resistant *Staphylococcus aureus* (MRSA). *Proc Natl Acad Sci U S A* **99**, 7687-7692, doi:10.1073/pnas.122108599 (2002).
- 8 Spellberg, B., Powers, J. H., Brass, E. P., Miller, L. G. & Edwards, J. E. Trends in antimicrobial drug development: implications for the future. *Clin Infect Dis* **38**, 1279-1286, doi:10.1086/420937 (2004).
- 9 Tan, C. M. *et al.* Restoring methicillin-resistant *Staphylococcus aureus* susceptibility to  $\beta$ -lactam antibiotics. *Sci Transl Med* **4**, 126ra135, doi:10.1126/scitranslmed.3003592 (2012).
- 10 Kohanski, M. A., Dwyer, D. J. & Collins, J. J. How antibiotics kill bacteria: from targets to networks. *Nat Rev Microbiol* **8**, 423-435, doi:10.1038/nrmicro2333 (2010).
- 11 Tomasz, A., Albino, A. & Zanati, E. Multiple antibiotic resistance in a bacterium with suppressed autolytic system. *Nature* **227**, 138-140 (1970).
- 12 Heidrich, C., Ursinus, A., Berger, J., Schwarz, H. & Höltje, J. V. Effects of multiple deletions of murein hydrolases on viability, septum cleavage, and sensitivity to large toxic molecules in *Escherichia coli*. *J Bacteriol* **184**, 6093-6099 (2002).
- 13 Fisher, A. C. & DeLisa, M. P. Laboratory evolution of fast-folding green fluorescent protein using secretory pathway quality control. *PLoS One* **3**, e2351, doi:10.1371/journal.pone.0002351 (2008).
- 14 Arnaud, M., Chastanet, A. & Debarbouille, M. New vector for efficient allelic replacement in naturally nontransformable, low-GC-content, gram-positive bacteria. *Appl. Environ. Microbiol.* **70**, 6887-6891, doi:10.1128/AEM.70.11.6887-6891.2004 (2004).

- 15 Guérout-Fleury, A. M., Shazand, K., Frandsen, N. & Stragier, P. Antibiotic-resistance cassettes for *Bacillus subtilis*. *Gene* **167**, 335-336 (1995).
- 16 Oshida, T. & Tomasz, A. Isolation and characterization of a *Tn551*-autolysis mutant of *Staphylococcus aureus*. *J Bacteriol* **174**, 4952-4959 (1992).
- 17 Veiga, H., Jorge, A. M. & Pinho, M. G. Absence of nucleoid occlusion effector Noc impairs formation of orthogonal FtsZ rings during *Staphylococcus aureus* cell division. *Mol. Microbiol.* **80**, 1366-1380, doi:10.1111/j.1365-2958.2011.07651.x (2011).
- 18 Pinho, M. & Errington, J. A *divIVA* null mutant of *Staphylococcus aureus* undergoes normal cell division. *FEMS Microbiol Lett* **240**, 145-149 (2004).
- 19 Loskill, P. *et al.* Reduction of the peptidoglycan crosslinking causes a decrease in stiffness of the *Staphylococcus aureus* cell envelope. *Biophys J* **107**, 1082-1089, doi:10.1016/j.bpj.2014.07.029 (2014).
- 20 Schneider, C. A., Rasband, W. S. & Eliceiri, K. W. NIH Image to ImageJ: 25 years of image analysis. *Nat Methods* **9**, 671-675 (2012).
- 21 Mattingly, S. J., Daneo-Moore, L. & Shockman, G. D. Factors regulating cell wall thickening and intracellular iodophilic polysaccharide storage in *Streptococcus mutans*. *Infect Immun* **16**, 967-973 (1977).
- 22 Lee, S. H. *et al.* Antagonism of chemical genetic interaction networks resensitize MRSA to  $\beta$ -lactam antibiotics. *Chem Biol* **18**, 1379-1389, doi:10.1016/j.chembiol.2011.08.015 (2011).
- 23 Huber, J. *et al.* Chemical genetic identification of peptidoglycan inhibitors potentiating carbapenem activity against methicillin-resistant *Staphylococcus aureus*. *Chem Biol* **16**, 837-848, doi:10.1016/j.chembiol.2009.05.012 (2009).
- 24 De Lencastre, H. *et al.* Antibiotic resistance as a stress response: complete sequencing of a large number of chromosomal loci in *Staphylococcus aureus* strain COL that impact on the expression of resistance to methicillin. *Microb Drug Resist* **5**, 163-175 (1999).
- 25 Berger-Bächli, B., Strässle, A., Gustafson, J. & Kayser, F. Mapping and characterization of multiple chromosomal factors involved in methicillin resistance in *Staphylococcus aureus*. *Antimicrob Agents Chemother* **36**, 1367-1373 (1992).
- 26 Adams, D. W. & Errington, J. Bacterial cell division: assembly, maintenance and disassembly of the Z ring. *Nat Rev Microbiol* **7**, 642-653, doi:10.1038/nrmicro2198 (2009).
- 27 Lara, B., Mengin-Lecreulx, D., Ayala, J. A. & van Heijenoort, J. Peptidoglycan precursor pools associated with *MraY* and *FtsW* deficiencies or antibiotic treatments. *FEMS Microbiol Lett* **250**, 195-200, doi:10.1016/j.femsle.2005.07.005 (2005).
- 28 Pinho, M. & Errington, J. Dispersed mode of *Staphylococcus aureus* cell wall synthesis in the absence of the division machinery. *Mol Microbiol* **50**, 871-881, doi:10.1046/j.1365-2958.2003.03719.x (2003).
- 29 Andreu, J. M. *et al.* The antibacterial cell division inhibitor PC190723 is an FtsZ polymer-stabilizing agent that induces filament assembly and condensation. *J Biol Chem* **285**, 14239-14246, doi:10.1074/jbc.M109.094722 (2010).

- 30 Haydon, D. J. *et al.* An inhibitor of FtsZ with potent and selective anti-staphylococcal activity. *Science* **321**, 1673-1675, doi:10.1126/science.1159961 (2008).
- 31 Pinho, M. G. & Errington, J. Recruitment of penicillin-binding protein PBP2 to the division site of *Staphylococcus aureus* is dependent on its transpeptidation substrates. *Mol. Microbiol.* **55**, 799-807, doi:10.1111/j.1365-2958.2004.04420.x (2005).
- 32 Nair, D. R. *et al.* Characterization of a novel small molecule that potentiates  $\beta$ -lactam activity against gram-positive and gram-negative pathogens. *Antimicrob Agents Chemother* **59**, 1876-1885, doi:10.1128/AAC.04164-14 (2015).
- 33 Memmi, G., Filipe, S., Pinho, M., Fu, Z. & Cheung, A. *Staphylococcus aureus* PBP4 Is Essential for beta-Lactam Resistance in Community-Acquired Methicillin-Resistant Strains. *Antimicrob. Agents. Chemother.* **52**, 3955-3966, doi:10.1128/AAC.00049-08 (2008).
- 34 Finan, J. E., Archer, G. L., Pucci, M. J. & Climo, M. W. Role of penicillin-binding protein 4 in expression of vancomycin resistance among clinical isolates of oxacillin-resistant *Staphylococcus aureus*. *Antimicrob Agents Chemother* **45**, 3070-3075, doi:10.1128/AAC.45.11.3070-3075.2001 (2001).
- 35 Wyke, A. W., Ward, J. B., Hayes, M. V. & Curtis, N. A. A role in vivo for penicillin-binding protein-4 of *Staphylococcus aureus*. *Eur J Biochem* **119**, 389-393 (1981).
- 36 Kuroda, M. *et al.* Two-component system VraSR positively modulates the regulation of cell-wall biosynthesis pathway in *Staphylococcus aureus*. *Mol Microbiol* **49**, 807-821, doi:3599 [pii] (2003).
- 37 Utaida, S. *et al.* Genome-wide transcriptional profiling of the response of *Staphylococcus aureus* to cell-wall-active antibiotics reveals a cell-wall-stress stimulon. *Microbiology* **149**, 2719-2732 (2003).
- 38 Lehár, J. *et al.* Chemical combination effects predict connectivity in biological systems. *Mol Syst Biol* **3**, 80, doi:10.1038/msb4100116 (2007).
- 39 Falconer, S. B., Czarny, T. L. & Brown, E. D. Antibiotics as probes of biological complexity. *Nat Chem Biol* **7**, 415-423, doi:10.1038/nchembio.590 (2011).
- 40 Errington, J., Daniel, R. A. & Scheffers, D. J. Cytokinesis in bacteria. *Microbiol Mol Biol Rev* **67**, 52-65, doi:10.1128/MMBR.67.1.52-65.2003 (2003).
- 41 Scheffers, D. J. & Pinho, M. G. Bacterial cell wall synthesis: New insights from localisation studies. *Microbiol. Mol. Biol. Rev.* **69**, 585-607, doi:10.1128/MMBR.69.4.585-607.2005 (2005).
- 42 Atilano, M. *et al.* Teichoic acids are temporal and spatial regulators of peptidoglycan cross-linking in *Staphylococcus aureus*. *Proc. Natl. Acad. Sci. U S A* **107**, 18991-18996, doi:10.1073/pnas.1004304107 (2010).
- 43 Weiss, D. S., Chen, J. C., Ghigo, J. M., Boyd, D. & Beckwith, J. Localisation of FtsI (PBP3) to the septal ring requires its membrane anchor, the Z ring, FtsA, FtsQ, and FtsL. *J Bacteriol* **181**, 508-520 (1999).
- 44 Scheffers, D. J., Jones, L. J. & Errington, J. Several distinct localisation patterns for penicillin-binding proteins in *Bacillus subtilis*. *Mol Microbiol* **51**, 749-764 (2004).

- 45 Pinho, M., de Lencastre, H. & Tomasz, A. An acquired and a native penicillin-binding protein cooperate in building the cell wall of drug-resistant staphylococci. *Proc Natl Acad Sci U S A* **98**, 10886-10891 (2001).
- 46 Monteiro, J. M. *et al.* Peptidoglycan synthesis drives an FtsZ-treadmilling-independent step of cytokinesis. *Nature*, doi:10.1038/nature25506 (2018).
- 47 Friedrich, C. L., Moyles, D., Beveridge, T. J. & Hancock, R. E. Antibacterial action of structurally diverse cationic peptides on gram-positive bacteria. *Antimicrob Agents Chemother* **44**, 2086-2092 (2000).
- 48 Straus, S. K. & Hancock, R. E. Mode of action of the new antibiotic for Gram-positive pathogens daptomycin: comparison with cationic antimicrobial peptides and lipopeptides. *Biochim Biophys Acta* **1758**, 1215-1223, doi:10.1016/j.bbamem.2006.02.009 (2006).
- 49 Xiong, Y. Q., Mukhopadhyay, K., Yeaman, M. R., Adler-Moore, J. & Bayer, A. S. Functional interrelationships between cell membrane and cell wall in antimicrobial peptide-mediated killing of *Staphylococcus aureus*. *Antimicrob Agents Chemother* **49**, 3114-3121, doi:10.1128/AAC.49.8.3114-3121.2005 (2005).
- 50 Calamita, H. G., Ehringer, W. D., Koch, A. L. & Doyle, R. J. Evidence that the cell wall of *Bacillus subtilis* is protonated during respiration. *Proc Natl Acad Sci U S A* **98**, 15260-15263, doi:10.1073/pnas.261483798 (2001).





# Chapter VI

---

## General Discussion and Conclusions

## **New approaches to study an old foe**

The pathogen *Staphylococcus aureus* constitutes one of the major human afflictions. Nearly a century of research into antibiotic development has resulted in a myriad of drugs efficient against *S. aureus* infections. Nevertheless this pathogen continues to adapt its biological processes to develop resistance to treatment. Great efforts have been made to develop antibiotics against a single target, but the frequency of acquisition of resistance to these types of drugs tends to be high. Nearly all of the most useful antibiotics discovered so far have various targets (different PBPs, ribosomal proteins encoded by several genes, membrane motifs), which makes development of resistance more difficult for bacteria. There is a clear need for new strategies to deal with MRSA (and other emerging drug-resistant bacteria) and I firmly believe that continued research into the biological processes of bacterial cells will provide knowledge of many potential pathways that can be exploited for drug development, with more success than single targets.

Despite its clinical relevance, less is known about the fundamental biology of the *S. aureus* cell than of laboratory workhorses *Escherichia coli* and *Bacillus subtilis*. This is partly because the small size of *S. aureus* cells (which average 1  $\mu\text{m}$  in diameter<sup>1</sup>, corresponding to only four times the resolution limit of conventional light microscopy) has hindered attempts to precisely measure morphological changes during the cell cycle; and partly due to

limited availability of molecular biology tools to study protein localisation *in vivo*<sup>2</sup>. In recent years the advent of Super-Resolution Microscopy techniques coupled with the development of new vectors to study protein localisation coming from our laboratory<sup>2</sup>, and others<sup>3,4</sup>, has allowed us to characterise in detail how *S. aureus* grows and divides and how it coordinates peptidoglycan synthesis with its cell cycle.

When investigating the *S. aureus* cell cycle I have often looked back at the earliest attempts, specifically the observations of Tzagoloff and Novick<sup>1</sup>, during the late 70s. Using time-lapse microscopy to follow single *S. aureus* cells during their lifecycle, the authors made two astute observations: firstly that “the cells began to swell in preparation for division” and secondly that “the separation of the two daughter cells occurs with a rather abrupt popping motion”<sup>1</sup>. Taking advantage of the increase in imaging resolution provided by SIM, we could elaborate on past observations. *S. aureus* cells grow continuously throughout their cell cycle, effectively doubling their size from an average initial volume of 0.47  $\mu\text{m}^3$  to a final volume of 0.91  $\mu\text{m}^3$ , and this growth is accompanied by slight cell elongation<sup>5</sup>. Therefore cell growth in *S. aureus* is more similar to rod-shaped bacteria than what was previously thought, as *B. subtilis*<sup>6</sup> and *E.coli*<sup>7</sup> also increase in cell volume continuously throughout the cell cycle. However, the increase of cell volume in rods is strictly due to cell elongation, as the width of the cell remains constant<sup>6</sup>, whereas in *S. aureus* both cell length and width increase with the cell cycle<sup>5</sup>. We

characterised the *S. aureus* cell cycle by assigning cells to three phases – Phase 1 (P1) cells have recently divided and have not started synthesising the septum; Phase 2 (P2) cells are synthesising the septum; Phase 3 (P3) cells have finished septum synthesis, which is undergoing maturation, and are going to generate two identical daughter cells. Cells spend half of their cell cycle in P1 and the other half equally on P2 and P3<sup>5</sup>. Cell growth is more pronounced during P3 (0.008  $\mu\text{m}^3/\text{min}$ ), corresponding to the swelling observed by Tzagaloff and Novick<sup>1</sup>, and only Phases 1 and 3 are periods of cell elongation.

We then wondered about the mechanisms behind this increase in cell volume. This could simply be a mechanical process, where the doubling of the cell's internal contents in preparation for division (including DNA replication and protein synthesis) would cause an increase in internal turgor pressure<sup>8</sup>, which would exert an outward force stretching the bacterial membrane and cell wall, leading to cell enlargement<sup>9</sup>. While peptidoglycan could be flexible enough to bear the stretching of the membrane<sup>10</sup>, it would ultimately lead to the overall thinning of the bacterial surface *in tandem* with the progression of the cell cycle. This was never observed in transmission electron microscopy imaging of *S. aureus*, where the peripheral cell wall appears homogeneous in thickness<sup>11,12</sup>. It is therefore more likely that both peptidoglycan synthesis and autolysis are necessary during the cell cycle, to retain cell surface integrity.

We considered two hypotheses for the increase in surface area during the cell cycle: **i)** the new wall material (which came from the septum of the mother cell) is selectively remodelled and enlarged during the cell cycle; or **ii)** the septum quickly reshapes into a curved surface during division and then the entire cell surface is remodelled during the cell cycle. We found that the latter hypothesis is correct based on two pieces of evidence. Firstly we saw that upon splitting of the mother cell and reshaping of the flat septum to a curved surface, the material coming from the septum only constitutes approximately 40% of each daughter cell surface<sup>5</sup>. With the progression of the cell cycle and concomitant cell growth, this percentage did not change i.e. the “new” wall material still constituted 40% of the cell surface at the end of the life cycle<sup>5</sup>. This showed that new wall material was not selectively remodelled to increase in surface area, compared to the rest of the cell wall, because if that was the case the new wall would expand to occupy an increased fraction of the cell surface. The second piece of evidence came when we used a fluorescent derivative of D-alanine that is incorporated in the stem peptide of PG precursors during PG synthesis<sup>13</sup>. We found that PG is incorporated all around the cell surface, particularly during Phase 1, and is dependent on the activity of the major PG synthases, the PBPs, similarly to septal PG insertion. When we deleted the non-essential PBP4, cells incorporated less peripheral PG<sup>5</sup>, in agreement with Gautam et al.<sup>14</sup>, and took a longer time to complete P1, suggesting that at least PBP4 is involved in this process.

Although we mostly focussed on the dynamics of PG incorporation, PG remodelling through autolytic activity is likely as important during the progression of the cell cycle, because chemical bonds in the existing structure must be broken to allow for the insertion of new material<sup>15</sup>. For example, the cytoskeleton machinery of *B. subtilis* includes LytE, a hydrolase that promotes cell elongation<sup>16</sup>; and LytM is required for the helical shape of *Helicobacter pylori*<sup>17</sup>. Accordingly, we saw that an *S. aureus* Atl mutant generated larger and less elongated cells than wild-type, implicating a function for Atl in cell size homeostasis and shape maintenance. Understanding how PG synthesis and remodelling are coordinated during the cell cycle is an exciting area of research with many open questions. One challenge is to explain how autolysins such as Atl specifically act on old glycan layers while leaving the nascent glycans intact. Perhaps autolysins localise to the outer layers of the cell wall and are unable to reach the inner layers or, alternatively, it is possible that new glycans are chemically modified to prevent premature autolysin activity and this modification is progressively removed during the cell cycle.

### **Dynamics of septum reshaping in *S. aureus***

Taken together, our data challenged the previous model for cellular growth in *S. aureus* stating that cocci only synthesised new PG at the septum during division, and that the doubling of the cell volume occurred upon splitting of the mother cell, when the flat

septum is reshaped into a curved hemisphere<sup>18</sup>. We therefore decided to revisit this question and investigate the dynamics of the reshaping of the flat septum, which correspond to the “popping” motion<sup>1</sup> described above. We used a fast camera to determine the timescale of this event and found that it is an extremely rapid process, occurring in less than 2 ms, which is the time resolution limit of our camera. Moreover, we found that there was no substantial increase in cell size immediately after popping, with each daughter cell having approximately half of the volume of their mother cell<sup>5</sup>. Because popping is so quick, we wondered whether this is purely a mechanical process driven by internal turgor or whether it requires enzymatic activity.

Previous studies using atomic force microscopy have revealed the presence of perforation holes around the outer edge of the septum, which become larger as synthesis of the septum proceeds<sup>19</sup>. It has been suggested that these holes result from the activity of autolysins, including Atl, which localises at the external edge of the septum and is important for cell splitting<sup>20,21</sup>. Autolysins Sle1 and LytN were also shown to localise to the septum through their LysM domains, as reported by Frankel and Schneewind<sup>22</sup>, who proposed that autolysin-mediated processive cleavage of the septum is required for cell separation. Alternatively, it has been suggested that cell splitting can be independent of hydrolase activity and simply result from high circumferential mechanical stress, which generates a crack that propagates throughout septal PG<sup>23</sup>. We have shown that a

mutant deficient of amidase Sle1 takes much longer to complete Phase 3 of the cell cycle, (corresponding to the period of septum maturation) with future daughter cells initiating the next division cycle before the complete splitting of the mother cell, suggesting that Sle1 has a role in cell separation<sup>5</sup>.

Even though autolysin activity is likely required for daughter cell splitting, it was still unclear whether it was necessary for the reshaping of the flat septum, as these could be two separate events. We found that popping is dependent on both internal turgor and autolytic activity, as we observed the presence of D-shaped cells (that is cells in which the flat septum failed to expand) in mutants deficient of autolysins Sle1 and LytM, which increased in frequency in high osmolarity conditions<sup>5</sup>. We proposed that during Phase 3 of the *S. aureus* cell cycle, autolysin activity creates nicks in septal peptidoglycan, which both facilitates daughter cell detachment and structurally loosens peptidoglycan, allowing turgor-driven expansion of the flat septum surface once cells separate<sup>5</sup>.

### **One peptidoglycan synthesis machinery - two locations**

Our studies of the cell shape dynamics during the *S. aureus* cell cycle revealed that peptidoglycan synthesis and incorporation occurs continuously during the lifecycle of these bacteria. One interesting observation was that the incorporation of PG precursors shifts from the periphery of the cell during Phase 1 of the cell cycle to



almost exclusively at mid-cell for initiation of the synthesis of the septum<sup>5</sup>. The rod-shaped organisms *E.coli* and *B. subtilis* possess two PG synthesis machineries dedicated to either peripheral or septal PG synthesis. In these organisms, peripheral PG synthesis is coordinated by the actin-like cytoskeletal protein MreB, while septal synthesis is coordinated by the tubulin homologue FtsZ. In contrast, *S. aureus* has a single machinery that must ensure PG incorporation at both the cell periphery and the septum<sup>18</sup>. Therefore the next question we asked was: what is the molecular cue that signals for the transition from peripheral to septal PG synthesis?

PG synthesis is one of the most conserved biochemical synthesis pathways in bacteria<sup>18</sup>. Most proteins involved in PG synthesis are essential, particularly those which catalyse the cytoplasmic<sup>24</sup> and inner membrane steps<sup>25</sup>. We reasoned that shifting PG synthesis from the periphery to mid-cell could be as simple as redirecting one core protein (or step) of PG synthesis to the right place at the right time. If this was true then this protein would have to localise exclusively to mid-cell in preparation for division, in order to direct PG incorporation there. We studied the localisation pattern of most PG synthesis proteins and found three possible candidates which strictly localised to the septum during division – the putative flippase MurJ, the putative transglycosylase FtsW and the transpeptidase PBP1<sup>26</sup>. Further, it seemed likely that the candidate protein would arrive early to the division site and therefore could be recruited to mid-cell during the assembly of the divisome, which has

been shown to occur in two stages in *B. subtilis*<sup>27</sup>. We performed co-localisation experiments with FtsZ and DivIB, as markers for the first and the second stages of divisome assembly, respectively, and found that FtsW and PBP1 arrive to the divisome approximately at the same time as DivIB, while MurJ arrived later than the remaining proteins. We showed that MurJ recruitment to the divisome was dependent on the assembly of the FtsL/DivIB/DivIC subcomplex, as depleting the expression of either protein prevented the recruitment of MurJ to the mid-cell<sup>26</sup>. Initially we were expecting the arrival of FtsW or PBP1 (or both) to the mid-cell to be the molecular cue directing PG synthesis to the septum, rather than of MurJ, due to their earlier recruitment to the divisome. On the contrary, PG incorporation at mid-cell was only observed when MurJ was present at mid-cell as well, indicating that MurJ is the PG synthesis protein that determines the shift from peripheral to mid-cell PG synthesis.

This led us to propose a model where the sole PG synthesis machinery of *S. aureus* incorporates lipid II all around the cell surface during the initial stages of the cell cycle. During divisome assembly, the DivIB-DivIC-FtsL complex recruits MurJ to the mid-cell which ensures that all lipid II translocation is occurring in that region. Substrate affinity<sup>28</sup> then diverts the major synthase PBP2 to mid-cell where it incorporates lipid II specifically in that region, leading to septal PG synthesis. This allows *S. aureus* to bypass the need for a cytoskeletal MreB-like machinery dedicated to peripheral PG synthesis and constitutes a novel mechanism in prokaryotes, where

PG is incorporated at two locations using the same multi-protein machinery.

The timing of MurJ arrival to the divisome is particularly interesting. It has been shown that the DivIB-DivIC-FtsL complex only assembles after FtsK localises to the divisome<sup>29</sup>. FtsK is part of a family of DNA translocases which pump DNA away from the division site, preventing bisection of the nucleoid by the septum<sup>30,31</sup>. The function of the DivIB-DivIC-FtsL complex can therefore constitute a checkpoint system that signals that DNA segregation is underway and, through MurJ recruitment, allows PG incorporation to initiate at the septum. Nevertheless, we did not investigate direct protein-protein interactions between the subcomplex and MurJ. It is therefore possible that another unknown factor is involved in the divisome hierarchy between the two proteins. It would also be interesting to explore the mechanisms of membrane synthesis at mid-cell. Similarly to PG synthesis, phospholipid incorporation at mid-cell must be coordinated by the assembly of the divisome, as we never observed septal membrane in cells where FtsZ polymerization was impaired<sup>26,32</sup> or in cells depleted of DivIB/DivIC/FtsL<sup>26</sup>. Perhaps both peptidoglycan and phospholipid incorporation have to occur precisely at the same time in order to maintain the integrity of the septum.

The functions of the SEDS putative TGase FtsW and transpeptidase PBP1 are still unclear. Our data shows that FtsW and

PBP1 are recruited to the divisome at approximately the same time, suggesting they could function together as a cognate SEDS/PBP pair involved in PG incorporation<sup>26</sup>. This would be similar in function to the RodA/PBPH and FtsW/PBP2B pairs, which were proposed by Meeske et al.<sup>33</sup> to be involved in PG polymerization during elongation and septation in *B. subtilis*, respectively. However, recruitment of FtsW/PBP1 to the divisome precedes that of MurJ and their activity presumably requires a flipped substrate. If MurJ is the sole flippase in the cell, why are FtsW/PBP1 recruited first to the divisome? It has been shown that FtsW can translocate lipid-linked precursors in purified *E. coli* membrane vesicles<sup>34</sup>, but flippase activity was not observed *in vivo*<sup>35</sup>. It is possible that the *S. aureus* FtsW/PBP1 pair functions in an early stage of septal synthesis where it both flips and incorporates a small initial pool of lipid II that provides a skeleton for subsequent mass PG incorporation, mediated by MurJ and PBP2. Accordingly, when we inhibited MurJ activity using DMPI we saw a drastic reduction in septal HADA incorporation but it was not completely abolished<sup>26</sup>, suggesting the presence of a MurJ-independent mechanism for HADA septal incorporation. However, it has been shown that PBP4 activity can directly exchange D-Ala termini by HADA in the stem peptides of mature PG<sup>14,36</sup>, which could explain why DMPI did not completely abolish HADA incorporation.

One curious aspect we noticed when investigating antibiotic effects on cell cycle progression of *S. aureus* was that cells treated with the FtsZ inhibitor PC190723 were uniformly and specifically stalled in

Phase 1 of the cell cycle<sup>26</sup>. While it was expected that cells that were in Phase 1 would not be able to synthesise a septum in the absence of a proper FtsZ ring and thus progress in the cell cycle, we were surprised to observe that the majority of cells in Phase 2 were perfectly able to complete the cell cycle. These data suggested that FtsZ treadmilling during septum synthesis (P2) was not required for cytokinesis, which contrasted with existing models. It has been proposed that the force for cytokinesis is provided by FtsZ, which generates a contractile force that, through membrane anchor FtsA, pulls the bacterial membrane inwards<sup>37,38</sup>. Alternatively it has been suggested that the force that drives cytokinesis could come from PG synthesis at the septum<sup>37,39</sup>. To investigate this, subsequent work done in our lab focussed on measuring the constriction rates of FtsZ rings during cytokinesis in the presence or absence of PC190723. In the absence of inhibitor, it was observed that FtsZ rings constrict in two stages, an initial slow stage and a second faster stage<sup>26</sup>. Inhibiting FtsZ treadmilling with PC19023 blocked constriction only of rings that were at the initial slow stage, indicating that another force independent of FtsZ treadmilling was responsible for the constriction of second stage Z-rings. Accordingly, the onset of the fast constriction step coincided with the arrival of MurJ (and PBP2) to the divisome. Furthermore, inhibition of MurJ halted the constriction of Z rings at all stages and prevented cytokinesis<sup>26</sup>. Taken together it seems that cytokinesis in *S. aureus* occurs in two steps: a slow first step where FtsZ treadmilling organises the assembly of the divisome and a

second, faster step, where MurJ recruitment to the divisome drives PG incorporation to the mid-cell, providing constrictive force required for cytokinesis.

### **Peptidoglycan crossbridges as targets for drug design**

The integrity of the peptidoglycan layer is paramount to the viability of most bacterial cells<sup>10</sup>. The PG layer protects the cell from environmental factors, including variations in osmolarity, pH and temperature. One of the main roles of PG is to withstand the cell's internal turgor, which is only possible due the flexibility of its cross-linked glycan chains<sup>10</sup>. In essence PG is akin to a mesh, or a spider web, in the sense that it is strong but flexible enough to dilate as the cell grows and expands its size without breaking.

We have shown that the pentaglycine crossbridges in *S. aureus* PG are required to withstand the cell's internal turgor. When we depleted expression of FemAB, the enzymes that add glycines 2-5 to lipid II-Gly<sub>1</sub>, we observed extensive membrane damage resulting in cell lysis, suggesting that in the absence of pentaglycine crosslinks PG loses structural integrity and the cell bursts. *S. aureus femAB* mutants have been isolated in the past through selective antibiotic pressure<sup>40</sup>. While a secondary suppressor or compensatory mutation was never found, it was shown that *femAB* mutants were able to survive by severely adapting their biochemical processes, presumably to alleviate turgor, including upregulating the expression of

transporters for osmoprotectant molecules such as glycerol and glycine betaine, or downregulating nitrogen metabolism<sup>41</sup>. It would be interesting to directly measure turgor pressure inside wild-type and adapted *femAB* mutant cells to determine the decrease in internal pressure required for the cell to survive without pentaglycine crosslinks.

In any case, modulation of metabolic pathways is apparently not sufficient by itself for the cell to survive without pentaglycine crosslinks. Adapted *femAB* null mutants also seem to have a starkly different PG structural organisation than wild-type, with longer glycan chains and lower percentage of cross-linked glycans<sup>40,42,43</sup>. When we depleted *femAB* expression, which results in the synthesis of lipid II species substituted with one glycine instead of five, we did not detect the appearance of extra peaks which could correspond to monoglycyl-substituted crosslinked di-, tri-, tetra- or pentamers. Rather we observed an overall decrease of all pentaglycine crosslinked species, suggesting that lipid II-gly<sub>1</sub> is not a valid substrate for PBP transpeptidation (TP). However, recent data from Suzanne Walker's group<sup>44</sup> has shown that PBP2 can use lipid II-gly<sub>1</sub> (and lipid II-gly<sub>3</sub>) as a substrate for TP *in vitro*, albeit to a lesser extent than lipid II-gly<sub>5</sub>. This was in contrast to other TPases such as PBP2A and PBP4 which did not act on lipid II-gly<sub>1</sub><sup>44</sup>. In light of this evidence we decided to revisit our data and noticed that in PG profiles of **i**) a conditional *femAB* mutant grown with low *femAB* expression and of **ii**) a *femA* point mutant carrying a KR180AA mutation (with reduced

FemA activity), there was a marked accumulation of a dimer species that had been previously detected in low amounts in *S. aureus*<sup>45</sup>, but with unknown chemical composition. This species could be a monoglycine substituted dimer resulting from PBP2 TP activity. Nevertheless, as mentioned above, we did not observe alternative higher order crosslinked species, indicating that perhaps PBP2 is able to crosslink monoglycine substituted monomers but loses activity on dimers, trimers, tetramers, etc.

Given the importance of pentaglycine crossbridges for the structural stability of the *S. aureus* peptidoglycan and since the *femAB* operon is exclusive to these bacteria, Fem proteins seem good candidates for MRSA-specific drug design. We have shown that depletion of FemAB effectively causes cell lysis due to loss of membrane integrity in CA-MRSA strain MW2, indicating that a FemA inhibitor could be potent against infections caused by MRSA. However, *femAB* mutants which have developed adaptations to survive with reduced crossbridges have been isolated in the past<sup>41,46-48</sup>, raising concerns that the same adaptation and, consequently, emergence of resistance could occur during therapy with a FemA inhibitor. The upside is that MRSA *femAB* mutants become hypersusceptible to  $\beta$ -lactams<sup>46,49</sup>, most likely because resistance determinant PBP2A is unable to crosslink monoglycyl substituted species<sup>44</sup>, even after rearrangements of PG tertiary structure<sup>42</sup>. Therefore a possible strategy would be to supply FemA inhibitors in combination therapy with a  $\beta$ -lactam antibiotic to treat MRSA



infections. To my knowledge the only FemA inhibitor which has been described so far is cyslabdan, a small nonantibiotic produced by *Streptomyces* K04-0144 isolated in Okinawa<sup>50</sup>. Although cyslabdan potentiated the effect of imipenem against MRSA, it was non-lethal by itself and HPLC analysis of mucopeptides revealed no changes in higher order cross-linking, which are indicative of reduced FemA activity<sup>51</sup>. Similarly to the *in vivo* effects, incubation of lipid II-gly<sup>1</sup> with FemA in the presence of cyslabdan led to a modest reduction of protein activity, indicating that cyslabdan is only a partial inhibitor of FemA<sup>51</sup>. Towards the future development of a more potent FemA inhibitor we have observed that mutations in the  $\alpha 6$  helix and in the 1B subdomain of FemA led to a severe decrease in transferase activity. We posited that the former region stabilises the entering glycyl –charged tRNA molecules while the latter has been previously suggested to be the binding channel for the lipid II-gly<sup>1</sup> substrate<sup>52,53</sup>. One possible avenue for specific FemA drug development could be the design of an analogue of a glycyl-charged tRNA molecule which would compete for the FemA active site, as presumably these are exclusively used by Fem proteins in the cell<sup>54</sup>. Such an analogue could be modelled to bind at the junction between the coiled-coil arms of FemA and the globular domain, stabilised by interactions with polar charged amino acids in the  $\alpha 6$  helix, which we have identified as important for protein activity.

## **Mode of action of antibiotics and drug synergy**

In the face of increasing bacterial resistance to antibiotics coupled with a generalised disinvestment towards research and development of new drugs to treat bacterial infections<sup>55</sup>, a clear understanding of the mechanisms behind antibiotic activity becomes essential. Part of this understanding comes from determining the mode of action of antibiotics, or in other words, what happens to the bacterial cell when faced with an inhibitor of a cellular function. Insights into antibiotic modes of action will allow us to predict (to some extent) which molecules will be more effective and the likelihood of bacteria developing resistance against different compounds<sup>56</sup>.

The effects of a direct drug-target interaction are relatively simple to characterise. For example, linezolid binds ribosomes and stalls protein synthesis<sup>57</sup>, which is essential to the cell; ciprofloxacin inhibits DNA gyrase stalling DNA replication<sup>58</sup>, therefore cells cannot divide; cefotaxime binds PBPs and halts PG biosynthesis<sup>59</sup>, which is essential for the integrity of the cell envelope; nisin binds lipid II, causing membrane holes that leak ions<sup>60</sup>, disrupting cell homeostasis. However, the direct effect of primary target inhibition by an antibiotic is often merely the initial stage of a complex multi-layered mechanism leading to cellular death, and these mechanisms are not as well understood<sup>56</sup>. An example which illustrates this complexity pertains to the mode of action of quinolones, where binding of the

quinolone to gyrase stalls DNA replication, which is by itself a bacteriostatic rather than bactericidal effect, in the sense that it prevents cell division without affecting cell viability. However, cell death then arises due to subsequent events during which the bacterial chromosomes are quickly fragmented. These events leading to cell death can be dependent on a variety of factors including deregulated protein synthesis, expression of toxin-antitoxin modules and the generation of reactive oxygen species<sup>58</sup>.

The mode of action of antibiotics increases in complexity when combination therapy is considered. If treatment with a combination of two (or more) drugs results in lowered MICs for each drug, when compared to the individual MIC, then these drugs are synergistic<sup>61</sup>. Synergy is often (but not exclusively) observed when two agents affect the same biochemical pathway in the cell<sup>56</sup>. Such is the case for the cyslabdan/imipenem combination described above. Cyslabdan potentiates imipenem activity against MRSA essentially because both agents impair the same chemical reaction: transpeptidation of glycan strands catalysed by PBPs. In this way, cyslabdan inhibits the synthesis of the substrate (lipid II-gly<sub>5</sub>) of transpeptidation while imipenem inhibits the catalyst (PBP). Similarly, treatment with MurJ inhibitor DMPI also potentiates imipenem activity<sup>62</sup>, because DMPI prevents the translocation of lipid II-gly<sub>5</sub> across the membrane<sup>26</sup>.

A less straightforward example relates to the synergy between PC190723 (which inhibits FtsZ treadmilling)<sup>63</sup> and  $\beta$ -lactam antibiotics. When investigating the mode of action of PC190723 in *S. aureus* cells we noticed that FtsZ localisation was altered from the normal mid-cell position, instead appearing as extra rings and arcs seemingly in random positions in the cell<sup>32</sup>. This implied that the assembly of the divisome was impaired when cells were treated with PC190723, indicating that FtsZ-treadmilling is required to stabilise the *S. aureus* divisome. Because divisome assembly is a hierarchical process that is dependent on the sequential recruitment of proteins to the mid-cell<sup>64</sup>, we reasoned that PC190723 would prevent the correct localisation of PG synthases to mid-cell. Accordingly, we observed that PBP2 becomes dispersed throughout the cell surface in cells treated with PC190723<sup>32</sup>, similarly to previous studies showing dependence of FtsZ for correct PBP2 localisation<sup>65</sup>. Therefore even though PC190723 is effective on its own against MRSA because it prevents correct Z ring placement, it also synergises with  $\beta$ -lactam antibiotics due to both agents affecting PG synthesis at the septum. This effect probably extends to other combinations of inhibitors of steps of divisome assembly with  $\beta$ -lactams. Importantly, the frequency of resistance (*i.e.* the likelihood of appearance of a spontaneous mutation conferring resistance) to PC190723 in MRSA is very close to the value which is acceptable for a single-agent antibiotic ( $\sim 10^{-8}$  events), with PC190723<sup>R</sup> spontaneous mutations invariably mapping to FtsZ<sup>32</sup>. On the other hand, MRSA PC190723<sup>R</sup>

isolates become markedly susceptible to  $\beta$ -lactam activity<sup>32</sup>, suggesting that this combination can constitute an option for antibiotic therapy.

When investigating the mode of action of DNAC-1, a novel small molecule isolated in a screening for compounds synergistic with  $\beta$ -lactams, we found that incubation of *S. aureus* cells with DNAC-1 led to extensive membrane damage<sup>66</sup>. Furthermore, this membrane effect seemed direct rather than a downstream consequence of other pathways failing, as DNAC-1 rapidly caused membrane depolarisation and cell lysis<sup>66</sup>. Surprisingly DNAC-1 revealed specific synergy with cell wall active antibiotics but not with other antibiotic classes, suggesting that its mode of action also involves perturbation of PG synthesis, directly or indirectly, in addition to membrane damage. In agreement, incubation of MRSA with DNAC-1 caused delocalisation of FtsZ and PG synthases PBP2/PBP4 within 15 minutes of exposure. Additionally, DNAC-1 caused mild activation of the cell wall stress response operon *vraSR*, which is triggered when PG synthesis is impaired<sup>66</sup>. Therefore the mode of action of DNAC-1 shares some similarities with another membrane active compound, nisin, which also targets PG synthesis. Nisin forms pores in the membrane through lipid II binding, which both leads to rapid cell permeabilisation and interrupts PG synthesis<sup>60,67</sup>. Scanning electron microscopy imaging of *E. coli* and *B. subtilis* cells treated with nisin showed extensive membrane blebbing, similarly to what we observed with DNAC-1<sup>68</sup>. Furthermore, studies

by Lages et al.<sup>69</sup> have shown that nisin delocalises the elongation specific PG synthases PbpH and PBP2A in *B. subtilis* but, surprisingly, septation-specific PBP2B was unaffected. As PBP2B recruitment to mid-cell is dependent on the assembly of the divisome<sup>70</sup>, it can also be inferred that FtsZ localisation is not affected by nisin, although this has never been shown. Therefore DNAC-1 and nisin have a similar mode of action in terms of membrane effects but nisin only interferes with PG synthesis, while DNAC-1 also inhibits the assembly of the divisome<sup>66</sup>. It would be interesting to elucidate the precise molecular target of DNAC-1 in the bacterial membrane. This could be a PG synthesis lipid intermediate, akin to the mechanisms of nisin binding<sup>67</sup>, or alternatively, a putative membrane microdomain which is required for the assembly of the divisome. Both hypotheses are consistent with the observed synergy between DNAC-1 and  $\beta$ -lactam antibiotics<sup>66</sup>, as binding to either molecular target would potentiate the effects of inhibition of PG synthesis. However, a more likely interpretation is that the primary mode of action through which DNAC-1 kills bacterial cells is through destabilisation of the bacterial membrane, and that delocalisation of FtsZ and PG synthesis proteins constitutes a secondary effect.

Antibiotics that disrupt bacterial membranes have quick bactericidal effects and the frequency of resistance is generally low<sup>71</sup>. Furthermore, these agents can disperse bacterial biofilms and readily kill metabolically dormant (persister) cells, which constitute an important factor associated with treatment failure due to inherent

resistance to most classes of antibiotics that target biosynthetic pathways<sup>71</sup>. As such, membrane active molecules such as DNAC-1 have the potential to become powerful tools to treat persistent bacterial infections. A concerted effort into both improving the specificity and understanding the mode of action of these molecules is highly desirable for antibiotic development.

## Final Remarks

In this thesis I have used different approaches to tackle the issue of escalating antibiotic resistance in bacteria, specifically focussing on clinically relevant *S. aureus*. My major goal was to investigate fundamental biological processes in this pathogen, specifically how it coordinates peptidoglycan synthesis and remodelling with the progression of its cell cycle. I then used this knowledge to study the mode of action of newly-developed antimicrobials, as well as to find new targets for antibiotic development.

Although I believe we have made significant advances to the study of cell biology in bacteria, many questions still remain. Having determined the mechanism and timing of the recruitment of PG synthesis to mid-cell in *S. aureus*, I am most interested in investigating how it coordinates with DNA segregation and membrane synthesis. The ultimate objective would be to arrive at a complete model to septum synthesis, integrating the order of assembly of proteins, the timings of each process, and the structural dynamics between each component of the septum. It is likely that with further advances in technology, particularly towards the development of microscopy techniques, we will come to a virtually complete understanding of how bacteria function, down to each single molecule. Such knowledge will definitely prove invaluable, not only towards the design of better and more efficient antibiotics, but also to further



exploit the potential of bacterial cells as biological machines that can be used for medical, technological and commercial applications.

## References

- 1 Tzagoloff, H. & Novick, R. Geometry of cell division in *Staphylococcus aureus*. *J. Bacteriol.* **129**, 343-350 (1977).
- 2 Pereira, P., Veiga, H., Jorge, A. & Pinho, M. Fluorescent reporters for studies of cellular localisation of proteins in *Staphylococcus aureus*. *Appl. Environ. Microbiol.* **76**, 4346-4353, doi:10.1128/AEM.00359-10 (2010).
- 3 Charpentier, E. *et al.* Novel cassette-based shuttle vector system for gram-positive bacteria. *Appl. Environ. Microbiol.* **70**, 6076-6085, doi:10.1128/AEM.70.10.6076-6085.2004 (2004).
- 4 Fisher, A. C. & DeLisa, M. P. Laboratory evolution of fast-folding green fluorescent protein using secretory pathway quality control. *PLoS One* **3**, e2351, doi:10.1371/journal.pone.0002351 (2008).
- 5 Monteiro, J. M. *et al.* Cell shape dynamics during the staphylococcal cell cycle. *Nat Commun* **6**, 8055, doi:10.1038/ncomms9055 (2015).
- 6 Burdett, I. D., Kirkwood, T. B. & Whalley, J. B. Growth kinetics of individual *Bacillus subtilis* cells and correlation with nucleoid extension. *J Bacteriol* **167**, 219-230 (1986).
- 7 Campos, M. *et al.* A constant size extension drives bacterial cell size homeostasis. *Cell* **159**, 1433-1446, doi:10.1016/j.cell.2014.11.022 (2014).
- 8 Rojas, E., Theriot, J. A. & Huang, K. C. Response of *Escherichia coli* growth rate to osmotic shock. *Proc Natl Acad Sci U S A* **111**, 7807-7812, doi:10.1073/pnas.1402591111 (2014).
- 9 Turner, R. D., Hurd, A. F., Cadby, A., Hobbs, J. K. & Foster, S. J. Cell wall elongation mode in Gram-negative bacteria is determined by peptidoglycan architecture. *Nat Commun* **4**, 1496, doi:10.1038/ncomms2503 (2013).
- 10 Vollmer, W., Blanot, D. & de Pedro, M. Peptidoglycan structure and architecture. *FEMS Microbiol Rev* **32**, 149-167 (2008).
- 11 Giesbrecht, P., Kersten, T., Maidhof, H. & Wecke, J. Staphylococcal cell wall: morphogenesis and fatal variations in the presence of penicillin. *Microbiol. Mol. Biol. Rev.* **62**, 1371-1414 (1998).
- 12 Touhami, A., Jericho, M. & Beveridge, T. Atomic force microscopy of cell growth and division in *Staphylococcus aureus*. *J Bacteriol* **186**, 3286-3295 (2004).
- 13 Kuru, E. *et al.* *In situ* probing of newly synthesized peptidoglycan in live bacteria with fluorescent D-amino acids. *Angew. Chem. Int Ed. Engl.* **51**, 12519-12523, doi:10.1002/anie.201206749 (2012).
- 14 Gautam, S., Kim, T. & Spiegel, D. A. Chemical probes reveal an extraseptal mode of cross-linking in *Staphylococcus aureus*. *J Am Chem Soc* **137**, 7441-7447, doi:10.1021/jacs.5b02972 (2015).
- 15 Vollmer, W., Joris, B., Charlier, P. & Foster, S. Bacterial peptidoglycan (murein) hydrolases. *FEMS Microbiol Rev* **32**, 259-286, doi:10.1111/j.1574-6976.2007.00099.x (2008).
- 16 Carballido-López, R. *et al.* Actin homolog MreBH governs cell morphogenesis by localisation of the cell wall hydrolase LytE. *Dev Cell* **11**, 399-409, doi:10.1016/j.devcel.2006.07.017 (2006).

- 17 Sycuro, L. K. *et al.* Peptidoglycan crosslinking relaxation promotes *Helicobacter pylori*'s helical shape and stomach colonization. *Cell* **141**, 822-833, doi:10.1016/j.cell.2010.03.046 (2010).
- 18 Pinho, M. G., Kjos, M. & Veening, J. W. How to get (a)round: mechanisms controlling growth and division of coccoid bacteria. *Nat Rev Microbiol* **11**, 601-614, doi:10.1038/nrmicro3088 (2013).
- 19 Touhami, A., Jericho, M. H. & Beveridge, T. J. Atomic force microscopy of cell growth and division in *Staphylococcus aureus*. *J. Bacteriol.* **186**, 3286-3295, doi:10.1128/JB.186.11.3286-3295.2004 (2004).
- 20 Sugai, M. *et al.* Identification of endo-beta-N-acetylglucosaminidase and N-acetylmuramyl-L-alanine amidase as cluster-dispersing enzymes in *Staphylococcus aureus*. *J. Bacteriol.* **177**, 1491-1496 (1995).
- 21 Yamada, S. *et al.* An autolysin ring associated with cell separation of *Staphylococcus aureus*. *J. Bacteriol.* **178**, 1565-1571 (1996).
- 22 Frankel, M. B. & Schneewind, O. Determinants of murein hydrolase targeting to cross-wall of *Staphylococcus aureus* peptidoglycan. *J Biol Chem* **287**, 10460-10471, doi:10.1074/jbc.M111.336404 (2012).
- 23 Zhou, X. *et al.* Bacterial division. Mechanical crack propagation drives millisecond daughter cell separation in *Staphylococcus aureus*. *Science* **348**, 574-578, doi:10.1126/science.aaa1511 (2015).
- 24 Barreteau, H. *et al.* Cytoplasmic steps of peptidoglycan biosynthesis. *FEMS Microbiol Rev* **32**, 168-207, doi:10.1111/j.1574-6976.2008.00104.x (2008).
- 25 Bouhss, A., Trunkfield, A. E., Bugg, T. D. & Mengin-Lecreulx, D. The biosynthesis of peptidoglycan lipid-linked intermediates. *FEMS Microbiol Rev* **32**, 208-233, doi:10.1111/j.1574-6976.2007.00089.x (2008).
- 26 Monteiro, J. M. *et al.* Peptidoglycan synthesis drives an FtsZ-treadmilling-independent step of cytokinesis. *Nature*, doi:10.1038/nature25506 (2018).
- 27 Gamba, P., Veening, J. W., Saunders, N. J., Hamoen, L. W. & Daniel, R. A. Two-step assembly dynamics of the *Bacillus subtilis* divisome. *J Bacteriol* **191**, 4186-4194, doi:10.1128/JB.01758-08 (2009).
- 28 Pinho, M. G. & Errington, J. Recruitment of penicillin-binding protein PBP2 to the division site of *Staphylococcus aureus* is dependent on its transpeptidation substrates. *Mol. Microbiol.* **55**, 799-807, doi:10.1111/j.1365-2958.2004.04420.x (2005).
- 29 Chen, J. C. & Beckwith, J. FtsQ, FtsL and FtsI require FtsK, but not FtsN, for co-localisation with FtsZ during *Escherichia coli* cell division. *Mol Microbiol* **42**, 395-413 (2001).
- 30 Kaimer, C., González-Pastor, J. E. & Graumann, P. L. SpoIIIE and a novel type of DNA translocase, SftA, couple chromosome segregation with cell division in *Bacillus subtilis*. *Mol Microbiol* **74**, 810-825, doi:10.1111/j.1365-2958.2009.06894.x (2009).
- 31 Crozat, E., Rousseau, P., Fournes, F. & Cornet, F. The FtsK family of DNA translocases finds the ends of circles. *J Mol Microbiol Biotechnol* **24**, 396-408, doi:10.1159/000369213 (2014).

- 32 Tan, C. M. *et al.* Restoring methicillin-resistant *Staphylococcus aureus* susceptibility to  $\beta$ -lactam antibiotics. *Sci Transl Med* **4**, 126ra135, doi:10.1126/scitranslmed.3003592 (2012).
- 33 Meeske, A. J. *et al.* SEDS proteins are a widespread family of bacterial cell wall polymerases. *Nature* **537**, 634-638, doi:10.1038/nature19331 (2016).
- 34 Mohammadi, T. *et al.* Identification of FtsW as a transporter of lipid-linked cell wall precursors across the membrane. *EMBO J* **30**, 1425-1432, doi:10.1038/emboj.2011.61 (2011).
- 35 Sham, L. T. *et al.* Bacterial cell wall. MurJ is the flippase of lipid-linked precursors for peptidoglycan biogenesis. *Science* **345**, 220-222, doi:10.1126/science.1254522 (2014).
- 36 Qiao, Y. *et al.* Detection of lipid-linked peptidoglycan precursors by exploiting an unexpected transpeptidase reaction. *J. Am. Chem. Soc.* **136**, 14678-14681, doi:10.1021/ja508147s (2014).
- 37 Coltharp, C. & Xiao, J. Beyond force generation: Why is a dynamic ring of FtsZ polymers essential for bacterial cytokinesis? *Bioessays* **39**, 1-11, doi:10.1002/bies.201600179 (2017).
- 38 Li, Z., Trimble, M. J., Brun, Y. V. & Jensen, G. J. The structure of FtsZ filaments *in vivo* suggests a force-generating role in cell division. *EMBO J* **26**, 4694-4708, doi:10.1038/sj.emboj.7601895 (2007).
- 39 Coltharp, C., Buss, J., Plumer, T. M. & Xiao, J. Defining the rate-limiting processes of bacterial cytokinesis. *Proc Natl Acad Sci U S A* **113**, E1044-1053, doi:10.1073/pnas.1514296113 (2016).
- 40 Strandén, A., Ehler, K., Labischinski, H. & Berger-Bächi, B. Cell wall monoglycine crossbridges and methicillin hypersusceptibility in a *femAB* null mutant of methicillin-resistant *Staphylococcus aureus*. *J Bacteriol* **179**, 9-16 (1997).
- 41 Hübscher, J. *et al.* Living with an imperfect cell wall: compensation of *femAB* inactivation in *Staphylococcus aureus*. *BMC Genomics* **8**, 307, doi:10.1186/1471-2164-8-307 (2007).
- 42 Kim, S. J., Chang, J. & Singh, M. Peptidoglycan architecture of Gram-positive bacteria by solid-state NMR. *Biochim Biophys Acta* **1848**, 350-362, doi:10.1016/j.bbamem.2014.05.031 (2015).
- 43 Sharif, S., Kim, S., Labischinski, H. & Schaefer, J. Characterization of peptidoglycan in *fem*-deletion mutants of methicillin-resistant *Staphylococcus aureus* by solid-state NMR. *Biochemistry* **48**, 3100-3108 (2009).
- 44 Srisuknimit, V., Qiao, Y., Schaefer, K., Kahne, D. & Walker, S. Peptidoglycan Cross-Linking Preferences of *Staphylococcus aureus* Penicillin-Binding Proteins Have Implications for Treating MRSA Infections. *J Am Chem Soc* **139**, 9791-9794, doi:10.1021/jacs.7b04881 (2017).
- 45 de Jonge, B. L., Chang, Y. S., Gage, D. & Tomasz, A. Peptidoglycan composition of a highly methicillin-resistant *Staphylococcus aureus* strain. The role of penicillin binding protein 2A. *J Biol Chem* **267**, 11248-11254 (1992).
- 46 Berger-Bächi, B. Insertional inactivation of staphylococcal methicillin resistance by *Tn551*. *J Bacteriol* **154**, 479-487 (1983).

- 47 Berger-Bächli, B., Barberis-Maino, L., Strässle, A. & Kayser, F. FemA, a host-mediated factor essential for methicillin resistance in *Staphylococcus aureus*: molecular cloning and characterization. *Mol Gen Genet* **219**, 263-269 (1989).
- 48 Rohrer, S., Ehlert, K., Tschierske, M., Labischinski, H. & Berger-Bächli, B. The essential *Staphylococcus aureus* gene *fmhB* is involved in the first step of peptidoglycan pentaglycine interpeptide formation. *Proc Natl Acad Sci U S A* **96**, 9351-9356 (1999).
- 49 Berger-Bächli, B., Strässle, A., Gustafson, J. & Kayser, F. Mapping and characterization of multiple chromosomal factors involved in methicillin resistance in *Staphylococcus aureus*. *Antimicrob Agents Chemother* **36**, 1367-1373 (1992).
- 50 Fukumoto, A. *et al.* Cyslabdan, a new potentiator of imipenem activity against methicillin-resistant *Staphylococcus aureus*, produced by *Streptomyces* sp. K04-0144. II. Biological activities. *J Antibiot (Tokyo)* **61**, 7-10, doi:10.1038/ja.2008.102 (2008).
- 51 Koyama, N. *et al.* The nonantibiotic small molecule cyslabdan enhances the potency of  $\beta$ -lactams against MRSA by inhibiting pentaglycine interpeptide bridge synthesis. *PLoS One* **7**, e48981, doi:10.1371/journal.pone.0048981 (2012).
- 52 Benson, T. *et al.* X-ray crystal structure of *Staphylococcus aureus* FemA. *Structure* **10**, 1107-1115 (2002).
- 53 Maillard, A. *et al.* Structure-based site-directed mutagenesis of the UDP-MurNAc-pentapeptide-binding cavity of the FemX alanine transferase from *Weissella viridescens*. *J Bacteriol* **187**, 3833-3838 (2005).
- 54 Berger-Bächli, B. & Tschierske, M. Role of fem factors in methicillin resistance. *Drug Resist Updat* **1**, 325-335 (1998).
- 55 Fernandes, P. Antibacterial discovery and development--the failure of success? *Nat Biotechnol* **24**, 1497-1503, doi:10.1038/nbt1206-1497 (2006).
- 56 Kohanski, M. A., Dwyer, D. J. & Collins, J. J. How antibiotics kill bacteria: from targets to networks. *Nat Rev Microbiol* **8**, 423-435, doi:10.1038/nrmicro2333 (2010).
- 57 Livermore, D. M. Linezolid in vitro: mechanism and antibacterial spectrum. *J Antimicrob Chemother* **51 Suppl 2**, ii9-16, doi:10.1093/jac/dkg249 (2003).
- 58 Aldred, K. J., Kerns, R. J. & Osheroff, N. Mechanism of quinolone action and resistance. *Biochemistry* **53**, 1565-1574, doi:10.1021/bi5000564 (2014).
- 59 Waxman, D. & Strominger, J. Penicillin-binding proteins and the mechanism of action of beta-lactam antibiotics. *Annu Rev Biochem* **52**, 825-869 (1983).
- 60 Breukink, E. *et al.* Lipid II is an intrinsic component of the pore induced by nisin in bacterial membranes. *J Biol Chem* **278**, 19898-19903, doi:10.1074/jbc.M301463200 (2003).
- 61 Foucquier, J. & Guedj, M. Analysis of drug combinations: current methodological landscape. *Pharmacol Res Perspect* **3**, e00149, doi:10.1002/prp2.149 (2015).

- 62 Huber, J. *et al.* Chemical genetic identification of peptidoglycan inhibitors potentiating carbapenem activity against methicillin-resistant *Staphylococcus aureus*. *Chem Biol* **16**, 837-848, doi:10.1016/j.chembiol.2009.05.012 (2009).
- 63 Elsen, N. L. *et al.* Mechanism of action of the cell-division inhibitor PC190723: modulation of FtsZ assembly cooperativity. *J Am Chem Soc* **134**, 12342-12345, doi:10.1021/ja303564a (2012).
- 64 Errington, J., Daniel, R. A. & Scheffers, D. J. Cytokinesis in bacteria. *Microbiol Mol Biol Rev* **67**, 52-65, doi:10.1128/MMBR.67.1.52-65.2003 (2003).
- 65 Pinho, M. & Errington, J. Dispersed mode of *Staphylococcus aureus* cell wall synthesis in the absence of the division machinery. *Mol Microbiol* **50**, 871-881, doi:10.1046/j.1365-2958.2003.03719.x (2003).
- 66 Nair, D. R. *et al.* Characterization of a novel small molecule that potentiates  $\beta$ -lactam activity against gram-positive and gram-negative pathogens. *Antimicrob Agents Chemother* **59**, 1876-1885, doi:10.1128/AAC.04164-14 (2015).
- 67 Wiedemann, I. *et al.* Specific binding of nisin to the peptidoglycan precursor lipid II combines pore formation and inhibition of cell wall biosynthesis for potent antibiotic activity. *J Biol Chem* **276**, 1772-1779, doi:10.1074/jbc.M006770200 (2001).
- 68 Prince, A. *et al.* Corrigendum: Lipid-II Independent Antimicrobial Mechanism of Nisin Depends On Its Crowding And Degree Of Oligomerization. *Sci Rep* **7**, 41346, doi:10.1038/srep41346 (2017).
- 69 Lages, M. C., Beilharz, K., Morales Angeles, D., Veening, J. W. & Scheffers, D. J. The localisation of key *Bacillus subtilis* penicillin binding proteins during cell growth is determined by substrate availability. *Environ Microbiol* **15**, 3272-3281, doi:10.1111/1462-2920.12206 (2013).
- 70 Corbin, B. D., Geissler, B., Sadasivam, M. & Margolin, W. Z-ring-independent interaction between a subdomain of FtsA and late septation proteins as revealed by a polar recruitment assay. *J Bacteriol* **186**, 7736-7744, doi:10.1128/JB.186.22.7736-7744.2004 (2004).
- 71 Hurdle, J. G., O'Neill, A. J., Chopra, I. & Lee, R. E. Targeting bacterial membrane function: an underexploited mechanism for treating persistent infections. *Nat Rev Microbiol* **9**, 62-75, doi:10.1038/nrmicro2474 (2011).

## **Curriculum Vitae**

**João Miguel Monteiro**

### **Institutional Address**

Bacterial Cell Biology Laboratory, Instituto de Tecnologia Química e Biológica António Xavier, Universidade Nova de Lisboa (ITQB-UNL), Avenida da República - EAN, 2780-157 Oeiras, Portugal.

**Phone:** (+351) 214 469 538

**E-mail:** [jmonteiro@itqb.unl.pt](mailto:jmonteiro@itqb.unl.pt)

**Web page:** [www.itqb.unl.pt/labs/bacterial-cell-biology](http://www.itqb.unl.pt/labs/bacterial-cell-biology)

### **Personal Details**

João Miguel da Silva Queiroga Monteiro, born in 19/04/1985 in Lisbon, Portugal; ID 12711867; resident in Rua Álvaro Perdigão, lote 6 4° esquerdo, 2900-163 Setúbal, Portugal.

**E-mail:** [jmonteiro85@gmail.com](mailto:jmonteiro85@gmail.com).

**Spoken languages:** Portuguese, English (fluent), Spanish (fluent), French (basic).

### **Academic Research Training**

**Since July 2011;** PhD student from ITQB/UNL. Thesis project: Mechanisms coordinating peptidoglycan synthesis with the cell cycle in *Staphylococcus aureus* (SFRH/BD/71993/2010, of the Fundação para a Ciência e Tecnologia – FCT) in the Bacterial Cell Biology Laboratory at ITQB-UNL, under the supervision of Prof. Mariana Gomes de Pinho.

**November 2013 to Jan 2014;** recipient of an EMBO Short-term Fellowship (Ref. ASTF 558-2013) with the project entitled “Studies on the function and activity of the *Staphylococcus aureus* VraTSR three-component system reconstituted in

liposomes” at the Institut für Medizinische Mikrobiologie, Immunologie und Parasitologie (IMMIP), in Bonn, Germany, under the supervision of Professor Gabriele Bierbaum.

**September 2012 to August 2013**; Research Training in the Pharmazeutische Mikrobiologie group in the University of Bonn, Germany, as part of the PhD studies, under the supervision of Professor Hans-Georg Sahl.

**January 2011 to November 2011**; ITQB PhD program at ITQB NOVA. Courses covered themes such as Biochemistry and Structural Biology, Biomolecular Chemistry, Microbial Physiology and Pathogenesis, Cell and Developmental Biology, Biotechnology and Bioentrepreneurship.

**September 2009 to January 2011**; Research training at ITQB-UNL in the Bacterial Cell Biology laboratory under the supervision of Prof. Mariana Gomes de Pinho.

**September 2007 to September 2009**; Master degree in Molecular Genetics and Biomedicine from the Faculdade de Ciências e Tecnologia (FCT) of UNL with Dissertation entitled “Localisation studies of the FemXAB protein family in *Staphylococcus aureus*”, under the supervision of Prof. Mariana Gomes de Pinho. Final classification: 18 (20).

**September 2003 to September 2007**; Bachelor degree in Applied Chemistry – Biotechnology from Faculdade de Ciências e Tecnologia (FCT) of UNL. Classification: 14 (20).

## **Scientific Publications**

**Monteiro JM\***, Pereira AR\*, Reichmann NT, Saraiva BM, Fernandes PB, Veiga H, Tavares AC, Santos M, Ferreira MT, Macário V, VanNieuhenhze MS, Filipe SR and Pinho MG. Peptidoglycan synthesis drives an FtsZ treadmilling-independent step of cytokinesis. *Nature*. doi:10.1038/nature25506 (2018).

Nair DR, Chen J, **Monteiro JM**, Josten M, Pinho MG, Sahl HG, Wu J and Cheung A. A quinolinol-based small molecule with anti-MRSA activity that targets the bacterial membrane and promotes fermentative metabolism. *Journal of Antibiotics* Oct;70(10):1009-1019. doi: 10.1038/ja.2017.79 (2017).

Serrano M, Crawshaw AD, Dembek M, **Monteiro JM**, Pereira FC, Pinho MG, Fairweather NF, Salgado PS and Henriques AO. The SpoIIQ-SpoIIIAH complex of *Clostridium difficile* controls forespore engulfment and late stages of gene



expression and spore morphogenesis. *Molecular Microbiology* Apr;100(1):204-28. doi: 10.1111/mmi.13311 (2016).

**Monteiro JM\***, Fernandes PB\*, Vaz F, Pereira AR, Tavares AC, Ferreira MT, Pereira PM, Veiga H., Kuru E, VanNieuwenhze MS, Brun YV, Filipe SR and Pinho MG. Cell shape dynamics during the staphylococcal cell cycle. *Nature Communications* 6, 8055; doi:10.1038/ncomms9055 (2015).

Nair DR, **Monteiro JM**, Memmi G, Thanassi J, Pucci M, Scharzman J, Pinho MG and Cheung A. Characterization of a novel small molecule that potentiates  $\beta$ -lactam activity against Gram-positive and Gram-negative pathogens. *Antimicrobial Agents and Chemotherapy* 59:1876–1885; doi:10.1128/AAC.04164-14 (2015).

Reichmann NT, Piçarra Cassona C, **Monteiro JM**, Bottomley AL, Corrigan RM, Foster SJ, Pinho MG, Gründling A. Differential localisation of LTA synthesis proteins and their interaction with the cell division machinery in *Staphylococcus aureus*. *Molecular Microbiology* Apr;92(2):273-86; doi: 10.1111/mmi.12551 (2014).

Tan CM\*, Therien AG\*, Lu J, Lee SH, Caron A, Gill CJ, Lebeau-Jacob C, Benton-Perdomo L, **Monteiro JM**, Pereira PM, Elsen NL, Wu J, Deschamps K, Petcu M, Wong S, Daigneault E, Kramer S, Liang L, Maxwell E, Claveau D, Vaillancourt J, Skorey K, Tam J, Wang H, Meredith TC, Sillaots S, Wang-Jarantow L, Ramtohl Y, Langlois E, Landry F, Reid JC, Parthasarathy G, Sharma S, Baryshnikova A, Lumb KJ, Pinho MG, Soisson SM and Roemer T. Restoring Methicillin-Resistant *Staphylococcus aureus* Susceptibility to  $\beta$ -Lactam Antibiotics. *Science Translational Medicine* 4. 126ra35; doi: 10.1126/scitranslmed.3003592 (2012).

## Technical skills

Fluorescence microscopy: Wide-field microscopy (WF), Super-resolution structured illumination (SIM), Photoactivated Localisation Microscopy (PALM), Total Internal Reflection Fluorescence (TIRF), Fluorescence Resonance Energy Transfer (FRET).

General Microbiology and Molecular Biology: culture and propagation of bacteria, DNA purification, gene cloning, site-directed mutagenesis, transformation/transduction of DNA.

Biochemistry: SDS-PAGE, western-blotting analysis, protein purification, membrane purification, bacterial cell wall extraction by HPLC, enzymatic activity assays.

Bioinformatics: DNA sequence analysis, BLAST, protein structure analysis, ImageJ, ZEN, Metamorph, PDB viewer.

### **Oral Presentations**

MurJ recruitment to the divisome drives peptidoglycan incorporation to mid-cell in *Staphylococcus aureus*; **Monteiro JM**. 5<sup>th</sup> Mol. Micro and 4<sup>th</sup> M4 meeting, University of Birmingham, Birmingham, UK, September 13-14 (2017).

The interplay between peptidoglycan biosynthesis and cell cycle dynamics in *Staphylococcus aureus*; **Monteiro JM**. 6<sup>th</sup> ITQB NOVA PhD students meeting, November 19 (2015).

### **Poster presentations in international conferences**

MurJ recruitment to the divisome drives peptidoglycan incorporation to mid-cell in *Staphylococcus aureus*; **Monteiro JM**, Reichmann NT, Saraiva BM, Fernandes PB, Veiga H, Tavares AC, Santos MS, Ferreira MT, Macário V, VanNieuwenhze MS, Pinho MG. The 5<sup>th</sup> Great Wall Symposium, Hotel de São Rafael, São Rafael, Portugal, September 24-27 (2017).

Subcellular localisation of the complete peptidoglycan biosynthesis pathway in *Staphylococcus aureus*. **Monteiro JM**, Fernandes PB, Ferreira T, Saraiva BM, Reichmann NT, Macário V, Santos MS, Sobral R, Krippahl L, Pinho MG. Gordon research Conference on staphylococcal diseases, Renaissance Tuscany Il Ciocco, Lucca, Italy, July 12-17 (2015).

Cell shape dynamics during the staphylococcal cell cycle. **Monteiro JM**, Fernandes PB, Vaz F, Pereira AR, Tavares AC, Ferreira MT, Kuru E, VanNieuwenhze, Brun Y, Filipe SR and Pinho MG. Gordon research Conference on staphylococcal diseases, Renaissance Tuscany Il Ciocco, Lucca, Italy, July 12-17 (2015).

The pentaglycine bridges in *Staphylococcus aureus* peptidoglycan are required to maintain cell integrity. **Monteiro JM** and Pinho MG. Gordon Research Conference on Bacterial Cell Surfaces . Mount Snow Resort, Mount Snow, Vermont, US, June 22-27 (2014).

**Participation in other scientific meetings/courses**

EMBL Advanced Course on Fluorescence Imaging Techniques, EMBL, Heidelberg, Germany, July 7-11 (2014).

The 2<sup>nd</sup> Great Wall Symposium, Cascais, Lisbon, Portugal, September 28-30 (2011).  
Part of the organising committee.

How Dead is Dead II – The Ins and Outs of Bacterial Dormancy, Tübingen, Germany, June 16-17 (2011).

Bacterial Cell Biology Symposium and Workshop on Microscopy in Microbial systems. Umea University, Umea, Sweden, June 14-18 (2009).





ITQB-UNL | Av. da República, 2780-157 Oeiras, Portugal  
Tel (+351) 214 469 100 | Fax (+351) 214 411 277

[www.itqb.unl.pt](http://www.itqb.unl.pt)